UNIVERSITAT JAUME I

Departamento de Química Inorgánica y Orgánica
Institute of Advanced Materials

Poly-N-Heterocyclic Carbene Ligands with Rigid Polyaromatic Linkers. Self-Assembly and Host-Guest Chemistry

Doctoral Thesis
Carmen Mejuto Nieblas

PhD. Supervisors: Eduardo Peris and Gregorio Guisado-Barrios
Castellón de la Plana, June 2017

Prof. Dr. Eduardo Peris Fajarnés, Catedrático de Química Inorgánica y Dr. Gregorio Guisado Barrios, Investigador Postdoctoral Juan de la Cierva de la Universitat Jaume I, pertenecientes al Departamento de Química Inorgánica y Orgánica de la Univesitat Jaume I

Certifican: Que la Tesis Doctoral con el título "Poly N-Heterocyclic Carbene Ligands with Rigid Polyaromatic Linkers. Self-Assembly and Host-Guest Chemistry" ha sido desarollada bajo su dirección, en el Departamento de Química Inorgánica y Orgánica de la Universitat Jaume I, por Carmen Mejuto Nieblas

Castellón de la Plana, Junio de 2017

Fdo. Prof. Dr. Eduardo Peris Fajarnés   Fdo. Dr. Gregorio Guisado Barrios

Acknowledgements /Agradecimientos

Chapter 3

Chapter 4

Chapter 5

Nomenclature

The nomenclature employed to name the compounds described in this work is:

Ligands or organic intermediates in the synthesis of imidazolium salt: letters of the alphabet (**A**-**G**). In the cases where a compound could bear different substituents, their nature (Me, Et, …) will be included next to the letter of the alphabet.

Ligands salts precursors: the ligand letter with the acidic protons and its counter-ion. For example, **[H₃B^Et](PF₆)₃** is the precursor salt of the ligand B which contains three acidic C-H bonds and three hexafluorophosphate as counter-ions.

Metal complexes with NHC ligands: the number followed by the letter of the coordinated ligand. The complexes have been sorted in order of appearance in the text.

List of Abbreviations

Δ	Refluxing temperature
Å	Ångström
η	Ligand hapticity
ϕ	Quantum yield
λ	Wavelength
ε_r	Relative error
ν	Frequency
Ar	Aryl
av	average
CCDC	Cambridge Crystallographic Data Centre
Cat.	Catalyst
Conv.	Conversion
COD	1,5-cyclooctadiene
Cp	Cyclopentadienyl
Cp*	1,2,3,4,5-pentamethylcyclopentadienyl
CV	Cyclic Voltammetry
DFT	Density Functional Theory
DMF	Dimethylformamide
DPV	Differential Pulse Voltammetry

DMSO	Dimethylsulfoxide
E	Potential
EA	Elemental Analysis
Et	Ethyl
EtOAc	Ethyl acetate
EtOH	Ethanol
Et$_2$O	Diethyl ether
ESI-MS	Electrospray Ionization Mass Spectrometry
ESI-TOF-MS	Electrospray Ionization Time-of-Flight Mass Spectrometry
Fc	Ferrocene
FT-IR	Fourier Transform Infrared
FVP	Flash Vacuum Pyrolysis
GC	Gas Chromatography
h	Hour
HR-MS	High Resolution Mass Spectrometry
I	Current intensity
ITC	Isothermal Titration Calorimetry
ICP-MS	Inductively Coupled Plasma Mass Spectrometry
iPrOH	2-propanol
KHMDS	Potassium bis(trimethyl)silylamide
L	Ligand
M	Metal
Me	Methyl
MeOH	Methanol
MeCN	Acetonitrile
Mes	2,4,6-trimethylphenyl
MIC	Mesoionic carbene
nBu	n-butyl
NaHMDS	Sodium bis(trimethyl)silylamide
NHC	N-heterocyclic carbene
NMR	Nuclear Magnetic Resonance

δ		Chemical shift
	br	broad
	d	doublet
	J	coupling constant
	m	multiplet
	ppm	parts per milion
	s	singlet
	t	triplet
OAc		Acetate
O*t*Bu		*tert*-butoxide
OTf		Triflate
PAH		Policyclic Aromatic Hydrocarbon
Ph		Phenyl
RT		Room Temperature
SCC		Supramolecular Coordination Complex
SCE		Saturated Calomel Electrode
SMe		Methyl Sulfide
t		Time
trz		triazolylidene
T		Temperature
*t*Bu		*tert*-butyl
TEP		Tolman Electronic Parameter
THF		Tetrahydrofuran
UV/Vis		Ultraviolet/Visible
V_{Bur}		Buried Volume

En aplicación de la normativa de estudios de doctorado sobre la elaboración de Tesis Doctorales según el programa RD 99/2011 por el que se establece que: "*La Tesis Doctoral escrita en una lengua diferente del valenciano o castellano, en el momento de ser depositada, debe contener un apartado suficientemente amplio en una de estas dos lenguas, y debe formar parte de la encuadernación de la tesis*". El siguiente capítulo en castellano contiene un resumen y conclusiones sobre el trabajo recogido en la presente Tesis Doctoral.

Presentación de la memoria

La presente Tesis Doctoral describe la síntesis de metalo-estructuras poliaromáticas basadas en carbenos poli-N-heterocíclicos (NHCs). La tesis se organiza en cinco capítulos, que comprenden una introducción (Capítulo 1), resultados y discusión (Capítulos 2-4), y una sección experimental (Capítulo 5).

El *Capítulo 1* es una introducción que incluye conceptos relevantes para la tesis, tales como el autoensamblaje o carbenos N-heterocíclicos. También se incluye una sección que detalla el trabajo previamente desarrollado por el grupo. La revisión se organiza secuencialmente, siguiendo el orden en que se discuten los temas en los capítulos siguientes, y finaliza con los principales objetivos establecidos para el proyecto.
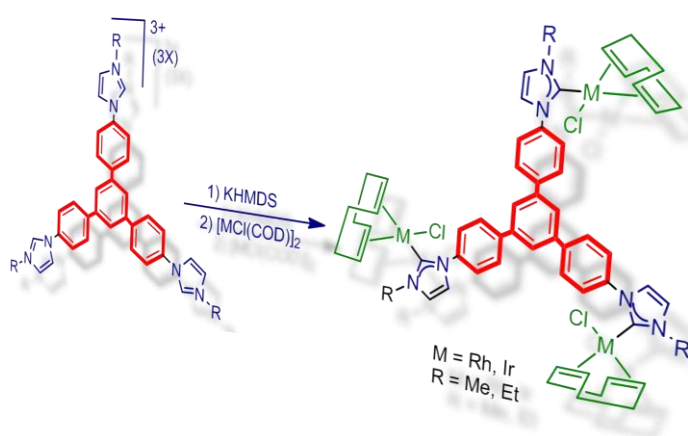
Figura 1. Imagen gráfica representativa del Capítulo 2

El ***Capítulo 2*** se dedica a la síntesis y caracterización de sales de tris-imidazolio y sales de tris-triazolio, basadas en un núcleo de 1,3,5-trifenilbenceno. Estas sales fueron empleadas como precursoras de carbenos N-heterocíclicos (NHCs) y carbenos mesoiónicos (MICs), y fueron coordinadas generando los correspondientes complejos metálicos. El capítulo se inicia con una breve introducción a los poli-NHCs, seguida de una discusión de los resultados. Se describe la síntesis de sales de tris-imidazolio y tris-triazolio. Los estudios de luminiscencia de compuestos de tris-imidazolio por emisión de fluorescencia muestran rendimientos cuánticos comparables a los del 1,3,5-tris (4-bromofenilbenceno). También se describe la síntesis de los correspondientes complejos trimetálicos de iridio[I], rodio[I] y níquel[II]. Los compuestos de rodio[I] e iridio[I] se sintetizaron por desprotonación de las sales de azolio KHMDS ó K_2CO_3 seguido de la adición de los correspondientes complejos [MCl(COD)$_2$]. Para la obtención de los derivados de níquel, se utilizó níqueloceno como precursor metálico. La caracterización espectroscópica confirma la simetría C_3 de todos los complejos. La preparación de los derivados de carbonilo de los complejos de Rh e Ir y la medida de las frecuencias de vibración CO, permitió hacer una evaluación de la capacidad δ-dadora de los correspondientes ligandos tri-NHC y tri-MIC.

Los complejos trimetálicos de rodio[I] se evaluaron como catalizadores para la adición de ácidos arilborónicos a cetonas α,β-insaturadas. La actividad catalítica es similar a la observada para los análogos monometálicos, sin que se observe una mejora para ligandos más donadores de electrones.
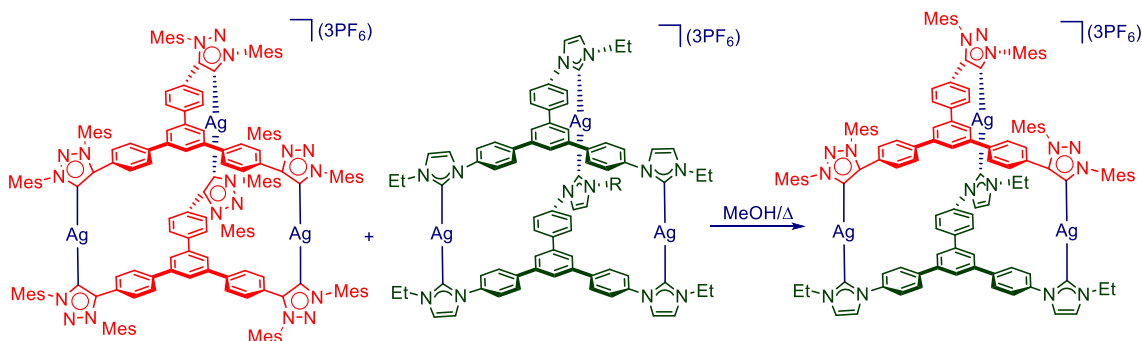
Figura 2. Imagen gráfica representativa del Capítulo 3

El ***Capítulo 3*** describe la síntesis de estructuras auto-ensambladas (*self-assembly structures*) basadas en ligandos carbeno NHC y MIC. En las primeras páginas se

muestra la síntesis de sistemas autoensamblados descritos en la literatura, y su utilización como estructuras supramoleculares. Se describe la síntesis de metalo-cajas de tris-NHC y tris-MIC con metales del grupo 11. La preparación de metalo-cajas de plata[I] se describe a partir de las sales precursoras de NHC y MIC descritas en el Capítulo 2. Seguidamente se describe la preparación de las metalo-cajas de oro[I] y cobre[I] por medio de transmetalación a partir de las metalo-cajas de plata[I]. En todos los casos se observa la formación de estructuras de geometría prismática trigonal, con una cavidad de tamaño nanométrico.

Por último, se describe la obtención de la primera metalo-caja heteroléptica, obtenida por la combinación de una sal precursora de NHC junto con, una sal precursora de MIC en presencia de Ag_2O. Además, esta caja de plata[I] heteroléptica también puede generarse usando otros procedimientos como es la mezcla de la metalo-caja homolépticas basada en ligandos NHC y MIC descritas anteriormente, produciéndose una reorganización molecular para la generación de metalo-caja heteroléptica. La estabilidad de estos complejos y las rutas sintéticas se analizaron y apoyaron adicionalmente mediante cálculos DFT.
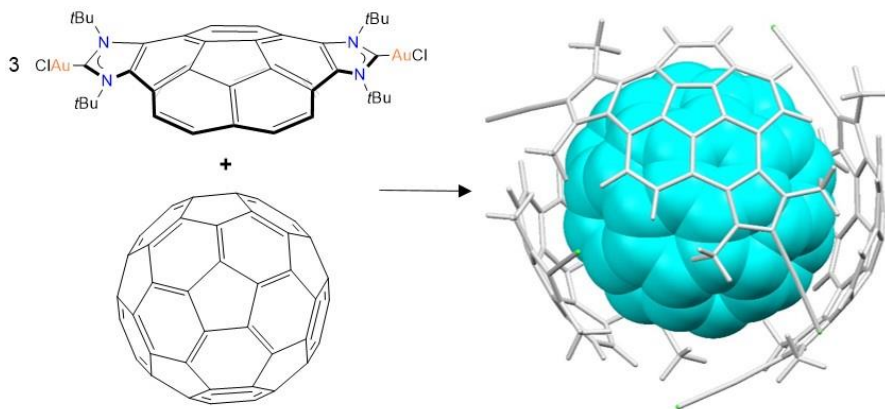
Figura 3. Imagen gráfica representativa del Capítulo 4.

El *Capítulo 4* se dedica a la síntesis de carbenos N-heterocíclicos a partir de unidades de basadas en coranuleno, la evaluación de su actividad catalítica y propiedades supramoleculares. El capítulo se inicia con una breve introducción sobre los NHC poliaromáticos planos *vs*. curvos. Se describe la síntesis de precursores de NHC de coranuleno a partir de tetrabromo-coranuleno, a través de una tetra-aminación de Buchwald-Hartwig seguida por la anulación con tri-butil ortoformiato. Dependiendo de

las condiciones de reacción empleadas, se pueden obtener dos sales precursoras de coranuleno con diferentes sustituyentes en el nitrógeno del anillo de imidazolio. Para la sal precursora que contiene el sustituyente más voluminoso (tert-butilo), se aisló y caracterizó su correspondiente carbeno libre. Por otro lado, se obtuvieron complejos dimetálicos de rodio[I] y oro[I] basados en dichos ligandos NHC previamente sintetizados. Además, se sintetizó el correspondiente derivado de di-rodio tetracarbonilo, lo que permitió el análisis y evaluación de las propiedades dadoras de los ligandos. Los valores de TEP indican un carácter menos dador a otros NHC poliaromáticos similares.

La actividad catalítica de los complejos de oro[I] se evaluó en la hidroaminación de alquinos y la ciclación de 2,5-dimetilfurano con alquinos terminales. En ambos casos, el rendimiento del catalizador fue sólo moderado.

Para el complejo oro[I] de coranuleno, se examinó la capacidad de reconocimiento de sistemas poliaromáticos fusionados, como el fulereno-C_{60} y el coroneno. Para ello se realizaron experimentos de valoración mediante RMN de protón y Calorimetría Isoterma de Titulación (ITC). Tras el análisis de los datos por ambas técnicas junto, con los cálculos teóricos realizados, se pudo concluir la formación de un sistema *host-guest* 3:1 una para el C_{60} y 1:1 para el caso del coroneno.

El *Capítulo 5* contiene la sección experimental, que recopila la caracterización completa de todos los compuestos discutidos en los capítulos anteriores, detallados con datos espectroscópicos (RMN de protón y carbono, análisis elemental, espectrometría de masas y espectroscopía infrarroja en los casos que requeridos) y el procedimiento experimental llevado a cabo en casa caso. En esta sección también están incluidos los datos de fluorescencia, tablas de cálculos teóricos, espectros de emisión y absorción, espectros de voltametría cíclica, experimentos de ITC y catálisis testadas. Por último, se detallan los datos de las estructuras de rayos X de monocristal obtenidas a lo largo de la tesis.

En resumen, en esta Tesis Doctoral se ha sintetizado una serie de ligandos politópicos basados en ligandos NHC y MIC mediante diferentes rutas sintéticas que dieron lugar a sistemas con arquitecturas muy sofisticadas. Se ha procedido a la formación de una gran variedad de complejos metálicos basados en dichas sales precursoras que permitieron la obtención de complejos mono-, di- y tri-metálicos homo y heterolépticos con diferentes geometrías. Se han analizado las propiedades luminiscentes de varias sales de

imidazolio, la actividad catalítica de algunos de los complejos metálicos obtenidos y se han llevado a cabo estudios de reconocimiento molecular *host-guest*.

Chapter 1

Introducción y Objetivos

1.1. Introducción

La presente Tesis Doctoral es el fruto de un trabajo de investigación centrado en la generación de nuevas entidades estructurales que puedan ser utilizadas para la formación de arquitecturas supramoleculares y el estudio de las interacciones entre ellas. Esta tarea se ha llevado a cabo combinando dos áreas diferentes de la química, como son la *química organometálica* y la *química supramolecular*. A lo largo de la tesis doctoral irán apareciendo una serie de conceptos básicos, que serán presentados y desarrollados en esta introducción, la cual servirá como preámbulo a otra introducción, más breve y específica, en cada uno de los siguientes capítulos.

1.1.1. Sistemas poliaromáticos funcionalizados con ligandos NHC

La química de los carbenos, y en particular de los carbenos N-heterocíclicos (NHC), ha sido estudiada desde hace décadas. Los primeros complejos metálicos con carbenos N-heterocíclicos fueron descritos en los años 60 por autores como Lappert[1], Öfele[2] y Wanzlick.[3] Posteriormente, en 1989 Bertrand y colaboradores consiguieron aislar el primer carbeno libre.[4] Sin embargo, no fue hasta 1991 cuando Arduengo y colaboradores[5] aislaron el primer carbeno N-heterocíclico.

La fortaleza del enlace metal-NHC y la versatilidad coordinativa de este tipo de ligandos son posiblemente, dos de las muchas propiedades que pueden haber ayudado al gran desarrollo de la química de los carbenos N-heterocíclicos.

La relativamente sencilla preparación de precursores de NHC (normalmente sales de azolio) ha permitido el acceso casi ilimitado a nuevas topologías organometálicas. Los imidazol-ilidenos (*NHC normales, abnormales o remotos*),[6] cuyos parámetros electrónicos y estéricos pueden ser modulados de forma controlada, han sido ampliamente estudiados e intensamente utilizados. Actualmente existe un amplio abanico de carbenos N-heterocíclicos, de entre los que merecen especial mención los 1,2,3-triazol-5-ilidenos (también conocidos como *NHC abnormales, o mesoionicos*), que fueron descritos más recientemente, y cuya capacidad electron-dadora es ligeramente superior a la de los *NHC normales*.[6-7]

Entre los diferentes tipos de ligandos NHC, los poli-carbenos N-heterocíclicos han suscitado un gran interés, ya que permiten la preparación de compuestos organometálicos con una gran variedad de geometrías.[8] Esta versatilidad topológica

puede facilitar la síntesis controlada de complejos cuyos ligandos puedan actuar como bis-quelato, pinza, tripodal o puente.

Los ligandos de tipo tris- y tetra-NHC son menos abundantes que los di-NHC, probablemente debido a que las sales de imidazolio tris- y tetra-catiónicas resultantes son a menudo difíciles de purificar dada su baja solubilidad en la mayoría de los disolventes orgánicos.[8b, 9]
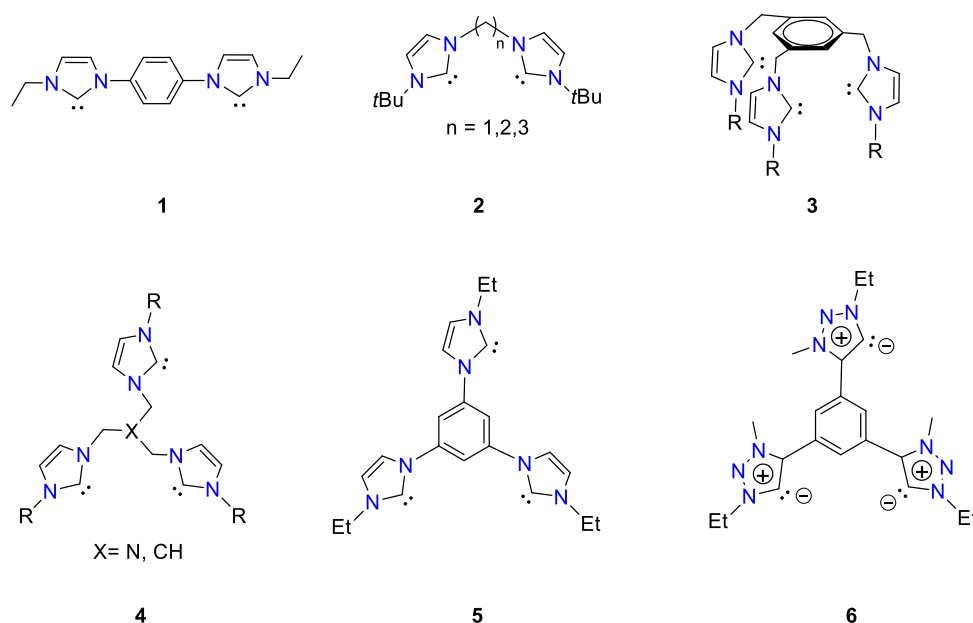
Figura 1.1. Ejemplos de ligandos carbenos poli-N-heterocíclicos

La síntesis de ligandos poli-NHC permite la obtención de complejos que pueden ser homo- o hetero-polimetálicos.[8a, 9b, d] La preparación de estos complejos polimetálicos se ha convertido en un foco de interés en el campo de la catálisis homogénea, ya que se ha comprobado que pueden presentar mayores actividades catalíticas que sus homólogos monometálicos (debido al fenómeno conocido como cooperatividad catalítica)[10] y porque además, en determinadas ocasiones pueden ser utilizados en catálisis tándem.[11]
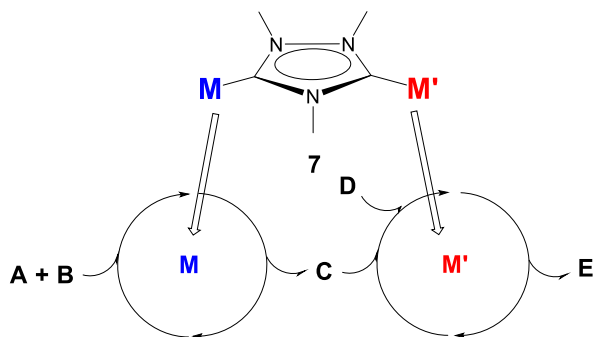
Esquema 1.1. Ejemplo de complejo hetero-bimetálico en catálisis tándem (esquema reproducido de la referencia [11c])

Gracias a su versatilidad coordinativa, recientemente los ligandos poli-NHC se han utilizado para el desarrollo de complejos de coordinación supramoleculares bi- y tri-dimensionales[9c, 12] (ver Sección 1.1.2). A modo de ejemplo, en el Esquema 1.2, se muestra cómo el ligando tris-NHC descrito por Hahn y colaboradores,[9c] y obtenido a partir de su sal precursora fenil-tris-imidazolio, puede servir para la generación de cajas moleculares como el complejo de Pd (**9**), o actuar como puente-quelato para generar el complejos dimetálicos de Rh o Ir (**10**).
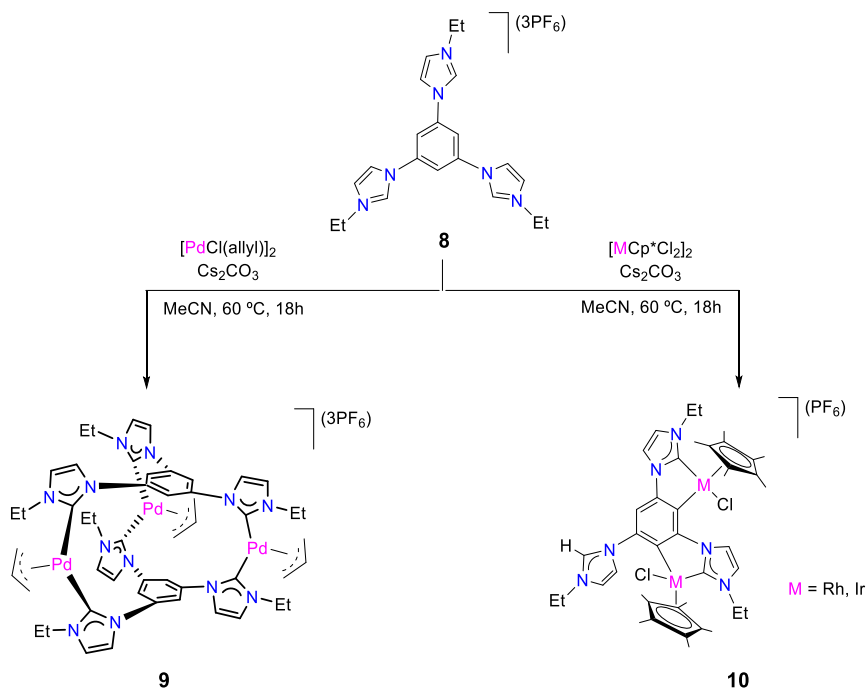
Esquema 1.2. Dos formas de coordinación de un tri-NHC[9c]

Este ejemplo ilustra cómo un mismo ligando poli-NHC se puede utilizar para la obtención de compuestos con estructuras muy variadas,[9d, 13] dependiendo del método de síntesis utilizado.

1.1.2. Reacciones de autoensamblaje (*Self-Assembly*)

El autoensamblaje es un proceso por el que un sistema desordenado sufre una organización espontánea y reversible de las unidades moleculares que lo componen, llegando a formar estructuras ordenadas por interacciones de naturaleza no covalente.
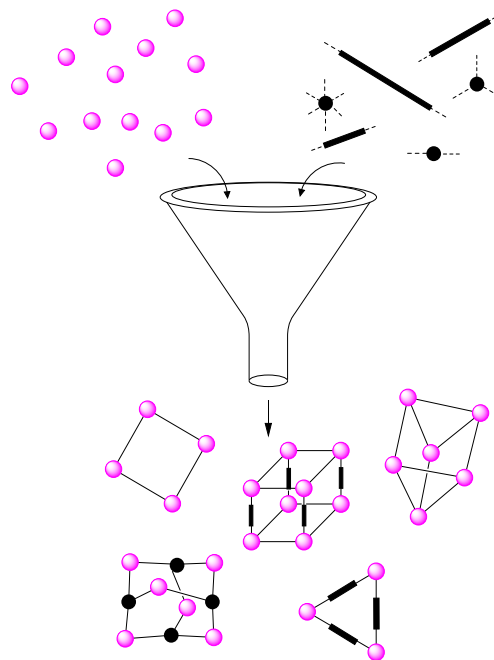
Esquema 1.3. Representación esquemática de la técnica de autoensamblaje[14]

El uso de metales de transición en procesos de autoensamblaje facilita la formación de sistemas con formas y tamaños bien definidos, tales como hélices o cajas. Los primeros trabajos en este campo de investigación se centraron en el desarrollo de diferentes métodos de autoensamblaje, gracias a los cuales se pudieron sintetizar diferentes metalociclos y metalocajas[14] (Esquema 1.3).

La combinación de un precursor metálico con un ligando bi- o tri-dentado con la geometría adecuada, puede formar espontáneamente enlaces metal-ligando que den lugar a productos termodinámicamente favorables.[15] Debido a que la formación de los enlaces metal-ligando es el motor de la obtención de la estructura supramolecular, a este tipo de proceso se le conoce como proceso de autoensambleje coordinativo (*coordination-driven self-assembly*). Los productos resultantes suelen mostrar estructuras altamente simétricas con cavidades bien definidas.[16] La presencia de la cavidad determina una reactividad única, que puede tener aplicaciones en catálisis,[17] reconocimiento molecular[18] y en la estabilización de especies altamente reactivas.[19]

Para la obtención de sistemas metálicos supramoleculares, es muy importante seleccionar adecuadamente la forma y tamaño de los ligandos (*spacers*), así como la naturaleza del fragmento metálico (*nodes*), que normalmente va a ocupar los vértices de la estructura poligonal o poliédrica. La selección del metal es muy importante, porque su capacidad coordinativa y los ángulos de coordinación van a determinar la forma del producto resultante. La mayoría de los esfuerzos invertidos en el diseño de arquitecturas metalo-supramolecules están basados en tratar de imitar el comportamiento de las enzimas. Por lo tanto, con la presencia de ligandos polidentados y la síntesis de sus correspondientes complejos metálicos, se persigue obtener cavidades que imiten el entorno en el que se encuentran los enzimas en la naturaleza.[20] Para la formación de dichas cavidades se necesita una matriz de varios metales, razón por la cual las moléculas metal-orgánicas con cavidades han sido definidas como 'complejos multimetálicos donde la coordinación del metal es necesaria para la formación de la cavidad'.[16b]

El diseño de estas estructuras metalo-supramoleculares permite crear arquitecturas bidimensionales (2D) como los metalo-cíclos, o tridimensionales (3D) como las metalo-cajas. En ambos casos las condiciones de reacción suelen ser suaves, obteniéndose altos rendimientos aislados. En el Esquema 1.4 se muestra un ejemplo de síntesis de una serie de metalo-cajas en las que, dependiendo del espaciador empleado, puede obtenerse una cavidad de mayor o menor tamaño. Dependiendo del tamaño de la caja, el volumen interior de la cavidad será mayor o menor, determinando de éste modo el número de moléculas neutras o cargadas que se pueden albergar en su interior.
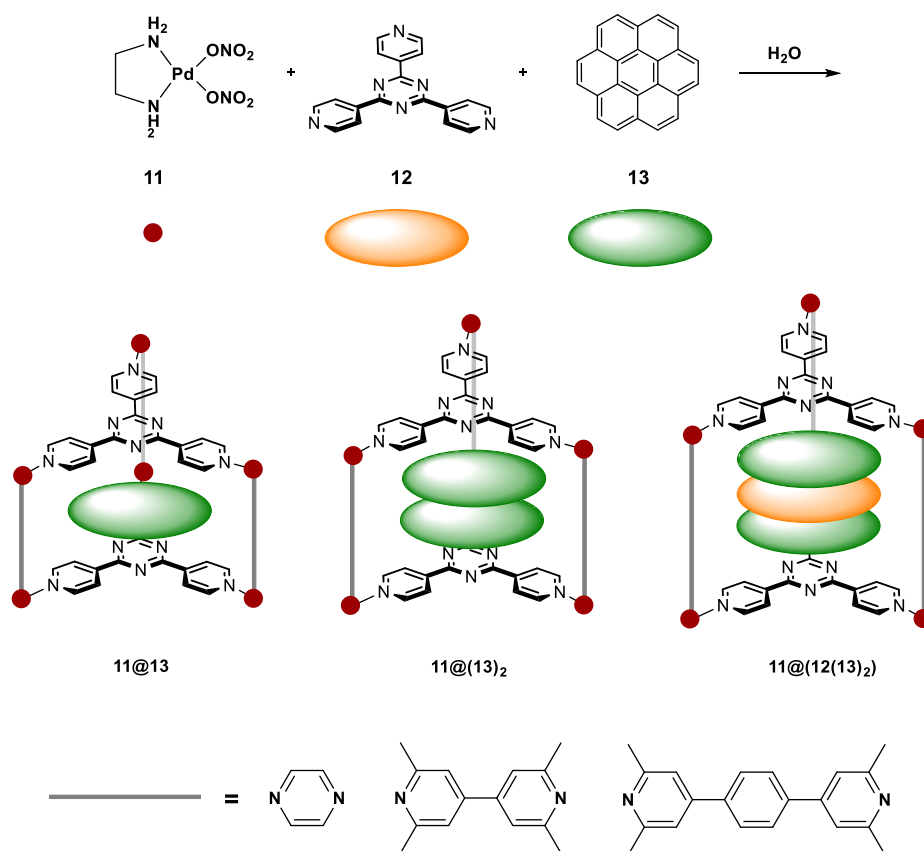
Esquema 1.4. Ejemplo de formación de un prima trigonal por autoensamblaje[15d]

A través de la metodología de autoensamblaje coordinativo, en nuestro grupo de investigación se ha sintetizado una serie de estructuras basadas en ligandos carbeno N-heterocíclicos que presentan cavidades en su estructura.[21]

1.1.3. Complejos de coordinación supramoleculares (*SCCs*)

Como se ha comentado anteriormente, la base para el diseño de sistemas metalo-supramoleculares es la disponibilidad de ligandos rígidos con dos o más puntos de anclaje, que en combinación con los metales adecuados, formen estructuras simétricas con formas y tamaños controlables. Los complejos de coordinación supramolecular (*Supramolecular Coordination Complexes*, SCCs)[15i, k] son estructuras moleculares basadas en sistemas poliaromáticos que pueden dar lugar a la formación de nanocavidades.[16a, 22]
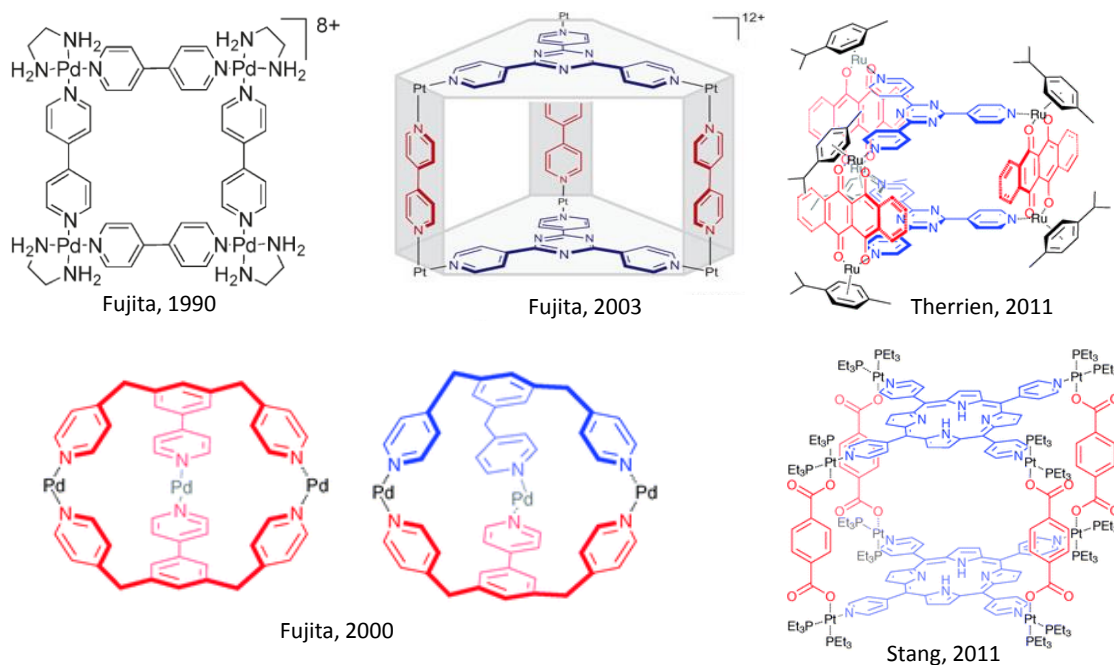
Figura 1.2. Ejemplos de complejos de coordinación supramolecular (*SSCs*)[15d, 23]

El resultado estructural de la síntesis metalo-supramolecular depende en gran medida de la naturaleza de los centros metálicos y los ligandos espaciadores (*linkers*) involucrados. Desde el punto de vista del diseño, dichos *linkers* son considerados como los elementos más importantes a tener en cuenta, ya que sus características topológicas, versatilidad y capacidad de ensamblaje, determinarán el tamaño, la geometría y la funcionalidad de las estructuras resultantes. Todo ello, combinado con la capacidad de coordinación de los metales de transición, da a este tipo de compuestos ventajas sobre los receptores orgánicos tradicionales,[15d, e, i, k, 24] que para lograr objetivos similares a menudo requieren procedimientos de síntesis muy laboriosos, altamente sofisticados y normalmente poco eficientes.

La mayoría de los sistemas metalo-supramoleculares descritos en la literatura, están basados en la utilización de ligandos polidentados de tipo Werner, por tanto están unidos a través de átomos de nitrógeno o de oxígeno. Algunos ejemplos representativos de este tipo de estructuras se muestran en la Figura 1.2.

Recientemente, el grupo de Hahn[13b, 25] y colaboradores han descrito un gran número de *SCCs* basados principalmente en carbenos poli-N-heterocíclicos (NHC).[8b, 26] Dichos *SCCs* presentan diversas geometrías, que incluyen cuadrados, rectángulos, triángulos[13b, 21a, 25a, 27] o cilindros[12b, 13a, 21b, c, 28] moleculares.

A pesar de la gran variedad de ejemplos recientes de estructuras bi- y tridimensionales basadas en el uso de ligandos poli-NHC, en la mayoría de los casos el volumen disponible de la cavidad es relativamente insuficiente para alojar determinadas moléculas orgánicas de interés. Este hecho podría ser el motivo por el cual existen muy pocos ejemplos de compuestos supramoleculares con ligandos NHC que hayan sido empleados como receptores para moléculas orgánicas. A consecuencia de lo anterior, a pesar del creciente número de conjuntos organometálicos *SCCs* conocidos, su aplicación al estudio de interacciones supramoleculares de tipo *host-guest* es poco frecuente, lo cual nos indujo a plantear parte de la investigación que se plantea en la presente memoria, abriendo así una nueva línea de investigación en nuestro grupo.

1.1.4. Antecedentes en nuestro grupo de investigación: Química Organometálica y Catálisis Homogénea (QOMCAT)

Gracias a los diferentes trabajos desarrollados en nuestro grupo de investigación, se ha podido demostrar cómo algunos catalizadores homogéneos basados en sistemas poliaromáticos, poseen propiedades claramente diferentes a las mostradas por sus análogos que no presentan sistemas poliaromáticos.[8a] La interpretación de estas diferencias se basa en la capacidad de los grupos poliaromáticos para producir interacciones no covalentes con moléculas aromáticas.[8a]

En la Figura 1.3 se muestran algunos de los complejos polimetálicos con ligandos poliaromáticos sintetizados durante los últimos años en nuestro grupo de investigación.[29] Estos complejos polimetálicos han sido probados en diferentes transformaciones catalíticas, en las que se ha comprobado cómo en muchos casos la actividad catalítica de los complejos polimetálicos es sensiblemente mayor que la mostrada por sus análogos monometálicos.
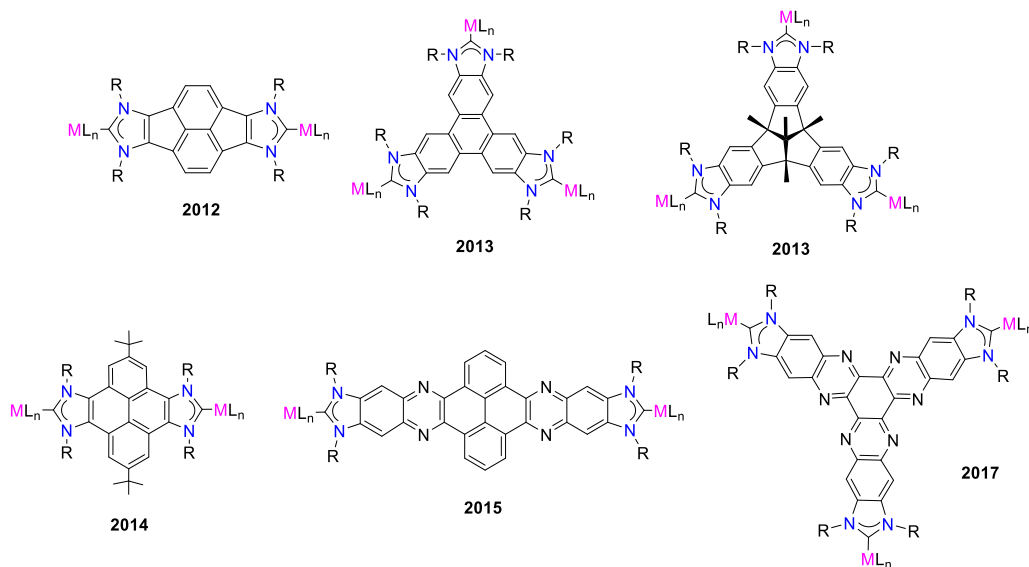
Figura 1.3. Ejemplos de complejos polimetálicos sintetizados en el grupo de investigación

Tal y como clasificaron Raynal y colaboradores en 2014,[17e, 30] las interacciones supramoleculares que pueden darse en catálisis homogénea son básicamente de tres tipos: interacciones ligando-ligando, interacciones aditivo-ligando e interacciones ligando-sustrato (Figura 1.4). Todas estas interacciones pueden afectar notablemente la eficacia de las reacciones catalíticas. Durante los últimos tres años, nuestro grupo de investigación ha dedicado un gran esfuerzo a estudiar de forma sistemática cómo estos tipos de interacción afectan al uso de catalizadores con ligandos NHC con sistemas poliaromáticos.
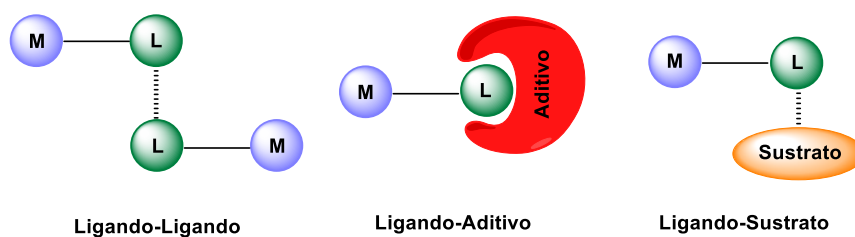
Figura 1.4. Interacciones supramoleculares en catalizadores homogéneos

Paralelamente a los trabajos dedicados a estudiar la influencia de las interacciones supramoleculares en catálisis homogénea, a partir de la técnica de autoensamblaje (*self-assembly*)[14, 15b, d, f] nuestro grupo ha logrado sintetizar una serie de complejos de coordinación supramoleculares basados en ligandos pireno-di-NHC. La Figura 1.5

muestra dos de estos compuestos, formados por cuatro centros metálicos de [Ni^{II}Cp] unidos por ligandos puentes pireno-di-NHC y bipiridina (**14**) o pirazina (**15**). Estos complejos son capaces de actuar como receptores para el reconocimiento de hidrocarburos policíclicos aromáticos (pireno, trifenileno, fenantreno y antraceno). Las contantes de asociación con estos sustratos fueron determinadas a partir de estudios de titración por espectroscopía de RMN de ^{1}H.
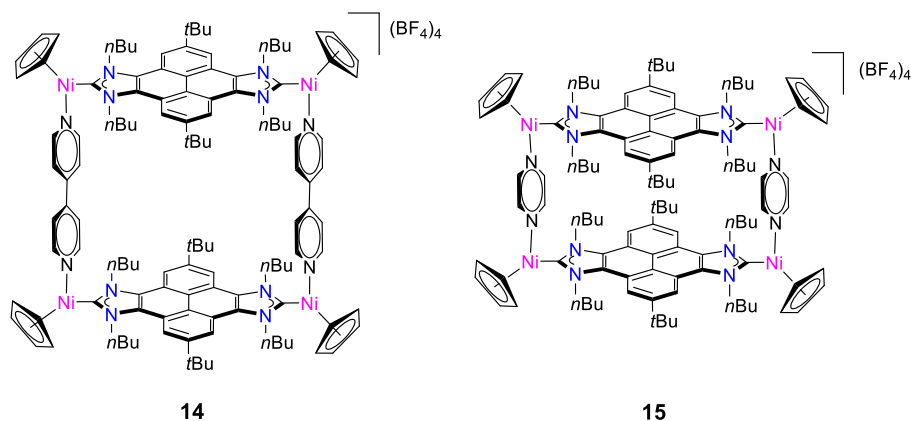
Figura 1.5. Ejemplos de receptores de hidrocarburos policíclicos aromáticos (PAHs)

Estos compuestos también se utilizaron como 'secuestradores' de hidrocarburos policíclicos aromáticos (*PAH-scavengers*). La adición de las cajas de níquel a disoluciones de heptano que contienen PAHs, produce la encapsulación del compuesto policíclico en el interior de la caja molecular, que al ser insoluble, puede separarse del medio por simple filtración.[21d] Teniendo en cuenta los efectos altamente perjudiciales de muchos de los PAHs en el medio ambiente,[31] este hallazgo puede tener implicaciones importantes para proporcionar formas efectivas de extracción de PAHs.

La introducción de centros metálicos en el diseño de receptores moleculares puede proporcionar algunos beneficios en comparación con el uso de los receptores de base orgánica más ampliamente utilizados, ya que la química de coordinación a menudo proporciona estructuras predecibles y bien definidas que facilitan que los receptores diseñados tengan una forma y tamaño idónea para el reconocimiento de moléculas de interés médico o biológico.

1.1.5. Hidrocarburos policíclicos aromáticos (*PAHs*)

Los hidrocarburos policíclicos aromáticos fusionados (*Policyclic Aromatic Hydrocarbons,* PAHs)[32] son compuestos orgánicos basados en uno o más anillos aromáticos fusionados entre sí. La gran mayoría de estos sistemas presentan estructuras planas, aunque éstas pueden verse modificadas con la introducción de anillos de cinco miembros en el esqueleto de la mismas, dando lugar a sistemas con geometrías curvas.

El trabajo realizado por nuestro grupo de investigación durante los últimos años ha estado centrado en la funcionalización de sistemas poliaromáticos planos con ligandos carbeno N-heterocíclico, lo que ha facilitado la incorporación de centros metálicos, y el estudio de sus aplicaciones.

Si bien hasta el momento, la mayor parte de la atención se había centrado en los PAHs basados sistemas π–conjugados planos, los PAHs curvos (no-planos) han resultado tener sorprendentes propiedades físicas, químicas y de ensamblaje.[33] Al mismo tiempo, permiten crear estructuras con geometrías imposibles de alcanzar con sistemas planos, como pueden ser, hélices, esferas, cilindros o cúpulas, entre otros.[34]

El Esquema 1.5 muestra las posibles subunidades de superficie curvada (coranuleno y sumaneno) que pueden derivar de un sistema esférico como es el fulereno C_{60}.
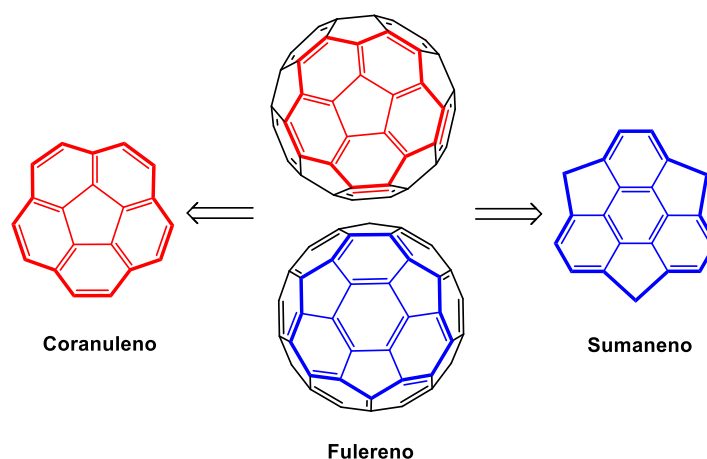
Esquema 1.5. Algunos ejemplos de hidrocarburos policíclicos aromáticos curvos

La estructura del coranuleno ($C_{20}H_{10}$), considerada como una tercera parte de un fulereno (C_{60}), es la unidad más pequeña basada en una sistema policíclico aromático fusionado que conserva su superficie curvada.

Hace aproximadamente medio siglo, Lawton and Barth[35] lograron publicar la primera síntesis del coranuleno, basada en 17 pasos de reacción, la cual tenía un rendimiento

global menor del 1%. En 1991 el grupo Scott[36] publicó una nueva ruta sintética en la que se mejoraba el rendimiento, y donde la obtención del coranuleno está basaba en la FVP (*Flash Vacuum Pyrolysis*). A lo largo de los años, se ha ido mejorando la ruta sintética para su obtención, hasta poder sintetizarse en escala de kilogramos. En el Esquema 1.6 se muestra una de las rutas sintéticas "*multi-kilogram scale*" descritas recientemente por el grupo del Prof. Jay S. Siegel.[37]
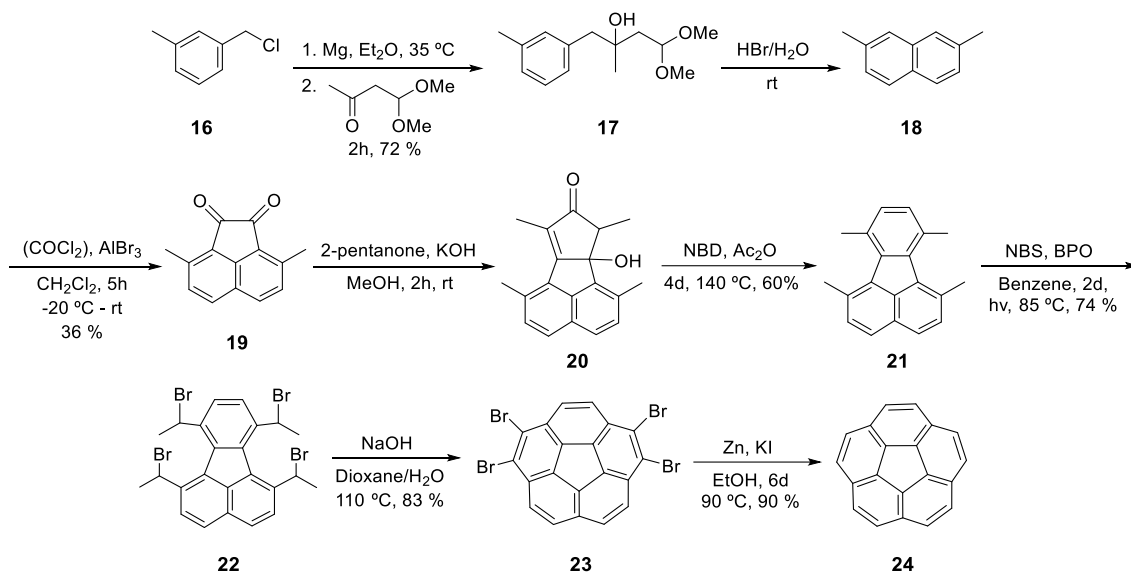
Esquema 1.6. Esquema de la "*multi-kilogram scale*" síntesis del coranuleno

En la bibliografía podemos encontrar una gran cantidad de trabajos basados en derivados del coranuleno,[38] que en muchos casos se utilizan como precursores para la síntesis de nuevos materiales con múltiples aplicaciones. Cristales líquidos, superficies grafíticas, ciclofanos, polímeros o incluso dendrímeros son algunos de los ejemplos de estos materiales.[39]

A pesar de la existencia de un elevado número de derivados orgánicos del coranuleno, el número de ejemplos funcionalizados con metales de transición es muy bajo,[34b, 40] lo que evidentemente justifica el escaso número de publicaciones que describen estudios de estos compuestos en campos como la catálisis, la química supramolecular o el reconocimiento molecular.
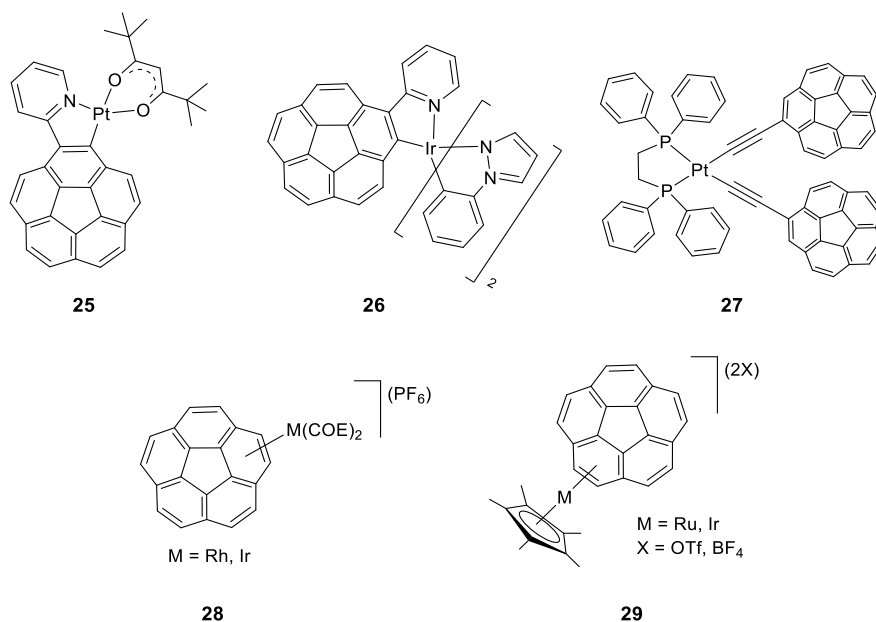
Figura 1.6. Algunos de los ejemplos de complejos basados en coranuleno

Actualmente no existen ejemplos de complejos metálicos con ligandos N-heterocíclico funcionalizados con coranuleno. La obtención de este tipo de ligandos podría abrir un amplio campo de posibilidades a nuevas aplicaciones, tanto en el campo de la catálisis como en el de la química supramolecular *host-guest*. Este es el motivo principal que nos llevó a desarrollar la investigación que se describe en el Chapter 4.

1.1.6. Química *Host-Guest* y receptores supramoleculares

La química supramolecular *host-guest* se centra en el estudio de las interacciones entre un receptor (*host*) y un huésped (*guest*). Por lo general, el *host* es una especie de mayor tamaño que el *guest* y presenta una cavidad en su estructura.

Existen numerosos ejemplos de *host*s. Entre ellos, cabe destacar los curcubiturilos, las ciclodextrinas o los calixarenos. Todos estos sistemas son capaces de modular su forma para crear una cavidad. El *guest* debe tener una forma complementaría al *host*, lo que permitirá la afinidad y selectividad entre ambos. Cuando ambas especies interaccionan entre sí se genera el denominado complejo *host-guest*.[41]

El objetivo final de la química *host-guest* es estudiar la fortaleza, naturaleza y selectividad de las interacciones no-covalentes entre un determinado *host* y un *guest*, para provocar que el reconocimiento molecular sea más efectivo y selectivo.

1.1.6.1. Receptores moleculares para la separación de fulerenos

Los fulerenos se pueden extraer fácilmente del hollín, pero encontrar una estrategia eficiente para obtenerlos de forma pura sigue siendo difícil, especialmente para derivados superiores a C_{70}.

Los primeros ejemplos descritos para la purificación de los fulerenos se basaron en la sublimación controlada del hollín de carbono, en la extracción con disolventes orgánicos, o en la purificación por cristalización. Actualmente, las técnicas cromatográficas que se usan para la purificación de fulerenos requieren enormes cantidades de disolvente y pueden provocar su descomposición. Por todo lo anterior, diseñar una metodología mejorada de purificación de fulereno es una meta muy perseguida.

Como alternativa a los métodos descritos anteriormente, actualmente se está prestando gran interés al uso de receptores moleculares para la separación selectiva de fulerenos mediante interacciones *host-guest*. Este método no requiere un equipo especializado y además se pueden llegar a diseñar sistemas reciclables.

Los arenos basados en ciclodextrinas,[42] calixarenos,[43] porfirinas,[44] o metaloporfirinas,[45] son algunos de los ejemplos de receptores de fulerenos más eficientes, especialmente cuando dos o más de estas unidades se asocian entre sí. Dichas asociaciones permiten a estos sistemas formar ensamblajes en forma de cajas moleculares,[46] capaces de impedir o permitir la entrada de moléculas según su tamaño, lo que les convierte en excelentes sistemas para la separación de fulerenos según el número de átomos de carbono que contengan.
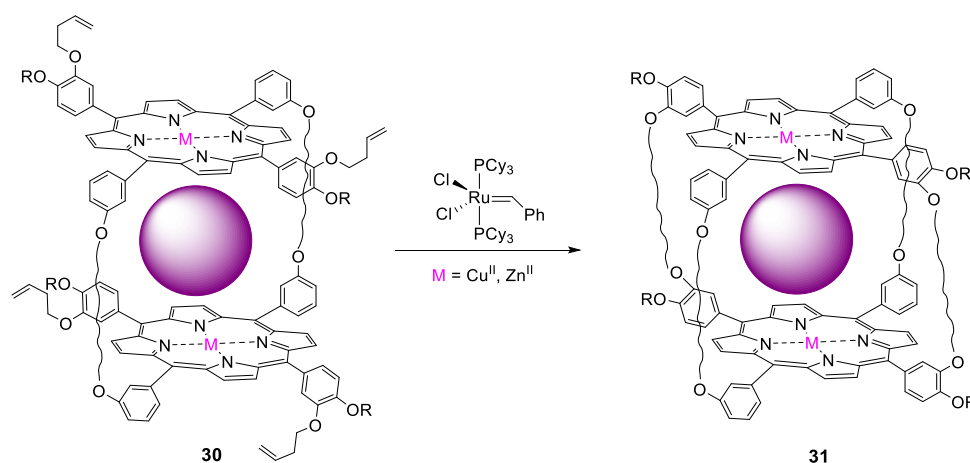
Figura 1.7. Ejemplo de caja molecular con fulereno C_{60}

Mediante el empleo de estas cajas moleculares, se ha demostrado que es posible una recuperación eficiente de los fulerenos encapsulados mediante diferentes estrategias que van desde tratamientos térmicos o ácidos, a reordenamientos conformacionales y estructurales, siendo éstos últimos los más prometedores ya que el *host* también puede ser parcialmente recuperado en este caso.

Por otro lado, a raíz del descubrimiento de los fulerenos[47] y de las redes poliaromáticas de superficie curvada, surgió un gran interés por el estudio de las posibles interacciones supramoleculares derivadas del apilamiento entre ambos sistemas.[48]

Los estudios más recientes basados en el reconocimiento molecular de fulerenos tienen en común la presencia de más de un sistema poliaromático curvado. Estos sistemas son capaces de "abrazar" al fulereno como si de una pinza se tratara, dando lugar a la formación de un complejo *host-guest*, creándose una interacción π-π entre el *host* (ligando pinza) y el *guest* (fulereno), generando situación de gran estabilidad termodinámica.

En el Capítulo 4 de esta tesis doctoral se detallará y demostrará como sistemas que contienen tres unidades de coranuleno, son capaces de reconocer fulereno C_{60} con una elevada constante de asociación.

1.2. Objetivos

En base a la amplia colección de sistemas mono- y polimetálicos recogidos en la literatura, pero sobre todo en aquellos ejemplos desarrollados en los últimos años por nuestro grupo de investigación (QOMCAT) y así como de su gran versatilidad mostrada en diversas aplicaciones (catálisis, reconocimiento molecular, propiedades fotoluminiscentes, reacciones de autoensambaje, etc.), el objetivo general de la presente Tesis Doctoral es el desarrollo de complejos de coordinación supramolecular y receptores moleculares bimetálicos basados ligandos poliaromáticos. Éste objetivo general puede dividirse en los siguientes objetivos más específicos:

- Síntesis de sales de poli-azolio a partir de polifenilenos o sistemas aromáticos fusionados de superficie curvada para la obtención de ligandos poli-NHCs.

- Coordinación de los poli-NHCs a diferentes fragmentos metálicos, estudio de sus propiedades electrónicas y evaluación de su actividad catalítica.

- Obtención de complejos de coordinación supramolecular (*SCCs*) por autoensamblaje a partir de sistemas poliaromáticos funcionalizados con poli-NHCs.

- Estudio de las interacciones supramoleculares tipo *host-guest* existentes entre sistemas basados en superficies curvadas.

1.3. Referencias

[1] a) D. J. Cardin, B. Cetinkaya and M. F. Lappert, *Chem. Rev.* **1972**, *72*, 545-574; b) D. J. Cardin, B. Cetinkaya, M. J. Doyle and M. F. Lappert, *Chem. Soc. Rev.* **1973**, *2*, 99-144; c) M. F. Lappert, *J. Organomet. Chem.* **1988**, *358*, 185-214; d) M. V. Baker, S. K. Brayshaw, B. W. Skelton, A. H. White and C. C. Williams, *J. Organomet. Chem.* **2005**, *690*, 2312-2322.

[2] K. Ofele, *J. Organomet. Chem.* **1968**, *12*, 42.

[3] H. W. Wanzlick and H. J. Schönherr, *Angew. Chem. Int. Ed.* **1968**, *7*, 141.

[4] D. Bourissou, O. Guerret, F. P. Gabbai and G. Bertrand, *Chem. Rev.* **2000**, *100*, 39.

[5] A. J. Arduengo, R. L. Harlow and M. Kline, *J. Am. Chem. Soc.* **1991**, *113*, 361-363.

[6] R. H. Crabtree, *Coord. Chem. Rev.* **2013**, *257*, 755-766.

[7] G. Guisado-Barrios, J. Bouffard, B. Donnadieu and G. Bertrand, *Angew. Chem. Int. Ed.* **2010**, *49*, 4759-4762.

[8] a) E. Peris, *Chem. Commun.* **2016**, *52*, 5777-5787; b) M. Poyatos, J. A. Mata and E. Peris, *Chem. Rev.* **2009**, *109*, 3677-3707.

[9] a) R. Maity, M. van der Meer and B. Sarkar, *Dalton Trans.* **2015**, *44*, 46-49; b) R. Maity, H. Koppetz, A. Hepp and F. E. Hahn, *J. Am. Chem. Soc.* **2013**, *135*, 4966-4969; c) R. Maity, A. Rit, C. Schulte to Brinke, C. G. Daniliuc and F. E. Hahn, *Chem. Commun.* **2013**, *49*, 1011-1013; d) R. Maity, C. Schulte to Brinke and F. E. Hahn, *Dalton Trans.* **2013**, *42*, 12857-12860.

[10] a) M. E. Broussard, B. Juma, S. G. Train, W. J. Peng, S. A. Laneman and G. G. Stanley, *Science* **1993**, *260*, 1784-1788; b) W. J. Peng, S. G. Train, D. K. Howell, F. R. Fronczek and G. G. Stanley, *Chem. Commun.* **1996**, 2607-2608.

[11] a) S. Sabater, J. A. Mata and E. Peris, *Chem. Eur. J.* **2012**, *18*, 6380-6385; b) J. A. Mata, F. E. Hahn and E. Peris, *Chem. Sci.* **2014**, *5*, 1723; c) S. Sabater, J. A. Mata and E. Peris, *Nat. Commun.* **2013**, *4*, 2553; d) S. Sabater, J. A. Mata and E. Peris, *Eur. J. Inorg. Chem.* **2013**, 4764-4769.

[12] a) A. Rit, T. Pape and F. E. Hahn, *Organometallics* **2011**, *30*, 6393-6401; b) A. Rit, T. Pape, A. Hepp and F. E. Hahn, *Organometallics* **2011**, *30*, 334-347.

[13] a) C. Radloff, H. Y. Gong, C. Schulte to Brinke, T. Pape, V. M. Lynch, J. L. Sessler and F. E. Hahn, *Chem. Eur. J.* **2010**, *16*, 13077-13081; b) M.

Schmidtendorf, T. Pape and F. E. Hahn, *Angew. Chem. Int. Ed.* **2012**, *51*, 2195-2198.

[14] B. J. Holliday and C. A. Mirkin, *Angew. Chem. Int. Ed.* **2001**, *40*, 2022-2043.

[15] a) E. C. Constable, *Coord. Chem. Rev.* **2008**, *252*, 842-855; b) M. Fujita, M. Tominaga, A. Hori and B. Therrien, *Acc. Chem. Res.* **2005**, *38*, 369-378; c) M. Fujita, *Chem. Soc. Rev.* **1998**, *27*, 417-425; d) R. Chakrabarty, P. S. Mukherjee and P. J. Stang, *Chem. Rev.* **2011**, *111*, 6810-6918; e) S. Leininger, B. Olenyuk and P. J. Stang, *Chem. Rev.* **2000**, *100*, 853-907; f) P. J. Stang and B. Olenyuk, *Acc. Chem. Res.* **1997**, *30*, 502-518; g) A. M. Castilla, W. J. Ramsay and J. R. Nitschke, *Acc. Chem. Res.* **2014**, *47*, 2063-2073; h) L. Chen, Q. Chen, M. Wu, F. Jiang and M. Hong, *Acc. Chem. Res.* **2015**, *48*, 201-210; i) T. R. Cook and P. J. Stang, *Chem. Rev.* **2015**, *115*, 7001-7045; j) X. Su and I. Aprahamian, *Chem. Soc. Rev.* **2014**, *43*, 1963-1981; k) T. R. Cook, Y.-R. Zheng and P. J. Stang, *Chem. Rev.* **2013**, *113*, 734-777; l) B. Linton and A. D. Hamilton, *Chem. Rev.* **1997**, *97*, 1669-1680.

[16] a) P. Ballester, M. Fujita and J. Rebek, Jr., *Chem. Soc. Rev.* **2015**, *44*, 392-393; b) P. D. Frischmann and M. J. MacLachlan, *Chem. Soc. Rev.* **2013**, *42*, 871-890.

[17] a) C. J. Brown, F. D. Toste, R. G. Bergman and K. N. Raymond, *Chem. Rev.* **2015**, *115*, 3012-3035; b) S. H. A. M. Leenders, R. Gramage-Doria, B. de Bruin and J. N. H. Reek, *Chem. Soc. Rev.* **2015**, *44*, 433-448; c) P. Dydio and J. N. H. Reek, *Chem. Sci.* **2014**, *5*, 2135-2145; d) T. S. Koblenz, J. Wassenaar and J. N. H. Reek, *Chem. Soc. Rev.* **2008**, *37*, 247-262; e) M. Raynal, P. Ballester, A. Vidal-Ferran and P. W. N. M. van Leeuwen, *Chem. Soc. Rev.* **2014**, *43*, 1660-1733.

[18] a) S. Dong, B. Zheng, F. Wang and F. Huang, *Acc. Chem. Res.* **2014**, *47*, 1982-1994; b) K. Ariga, H. Ito, J. P. Hill and H. Tsukube, *Chem. Soc. Rev.* **2012**, *41*, 5800-5835; c) B. Chen, S. Xiang and G. Qian, *Acc. Chem. Res.* **2010**, *43*, 1115-1124.

[19] A. Galan and P. Ballester, *Chem. Soc. Rev.* **2016**, *45*, 1720-1737.

[20] J.-N. Rebilly, B. Colasson, O. Bistri, D. Over and O. Reinaud, *Chem. Soc. Rev.* **2015**, *44*, 467-489.

[21] a) C. Mejuto, G. Guisado-Barrios, D. Gusev and E. Peris, *Chem. Commun.* **2015**, *51*, 13914-13917; b) N. Sinha, F. Roelfes, A. Hepp, C. Mejuto, E. Peris and F. E. Hahn, *Organometallics* **2014**, *33*, 6898-6904; c) C. Segarra, G. Guisado-Barrios,

F. E. Hahn and E. Peris, *Organometallics* **2014**, *33*, 5077-5080; d) V. Martínez-Agramunt, S. Ruiz-Botella and E. Peris, *Chem. Eur. J.* **2017**, *23*, 1-8.

[22] a) C. Garcia-Simon, R. Gramage-Doria, S. Raoufmoghaddam, T. Parella, M. Costas, X. Ribas and J. N. H. Reek, *J. Am. Chem. Soc.* **2015**, *137*, 2680-2687; b) F. Hof, S. L. Craig, C. Nuckolls and J. Rebek, *Angew. Chem. Int. Ed.* **2002**, *41*, 1488-1508.

[23] a) M. Fujita, J. Yazaki and K. Ogura, *J. Am. Chem. Soc.* **1990**, *112*, 5645-5647; b) N. P. E. Barry, O. Zava, P. J. Dyson and B. Therrien, *Chem. Eur. J.* **2011**, *17*, 9669-9677; c) K. Kumazawa, K. Biradha, T. Kusukawa, T. Okano and M. Fujita, *Angew. Chem. Int. Ed.* **2003**, *42*, 3909-3913.

[24] a) C. J. Jones, *Chem. Soc. Rev.* **1998**, *27*, 289-299; b) Y.-F. Han, H. Li and G.-X. Jin, *Chem. Commun.* **2010**, *46*, 6879-6890; c) S.-S. Li, B. H. Northrop, Q.-H. Yuan, L.-J. Wan and P. J. Stang, *Acc. Chem. Res.* **2009**, *42*, 249-259.

[25] a) F. M. Conrady, R. Fröhlich, C. Schulte to Brinke, T. Pape and F. E. Hahn, *J. Am. Chem. Soc.* **2011**, *133*, 11496-11499; b) M. Schmidtendorf, T. Pape and F. E. Hahn, *Dalton Trans.* **2013**, *42*, 16128-16141; c) M. Schmidtendorf, C. S. T. Brinke and F. E. Hahn, *J. Organomet. Chem.* **2014**, *751*, 620-627.

[26] J. A. Mata, M. Poyatos and E. Peris, *Coord. Chem. Rev.* **2007**, *251*, 841-859.

[27] a) F. E. Hahn, C. Radloff, T. Pape and A. Hepp, *Organometallics* **2008**, *27*, 6408-6410; b) C. Radloff, F. E. Hahn, T. Pape and R. Fröhlich, *Dalton Trans.* **2009**, 7215-7222; c) M. Viciano, M. Sanau and E. Peris, *Organometallics* **2007**, *26*, 6050-6054.

[28] a) F. E. Hahn, C. Radloff, T. Pape and A. Hepp, *Chem. Eur. J.* **2008**, *14*, 10900-10904; b) A. Rit, T. Pape and F. E. Hahn, *J. Am. Chem. Soc.* **2010**, *132*, 4572-4573; c) D. H. Wang, B. G. Zhang, C. He, P. Y. Wu and C. Y. Duan, *Chem. Commun.* **2010**, *46*, 4728-4730.

[29] a) A. Prades, E. Peris and M. Alcarazo, *Organometallics* **2012**, *31*, 4623-4626; b) S. Ibanez-Maella, M. Poyatos and E. Peris, *Chem. Commun.* **2017**; c) S. Gonell, M. Poyatos and E. Peris, *Angew. Chem. Int. Ed.* **2013**, *52*, 7009-7013; d) C. Segarra, J. Linke, E. Mas-Marza, D. Kuck and E. Peris, *Chem. Commun.* **2013**, *49*, 10572-10574; e) S. Gonell, M. Poyatos and E. Peris, *Chem. Eur. J.* **2014**, *20*, 9716-9724; f) H. Valdes, M. Poyatos and E. Peris, *Organometallics* **2015**, *34*, 1725-1729.

[30] M. Raynal, P. Ballester, A. Vidal-Ferran and P. W. N. M. van Leeuwen, *Chem. Soc. Rev.* **2014**, *43*, 1734-1787.

[31] a) I. J. Keyte, R. M. Harrison and G. Lammel, *Chem. Soc. Rev.* **2013**, *42*, 9333-9391; b) A. K. Haritash and C. P. Kaushik, *J. Hazard. Mater.* **2009**, *169*, 1-15; c) C. L. Lemieux, A. B. Lambert, S. Lundstedt, M. Tysklind and P. A. White, *Environ. Toxicol. Chem.* **2008**, *27*, 978-990; d) K. Srogi, *Environ. Chem. Lett.* **2007**, *5*, 169-195.

[32] a) L. Zhang, Y. Cao, N. S. Colella, Y. Liang, J. L. Bredas, K. N. Houk and A. L. Briseno, *Acc. Chem. Res.* **2015**, *48*, 500-509; b) L. T. Scott, *Chem. Soc. Rev.* **2015**, *44*, 6464-6471; c) P. G. Ghasemabadi, T. G. Yao and G. J. Bodwell, *Chem. Soc. Rev.* **2015**, *44*, 6494-6518.

[33] N. Martin and L. T. Scott, *Chem. Soc. Rev.* **2015**, *44*, 6397-6400.

[34] a) P. W. Rabideau and A. Sygula, *Acc. Chem. Res.* **1996**, *29*, 235-242; b) Y.-T. Wu and J. S. Siegel, *Chem. Rev.* **2006**, *106*, 4843-4867; c) V. M. Tsefrikas and L. T. Scott, *Chem. Rev.* **2006**, *106*, 4868-4884; d) T. Higashino, J. M. Lim, T. Miura, S. Saito, J.-Y. Shin, D. Kim and A. Osuka, *Angew. Chem. Int. Ed.* **2010**, *49*, 4950-4954; e) T. Amaya and T. Hirao, *Chem. Commun.* **2011**, *47*, 10524-10535; f) M. Stepien, N. Sprutta and L. Latos-Grazynski, *Angew. Chem. Int. Ed.* **2011**, *50*, 4288-4340; g) M. Stepien, B. Szyszko and L. Latos-Grazynski, *J. Am. Chem. Soc.* **2010**, *132*, 3140-3152; h) S. Higashibayashi and H. Sakurai, *Chem. Lett.* **2011**, *40*, 122-128; i) A. Sygula, *Eur. J. Org. Chem.* **2011**, 1611-1625; j) T. Higashino, B. S. Lee, J. M. Lim, D. Kim and A. Osuka, *Angew. Chem. Int. Ed.* **2012**, *51*, 13105-13108; k) Y. Shen and C.-F. Chen, *Chem. Rev.* **2012**, *112*, 1463-1535; l) H. Omachi, Y. Segawa and K. Itami, *Acc. Chem. Res.* **2012**, *45*, 1378-1389; m) E. Gonka, P. J. Chmielewski, T. Lis and M. Stepien, *J. Am. Chem. Soc.* **2014**, *136*, 16399-16410; n) K. Y. Cheung, X. Xu and Q. Miao, *J. Am. Chem. Soc.* **2015**, *137*, 3910-3914; o) T. Amaya and T. Hirao, *Chemical Record* **2015**, *15*, 310-321.

[35] a) R. G. Lawton and W. E. Barth, *J. Am. Chem. Soc.* **1971**, *93*, 1730-1745; b) W. E. Barth and R. G. Lawton, *J. Am. Chem. Soc.* **1966**, *88*, 380-&.

[36] L. T. Scott, M. M. Hashemi, D. T. Meyer and H. B. Warren, *J. Am. Chem. Soc.* **1991**, *113*, 7082-7084.

[37] A. M. Butterfield, B. Gilomen and J. S. Siegel, *Org. Process Res. Dev.* **2012**, *16*, 664-676.

[38] a) Y. T. Wu, D. Bandera, R. Maag, A. Linden, K. K. Baldridge and J. S. Siegel, *J. Am. Chem. Soc.* **2008**, *130*, 10729-10739; b) T. J. Seiders, K. K. Baldridge, G. H. Grube and J. S. Siegel, *J. Am. Chem. Soc.* **2001**, *123*, 517-525; c) H. A. Reisch, M. S. Bratcher and L. T. Scott, *Org. Lett.* **2000**, *2*, 1427-1430; d) L. T. Scott, *Pure Appl. Chem.* **1996**, *68*, 291-300.

[39] D. Miyajima, K. Tashiro, F. Araoka, H. Takezoe, J. Kim, K. Kato, M. Takata and T. Aida, *J. Am. Chem. Soc.* **2009**, *131*, 44.

[40] a) B. Topolinski, B. M. Schmidt, S. Schwagerus, M. Kathan and D. Lentz, *Eur. J. Inorg. Chem.* **2014**, 5391-5405; b) J. W. Facendola, M. Seifrid, J. Siegel, P. I. Djurovich and M. E. Thompson, *Dalton Trans.* **2015**, *44*, 8456-8466; c) R. Maag, B. H. Northrop, A. Butterfield, A. Linden, O. Zerbe, Y. M. Lee, K.-W. Chi, P. J. Stang and J. S. Siegel, *Org. Biomol. Chem.* **2009**, *7*, 4881-4885; d) P. A. Vecchi, C. M. Alvarez, A. Ellern, R. J. Angelici, A. Sygula, R. Sygula and P. W. Rabideau, *Organometallics* **2005**, *24*, 4543-4552; e) T. J. Seiders, K. K. Baldridge, J. M. Oconnor and J. S. Siegel, *J. Am. Chem. Soc.* **1997**, *119*, 4781-4782; f) J. S. Siegel, K. K. Baldridge, A. Linden and R. Dorta, *J. Am. Chem. Soc.* **2006**, *128*, 10644-10645; g) T. J. Seiders, K. K. Baldridge, J. M. O'Connor and J. S. Siegel, *Chem. Commun.* **2004**, 950-951; h) C. M. Alvarez, L. A. Garcia-Escudero, R. Garcia-Rodriguez, J. M. Martin-Alvarez, D. Miguel and V. M. Rayon, *Dalton Trans.* **2014**, *43*, 15693-15696.

[41] a) H. Yang, B. Yuan, X. Zhang and O. A. Scherman, *Acc. Chem. Res.* **2014**, *47*, 2106-2115; b) P. J. Altmann and A. Pothig, *J. Am. Chem. Soc.* **2016**, *138*, 13171-13174.

[42] Y. Liu, H. Wang, P. Liang and H. Y. Zhang, *Angew. Chem. Int. Ed.* **2004**, *43*, 2690-2694.

[43] J. L. Atwood, G. A. Koutsantonis and C. L. Raston, *Nature* **1994**, *368*, 229-231.

[44] Y. B. Wang and Z. Y. Lin, *J. Am. Chem. Soc.* **2003**, *125*, 6072-6073.

[45] K. Tashiro, T. Aida, J. Y. Zheng, K. Kinbara, K. Saigo, S. Sakamoto and K. Yamaguchi, *J. Am. Chem. Soc.* **1999**, *121*, 9477-9478.

[46] D. Canevet, E. M. Perez and N. Martin, *Angew. Chem. Int. Ed.* **2011**, *50*, 9248-9259.

[47] H. W. Kroto, J. R. Heath, S. C. Obrien, R. F. Curl and R. E. Smalley, *Nature* **1985**, *318*, 162-163.

[48] A. Sygula, *Synlett* **2016**, *27*, 2070-2080.

Chapter 2

Metal Complexes with Tris-NHC and Tris-MIC Ligands Based on a 1,3,5-Triphenylbenzene Core

2.1 Introduction

Highly symmetrical poly-N-heterocyclic carbene ligands (poly-NHCs) and their corresponding poly-metallic complexes have been subject of increasing attention because they allow the preparation of a wide variety of multifunctional materials.[1] The design of architectures with geometrically isolated carbenes has allowed the development of NHC-based materials,[2] which are potentially useful for the preparation of organometallic polymers with sensing, magnetic, optical, and catalytic properties.[2] This special type of poly-carbenes may generate multimetallic catalysts that can find important applications, specially towards the design of sophisticated tandem catalytic processes.[3] Additionally, the catalytic activity of the multimetallic complexes can be compared with the activity of their related monometallic counter-parts, providing some insight into catalytic cooperativity between the metals comprised in the multimetallic systems.[4]
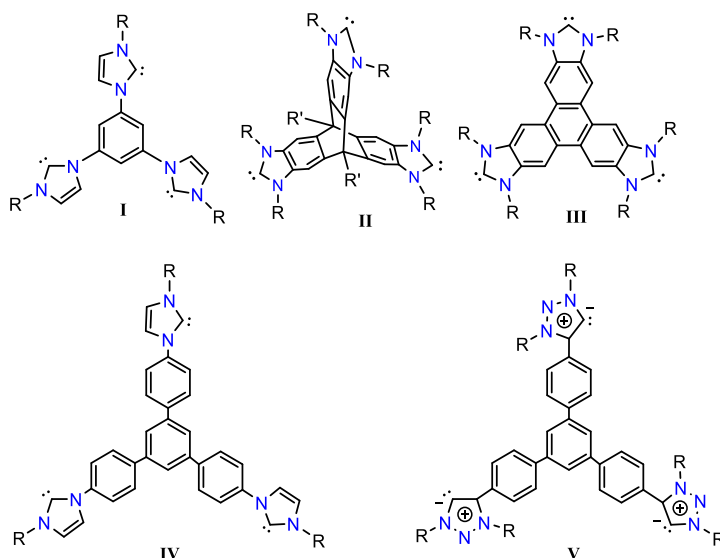
Chart 2.1. Representative examples of C_3-symmetry tris-carbene ligands

Chart 2.1 shows some known C_3-symmetry tris-carbenes (**I-III**),[5] together with those that will be subject of study in this work (**IV** and **V**). While **I**[6] and **II**[7] display electronically disconnected carbenes, **III**[4] holds three carbenes connected through a π-delocalized polyaromatic system. However, studies on the electronic communication between the metals bound to **III**, demonstrated that the communication seems to be disrupted,[8] probably due to the negligible d_M–p_L overlap as a consequence of the lack of π-backdonation. It is worth mentioning that the tris-carbene **III** allowed the preparation of trimetallic catalysts, whose activities were significantly improved

27

compared to their monometallic analogues in several benchmark homogeneously catalyzed reactions.[9]

Prompted by these previous findings, we decided to design a new type of C_3-symmetry ligands (**IV** and **V**), in which a 1,3,5-triphenylbenzene core connects all three carbene moieties.[10] It is worth mentioning, that **V** constitutes an important development on MIC chemistry, because MICs were only very recently unveiled,[11] and therefore, the development of MIC-based poly-metallic complexes is still in its infancy. Parallel to the preparation of trimetallic complexes with C_3-symmetry, we believe that both, **IV** and **V**, could potentially be used for the preparation of novel supramolecular assemblies, as will be reflected in the following Chapters.

In addition, polyphenylenes have been subject of increasing attention due to their luminescence properties.[12] In this context, symmetrically-trisubstituted benzenes derived from polyphenylenes are known to provide high quantum yield (Φ_f) values. [12b, 13] Herein, the study of the luminescence properties of new 1,3,5-triphenylbenzene based NHC ligands (**IV**) will be presented and discussed in the next section. Finally, this Chapter will describe the coordination studies of **IV** and **V** to Rh[(I)], Ir[(I)] and Ni[(II)], together with some preliminary studies on their catalytic activities.

2.2 Results and discussion

2.2.1 Synthesis and characterization of C_3-symmetry tris-azolium salts

Chart 2.2 shows the tris-imidazolium and tris-triazolium salts that will be used as tris-NHC and tris-MIC precursors all along this Chapter. As a common feature, both salts contain a 1,3,5-triphenylbenzene core.

[H₃B^Me](CF₃SO₃)₃ (R = Me)
[H₃B^Et](X)₃   (R = Et, X = BF₄, Br, PF₆)

[H₃C^Mes](PF₆)₃

Mes = mesityl
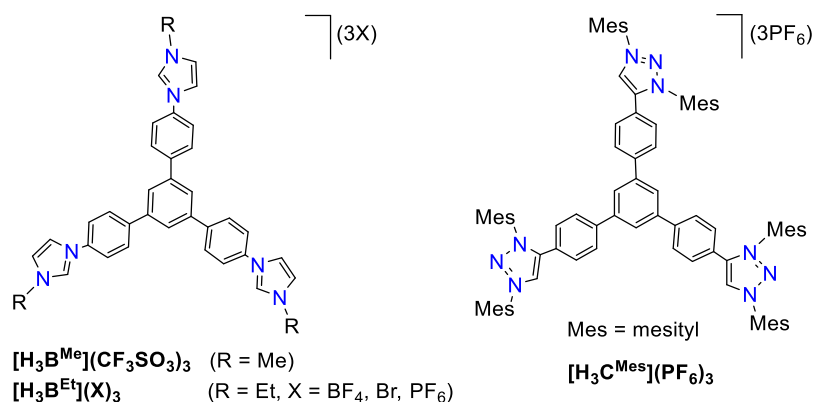
Chart 2.2. Tris-azolium salts

2.2.1.1 *C₃*-symmetry tris-imidazolium salts. Synthesis and characterization

The tris-imidazolium salts were obtained by using the Ullmann C-C coupling reaction according to the synthetic procedure depicted in Scheme 2.1. This methodology has been described by Hahn and co-workers for the preparation of related 1,3,5-phenylene-tris-imidazolium salts.[6, 14]

The reaction of 1,3,5-tris(4-bromophenylbenzene) with imidazole in the presence of $CuSO_4$ and K_2CO_3, afforded the corresponding 1,3,5-tris(4-bromophenylbenzene) compound, in 65% yield. Subsequent quaternization of the nitrogen atoms at the tris-imidazole compound **A** using different alkylating agents (methyl triflate, triethyloxonium tetrafluoroborate or bromoethane), yielded the corresponding salts.
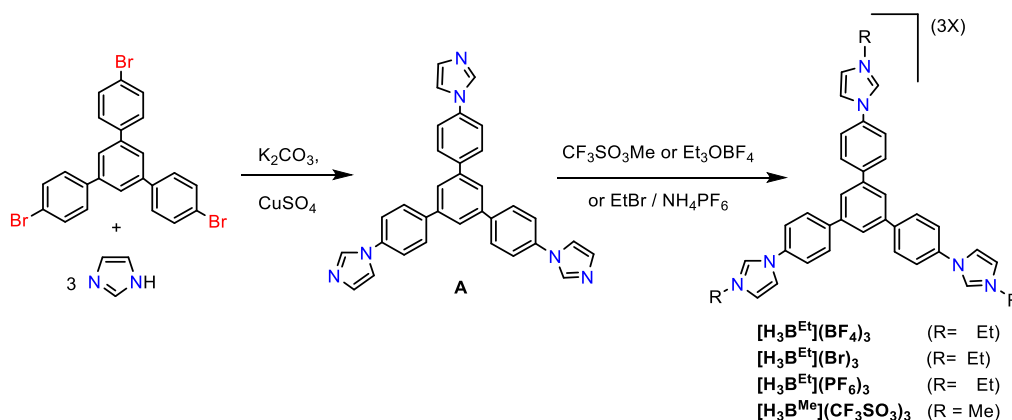
Scheme 2.1. Synthesis of tris-imidazolium salts

Compounds **A**, **[H₃B^Me](CF₃SO₃)₃** and **[H₃B^Et](X)₃** were characterized by means of NMR spectroscopy, mass spectrometry and elemental analysis. A common feature of their NMR spectra is that they all are consistent with their predicted *C₃*-symmetry. As an illustrative example, the ¹H NMR spectrum of **[H₃B^Me](CF₃SO₃)₃** is described below. For comparative purposes, the corresponding mono-imidazolium salt derivative **[HD^Et](BF₄)**, had also been synthesized. All details regarding the synthesis and spectroscopic features of compounds **A**, **[H₃B^Et](BF₄)₃**, **[H₃B^Et](Br)₃**, **[H₃B^Et](PF₆)₃** and **[HD^Et](BF₄)** can be found in the Experimental Section (Chapter 5).

^1H NMR spectrum of [H₃B^Me](CF₃SO₃)₃

Figure 2.1 shows ^1H NMR spectrum of **[H₃B^Me](CF₃SO₃)₃**. The number of signals and their integration are consistent with the C_3-symmetry of the molecule. The signal due to the acidic protons from the NC*H*N group (**a**) is displayed as a singlet at 9.52 ppm. The signals corresponding to the protons of 1,3,5-triphenylbenzene core (**d**, **e** and **f**) along with the protons of the imidazole ring (**b**) are displayed between 8.12-7.81 ppm. Finally, the signal due to the protons of the three methyl groups appears at 4.08 ppm (**c**).
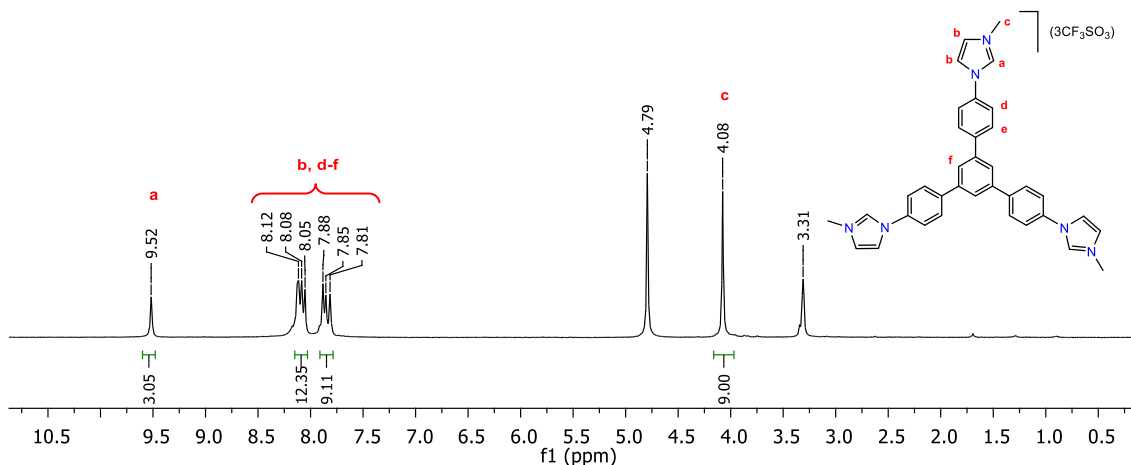
Figure 2.1. ^1H NMR spectrum of **[H₃B^Me](CF₃SO₃)₃** in CD₃OD

Molecular structure of [H₃B^Me](CF₃SO₃)₃

Crystals of **[H₃B^Me](CF₃SO₃)₃** suitable for X-Ray Diffraction analysis were obtained by slow diffusion of diethyl ether into a concentrated solution of the salt in MeOH.
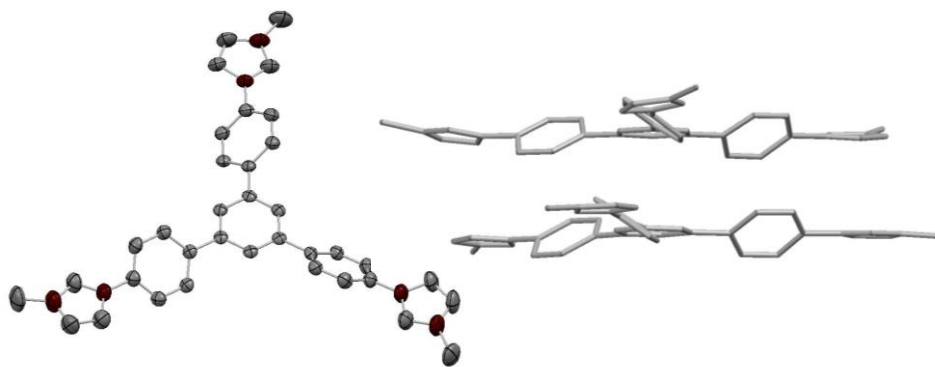
Figure 2.2. Molecular structure of **[H₃B^Me](CF₃SO₃)₃** (left). Hydrogen atoms and counterions (CF₃SO₃⁻) have been omitted for clarity. Ellipsoids at 50 % of probability. The figure on the right shows the π-stacking of two adjacent molecules

The molecular structure of **[H₃B^{Me}](CF₃SO₃)₃**, shown Figure 2.2, confirms the presence of the three imidazole rings connected to the tris-phenylbenzene core.

The crystal packing shows a one-dimensional π-stacking involving all four phenylene rings of each molecule separated by 3.605 Å. Although the molecule is not co-planar, the relative disposition of adjacent tris-imidazolium moieties shows that all aromatic rings are displayed in a quasi-parallel manner.

2.2.1.2 *C₃-symmetry tris-triazolium salt. Synthesis and characterization*

For comparative purposes we also aimed to prepare a 1,3,5-triphenylbenzene-based tris-triazolium salt, in order to gain further insights into the features of these systems.

The tris-triazolium salt **[H₃C^{Mes}](PF₆)₃** was obtained in 93% yield, by following the procedure depicted in Scheme 2.2. The reaction of 1,3,5-tris(4-ethynylphenylbenzene)[15] with 1,3-dimesityltriazene[11c] in the presence of KPF₆ and *^{t}*BuOCl at -78ºC, afforded the corresponding 1,3,5-triphenylbenzene-bridged tris-1,3-diaryl-1*H*-1,2,3-triazolium tris(hexafluorophosphate). This tris-triazolium salt was characterized by means of NMR and mass spectrometry and elemental analysis. The ¹H and ¹³C{¹H} NMR spectra of **[H₃C^{Mes}](PF₆)₃** confirmed the threefold symmetry of the molecule.
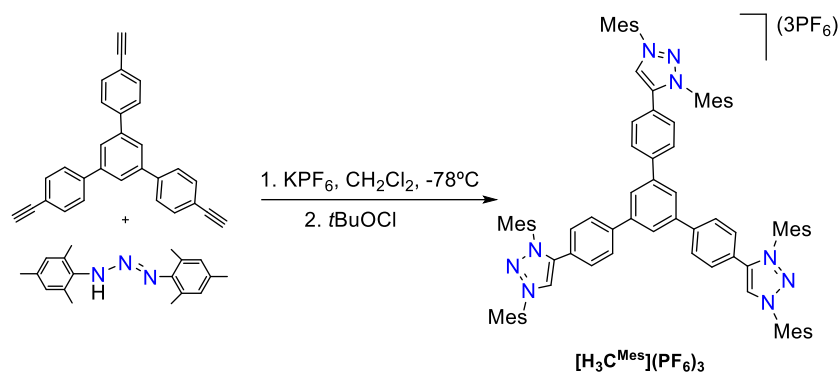
Scheme 2.2. Synthesis of tris-triazolium salts **[H₃C^{Mes}](PF₆)₃**

¹H NMR spectrum of [H₃C^{Mes}](PF₆)₃

Figure 2.3 shows the ¹H NMR spectrum of **[H₃C^{Mes}](PF₆)₃**. The number of signals and their integration are consistent, with the *C₃*-symmetry of the molecule, as previously observed for the imidazolium salts. The signal due to the acidic protons from the NC(*H*)N group (**a**) is displayed at 9.08 ppm. The signals assigned to the protons of the 1,3,5-triphenylbenzene core (**e**, **f** and **g**) are displayed between 7.78-7.58 ppm, and the signals for the aromatic protons of the mesityl groups (**d**) are shown at 7.13-7.15 ppm.

Finally, the signals due to the protons of the methyl groups at the mesityl groups appear between 2.43 and 2.06 ppm (**b** and **c**).
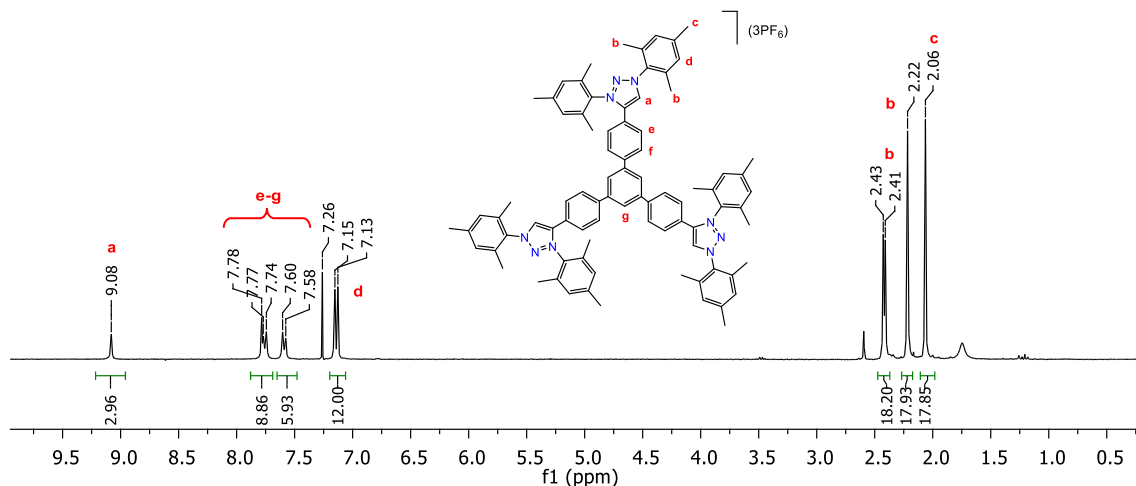
Figure 2.3. ^{1}H NMR spectrum of **[H₃C^Mes](PF₆)₃** in CDCl₃

2.2.2 Luminescence properties of the tris-imidazolium salts

Polyaromatic symmetrical cyclotrimers are often highly emissive.[12] In fact, 1,3,5-tris(4-bromophenylbenzene) possesses the highest quantum yields (Φ) in comparison with other benzenes bearing different number of phenyl substituents and located at different positions, and therefore constitutes an excellent scaffold for the design of luminiscent materials.[12a] We considered that it could be interesting to evaluate the photophysical changes produced by the incorporation of three imidazolium rings into the 1,3,5-triphenylbenzene core.
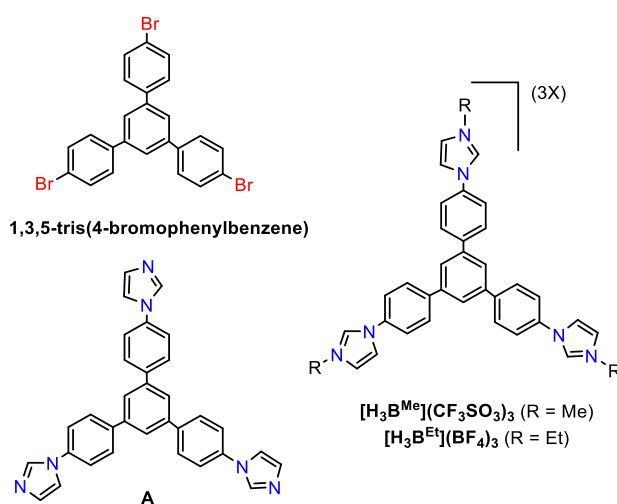
Chart 2.3. Polyaromatic systems under study

Table 2.1 summarizes the photochemical properties of the polyaromatic systems shown in Chart 2.3. The complete set of UV-Vis and fluorescence spectra of these compounds can be found in the Experimental Section (Chapter 5).

Table 2.1. Luminescence properties of **A**, **[H$_3$B^{Me}](CF$_3$SO$_3$)$_3$** and **[H$_3$B^{Et}](BF$_4$)$_3$**

Entry	Compound	λ_{abs} (nm) (log(ε))[a]	λ_{em} (nm)[b]	Φ_f[b]
1[c]	**1,3,5-tris(4-bromophenylbenzene)**	253 (4.71)	352	0.29
2	**A**	276 (4.83)	359	0.24
3	**[H$_3$B^{Me}](CF$_3$SO$_3$)$_3$**	268 (5.04)	351	0.16
4	**[H$_3$B^{Et}](BF$_4$)$_3$**	272 (5.00)	358	0.18

[a]Measurements performed in degassed MeCN under ambient conditions. Molar extinction coefficients (ε, in M^{-1}cm^{-1}) were determined from Beer's law plots. [b]Emission quantum yield was determined using as standard a 1N solution of quinine bisulfate in degassed H$_2$SO$_4$ (Φ_f = 0.55) exciting at 290 nm. [c]Values taken from reference [12a]

All three compounds **A**, **[H$_3$B^{Me}](CF$_3$SO$_3$)$_3$** and **[H$_3$B^{Et}](BF$_4$)$_3$** exhibit fluorescence emission in the 320-420 nm region, although their quantum yields are moderate (0.16-0.24). From the data given in Table 2.1, it can be observed that the cationic species **[H$_3$B^{Me}]$^{3+}$** and **[H$_3$B^{Et}]$^{3+}$** show similar quantum yields, and similar emission maximum wavelengths compared those of the neutral compound **A**. Furthermore, the absorption and emission properties are comparable to those provided by 1,3,5-tris(4-bromophenylbenzene) (entry 1). The fact that the photophysical properties of the tris-imidazolium molecules are maintained compared to those provided by triphenyl-benzene, may be considered as an advantage, if we take into account that the production of highly stable tri-cationic molecules such as **[H$_3$B^{Me}]$^{3+}$** and **[H$_3$B^{Et}]$^{3+}$** may give rise to molecules with tuneable physical properties such as solubility, or melting point, just by modifying the nature of the counter-anion and the N-substituents at the imidazole rings.

2.2.3 Synthesis and characterization of trimetallic complexes

A series of Rh$^{(I)}$, Ir$^{(I)}$ and Ni$^{(II)}$ complexes (see Chart 2.4) were prepared employing different metallation strategies depending on the metal precursors used. In the following

sections, the preparation and characterization of the complexes obtained will be explained in detail.
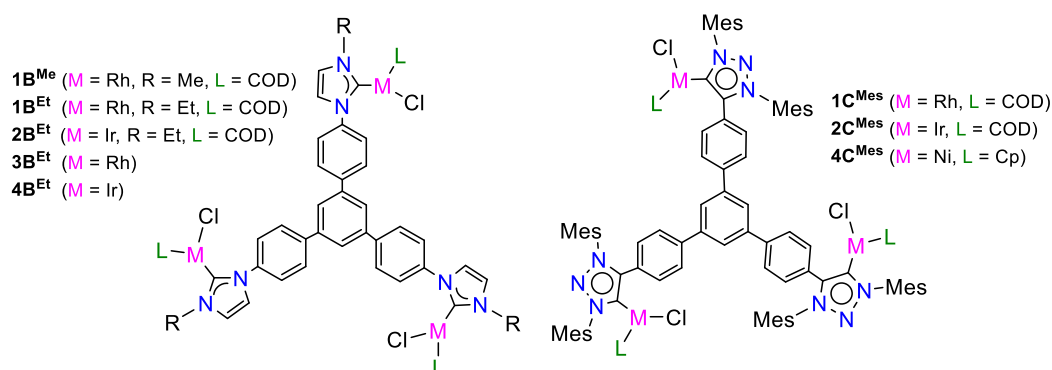
Chart 2.4. Tris-azolium complexes

2.2.3.1 Iridium(I) and rhodium(I) complexes

In this section, we will describe the coordination capabilities of the ligand starting from the tris-azolium salts previously described. By using $[MCl(COD)]_2$ (M = Rh or Ir) as metal precursors, we aimed to obtain the corresponding trimetallic complexes. In general, the reaction of the corresponding salt (tris-triazolium or tris-imidazolium) with $[MCl(COD)]_2$ (M = Rh or Ir) in presence of a base, allowed the preparation of all our complexes in moderate to good yields. Then, these complexes can be transformed into their corresponding carbonyl derivatives by bubbling CO through a solution of these metal complexes in methylene chloride.

Complexes with NHC ligands

The deprotonation of $[H_3B^{Et}](BF_4)_3$ (or $[H_3B^{Me}](CF_3SO_3)_3$) with potassium bis(trimethyl)silylamide (KHMDS) in THF, followed by the addition of $[MCl(COD)]_2$ (M = Rh, Ir), allowed the preparation of the corresponding tris-NHC complexes of rhodium ($1B^{Me}$ or $1B^{Et}$) and iridium ($2B^{Et}$) (Scheme 2.3).
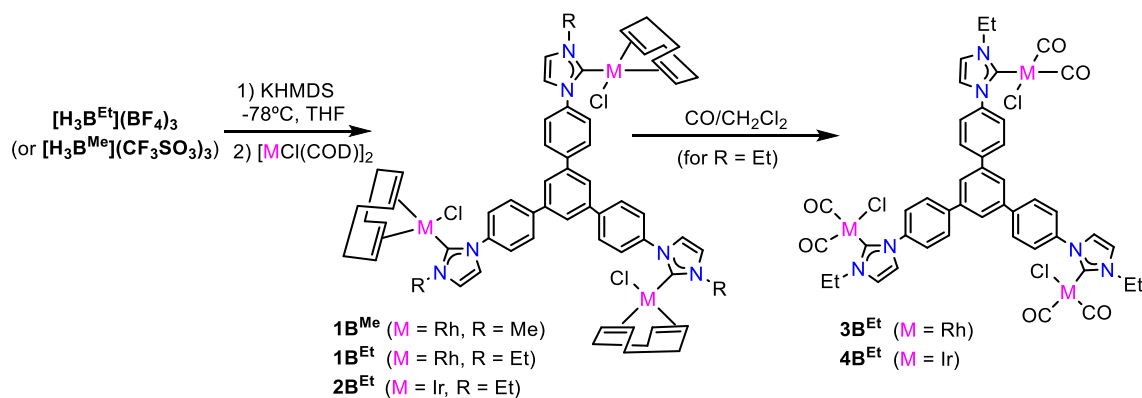
Scheme 2.3.Preparation of the metal complexes

Compounds **1B^{Et}** and **2B^{Et}** were converted into their corresponding carbonyl derivatives by bubbling CO through a solution of these complexes in methylene chloride at 0 ºC. Precipitation from a mixture CH$_2$Cl$_2$/hexane afforded the desired carbonylated compounds, **3B^{Et}** and **4B^{Et}**, in excellent yields (90% for **3B^{Et}** and 87% for **4B^{Et}**).

All new trimetallic complexes were characterized by NMR spectroscopy, mass spectrometry and elemental analysis. Due to the similarity between these compounds, only the ^{1}H NMR spectrum of **1B^{Et}** will be described below. All the details regarding the characterization of all other complexes, including the two monometallic Rh$^{(I)}$ and Ir$^{(I)}$ derivatives **1D^{Et}** and **2D^{Et}** respectively, can be found in the Experimental Section (Chapter 5).

As a common feature, the ^{1}H and ^{13}C{^{1}H} NMR spectra of these new complexes, are in agreement with their predicted threefold symmetry. For example, the ^{1}H NMR spectra of all complexes display two sharp signals assigned to the protons of the backbone of the three equivalent imidazolylidene rings. The ^{13}C{^{1}H} NMR spectra show single resonances due to the metallated carbene carbons, with the distinctive $^1J_{Rh-C}$ couplings for the case of the rhodium complexes (**1B^{Me}**: 183.8 ppm, $^1J_{Rh-C}$ = 51.2 Hz; **1B^{Et}**: 182.9 ppm, $^1J_{Rh-C}$ = 51.3 Hz; **2B^{Et}**: 180.1 ppm; **3B^{Et}**: 185.6 ppm, $^1J_{Rh-C}$ = 54.3 Hz; **4B^{Et}**: 181.1 ppm). As illustrative examples, the ^{1}H and ^{13}C{^{1}H} NMR spectra of **1B^{Et}** are described below.

^{1}H NMR spectrum of 1B^{Et}

Figure 2.4 shows the ^{1}H NMR spectrum of **1B^{Et}**. The absence of the signal due to the acidic protons of the NC*H*N groups is the first indication of the coordination of the

triphenylene-based tris-imidazolylidene ligand to RhCl(COD). The signals corresponding to the protons of the 1,3,5-triphenylbenzene scaffold (**d**, **e** and **f**) appear at 8.39, 7.96 and 7.25 ppm, respectively. The signals attributed to the protons of the C*H* groups of the imidazolylidenes are shown as two doublets at 7.94 and 7.06 ppm (**a**). The signals due to the protons of the tree ethyl groups appear at 4.78 and 1.66 ppm (**b** and **c,** respectively). The rest of the signals corresponding to the protons of the COD ligands are directly displayed on the spectrum.
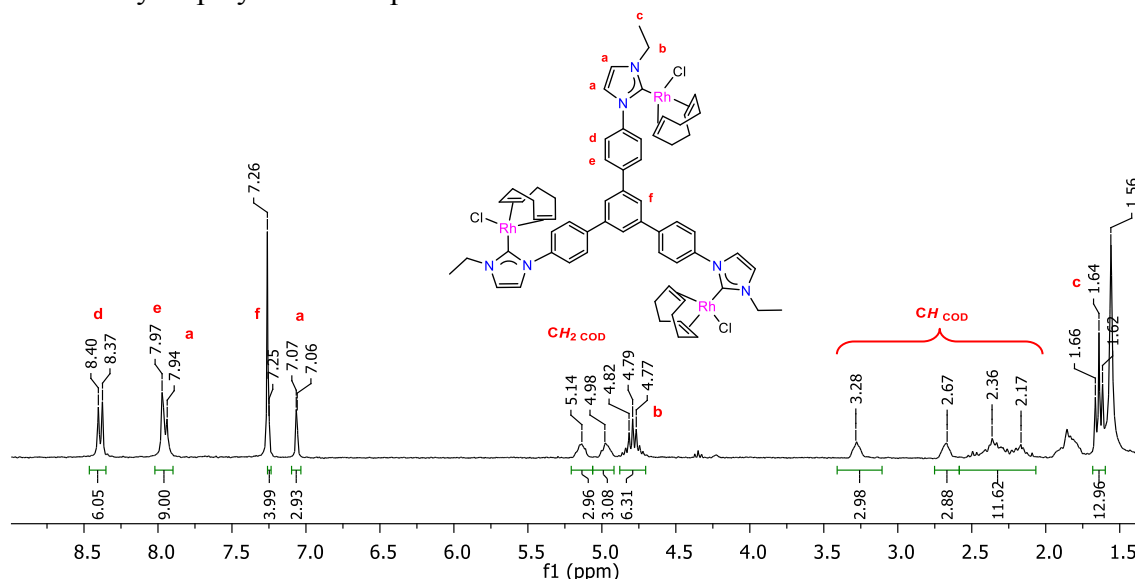
Figure 2.4. ^{1}H NMR spectrum of **1B^{Et}** in CDCl$_3$

^{13}C{^{1}H} NMR spectrum of 1B^{Et}

Figure 2.5 shows the ^{13}C{^{1}H} NMR spectrum of **1B^{Et}**. The most characteristic signal is that attributed to the metallated carbene-carbon (**1**), which is displayed as a doublet at 182.9 ppm ($^1J_{Rh-C}$ = 51.3 Hz).
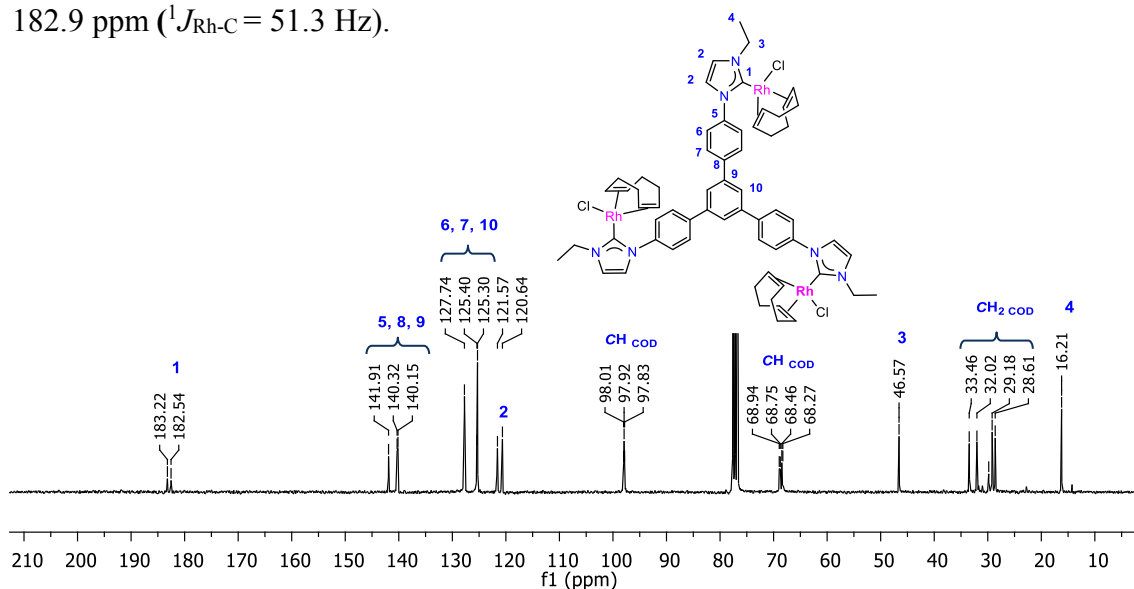
Figure 2.5. ^{13}C{^{1}H} NMR spectrum of **1B^{Et}** in CDCl$_3$

36

The signals corresponding to the carbons from the *C*H groups of the imidazolylidene rings (**2**) appear at 121.6 and 120.6 ppm. The signals attributed to the 1,3,5-triphenylbenzene core are displayed between 140.9-120.6 ppm. The signals due to the carbons of the three ethyl groups appear at 46.6 and 16.2 ppm (**3** and **4,** respectively). The rest of the signals corresponding to the carbon atoms of the COD ligands are conveniently displayed on the spectrum.

Although we tried our best to get single crystals suitable for the X-ray determination of the molecular structures of any of the trimetallic structures, all our attempts were in vain. In contrast, crystals suitable for X-ray analysis of the monometallic derivative **1D^{Et}** were obtained.

Molecular Structure of 1D^{Et}

The molecular diagram of the rhodium complex **1D^{Et}**, bearing a 1-phenyl-3-ethyl-imidazolylidene (Figure 2.6) is interesting because it represents the expected local molecular geometry of each of the metal fragments in the related trimetallic complex **1B^{Et}**. The details of the preparation of this complex can be found in the Experimental Section, Chapter 5.
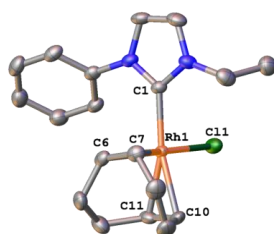
Figure 2.6. Molecular diagram of complex **1D^{Et}**. Ellipsoids at 50% probability level. Hydrogens omitted for clarity.

The molecular structure consists of a NHC ligand bound to a Rh(I) center, which is completing its coordination sphere with a chloride and a COD ligand. The Rh-C$_{carbene}$ bond distance is 2.033(2) Å (see Table 2.2). The high *trans* influence of the NHC ligand is illustrated by the longer distance between the rhodium atom and the olefin in the trans position related to the NHC ligand (compare 2.195 Å for the average Rh-C distances of the olefinic carbons *trans* to the NHC, with the 2.103 Å for the average distance between Rh and the carbons of the olefin trans to Cl).

Table 2.2. Selected bond lengths and angles of complex **1D**[Et]

Bond lengths (Å)		Bond angles (º)	
Rh(1)-C(1)	2.023(2)	C(1)-Rh(1)-Cl(1)	88.47(6)
Rh(1)-Cl(1)	2.382(6)	C(1)-Rh(1)-C(7)	89.42(8)
Rh(1)-C(7)	2.099(2)	C(1)-Rh(1)-C(10)	161.99(10)
Rh(1)-C(6)	2.105(2)		
Rh(1)-C(10)	2.208(2)		

Complexes with MIC ligands

The synthesis of the MIC-based complex **1C**[Mes], was carried out following the same methodology employed for the synthesis of **1B**[Et], which involves the deprotonation of the tris-triazolium salt **[H₃C**[Mes]**](PF₆)₃** with potassium bis(trimethyl)silylamide (KHMDS) in THF, followed by the addition of [RhCl(COD)]₂.

Scheme 2.4. Synthesis of **1C**[Mes]
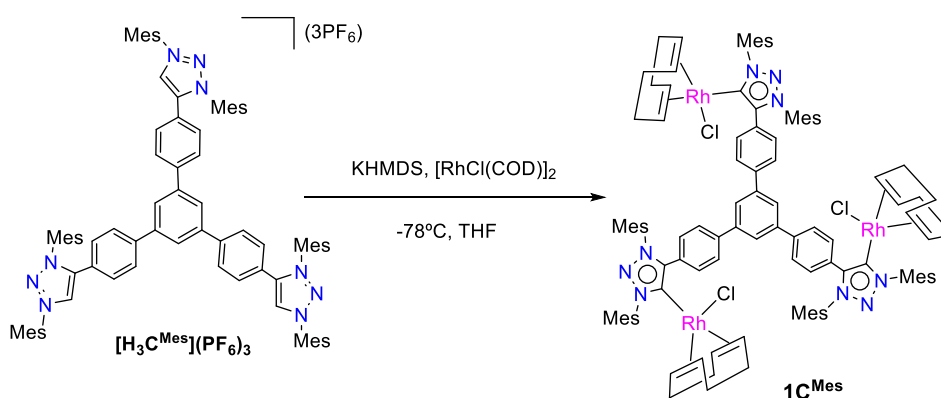
In the case of **2C**[Mes], an alternative synthetic strategy was followed. The tris-triazolium salt **[H₃C**[Mes]**](PF₆)₃** was deprotonated in acetone using K_2CO_3 in the presence of [IrCl(COD)]₂ under reflux (see Scheme 2.5).

Compound **1C**[Mes] can be easily transformed into the corresponding carbonyl derivative by bubbling CO through a solution of this complex in dichloromethane at 0ºC. Precipitation from a mixture CH_2Cl_2/hexane afforded the desired carbonylated compound **3C**[Mes] in excellent yield.
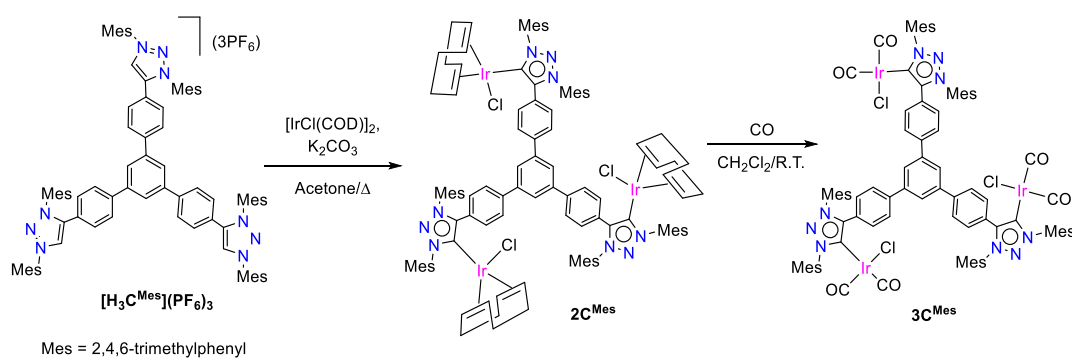
Scheme 2.5. Synthesis of **2C^Mes** and **3C^Mes**

All new trimetallic complexes were characterized by NMR spectroscopy, mass spectrometry and elemental analysis. The ^{1}H and ^{13}C{^{1}H} NMR spectra of these new complexes, are consistent with their predicted threefold symmetries. For example, two sharp signals assigned to the protons of the backbone of the three equivalent imidazolylidene rings are observed in the ^{1}H NMR spectra. A single resonance due to the metallated carbene carbons is found in the ^{13}C{^{1}H} NMR spectra, with the characteristic $^1J_{Rh-C}$ couplings for the case of the rhodium complexes (**1C^Mes**: 173.4 ppm, $^1J_{Rh-C}$ = 41.5 Hz; **2C^Mes**: 172.1 ppm, **3C^Mes**: 181.0 ppm).

As an example, the ^{1}H and ^{13}C NMR spectra of **2C^Mes** are described below. All the details regarding the characterization of **1C^Mes** and **3C^Mes** can be found in the Experimental Section (Chapter 5).

^{1}H NMR spectrum of 2C^Mes

Figure 2.7 shows the ^{1}H NMR spectrum of **2C^Mes**. The absence of the signal due to the protons of the N*H*CC groups, and the appearance of the signals corresponding to the COD ligand are indicative of the coordination of the tris-MIC ligand **C^Mes** to the Ir$^{(I)}$ fragment. The signals assigned to the protons of the 1,3,5-triphenylbenzene core (**a**, **c** and **b**) are displayed at 8.05, 7.78 and 7.63 ppm. The signals due to the aromatic protons of the mesityl groups appear between 7.08-7.00 ppm, and those due to the methyl groups appear between 2.45 and 2.04 ppm. The signals corresponding to the protons of the carbon atoms of the COD ligands are displayed on the spectrum.
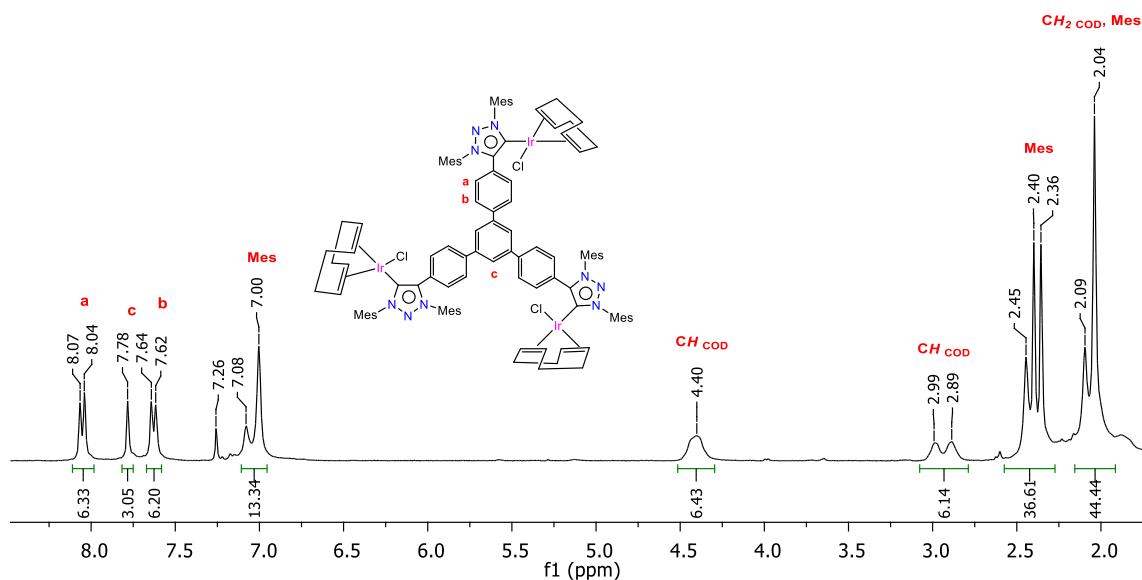
Figure 2.7. ^{1}H NMR spectrum of **2C**[Mes] in CDCl$_3$

$^{13}C\{^1H\}$ NMR spectrum of 2C[Mes]

Figure 2.8 shows the ^{13}C{^{1}H} NMR spectrum of **2C**[Mes]. The most characteristic signal is that attributed to the metallated carbene-carbon (**1**), which is displayed at 172.1 ppm. The signals attributed to the 1,3,5-triphenylbenzene core along with signals due to the aromatic carbons of the mesityl groups are displayed between 146.3-125.3 ppm. The signals due to the carbons of the three methyl groups of the mesityls appear between 21.4 and 17.7 ppm. The signals corresponding to the carbons of the COD ligand are conveniently displayed on the spectrum.
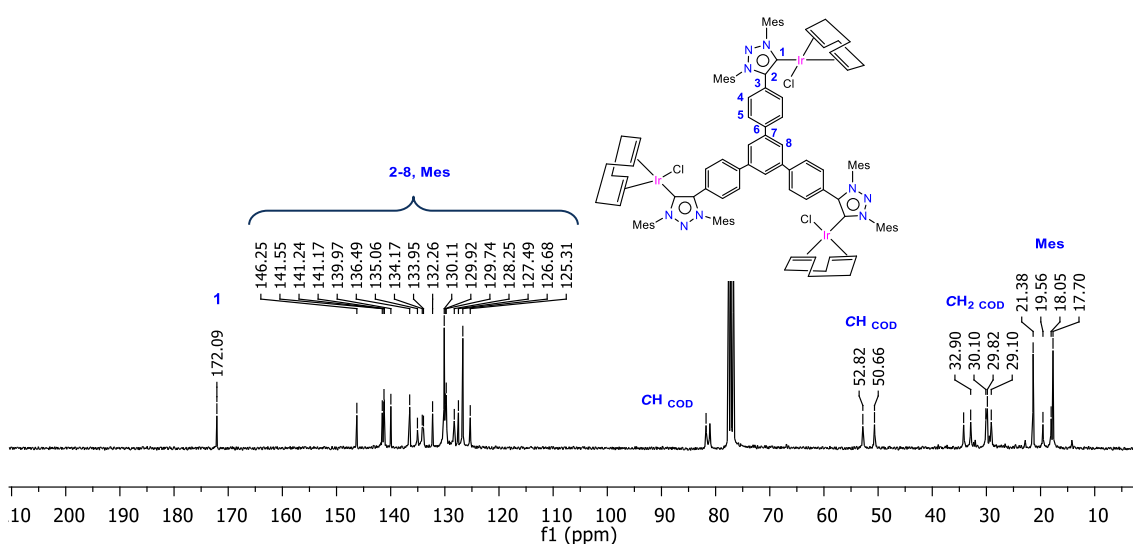
Figure 2.8. ^{13}C{^{1}H} NMR spectrum of **2C**[Mes] in CDCl$_3$

40

2.2.3.2 NiCpCl complexes

Prompted by the success in the synthesis of the Rh[I] and Ir[I] complexes, we decided to explore the coordination abilities of **[H₃B^Et](X)₃** (X = BF₄, PF₆, Br) and **[H₃C^Mes](PF₆)₃** with first row transition metals, such as iron and nickel. This work was done in collaboration with the group of Dr. Beatriz Royo from the *Instituto de Tecnologia Química e Biológica da Universidade Nova de Lisboa*, as a consequence of a research stay in her laboratory. As a result, a nickel complex based on the tris-MIC ligand was obtained. Unfortunately, all our attempts to obtain related Fe-based complexes failed. The synthetic procedure for the preparation of the tris-Ni complex **4C^Mes** is described in Scheme 2.6. The reaction of **[H₃C^Mes](PF₆)₃** with nickelocene ([NiCp₂]) in the presence of [NEt₄](Cl) in 1,4-dioxane under reflux, afforded the corresponding tris-MIC complex of Ni^(II) **4C^Mes**, as a red solid, in 40% yield after purification.
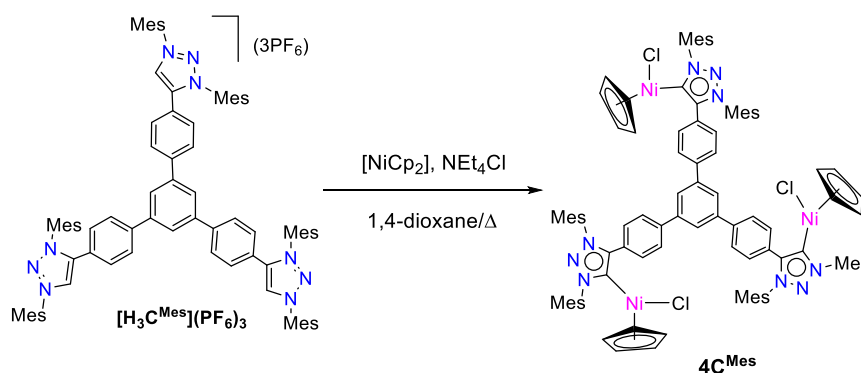
Scheme 2.6. Preparation of **4C^Mes**

The threefold symmetry of complex **4C^Mes** was confirmed by its ^{1}H NMR spectrum, which revealed a singlet due to the 15 protons at the three cyclopentadienyl ligands. The spectrum shows broad signals, probably as a consequence of the fluxionality due to the rotation about the C-C sigma bonds of the tris-MIC ligand, and the $C_{carbene}$-Ni bond (see Figure 2.9). The ^{13}C{^{1}H} NMR spectrum of **4C^Mes** displays the distinctive signal due to the equivalent metallated carbene carbons at 151.4 ppm, which falls close to the chemical shift shown by a previously reported [NiCpCl(trz)] (trz = triazolylidene) complex (148 ppm).[16] The trimetallic nature of the complex was confirmed by mass spectrometry, which revealed a peak at a *m/z* value of 810.7, assigned to [M-2Cl]²⁺. This compound is very interesting, because despite the fact that many [NiCpX(NHC)]

complexes have already been reported,[17] to our knowledge, this is the first Ni trimetallic complex featuring a tris-MIC ligand described so far.
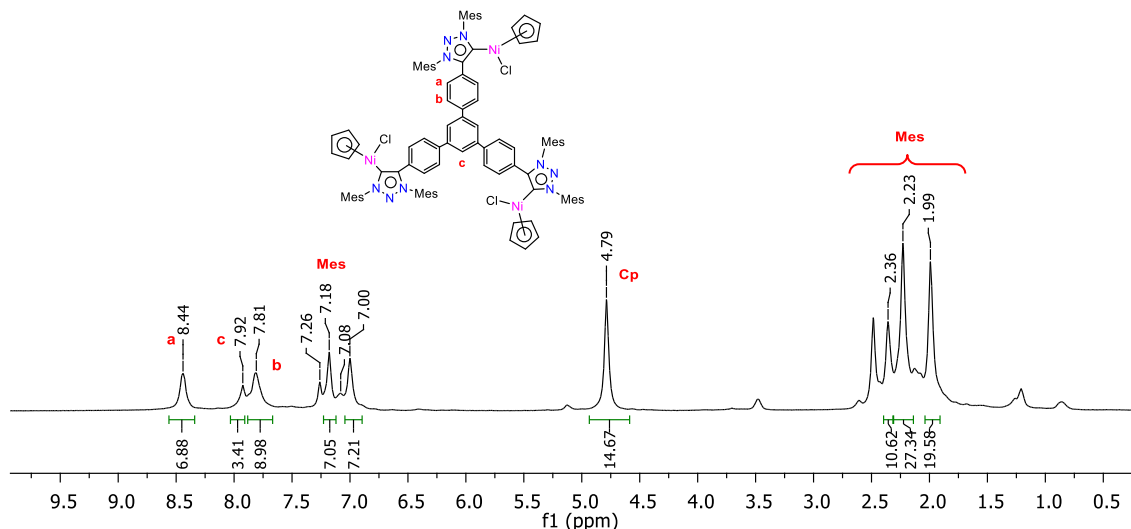
Figure 2.9. ^{1}H NMR spectrum of **4C**[Mes] in CDCl$_3$

2.2.4 Electronic properties of tri- *vs.* mono-metallic complexes

In order to assess the electron-donating abilities of the ligands described in the previous sections, two different approaches were followed. The first one involved the preparation of the carbonyl derivatives of complexes **3B**[Et], **4B**[Et] and **3C**[Mes], and the measurement of their corresponding ν(CO) stretching frequencies by means of IR spectroscopy. This provided us an indirect estimation of the TEP (Tolman Electronic Parameter). The second approach involves electrochemical measurements.

2.2.4.1 Carbonyl derivatives

Carbonyl complexes of the type [IrCl(L)(CO)$_2$] (L = NHC or MIC) have become broadly used for estimating TEP values,[18] avoiding the disadvantages of the [LNi(CO)$_3$] system, which is highly toxic and difficult to obtain. The first correlations were established by the Crabtree's and then by the Nolan's groups. These research groups proposed a simple equation to determine the TEP values from the ν_{av}(CO) frequencies of [IrCl(L)(CO)$_2$] complexes.[19] Some years later, Wolf and Plenio extended their correlation to the use of [RhCl(L)(CO)$_2$][20] complexes.

In order to evaluate the electron-donating character of our tris-NHC and tris-MIC ligands, the corresponding rhodium and iridium hexacarbonyl complexes (**4B**[Et] and **3C**[Mes]) were obtained (Chart 2.5). These complexes were obtained by bubbling carbon

monoxide into a solution of **2B**[Et] and **2C**[Mes] complexes in methylene chloride. (See Scheme 2.3 and Scheme 2.5)
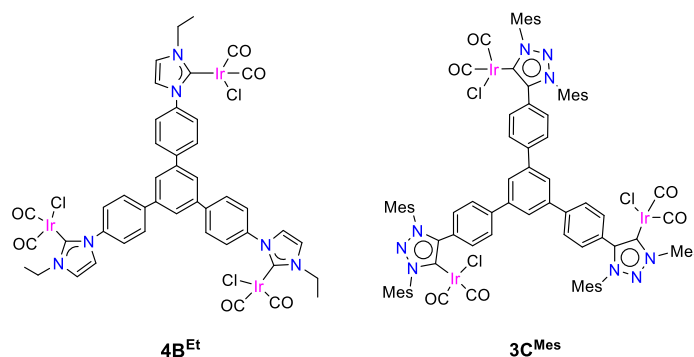
Chart 2.5. Schematic representation of complexes **4B**[Et] and **3C**[Mes]

The average C-O stretching frequencies $[\nu(CO)_{av}\ (cm^{-1})]$ of the tris- and mono-NHC and MIC complexes were determined by IR spectroscopy, and then the TEP values were estimated utilizing the well-known correlations. These data are shown in Table 2.3.

Table 2.3. Carbonyl stretching frequencies and TEP values for complexes **4B**[Et] and **3C**[Mes]

Entry	Complex	$\nu(CO)_{av}\ (cm^{-1})$[a]	TEP (cm^{-1})[b]
1	**4B**[Et]	2018	2045
2	**3C**[Mes]	2014	2042
3		2027[21]	2053
4		2019[11c]	2046

[a]IR data obtained in CH$_2$Cl$_2$. [b]Value calculated by linear regression from the experimentally measured $\nu_{av}(CO)$ of the [LIrCl(CO)$_2$] complex using TEP = $0.847\nu_{av}(CO) + 336$ (cm^{-1})[19b]

The higher TEP value observed for **4B**[Et] compared to that shown by **3C**[Mes] (entries 1 and 2) is indicative of the stronger electron-donating character of **C**[Mes]. This observation is in agreement with the TEP values obtained for the corresponding monometallic derivatives bearing the related NHC and MIC ligands (entries 3 and 4).[11c, 21] It should

43

be taken into account that **B^{Et}** and **C^{Mes}**, differ not only on their structural character (NHC *vs.* MIC), but also on their substituents at the nitrogen atom (alkyl *vs.* aryl), therefore this may also influence the electronic nature of the ligands.

In addition, the TEP value of **4B^E** differs on -8 cm^{-1} compared to its monometallic derivative (compare entries 1 and 3), which indicates that the tris-NHC ligand presents a stronger electron-donating character than its mono-NHC analogue. In a similar way, the TEP of **3C^{Me}** differs on -4 cm^{-1} with respect to its monometallic derivative (entries 2 and 4).

The results clearly indicate that the tritopic nature of **B^{Et}** and **C^{Mes}** is significantly improving the electron-donating ability of the ligands, thus suggesting that the tris-carbene ligands should not simply be regarded as the combination of the three monocarbenes that constitute their structures.

2.2.4.2 Electrochemical properties

Cyclic Voltammetry (CV) studies were also employed to evaluate the electronic properties of the carbene ligands. The first reports using this technique were those by Plenio, Crabtree, Peris and co-workers,[17a, d, 22] who performed their studies by using a selected series of rhodium, iridium and nickel complexes. This technique is also a valuable tool for determining the metal-to-metal electronic communication in multimetallic systems.[23]

We performed cyclic voltammetric studies of complexes **1B^{Et}** and **2B^{Et}** (Chart 2.6). Both species showed irreversible redox event, probably due to the low steric shielding about the metal, which makes the oxidised species to be highly unstable, as previously described in the literature for similar systems.[24] For comparative purposes, the results provided by these two trimetallic complexes were compared to their monometallic analogues, **1D^{Et}** and **2D^{Et}**, which were specifically synthesized for this purpose.
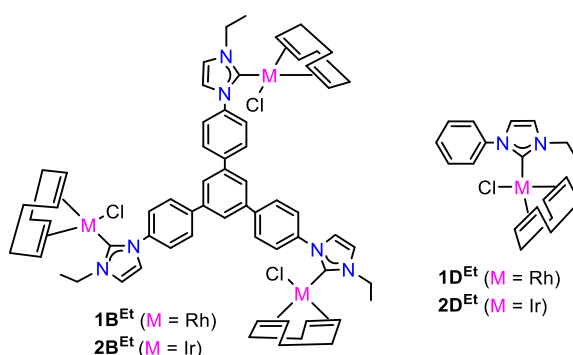
Chart 2.6. Rh^I and Ir^I metal complexes containing tris-NHC and mono-NHC ligands

The cyclic voltammetric diagrams obtained for the two iridium complexes **2B^{Et}** and **2D^{Et}** (Figure 2.10), display oxidation waves at a similar wave potential (E$_{oxid}$ = 0.71 V). This result indicates that both ligands (the tris-NHC ligand in **2B^{Et}** and the mono-NHC in **2D^{Et}**) provide a similar electron-donating ability.[20, 22a] By comparing the curves obtained from the Differencial Pulse Voltammetry (DPV) it can be observed that there is not any detectable broadening of the signal provided by the trimetallic complex, compared to that generated by the monometallic one. This result indicates that the tri-metallic complex **2B^{Et}** contains three essentially decoupled iridium fragments. A bi- or tri-metallic system with effective metal-to-metal communication should be expected to show two or three independent waves, each one assigned to the oxidation of each metal center. Alternatively, a significant broadening of the redox wave should be expected for a weakly electronically coupled system.
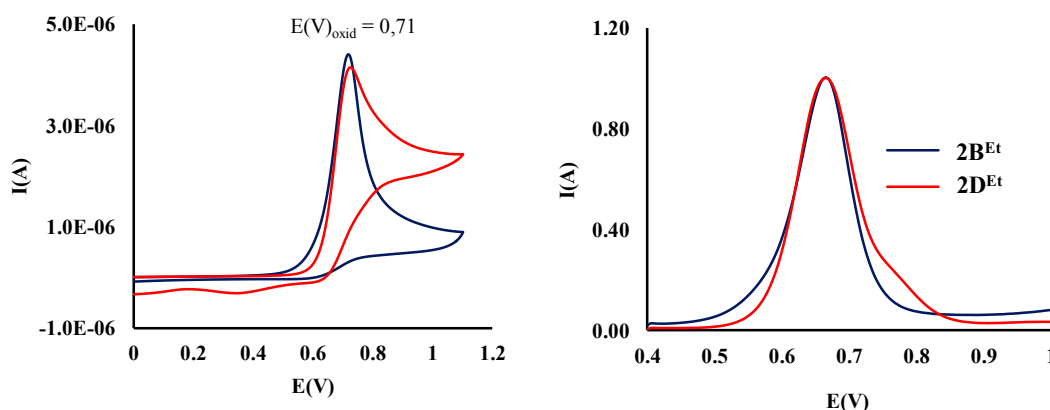
Figure 2.10. CV plot (left) and relevant DPV section (right) of complexes **2B^{Et}** and **2D^{Et}** (1mM in dry CH$_2$Cl$_2$ with 0.1M [NBu$_4$][PF$_6$] as the supporting electrolyte, 50 mVs^{-1} scan rate, Fc$^+$/Fc used as internal standard with E$_{1/2}$ (Fc/Fc$^+$) = 0.44 V *vs.* SCE)

The cyclic voltammetry studies of **1C^{Mes}**, **2C^{Mes}** and **4C^{Mes}** were also performed to gain further insight into the electronic properties of the tris-MIC ligands.

1C^{Mes} (M = Rh, L = COD)
2C^{Mes} (M = Ir, L = COD)
4C^{Mes} (M = Ni, L = Cp)
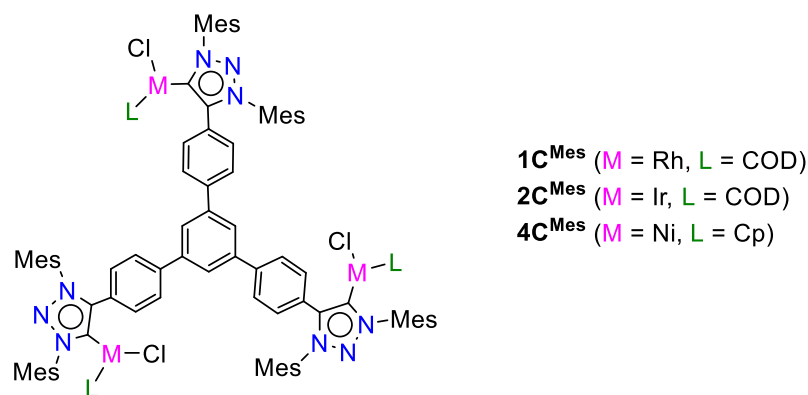
Chart 2.7. Tris-MIC complexes under study

The rhodium complex **1C^{Mes}** showed an irreversible redox event at E_{oxid} = 0.65 V (Figure 2.10, solid line), while the iridium complex **2C^{Mes}** (Figure 2.10, dotted line), showed a pseudo-reversible redox event at E_{oxid} = 0.69 V. Compared to the cyclic voltammetry data for the analogue complexes of rhodium and iridium with the tris-NHC ligand **B^{Et}** (E_{oxid} = 0.71 V, for both complexes),[10a] the lower E_{oxid} value for **1C^{Mes}** and **2C^{Mes}** is consistent with a higher electron-donating character of the tris-MIC ligand **C^{Mes}**. Again, the appearance of only one redox wave for both complexes, **1C^{Mes}** and **2C^{Mes}**, is consistent with the lack of electronic communication between the three metal centers for both trimetallic complexes.
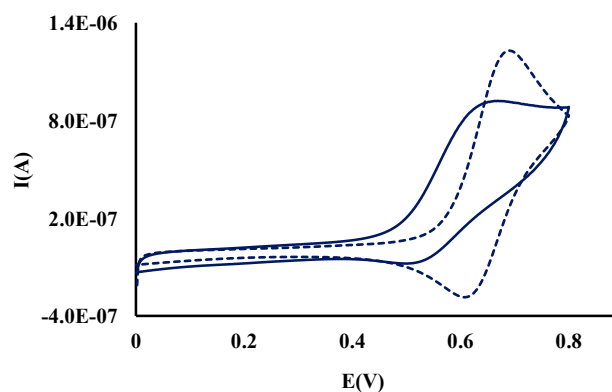
Figure 2.10. CV plots of complexes **1C^{Mes}** (solid line), and **2C^{Mes}** (dotted line). Experiments carried out using 1mM solutions of the complexes in dry CH_2Cl_2 with 0.1M [NBu$_4$][PF$_6$] as the supporting electrolyte, 100 mVs^{-1} scan rate, Fc$^+$/Fc used as internal standard with $E_{1/2}$ (Fc/Fc$^+$) = 0.44 V *vs.* SCE

[NiClCp(NHC)] often show reversible and well-behaved electrochemical responses,[17a, d] and are known to serve as excellent proves for the evaluation of the electron-donating character of their NHC ligands. In addition, to our knowledge there are not examples of

cyclic voltammetry studies on [NiClCp(MIC)] complexes. The cyclic voltammetry diagram of the tris-Ni$^{(II)}$ complex **4C^{Mes}** is shown in Figure 2.11, together with the relevant section of the DPV plot. The complex showed a quasi-reversible wave at a half-wave potential of $E_{1/2} = 0.64$ V, which is significantly lower than the half-wave potential shown by complex [NiCpCl(IMes)] (IMes = 1,3-mesityl-imidazolylidene),[17a] which showed a half-wave potential of $E_{1/2} = 0.72$ V. As expected, this result is consistent with the higher degree of electron-donating character for the ligand in **4C^{Mes}** compared to IMes. It can be established that there is only one redox event taking place, and thus it becomes evident that the tri-metallic complex **4C^{Mes}** contains three essentially decoupled nickel fragments.
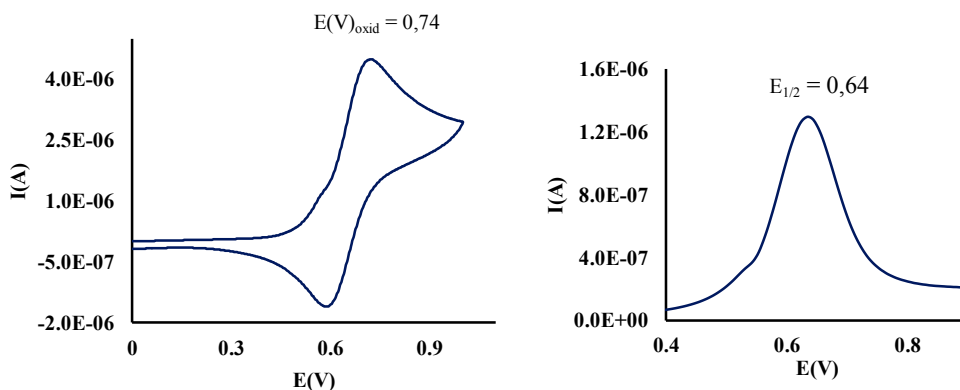
Figure 2.11. CV plot (left) and relevant DPV section (right) of complex **4C^{Mes}** (1mM in dry CH$_2$Cl$_2$ with 0.1M [NBu$_4$][PF$_6$] as the supporting electrolyte, 50 mVs^{-1} scan rate, Fc$^+$/Fc used as internal standard with $E_{1/2}$ (Fc/Fc$^+$) = 0.44 V *vs*. SCE).

2.2.5 Catalytic studies

2.2.5.1 Catalytic activity of the trimetallic rhodium complexes: 1,4-Addition of Arylboronic Acids to Cyclohex-2-one

The 1,4-addition of nucleophiles to α,β-unsaturated compounds represents one of the main organic transformation for the production of key intermediates in the pharmaceutical industry.[25] This process is a convenient synthetic pathway for the formation of C–C bonds.[26] Although copper is the most widely used metal for this type of reactions,[27] it shows, together with Grignard reagents, some important disadvantages, such as low temperature thresholds and high water sensitivity.

Rhodium catalysts have recently shown to provide some benefits into this reaction, especially since they allow the use of mild organometallic reagents and often afford high chemoselectivities. Rhodium catalysts also allow the use of aryl nucleophiles, which cannot be coupled when Cu-based catalysts are used.[28]

In this context, Nolan and co-workers reported an efficient rhodium catalyst that combines the presence of a strongly electron-donating N-heterocyclic carbene and a poorly electron-donating bidentate cyclooctadiene ligand.[29]

Prompted by these results, we decided to evaluate the catalytic activity of our rhodium complexes in the addition of arylboronic acids to an α,β-unsaturated ketone, such as cyclohex-2-one (Scheme 2.7).[29-30]

First, we studied the catalytic activity of the tris-NHC-rhodium complex (**1B**^{Et}), which was compared with its monometallic analogue (**1D**^{Et}) (Chart 2.8). Then, for comparison, we decided to study the activity of the complex tris-MIC rhodium complex **1C**^{Mes} for the same reaction.
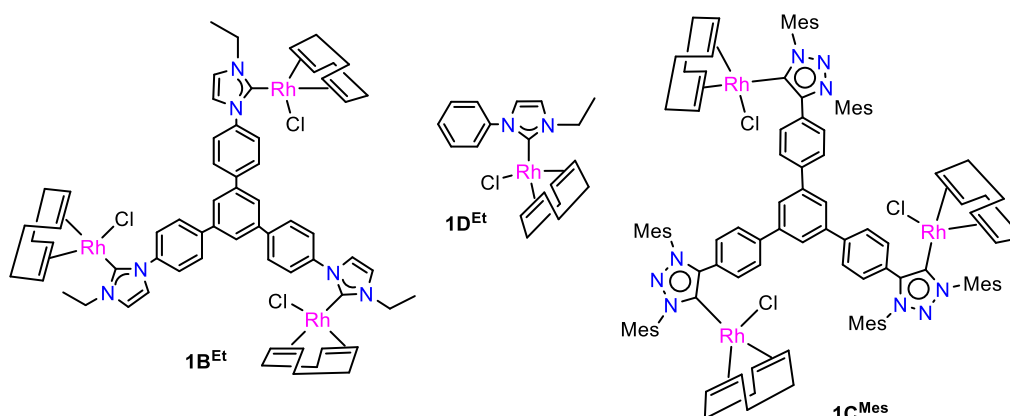
Chart 2.8. Schematic representation of complexes **1B**^{Et}, **1C**^{Mes} and **1D**^{Et}

The fact that the three metal centers in **1B**^{Et} and **1C**^{Mes} are essentially electronically disconnected, suggests that the ligand may be used to support different metal fragments without detriment of their potential catalytic properties, and thus should constitute a good opportunity to study cooperative effects. Also, the fact that the mono-NHC ligand in **1D**^{Et} provides with almost identical stereoelectronic properties as those offered by the tri-NHC ligand in **1B**^{Et}, gives us an excellent opportunity to compare the catalytic activities provided by the trimetallic complexes and their monometallic analogues.

Table 2.4 shows some selected results on the addition of arylboronic acids to cyclohex-2-one. As can be observed from the data shown, higher conversions were obtained when

the reactions were carried out in toluene, than in a mixture of THF/H$_2$O. This result is rather surprising, if we take into account that this reaction is generally performed in the presence of water,[30d] and the examples in which dry toluene is used have been regarded as rare, and only promoted when OH groups are forming part of the ancillary ligands, which is not our case.
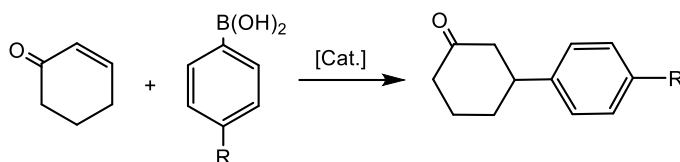
Scheme 2.7. 1,4-Addition of aryl boronic acids to cyclohex-2-one

Table 2.4. 1,4-Addition of arylboronic acids to cyclohex-2-one[a] using **1B^{Et}** (trimetallic) and **1D^{Et}** (monometallic) as catalysts

Entry	[Cat.] (mol %)	Solvent	R	[Cat.]	Conv.(%)[b]
1	0.066	THF/H$_2$O	H	**1B^{Et}**	56(45)
2	0.2	THF/H$_2$O	H	**1D^{Et}**	58(46)
3	0.066	THF/H$_2$O	Me	**1B^{Et}**	63(53)
4	0.2	THF/H$_2$O	Me	**1D^{Et}**	74(50)
5	0.066	Toluene	H	**1B^{Et}**	100(91)
6	6.6 10^{-3}	Toluene	H	**1B^{Et}**	71(68)
7	0.2	Toluene	H	**1D^{Et}**	96(90)
8	0.02	Toluene	H	**1D^{Et}**	61(48)
9	0.066	Toluene	Me	**1B^{Et}**	85(69)
10	0.2	Toluene	Me	**1D^{Et}**	69(55)
11[c]	0.066	Toluene	OMe	**1B^{Et}**	48(16)
12[c]	0.2	Toluene	OMe	**1D^{Et}**	47(14)

[a]Conditions: Cyclohexen-2-one (0.5 mmol), KOH (0.09 mmol), ArB(OH)$_2$ (0.6 mmol), dry solvent for entries 5-12. [b]Conversions determined by gas chromatography (GC), using anisole as internal standard. Yields given in parenthesis. [c]Using 2,4,6-trimethylphenol as standard

It is worth mentioning that we did not need additives to the reaction mixtures, in order to improve the catalytic outcomes. Regardless of the type of solvent used, the two

catalysts afforded very similar reaction outcomes, therefore suggesting that the higher nanolocal concentration provided by the trimetallic complex (dendrimer effect),[31] did not have any significant effect in its activity. This means that the trimetallic nature of **1B**^{Et} does not provide any improvement compared to its monometallic analogue. The representation of the reaction profiles for the reaction between phenylboronic acid and cyclohex-2-one (Figure 2.12), gives a good illustration of the quasi-identical behavior of the two catalysts.
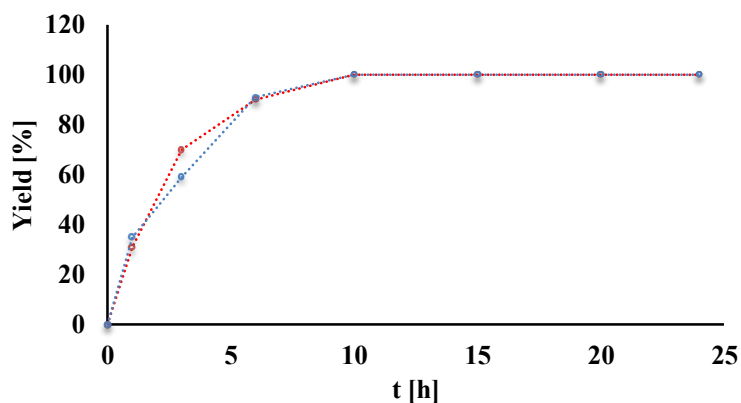
Figure 2.12. Time course for the addition of phenyl boronic acid to cyclohex-2-one. Reactions carried out in toluene at 100ºC, with a 0.06 (**1B**^{Et}: blue) or 0.2 (**1D**^{Et}: red) mol % of catalyst loading. Yields were determined by GC, using anisole as internal standard

This observation is interesting, and may be related to previous observations made by our research group, in which the use of π-extended polyaromatic-based di- and tri-NHC ligands produced significant improvements of the catalytic activities of their related complexes, compared to their monometallic analogues.[4, 32] In those cases, the catalytic benefits were attributed to the π-stacking between the substrates and the core of the π-extended polyaromatic ligand, a situation that may not be reproduced in this new case, in which the NHC moieties are π-disconnected from the polyaromatic core. It is also worth mentioning that for the reactions carried out at catalyst loadings of 6.6×10^{-3} and 0.02 mol % for **1B**^{Et} and **1D**^{Et}, respectively (entries 11 and 12), the yields obtained after 6h are moderately high, therefore illustrating the high activity of the catalysts even at very low catalyst loadings.

We observed that a side-reaction involving the deborylation of the aryl boronic acid is also taking place in this reaction. This would explain the differences found between conversions and yields for most of the reactions that we studied. This observation is

more relevant in the case of phenylboronic acid, for which the formation of anisole from 4-methoxy-phenylboronic acid is the dominant process (entries 11 and 12).

In order to compare the activity of the tri-NHC complex **1B**[Et] with the tri-MIC complex **1C**[Mes], catalyst **1C**[Mes] was also tested in the 1,4-addition of arylboronic acids to cyclohex-2-one, using the same reaction conditions. Table 2.5 shows the results obtained, together with the results given by the use of the tris-NHC catalyst **1B**[Et] to facilitate a direct comparison.
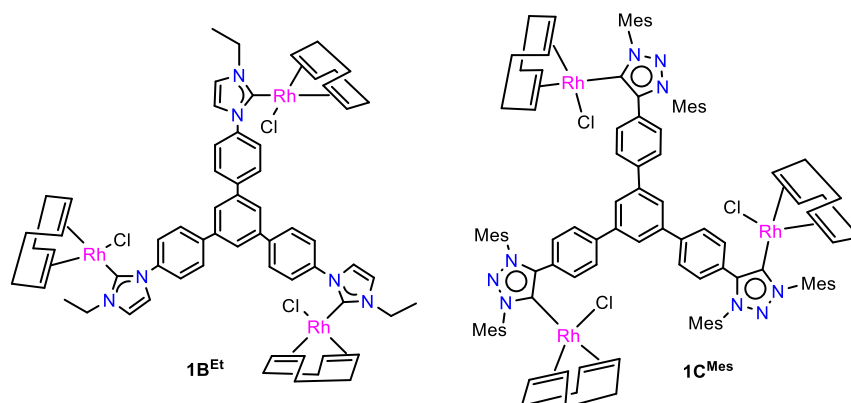
Chart 2.9. Schematic representation of catalysts **1B**[Et] and **1C**[Mes]

Table 2.5. 1,4-Addition of arylboronic acids to cyclohex-2-one[a] using **1B**[Et] and **1C**[Mes] as catalysts

Entry	R	[Cat.]	Conv.(%)
1	H	**1B**[Et]	100(91) [a]
2	H	**1C**[Mes]	66(43) [b]
3	Me	**1B**[Et]	85(69) [a]
4	Me	**1C**[Mes]	63(34) [b]
5	OMe	**1B**[Et]	48(16) [b]
6	OMe	**1C**[Mes]	52(15) [b]

Reaction conditions: Catalyst (0.066 mol %), 2-cyclohexen-1-one (0.5 mmol), KOH (0.09 mmol), ArB(OH)$_2$ (0.6 mmol), dry toluene (3 mL). Conversions determined by gas chromatography (GC), using [a]anisole or [b]2,4,6-trimethylphenol as internal standards. Yields are given in parenthesis. The results given for the use of complex **1B**[Et] were taken from ref [10a].

From the results shown, it can be observed that the activity of complex **1C**[Mes] is lower than the activity shown by **1B**[Et], both in terms of conversion and selectivity. For all the

reactions where **1C^Mes** was used, a side-reaction involving the deborylation of the aryl boronic acid was observed. This justifies the large differences found between conversions and yields for all of the reactions that we have studied. This observation is more pronounced in the case of 4-methoxy-phenylboronic acid, for which the formation of anisole is the dominant process (entries 5 and 6).

2.3 Conclusions

In this Chapter we described the synthesis and characterization of several tris-imidazolium and tris-triazolium salt precursors based on a triphenylbenzene core. The photophysical properties of the tris-imidazolium salts were evaluated, indicating that some of salts precursors exhibit fluorescence emission in the 320-420 nm region and moderate quantum yields.

These salts were used as tris-carbene ligand precursors, which were coordinated to Rh^(I), Ir^(I) and Ni^(II). The complexes were fully characterized by standard spectroscopic and microanalytical techniques. Some of the monometallic analogues were also synthesized and characterized for comparative purposes.

The electron-donating character of the triscarbene ligands was established by means of IR spectroscopy and electrochemical measurements. The electronic communication between metals was found to be almost negligible.

The catalytic activity of the tri- and monometallic rhodium complexes was evaluated toward the addition of arylboronic acids to an α,β-unsaturated ketone, showing that the catalytic activity of the trimetallic complex is comparable to itse monometallic counterpart. In addition, it was concluded that for this particular reaction, the performance of the metal complex containing the strong electron-donating tris-MIC ligand does not afford an improvement on the catalytic activity compared to the related tris-NHC-based complex for this specific reaction.

In summary, this Chapter illustrates the high coordination versatility of the new tris-NHC and tris-MIC ligands, their photochemical, electronic and catalytic properties.

2.4 References

[1]   a) J. A. Mata, M. Poyatos and E. Peris, *Coord. Chem. Rev.* **2007**, *251*, 841-859; b) M. Poyatos, J. A. Mata and E. Peris, *Chem. Rev.* **2009**, *109*, 3677-3707.

[2]   a) K. A. Williams, A. J. Boydston and C. W. Bielawski, *Chem. Soc. Rev.* **2007**, *36*, 729-744; b) B. C. Norris and C. W. Bielawski, *Macromolecules* **2010**, *43*, 3591-3593; c) A. B. Powell, C. W. Bielawski and A. H. Cowley, *Comments Inorg. Chem.* **2010**, *31*, 75-82; d) O. Schuster, L. Mercs and M. Albrecht, *Chimia* **2010**, *64*, 184-187; e) B. M. Neilson, A. G. Tennyson and C. W. Bielawski, *J. Phys. Org. Chem.* **2012**, *25*, 531-543.

[3]   J. A. Mata, F. E. Hahn and E. Peris, *Chem. Sci.* **2014**, *5*, 1723.

[4]   S. Gonell, M. Poyatos and E. Peris, *Angew. Chem. Int. Ed.* **2013**, *52*, 7009-7013.

[5]   S. Gonell, M. Poyatos and E. Peris, *Chem. Eur. J.* **2014**, *20*, 5746-5751.

[6]   A. Rit, T. Pape and F. E. Hahn, *J. Am. Chem. Soc.* **2010**, *132*, 4572-4573.

[7]   K. A. Williams and C. W. Bielawski, *Chem. Commun.* **2010**, *46*, 5166-5168.

[8]   S. Gonell, R. G. Alabau, M. Poyatos and E. Peris, *Chem. Commun.* **2013**, *49*, 7126-7128.

[9]   E. Peris, *Chem. Commun.* **2016**, *52*, 5777-5787.

[10]   a) C. Mejuto, G. Guisado-Barrios and E. Peris, *Organometallics* **2014**, *33*, 3205-3211; b) N. Sinha, F. Roelfes, A. Hepp, C. Mejuto, E. Peris and F. E. Hahn, *Organometallics* **2014**, *33*, 6898-6904; c) C. Mejuto, G. Guisado-Barrios, D. Gusev and E. Peris, *Chem. Commun.* **2015**, *51*, 13914-13917; d) C. Mejuto, B. Royo, G. Guisado-Barrios and E. Peris, *Beilstein J. Org. Chem.* **2015**, *11*, 2584-2590.

[11]   a) P. Mathew, A. Neels and M. Albrecht, *J. Am. Chem. Soc.* **2008**, *130*, 13534-13535; b) G. Guisado-Barrios, J. Bouffard, B. Donnadieu and G. Bertrand, *Angew. Chem. Int. Ed.* **2010**, *49*, 4759-4762; c) J. Bouffard, B. K. Keitz, R. Tonner, G. Guisado-Barrios, G. Frenking, R. H. Grubbs and G. Bertrand, *Organometallics* **2011**, *30*, 2617-2627.

[12]   a) I. A. Khotina, V. A. Izmrudov, N. V. Tchebotareva and A. L. Rusanov, *Macromol. Chem. Phys.* **2001**, *202*, 2360-2366; b) N. I. Nijegorodov and W. S. Downey, *Spectrochimi. Acta A* **1995**, *51*, 2335-2346.

[13]   a) N. I. Nizhegorodov, V. P. Zvolinskii and E. N. Smirnova, *Zh. Fiz. Khim.* **1992**, *66*, 3060-3065; b) I. B. Berlman, *J. Chem. Phys.* **1970**, *52*, 5616.

[14] a) C. Segarra, G. Guisado-Barrios, F. E. Hahn and E. Peris, *Organometallics* **2014**, *33*, 5077-5080; b) A. Rit, T. Pape, A. Hepp and F. E. Hahn, *Organometallics* **2011**, *30*, 334-347.

[15] S. H. Lim and S. M. Cohen, *Inorg. Chem.* **2013**, *52*, 7862-7872.

[16] Y. Wei, A. Petronilho, H. Mueller-Bunz and M. Albrecht, *Organometallics* **2014**, *33*, 5834-5844.

[17] a) O. R. Luca, B. A. Thompson, M. K. Takase and R. H. Crabtree, *J. Organomet. Chem.* **2013**, *730*, 79-83; b) C. D. Abernethy, A. H. Cowley and R. A. Jones, *J. Organomet. Chem.* **2000**, *596*, 3-5; c) R. A. Kelly, N. M. Scott, S. Diez-Gonzalez, E. D. Stevens and S. P. Nolan, *Organometallics* **2005**, *24*, 3442-3447; d) H. Valdes, M. Poyatos, G. Ujaque and E. Peris, *Chem. Eur. J.* **2015**, *21*, 1578-1588.

[18] C. A. Tolman, *Chem. Rev.* **1977**, *77*, 313-348.

[19] a) A. R. Chianese, X. W. Li, M. C. Janzen, J. W. Faller and R. H. Crabtree, *Organometallics* **2003**, *22*, 1663-1667; b) R. A. Kelly, III, H. Clavier, S. Giudice, N. M. Scott, E. D. Stevens, J. Bordner, I. Samardjiev, C. D. Hoff, L. Cavallo and S. P. Nolan, *Organometallics* **2008**, *27*, 202-210.

[20]　S. Wolf and H. Plenio, *J. Organomet. Chem.* **2009**, *694*, 1487-1492.

[21] D. G. Gusev, *Organometallics* **2009**, *28*, 6458-6461.

[22] a) S. Leuthausser, D. Schwarz and H. Plenio, *Chem. Eur. J.* **2007**, *13*, 7195-7203; b) S. Wolf and H. Plenio, *J. Organomet. Chem.* **2010**, *695*, 2418-2422; c) H. Valdes, M. Poyatos and E. Peris, *Organometallics* **2014**, *33*, 394-401.

[23] a) A. G. Tennyson, E. L. Rosen, M. S. Collins, V. M. Lynch and C. W. Bielawski, *Inorg. Chem.* **2009**, *48*, 6924-6933; b) L. Mercs, A. Neels and M. Albrecht, *Dalton Trans.* **2008**, 5570-5576; c) S. Sabater, J. A. Mata and E. Peris, *Organometallics* **2012**, *31*, 6450-6456; d) R. Sakamoto, T. Kambe, S. Tsukada, K. Takada, K. Hoshiko, Y. Kitagawa, M. Okumura and H. Nishihara, *Inorg. Chem.* **2013**, *52*, 7411-7416.

[24] a) R. Ballardini, G. Varani, M. T. Indelli and F. Scandola, *Inorg. Chem.* **1986**, *25*, 3858-3865; b) D. Tapu, C. Owens, D. VanDerveer and K. Gwaltney, *Organometallics* **2009**, *28*, 270-276.

[25] a) R. Brehme, D. Enders, R. Fernandez and J. M. Lassaletta, *Eur. J. Org. Chem.* **2007**, 5629-5660; b) P. Tian, H.-Q. Dong and G.-Q. Lin, *Acs Catalysis* **2012**, *2*, 95-119.

[26]   a) K. Fagnou and M. Lautens, *Chem. Rev.* **2003**, *103*, 169-196; b) T. Hayashi and K. Yamasaki, *Chem. Rev.* **2003**, *103*, 2829-2844; c) L. Zhao, Y. Ma, F. He, W. Duan, J. Chen and C. Song, *J. Org. Chem.* **2013**, *78*, 1677-1681; d) V. Lillo, A. Prieto, A. Bonet, M. M. Diaz-Requejo, J. Ramirez, P. J. Perez and E. Fernandez, *Organometallics* **2009**, *28*, 659-662.

[27]   T. Jerphagnon, M. G. Pizzuti, A. J. Minnaard and B. L. Feringa, *Chem. Soc. Rev.* **2009**, *38*, 1039-1075.

[28]   H. J. Edwards, J. D. Hargrave, S. D. Penrose and C. G. Frost, *Chem. Soc. Rev.* **2010**, *39*, 2093-2105.

[29]   B. J. Truscott, G. C. Fortman, A. M. Z. Slawin and S. P. Nolan, *Org. Biomol. Chem.* **2011**, *9*, 7038-7041.

[30]   a) M. Pucheault, S. Darses and J. P. Genet, *Tetrahedron Lett.* **2002**, *43*, 6155-6157; b) M. Pucheault, S. Darses and J. P. Genet, *Eur. J. Org. Chem.* **2002**, 3552-3557; c) M. Sakai, H. Hayashi and N. Miyaura, *Organometallics* **1997**, *16*, 4229-4231; d) T. Hayashi, M. Takahashi, Y. Takaya and M. Ogasawara, *J. Am. Chem. Soc.* **2002**, *124*, 5052-5058; e) I. Penafiel, I. M. Pastor, M. Yus, M. A. Esteruelas and M. Olivan, *Organometallics* **2012**, *31*, 6154-6161; f) I. Bratko, G. Guisado-Barrios, I. Favier, S. Mallet-Ladeira, E. Teuma, E. Peris and M. Gómez, *Eur. J. Org. Chem.* **2014**, 2160-2167.

[31]   a) B. Helms and J. M. J. Frechet, *Adv. Synth. Catal.* **2006**, *348*, 1125-1148; b) D. Astruc, *C. R. Chimie* **2005**, *8*, 1101-1107; c) J. N. H. Reek, S. Arevalo, R. Van Heerbeek, P. C. J. Kamer and P. Van Leeuwen in *Dendrimers in catalysis*, *Vol. 49* **2006**, pp. 71-151.

[32]   G. Guisado-Barrios, J. Hiller and E. Peris, *Chem. Eur. J.* **2013**, *19*, 10405-10411.

Chapter 3

Homoleptic and Heteroleptic Coordination Cages with NHC and MIC Ligands

3.1 Introduction

In 1987, Lehn and co-workers described the preparation of a dinuclear helicate complex by reacting $Cu^{(I)}$-based precursors with 2,2-bipyridine,[1] a work that constituted the first example of a metal-directed self-assembly process. A few years later, Constable defined metallo-supramolecular chemistry as '*the chemistry involving the combination of bridging organic ligands with metal units to synthesize discrete or polymeric assemblies*'.[2] Hence, the basis for metallosupramolecular design is the availability of (often rigid) ligands with two or more binding sites that must be able to combine with suitable metal fragments to form symmetrical structures with a variety of shapes and sizes. Nowadays, a large number of self-assembly metallosupramolecular structures featuring different shapes, sizes and properties are associated with the names of Fujita,[3] Raymond,[4] Stang,[5] Nitschke[6] and Constable,[7] among others.[8] Most efforts in the design of metallosupramolecules are based on mimicking enzymes, and therefore well-defined hydrophobic cavities are pursued, but again, the design of biomimetic complexes relies on the synthesis of metal complexes with polydentate ligands that mimic the environment found in nature. For the formation of the cavities an array of several metals is needed, and this is the reason why metallorganic molecules with cavities (metallocavitands) have been defined as '*multimetallic complexes where the metal coordination is necessary for cavity formation*'.[9]

The construction of metallosupramolecular structures can be achieved by using multitopic ligands bearing two or more binding domains separated by spacers which, by combination with the suitable metal fragments, may form assemblies with various sizes and geometries.[6a, b, 7b, 10] In this context, extended poly-N-heterocyclic-carbene (NHC) ligands[11] have recently shown to be suitable scaffolds for the preparation of supramolecular assemblies. The topological diversity of poly-NHCs has allowed the preparation of a variety of supramolecular assemblies that include molecular squares and triangles,[12] cylinder-like structures[13] and organometallic polymers.[14]

The $Ag^{(I)}$-mediated self-assembly of supramolecular assemblies from poly-NHC ligands has developed an emerging field of organometallic chemistry due to their facile preparation.[15] $Ag^{(I)}$-NHC complexes are readily obtained reacting Ag_2O with the corresponding NHC precursor (normally an imidazolium salt). In addition, they can easily be converted into different metal complexes *via* transmetalation reactions. This methodology has permitted the preparation of the cylinder-like assemblies with three

(**I**), four (**II**) and even six metal centers (**III**) (Chart 3.1). However, these molecular assemblies derived from NHC substituted phenylenes feature a rather small cavity, limiting the incorporation of guests. Therefore, the development of new supramolecular assemblies based on poly-NHC ligands having a larger π-conjugated framework could allow the preparation of novel structures, and also facilitate the recognition of guests.

M = Ag, Au, R = *n*-Bu, Et
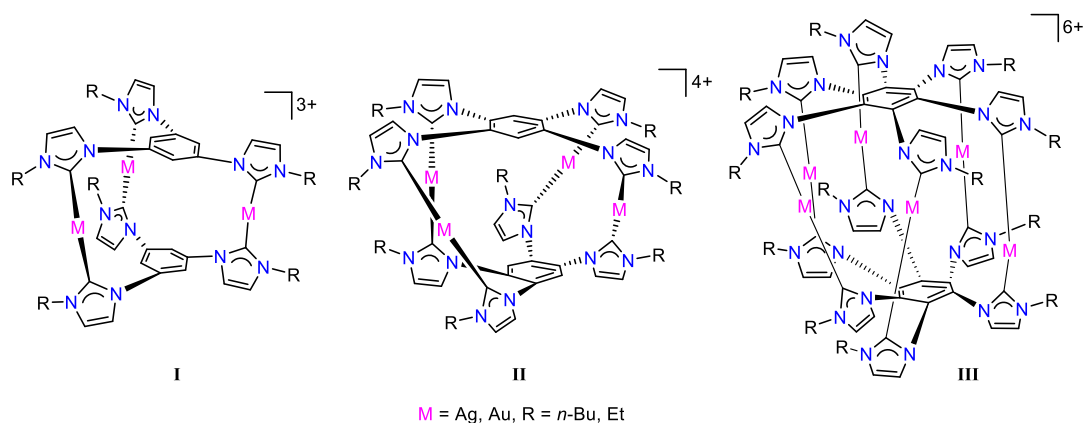
Chart 3.1. Cylinder-like assemblies from benzene derived tris-, tetra- or hexa-NHC ligands

We thought that we could apply our expertise in the preparation of rigid poly-NHC[16] and poly-MIC[17] ligands for the design of novel metallo-organic macromolecular cylinders. Self-assembled cages based on mesoionic carbenes are especially interesting, because they were not reported prior to this work. Such structures may offer some advantages and intriguing chemical properties, and they may be potentially useful for the selective recognition of small neutral or ionic molecules.[9c, 18] This Chapter deals with the preparation of several homoleptic and heteroleptic coordination cages based on tris-NHC and tris-MIC ligands and the study of their reactivity.

3.2 Results and discussion

3.2.1 Synthesis and characterization of homoleptic compounds

In this section we will describe the preparation of homoleptic nanometer-sized cylinder-like assemblies with coinage metals (Chart 3.2) derived from the 1,3,5-triphenylbenzene bridged tris-imidazolium and tris-triazolium salts in Chapter 2.[13g, 19] In addition, the synthesis and reactivity of heteroleptic coordination cages of Ag[(I)] will also be described.

NHC-NHC   **MIC-MIC**

[5B^{Et}](PF$_6$)$_3$ (M = Ag)
[6B^{Et}](PF$_6$)$_3$ (M = Au)
[7B^{Et}](PF$_6$)$_3$ (M = Cu)

[5C^{Mes}](PF$_6$)$_3$ (M = Ag)
[6C^{Mes}](AuCl$_2$)$_3$ (M = Au)
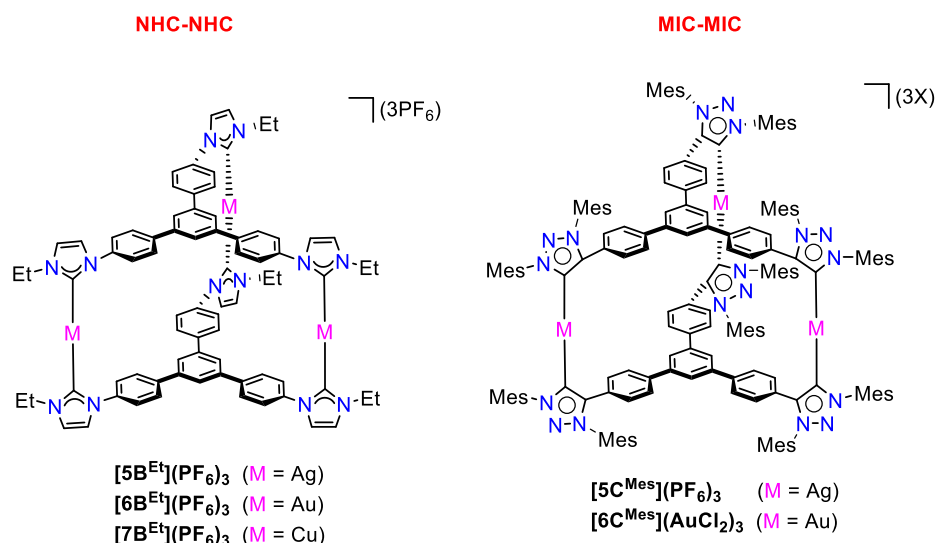
Chart 3.2. Cylinder-like assemblies from triphenylbenzene tris-NHC and tris-MIC ligands

3.2.1.1 Tris-NHC metallacages

The following work is a result of a collaboration between the group of Prof. Ekkehardt Hahn (Münster, Germany) and our research group in Castellón. The tris-imidazolium salt **[H$_3$B^{Et}](PF$_6$)$_3$** (Scheme 3.1) described in Chapter 2 was employed as ligand precursor. Scheme 3.1 displays the synthetic procedure for the preparation of the self-assembly structures of Ag, Au and Cu. The reaction of 2 equiv. of **[H$_3$B^{Et}](PF$_6$)$_3$** with 3 equiv. of Ag$_2$O in acetonitrile at 60 °C under the exclusion of light afforded the homoleptic trinuclear Ag$^{(I)}$-NHC cage complex **[5B^{Et}](PF$_6$)$_3$** in 77% yield, as a white solid.
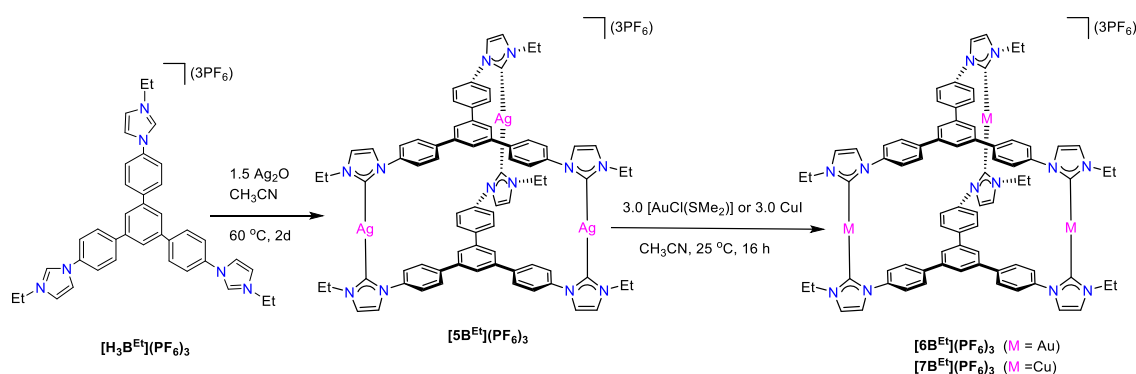
Scheme 3.1. Synthesis of complex **[5B^{Et}](PF$_6$)$_3$** and transmetalation to **[6B^{Et}](PF$_6$)$_3$** and **[7B^{Et}](PF$_6$)$_3$** complexes

Since Ag$^{(I)}$-NHC complexes are good carbene transfer agents,[15] we replaced the Ag$^{(I)}$ ions in **[5B^{Et}](PF$_6$)$_3$** by Au$^{(I)}$ by stirring a solution of **[5B^{Et}](PF$_6$)$_3$** in acetonitrile with 3

equiv. of [AuCl(SMe$_2$)] for 16 h at room temperature. This reaction allowed the formation of the trinuclear Au$^{(I)}$ hexacarbene complex **[6B^{Et}](PF$_6$)$_3$** as an air- and moisture-stable white solid, in 70% yield.

Similarly, the transmetalation of the tris-Ag$^{(I)}$-NHC complex **[5B^{Et}](PF$_6$)$_3$** with 3 equiv. of CuI in acetonitrile at room temperature yielded the trinuclear Cu$^{(I)}$ hexacarbene complex **[7B^{Et}](PF$_6$)$_3$**, as a white solid in 64% yield. The reaction allowed the retention of the metallosupramolecular structure.

All compounds were characterized by NMR spectroscopy, mass spectrometry and elemental analysis. All details regarding the characterization of compounds **[6B^{Et}](PF$_6$)$_3$** and **[7B^{Et}](PF$_6$)$_3$** can be found in the Experimental Section (Chapter 5). Probably, the most relevant features of their NMR characterization arise from the appearance of the signal due to the metallated carbons in the ^{13}C{^{1}H NMR spectra, at (**[5B^{Et}](PF$_6$)$_3$**: 178.3 ppm; **[6B^{Et}](PF$_6$)$_3$**: 180.6 ppm; **[7B^{Et}](PF$_6$)$_3$**: 174.3 ppm). As an illustrative example, the ^{1}H NMR spectrum of **[5B^{Et}](PF$_6$)$_3$** is described below.

^{1}H NMR spectrum of [5B^{Et}](PF$_6$)$_3$

Figure 3.1 shows the ^{1}H NMR spectrum of **[5B^{Et}](PF$_6$)$_3$**. The signals attributed to the protons of the C*H* groups of the imidazolylidenes are shown at 7.99 and 7.87 ppm (**c** and **d**). The signals corresponding to the protons of 1,3,5-triphenylbenzene core (**e**, **f** and **g**) are displayed at 7.79 and 7.65 ppm. The signals due to the protons of the six ethyl groups appear at 4.43 and 1.61 ppm (**b** and **a**, for the CH$_2$ and CH$_3$ groups, respectively).
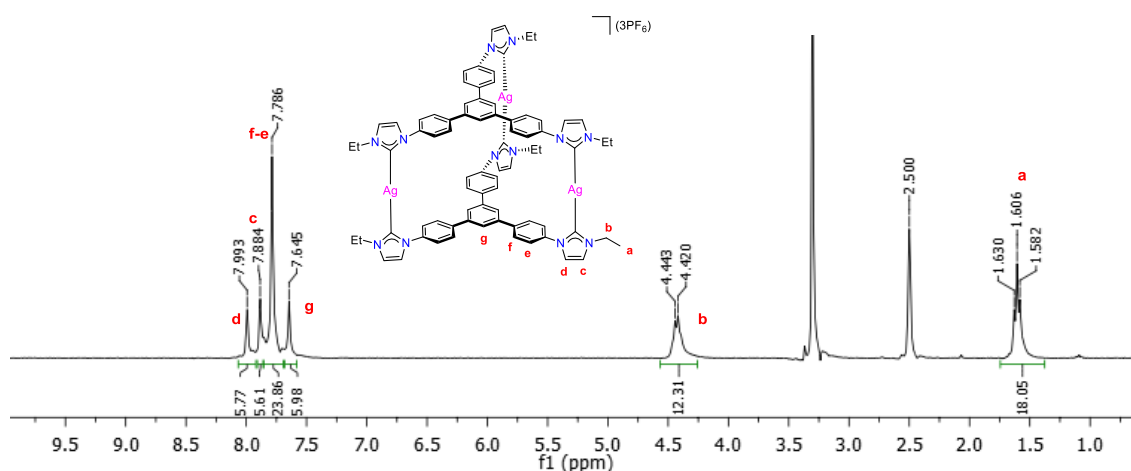
Figure 3.1. ^{1}H NMR spectrum of **[5B^{Et}](PF$_6$)$_3$** in DMSO-*d^6*

Molecular structures of [6B^{Et}](PF$_6$)$_3$

Single crystals of the gold-cage **[6B^{Et}](PF$_6$)$_3$** suitable for an X-ray diffraction study were obtained by slow vapor diffusion of diethyl ether into a saturated acetonitrile solution of the compound. The structure revealed two tris-NHC ligands sandwiching the three Au$^{(I)}$ atoms (Figure 3.2).
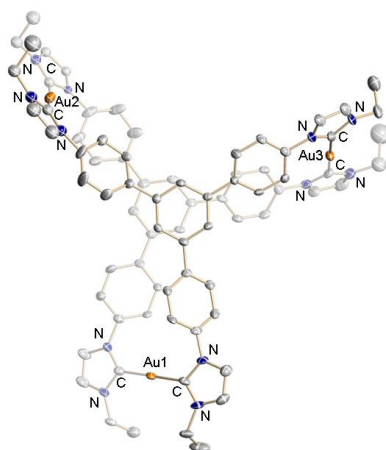
Figure 3.2. Molecular structure (top view) of trication **[6B^{Et}]$^{3+}$** in **[6B^{Et}](PF$_6$)$_3$**·CH$_3$CN·5Et$_2$O (hydrogen atoms, counterion and solvent molecules have been omitted for clarity, 50% probability ellipsoids)

Table 3.1. Selected range bond lengths and angles of complex **[6B^{Et}](PF$_6$)$_3$**

Bond lengths (Å)		Bond angles (°)	
Au(1)-C$_{NHC}$	1.918(14)–2.096(14)	**N-C$_{NHC}$-N**	101.5(10)–105.1(12)
		C$_{NHC}$-Au- C$_{NHC}$	170.5(7)–178.6(5)

The metric parameters observed in cation **[6B^{Et}]$^{3+}$** [Au-C$_{NHC}$, 1.918(14)-2.096(14) Å; C$_{NHC}$-Au-C$_{NHC}$, 170.5(7)-178.6(5)°] (Table 3.1) fall within the range of other dicarbene gold complexes reported in the literature.[12e, 13f, 20] The three gold atoms form a triangle featuring Au···Au separations of about 1.4 nm. The two central phenyl rings of the tris-NHC ligands are oriented in a nearly coplanar fashion where the separation between the two centroids is about 3.644 Å. We take this short separation as an indication for the presence of π··· π interactions between these rings. Related trinuclear cylinder-like assemblies obtained from tris-NHC ligands only linked by a phenylene group (see Chart 3.1) feature a much longer separation of the midpoints of the phenylene groups (M = Ag: 4.914 Å; M = Au: 4.762 Å; M = Cu: 4.239 Å).[13e] The convex distortion of **[6B^{Et}](PF$_6$)$_3$** is only possible with the 1,3,5-triphenylbenzene core. In addition, the NHC

donors are not oriented perpendicular to the aromatic backbone also contributing to the short separation of the central phenylene rings.

By assuming the molecule to adopt a pseudo-triangular prismatic structure, we may estimate the internal volume of the cavity as 360 Å^3, which is significantly larger than the volume estimated for the previously reported tri-Au$^{(I)}$ structures by Hahn and co-workers[13c, e] (the volume of the cavity of this previously reported structure is estimated as 72 Å^3) (see Chart 3.1, **I**). To accommodate the C_{NHC}-Au-C_{NHC} bonds of about 4.0 Å, the imidazolium rings are pushed out of the plane of the central phenyl group towards the outside of the cylinder giving the tris-carbene a convex geometry (Figure 3.3)
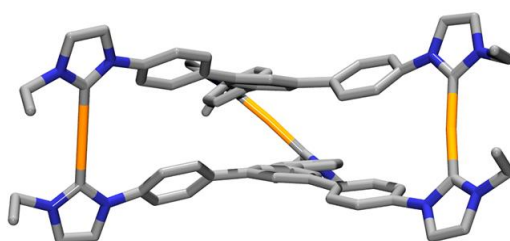
Figure 3.3. Schematic representation of the molecular structure (side view) of cation **[6B^{Et}](PF$_6$)$_3$** showing the the π···π interactions between the two central phenyl rings and the non-planar geometry of the tris-carbene ligands.

3.2.1.2 Tris-MIC metallacages

Parallel to the rapid growth of NHCs, mesoionic carbenes (MICs)[21] have recently emerged as a powerful subclass of NHCs due to their ease of accessibility and their arguably stronger electron donor properties compared to the classical NHC-analogues.[22] While monometallic complexes bearing mono-MIC ligands are widely used, poly-MIC ligands are not common,[17, 23] and this explains why MIC-based supramolecular assemblies were unknown before we started our work in the field.

The synthesis and characterization of the tris-triazolium salt **[H$_3$C^{Mes}](PF$_6$)$_3$** (Scheme 3.2) was described in Chapter 2. The reaction of **[H$_3$C^{Mes}](PF$_6$)$_3$** with 1.5 equivalents of Ag$_2$O in MeOH at 60 °C, afforded the tris-Ag$^{(I)}$–MIC-cage **[5C^{Mes}](PF$_6$)$_3$** in 42% yield. Compound **[H$_3$C^{Mes}](PF$_6$)$_3$** is the first MIC-based self-assembly structure reported to date.
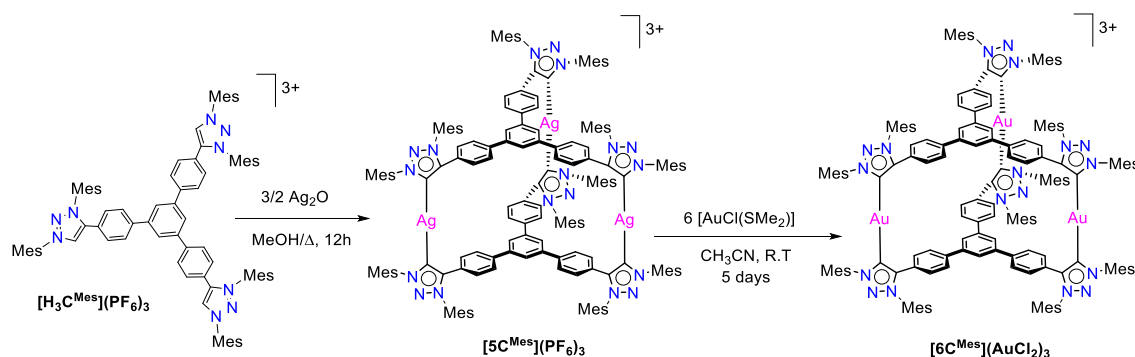
Scheme 3.2. Synthesis of **[5C^{Mes}](PF₆)₃** and **[6C^{Mes}](AuCl₂)₃**

The reaction of **[5C^{Mes}](PF₆)₃** with six equivalents of [AuCl(SMe₂)] in acetonitrile at room temperature during 5 days, led to the formation of the trinuclear hexa-MIC complex **[6C^{Mes}](AuCl₂)₃**, as an air-stable white solid, in 63% yield. The use of the excess of Au explains the formation of **[6C^{Mes}](AuCl₂)₃** with three (AuCl₂)⁻ counter-anions.

Compounds **[5C^{Mes}](PF₆)₃** and **[6C^{Mes}](AuCl₂)₃** were characterized by means of NMR spectroscopy, mass spectrometry and elemental analysis. All the details regarding the characterization of compound **[6C^{Mes}](AuCl₂)₃** can be found in the Experimental Section (Chapter 5).

The $^{13}C\{^1H\}$ NMR spectrum of **[5C^{Mes}](PF₆)** shows the resonance due to the equivalent metallated carbene-carbon atoms at 169.7 ppm, exhibiting the coupling to both silver isotopes ($^1J_{C-Ag(107)}$ = 165.0 Hz, $^1J_{C-Ag(109)}$ = 190.5 Hz). The $^{13}C\{^1H\}$ NMR spectrum of **[6C^{Mes}](AuCl₂)₃** shows a single signal at 161.1 ppm. As an illustrating example of the NMR characterization of the compounds, the ^1H NMR spectrum of **[5C^{Mes}](PF₆)₃** is described below.

^1H NMR spectrum of [5C^{Mes}](PF₆)₃

The ^1H NMR spectrum of **[5C^{Mes}](PF₆)₃** (Figure 3.4) indicates that the compound is highly symmetric, as shown by the appearance of four signals due to the protons of the methyl at the mesityl groups (four signals with relative integrals 18:18:36:36). The absence of the signal due to the acidic protons of the N*H*CC groups, provides a preliminary indication that the coordination of **[H₃C^{Mes}](PF₆)₃** to Ag$^{(I)}$ has occurred. The signals assigned to the protons of the 1,3,5-triphenylbenzene core (**a**, **c** and **b**) are displayed at 7.52, 7.43 and 7.36 ppm, respectively. The signals due to the aromatic

protons of the mesityl groups appear at 7.05 and 7.00 ppm, and those due to the methyl groups appear as four singlets between 2.04 and 2.54 ppm.
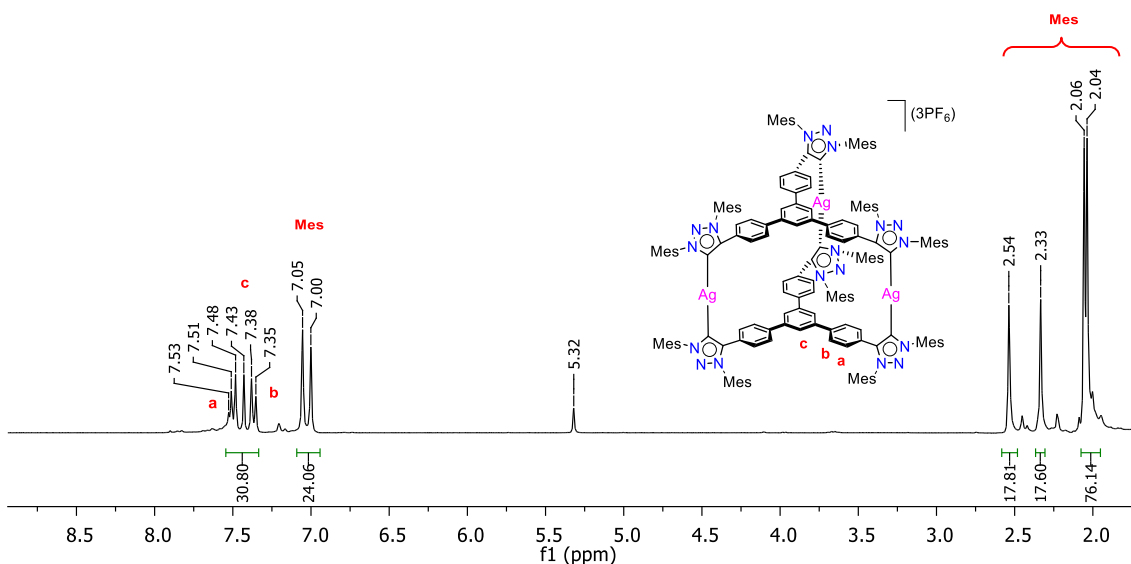
Figure 3.4. ^{1}H NMR spectrum of **[5C^{Mes}](PF$_6$)$_3$** in CD$_2$Cl$_2$

Molecular structure of [5C^{Mes}](PF$_6$)$_3$

The molecular structure of **[5C^{Mes}](PF$_6$)$_3$** was confirmed by X-ray diffraction studies (Figure 3.5). The structure consists of two tris-MIC ligands sandwiching the three silver atoms, thus rendering a hexacarbene complex cation, with three PF$_6$$^-$ counter-anions.

Figure 3.5. Molecular structure of complex **[5C^{Mes}](PF$_6$)$_3$** from different views (hydrogen atoms and counterions (3PF$_6$$^-$) omitted for clarity. Mesityl groups are represented as wireframes for clarity. Ellipsoids at 50% of probability.
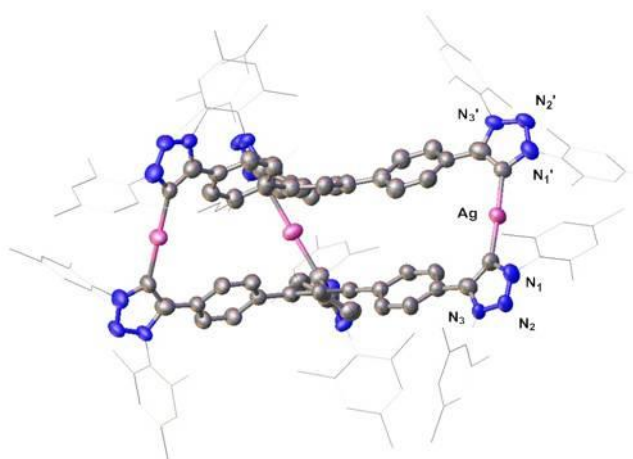
The average distance of the Ag-C$_{MIC}$ bonds is 2.105(7) Å, and the C$_{MIC}$-Ag-C$_{MIC}$ angle is 177.0°. The distance between the two central phenylene rings is of 4.318 Å. The three

silver atoms form a triangle, with an average Ag-Ag separation of about 13.96 Å. (Table 3.2)

Table 3.2. Selected bond lengths and angles of complex **[5C^{Mes}](PF$_6$)$_3$**

Bond lengths (Å)		Bond angles (°)	
Ag(1)-C$_5$	2.113 (7)	**N$_1$-C$_5$-N$_4$**	101.4 (6)
Ag(1)-C$_{5'}$	2.097 (7)	**N$_{1'}$-C$_{5'}$-N$_{4'}$**	103.5 (6)
		C$_5$-Ag- C$_{5'}$	177.9 (3)

3.2.2 Synthesis and characterization of a MIC-NHC mixed metallacage

Albrecht and Cazin recently described a methodology for the preparation of heteroleptic metal complexes based on coinage metals featuring either two bis-MIC or bis-NHC ligands.[21c, 24] Interestingly, the spontaneous recombination of MIC-ligands in the presence of silver salts allowed the preparation of bis-MIC-Au complexes.[24] Due to the similarities between NHC and MIC ligands and their complex-cage derivatives, we decided to see if we could obtain a cylinder-type coordination complex combining the presence of both, tris-NHC and tris-MIC ligands. The preparation of such type of complex is very interesting because it would allow us to design a methodology for obtaining coordination cages with two different types of carbenes. In order to prepare this heteroleptic cage, we decided to directly react an equimolecular amount of the tris-azolium salts **[H$_3$C^{Mes}](PF$_6$)$_3$** and **[H$_3$B^{Et}](PF$_6$)$_3$**, in the presence of three equivalents of Ag$_2$O in MeOH at 60°C for 12 hours (Scheme 3.3).

Assuming a random distribution of the two ligands over the three metal centers, this reaction should allow us to obtain the mixed NHC-MIC cage in 50% yield, together with 25% of each homoleptic cage. However, our expectations were exceeded, because the mixed NHC-MIC cage was the only metal-based species detected when we analyzed the reaction products by ESI mass spectroscopy (a main peak at *m/z* 1136.8 assigned to [M+PF$_6$]$^{2+}$ was observed). The purification of the resulting metal complex, allowed us to obtain the mixed NHC-MIC cage (**[1B^{Et}C^{Mes}](PF$_6$)$_3$**) in 45 % yield, which is very close to the yield that we should have expected for the formation of this compound, assuming a random distribution of the two ligands about the trimetallic structure (50%), as mentioned previously.
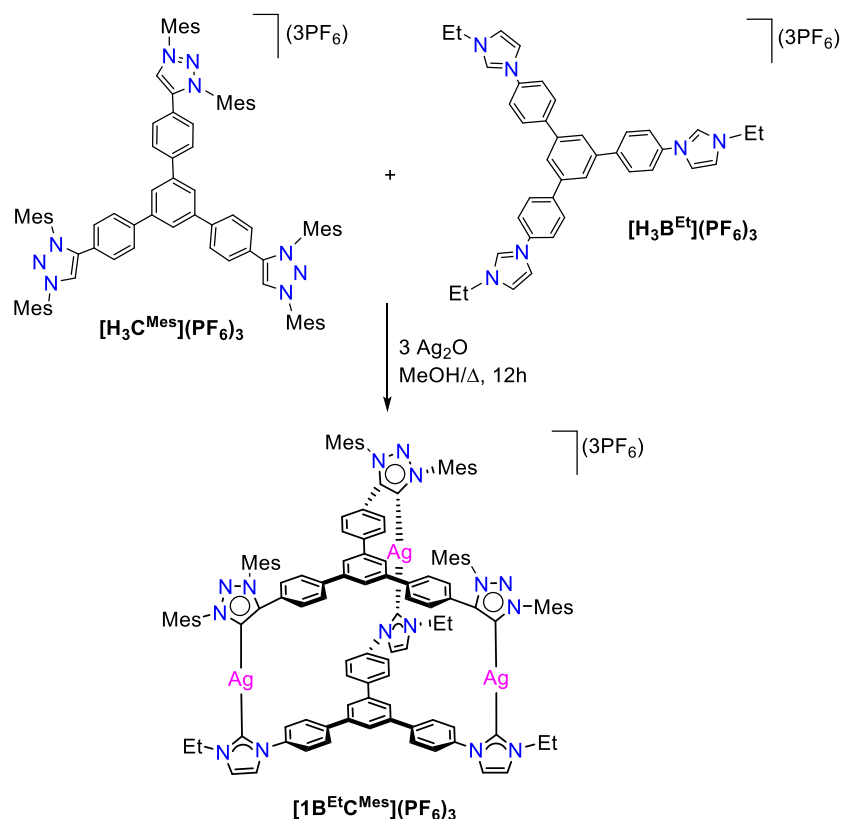
Scheme 3.3. Synthesis of **[1B^{Et}C^{Mes}](PF_6)_3**

The mixed NHC-MIC silver-based coordination cage **[1B^{Et}C^{Mes}](PF_6)_3** was characterized by NMR spectroscopy, mass spectrometry and elemental analysis.

*^1H NMR spectrum of **[1B^{Et}C^{Mes}](PF_6)_3***

The ^1H NMR spectrum of **[1B^{Et}C^{Mes}](PF_6)_3** (Figure 3.6) revealed the presence of the two different types of tris-carbene ligands. The number of signals and their integration are consistent with the threefold symmetry of the complex.
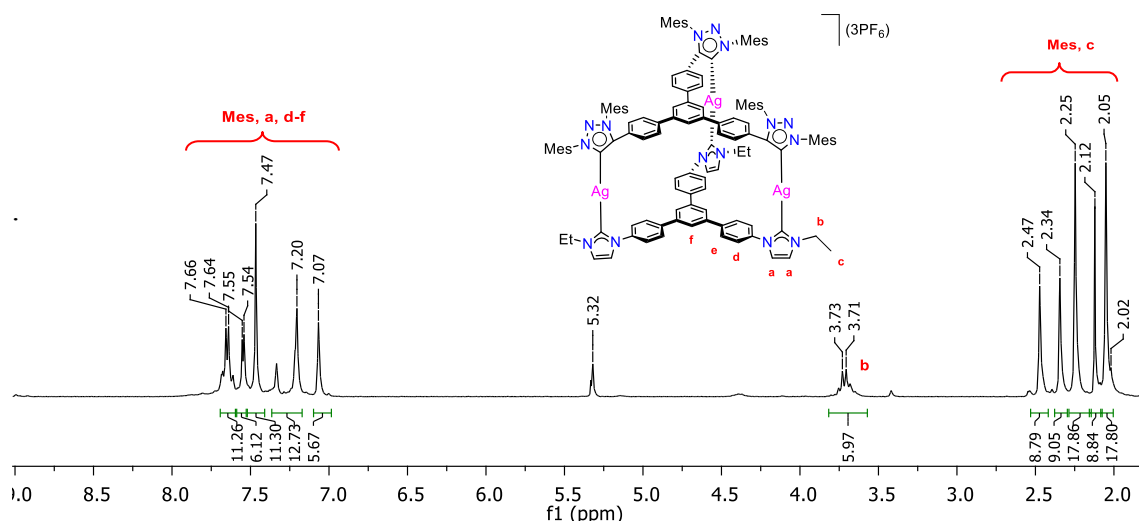
Figure 3.6. ^1H NMR spectrum of **[1B^{Et}C^{Mes}](PF_6)_3** in CD_2Cl_2

$^{13}C\{^1H\}$ NMR spectrum of [1B^{Et}C^{Mes}](PF$_6$)$_3$

The $^{13}C\{^1H\}$ NMR spectrum of **[1B^{Et}C^{Mes}](PF$_6$)$_3$** shows the distinct signals due to the presence of the two types of carbene carbons (**1**) and (**1'**), both displaying the coupling with the two silver isotopes, and therefore appearing as four doublets, two centered at 179.5 ($^1J_{C-Ag(107)}$ = 177.8 Hz, $^1J_{C-Ag(109)}$ = 205.5 Hz), and the other two at 169.5 ppm ($^1J_{C-Ag(107)}$ = 177.8 Hz, $^1J_{C-Ag(109)}$ = 168.8 Hz), for the NHC and MIC carbene carbons, respectively. These resonances are practically unshifted compared to the resonances of the di-(tris-NHC) and the di-(tris-MIC) silver complexes **[5B^{Et}](PF$_6$)$_3$** (178.3 ppm) and **[5C^{Mes}](PF$_6$)$_3$** (169.7 ppm, $^1J_{C-Ag(107)}$ = 165.0 Hz, $^1J_{C-Ag(109)}$ = 190.5 Hz).[13g]
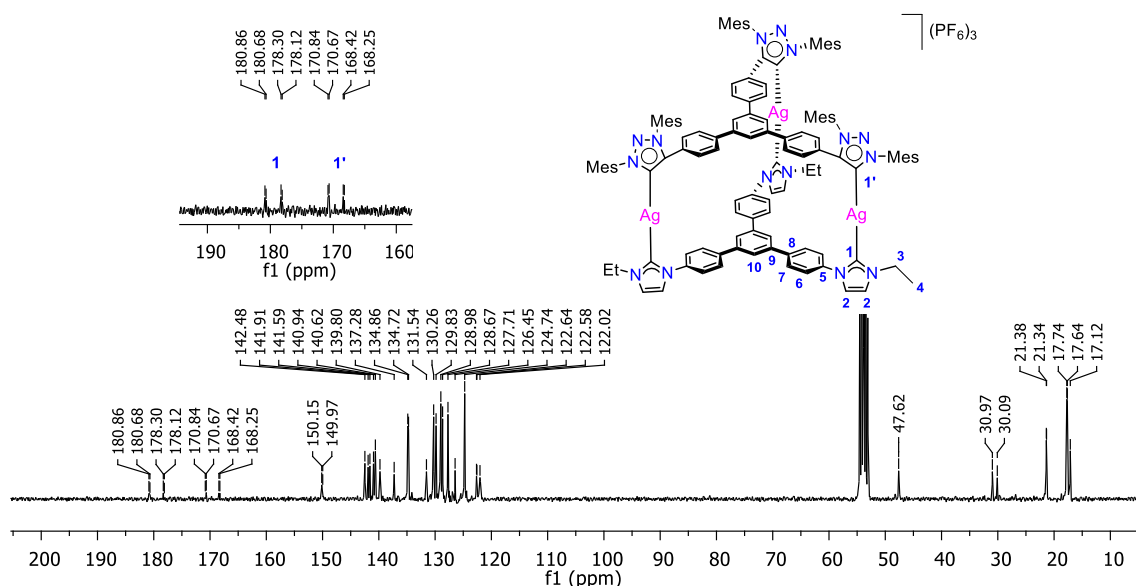
Figure 3.7. $^{13}C\{^1H\}$ NMR spectrum of **[1B^{Et}C^{Mes}](PF$_6$)$_3$** in CD$_2$Cl$_2$

3.2.2.1 Reactivity studies and ligand exchange reactions

Prompted by these encouraging results, we decided to explore a combinatorial synthetic route for the preparation of **[1B^{Et}C^{Mes}](PF$_6$)$_3$**. The reactions that we studied were: i) the reorganization of the preformed homo-MIC (**[5C^{Mes}](PF$_6$)$_3$**) and homo-NHC (**[5B^{Et}](PF$_6$)$_3$**) cages; ii) the reaction between the cage **[5C^{Mes}](PF$_6$)$_3$** and the salt **[H$_3$B^{Et}](PF$_6$)$_3$**, and iii) the reaction between the cage **[5B^{Et}](PF$_6$)$_3$** and the salt **[H$_3$C^{Mes}](PF$_6$)$_3$**. All reactions were carried out in MeOH at 60°C for 12 h. The schematic representation of these processes is depicted in Scheme 3.4).
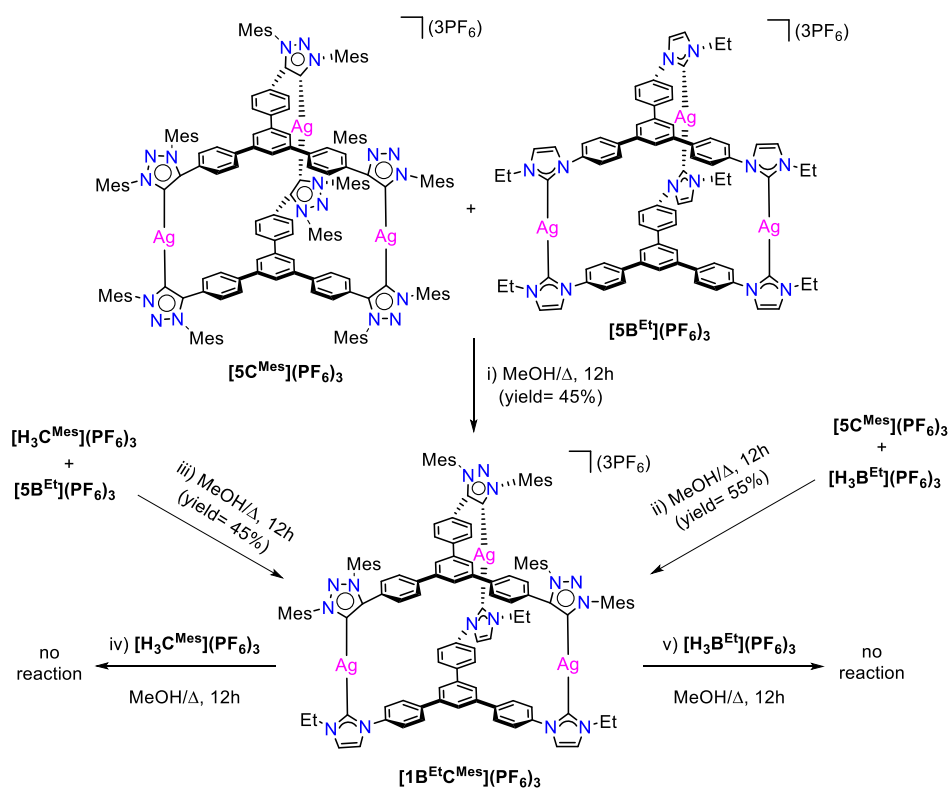
Scheme 3.4. Study of reactivity

The study of the products resulting from each reaction revealed that processes, i), ii) and iii) produced the mixed NHC-MIC cage **[1B^Et^C^Mes^](PF₆)₃** in 40-50 % yield, as the only detected (mass spectrometry) and isolable product. Processes iv) and v) (Scheme 3.4), involving the reaction of equimolecular amounts of **[1B^Et^C^Mes^](PF₆)₃** and **[H₃C^Mes^](PF₆)₃** (iv), and the reaction of equimolecular amounts of **[1B^Et^C^Mes^](PF₆)₃** and **[H₃B^Et^](PF₆)₃** (v), did not show any reorganization of the carbene ligands, and complex **[1B^Et^C^Mes^](PF₆)₃** was quasi-quantitatively recovered from the reaction mixtures.

DFT studies

These results indicate that, regardless of the thermodynamic of the overall reactions, the mixed MIC-NHC complex **[1B^Et^C^Mes^](PF₆)₃** can be formed and isolated from reactions involving the combination of the two tris-carbene-based metallocages, or by reaction of each tris-carbene-based metallocages with the related azolium salt, as depicted in Scheme 3.4. The reorganization of the ligand is also kinetically favored, as silver carbenes are often used for carbene transfer processes,[15b, 25] although in our case, we

show an unusual example of carbene transfer affording an intermolecular recombination of ligands.

In order to shed some light on these results, and to determine if the formation of the mixed MIC-NHC complex **[1B^{Et}C^{Mes}](PF$_6$)$_3$** is thermodynamically favorable compared to **[5C^{Mes}](PF$_6$)$_3$** and **[5B^{Et}](PF$_6$)$_3$**, we decided to calculate the thermodynamic parameters of reaction i) shown in Scheme 3.4 by M06L DFT calculations. Since good-quality computational modelling of the complete structures **[5C^{Mes}](PF$_6$)$_3$**, **[5B^{Et}](PF$_6$)$_3$**, and **[1B^{Et}C^{Mes}](PF$_6$)$_3$** is impossible, the calculations were performed on the mononuclear analogues, which optimized geometries are shown in Figure 3.8. These studies were performed by Prof. Dmitri Gusev (Wilfrid Laurier University, Canada).
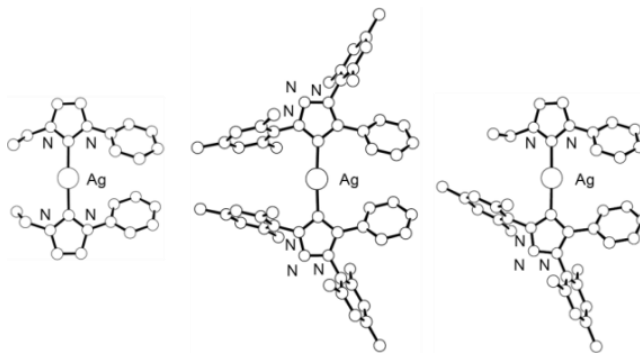
Figure 3.8. Calculated structures of [Ag(NHC)$_2$]$^+$, [Ag(MIC)$_2$]$^+$, and [Ag(MIC)(NHC)]$^+$ complexes (all hydrogen atoms are omitted for clarity).

In methanol, the formation of the mixed carbene complex, [Ag(NHC)$_2$]$^+$ + [Ag(MIC)$_2$]$^+$ → 2 [Ag(NHC)(MIC)]$^+$, is thermo-neutral: ΔH = 0.0 kcal/mol, whereas in the benzene (less polar) this reaction is slightly favorable: ΔH = -1.6 kcal/mol. The calculated Ag-C bond enthalpy is stronger for the MIC-Ag bond than for the NHC-Ag one in [Ag(NHC)(MIC)]$^+$ (44.0 *vs.* 41.8 kcal/mol in methanol).
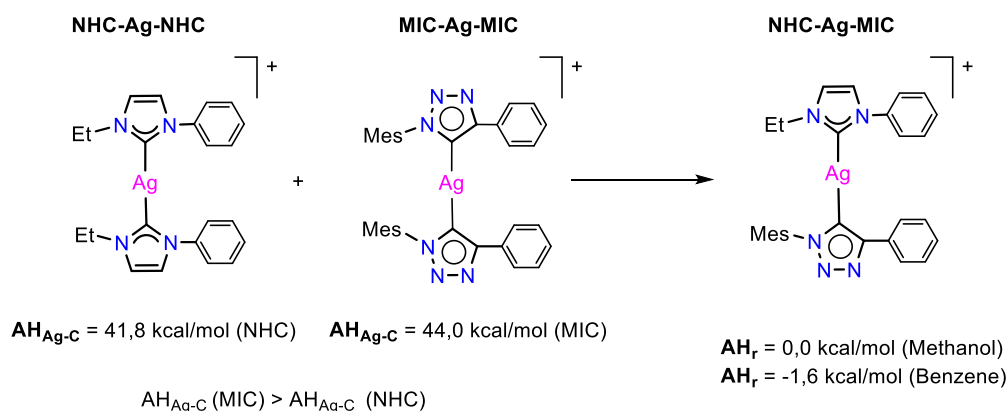
Scheme 3.5. Standard enthalpy of the formation of a NHC-Ag-MIC complex

Based on the computed energies, the mixed carbene complex is predicted to be the main species under equilibrium conditions, and the reasons to be the only isolated complex should be attributed to factors beyond those that we should take into account by DFT studies (solubility of the complex, interactions of **[5C^{Mes}](PF$_6$)$_3$**, **[5B^{Et}](PF$_6$)$_3$**, and **[1B^{Et}C^{Mes}](PF$_6$)$_3$** with the counter-ions [PF$_6$]$^-$, or explicit interactions with the solvent).

3.3 Conclusions

In this Chapter we described the synthesis of a new family of nanometer-sized cylinder-like trinuclear cages based on coinage metals using tris-NHC and tris-MIC ligands. The homoleptic Ag$^{(I)}$-cages (**[5B^{Et}](PF$_6$)$_3$** and **[5C^{Mes}](PF$_6$)$_3$**) can be readily prepared via metal-controlled self-assembly. The trinuclear silver complex **[5B^{Et}](PF$_6$)$_3$** undergoes transmetallation with [AuCl(SMe$_2$)] or CuI to form the corresponding homotrinuclear hexacarbene complexes **[6B^{Et}](PF$_6$)$_3$**, **[7B^{Et}](PF$_6$)$_3$** respectively. Parallel to this, trinuclear gold complex **[6C^{Mes}](PF$_6$)$_3$** was also obtained via transmetallation by reacting **[5C^{Mes}](PF$_6$)$_3$** with [AuCl(SMe$_2$)]. In all cases, the cylinder-like architecture was maintained. Two of these cages have been characterised by X-ray diffraction. The new structures show a large cavity volume, and may be related to previous cylinder-like hexa-NHC structures developed by our group.[13f] The presence of the cavity suggests that further studies may be needed for the utilization of these species for the encapsulation of aromatic guests.

Finally, we were able to synthesize a unique heteroleptic NHC-MIC cylinder-shaped cage (**[1B^{Et}C^{Mes}](PF$_6$)$_3$**), by the recombination of the ligands in the related MIC- and NHC-based cylinders, and by several other combinations. This reaction involves an

unusual rearrangement, which clearly illustrates the liability of the tris-NHC and tris-MIC ligands on silver in solution, paving the way for new applications such as guest release, or latent catalysis.

3.4 References

[1]   J. M. Lehn, A. Rigault, J. Siegel, J. Harrowfield, B. Chevrier and D. Moras, *Proc. Natl. Acad. Sci. U. S. A.* **1987**, *84*, 2565-2569.

[2]   E. C. Constable, *Chem. Ind.* **1994**, 56-59.

[3]   a) M. Fujita, *Chem. Soc. Rev.* **1998**, *27*, 417-425; b) M. Fujita, M. Tominaga, A. Hori and B. Therrien, *Acc. Chem. Res.* **2005**, *38*, 369-378.

[4]   D. L. Caulder and K. N. Raymond, *Acc. Chem. Res.* **1999**, *32*, 975-982.

[5]   a) P. J. Stang and B. Olenyuk, *Acc. Chem. Res.* **1997**, *30*, 502-518; b) S. Leininger, B. Olenyuk and P. J. Stang, *Chem. Rev.* **2000**, *100*, 853-907; c) R. Chakrabarty, P. S. Mukherjee and P. J. Stang, *Chem. Rev.* **2011**, *111*, 6810-6918; d) T. R. Cook, Y.-R. Zheng and P. J. Stang, *Chem. Rev.* **2013**, *113*, 734-777.

[6]   a) J. R. Nitschke, *Acc. Chem. Res.* **2007**, *40*, 103-112; b) M. M. J. Smulders, I. A. Riddell, C. Browne and J. R. Nitschke, *Chem. Soc. Rev.* **2013**, *42*, 1728-1754; c) A. M. Castilla, W. J. Ramsay and J. R. Nitschke, *Acc. Chem. Res.* **2014**, *47*, 2063-2073; d) S. Zarra, D. M. Wood, D. A. Roberts and J. R. Nitschke, *Chem. Soc. Rev.* **2015**, *44*, 419-432.

[7]   a) E. C. Constable, *Chem. Soc. Rev.* **2007**, *36*, 246-253; b) E. C. Constable, *Coord. Chem. Rev.* **2008**, *252*, 842-855; c) E. C. Constable, *Chem. Soc. Rev.* **2013**, *42*, 1637-1651.

[8]   a) P. J. Steel and C. M. Fitchett, *Coord. Chem. Rev.* **2008**, *252*, 990-1006; b) M. D. Ward, *Chem. Commun.* **2009**, 4487-4499; c) P. Dydio and J. N. H. Reek, *Chem. Sci.* **2014**, *5*, 2135-2145.

[9]   a) M. D. Pluth and K. N. Raymond, *Chem. Soc. Rev.* **2007**, *36*, 161-171; b) B. Birkmann, A. W. Ehlers, R. Frohlich, K. Lammertsma and F. E. Hahn, *Chem. Eur. J.* **2009**, *15*, 4301-4311; c) Y.-F. Han, W.-G. Jia, Y.-J. Lin and G.-X. Jin, *Angew. Chem. Int. Ed.* **2009**, *48*, 6234-6238; d) P. Mal, B. Breiner, K. Rissanen and J. R. Nitschke, *Science* **2009**, *324*, 1697-1699; e) J. W. Leeland, F. J. White and J. B. Love, *J. Am. Chem. Soc.* **2011**, *133*, 7320-7323; f) P. D. Frischmann and M. J. MacLachlan, *Chem. Soc. Rev.* **2013**, *42*, 871-890.

[10]   a) F. Wurthner, C. C. You and C. R. Saha-Moller, *Chem. Soc. Rev.* **2004**, *33*, 133-146; b) P. J. Steel, *Acc. Chem. Res.* **2005**, *38*, 243-250.

[11]   a) J. A. Mata, M. Poyatos and E. Peris, *Coord. Chem. Rev.* **2007**, *251*, 841-859; b) M. Poyatos, J. A. Mata and E. Peris, *Chem. Rev.* **2009**, *109*, 3677-3707.

[12] a) M. Viciano, M. Sanau and E. Peris, *Organometallics* **2007**, *26*, 6050-6054; b) F. E. Hahn, C. Radloff, T. Pape and A. Hepp, *Organometallics* **2008**, *27*, 6408-6410; c) C. Radloff, F. E. Hahn, T. Pape and R. Fröhlich, *Dalton Trans.* **2009**, 7215-7222; d) C. Radloff, J. J. Weigand and F. E. Hahn, *Dalton Trans.* **2009**, 9392-9394; e) F. M. Conrady, R. Fröhlich, C. Schulte to Brinke, T. Pape and F. E. Hahn, *J. Am. Chem. Soc.* **2011**, *133*, 11496-11499; f) M. Schmidtendorf, T. Pape and F. E. Hahn, *Angew. Chem. Int. Ed.* **2012**, *51*, 2195-2198.

[13] a) F. E. Hahn, C. Radloff, T. Pape and A. Hepp, *Chem. Eur. J.* **2008**, *14*, 10900-10904; b) C. Radloff, H. Y. Gong, C. Schulte to Brinke, T. Pape, V. M. Lynch, J. L. Sessler and F. E. Hahn, *Chem. Eur. J.* **2010**, *16*, 13077-13081; c) A. Rit, T. Pape and F. E. Hahn, *J. Am. Chem. Soc.* **2010**, *132*, 4572-4573; d) D. H. Wang, B. G. Zhang, C. He, P. Y. Wu and C. Y. Duan, *Chem. Commun.* **2010**, *46*, 4728-4730; e) A. Rit, T. Pape, A. Hepp and F. E. Hahn, *Organometallics* **2011**, *30*, 334-347; f) C. Segarra, G. Guisado-Barrios, F. E. Hahn and E. Peris, *Organometallics* **2014**, *33*, 5077-5080; g) N. Sinha, F. Roelfes, A. Hepp, C. Mejuto, E. Peris and F. E. Hahn, *Organometallics* **2014**, *33*, 6898-6904.

[14] a) O. Guerret, S. Sole, H. Gornitzka, M. Teichert, G. Trinquier and G. Bertrand, *J. Am. Chem. Soc.* **1997**, *119*, 6668-6669; b) A. J. Boydston and C. W. Bielawski, *Dalton Trans.* **2006**, 4073-4077; c) L. Mercs, A. Neels and M. Albrecht, *Dalton Trans.* **2008**, 5570-5576; d) B. Karimi and P. F. Akhavan, *Chem. Commun.* **2009**, 3750-3752; e) L. Mercs, A. Neels, H. Stoeckli-Evans and M. Albrecht, *Dalton Trans.* **2009**, 7168-7178; f) J. Choi, H. Y. Yang, H. J. Kim and S. U. Son, *Angew. Chem. Int. Ed.* **2010**, *49*, 7718-7722; g) B. Karimi and P. F. Akhavan, *Chem. Commun.* **2011**, *47*, 7686-7688; h) B. Karimi and P. F. Akhavan, *Inorg. Chem.* **2011**, *50*, 6063-6072; i) C. Zhang, J. J. Wang, Y. Liu, H. Ma, X. L. Yang and H. B. Xu, *Chem. Eur. J.* **2013**, *19*, 5004-5008; j) S. Gonell, M. Poyatos and E. Peris, *Chem. Eur. J.* **2014**, *20*, 5746-5751.

[15] a) J. C. Garrison and W. J. Youngs, *Chem. Rev.* **2005**, *105*, 3978-4008; b) I. J. B. Lin and C. S. Vasam, *Coord. Chem. Rev.* **2007**, *251*, 642-670; c) J. C. Y. Lin, R. T. W. Huang, C. S. Lee, A. Bhattacharyya, W. S. Hwang and I. J. B. Lin, *Chem. Rev.* **2009**, *109*, 3561-3598.

[16] E. Peris, *Chem. Commun.* **2016**, *52*, 5777-5787.

[17] a) G. Guisado-Barrios, J. Bouffard, B. Donnadieu and G. Bertrand, *Organometallics* **2011**, *30*, 6017-6021; b) D. I. Bezuidenhout, G. Kleinhans, G.

Guisado-Barrios, D. C. Liles, G. Ung and G. Bertrand, *Chem. Commun.* **2014**, *50*, 2431-2433.

[18] a) W. W. H. Wong, M. S. Vickers, A. R. Cowley, R. L. Paul and P. D. Beer, *Organic & Biomolecular Chemistry* **2005**, *3*, 4201-4208; b) J. Yoon, S. K. Kim, N. J. Singh and K. S. Kim, *Chem. Soc. Rev.* **2006**, *35*, 355-360; c) M. Yoshizawa, M. Tamura and M. Fujita, *Science* **2006**, *312*, 251-254; d) M. D. Pluth, R. G. Bergman and K. N. Raymond, *Science* **2007**, *316*, 85-88; e) B. Birkmann, R. Froehlich and F. E. Hahn, *Chem. Eur. J.* **2009**, *15*, 9325-9329.

[19] a) C. Mejuto, G. Guisado-Barrios and E. Peris, *Organometallics* **2014**, *33*, 3205-3211; b) C. Mejuto, G. Guisado-Barrios, D. Gusev and E. Peris, *Chem. Commun.* **2015**, *51*, 13914-13917; c) C. Mejuto, B. Royo, G. Guisado-Barrios and E. Peris, *Beilstein J. Org. Chem.* **2015**, *11*, 2584-2590.

[20] a) Q.-X. Liu, Z.-Q. Yao, X.-J. Zhao, A.-H. Chen, X.-Q. Yang, S.-W. Liu and X.-G. Wang, *Organometallics* **2011**, *30*, 3732-3739; b) J. Cure, R. Poteau, I. C. Gerber, H. Gornitzka and C. Hemmert, *Organometallics* **2012**, *31*, 619-626.

[21] a) G. Guisado-Barrios, J. Bouffard, B. Donnadieu and G. Bertrand, *Angew. Chem. Int. Ed.* **2010**, *49*, 4759-4762; b) R. H. Crabtree, *Coord. Chem. Rev.* **2013**, *257*, 755-766; c) K. F. Donnelly, A. Petronilho and M. Albrecht, *Chem. Commun.* **2013**, *49*, 1145-1159.

[22] P. Mathew, A. Neels and M. Albrecht, *J. Am. Chem. Soc.* **2008**, *130*, 13534-13535.

[23] a) J. Cai, X. Yang, K. Arumugam, C. W. Bielawski and J. L. Sessler, *Organometallics* **2011**, *30*, 5033-5037; b) M. T. Zamora, M. J. Ferguson and M. Cowie, *Organometallics* **2012**, *31*, 5384-5395; c) E. C. Keske, O. V. Zenkina, R. Wang and C. M. Crudden, *Organometallics* **2012**, *31*, 456-461; d) E. C. Keske, O. V. Zenkina, R. Wang and C. M. Crudden, *Organometallics* **2012**, *31*, 6215-6221; e) R. Maity, S. Hohloch, C.-Y. Su, M. van der Meer and B. Sarkar, *Chem. Eur. J.* **2014**, *20*, 9952-9961; f) R. Maity, M. van der Meer and B. Sarkar, *Dalton Trans.* **2015**, *44*, 46-49; g) S. Hohloch, S. Kaiser, F. L. Duecker, A. Bolje, R. Maity, J. Kosmrlj and B. Sarkar, *Dalton Trans.* **2015**, *44*, 686-693; h) R. Maity, M. Van der Meer, S. Hohloch and A. Sarkar, *Organometallics* **2015**, *34*, 3090-3096.

[24] a) D. Canseco-Gonzalez, A. Petronilho, H. Mueller-Bunz, K. Ohmatsu, T. Ooi and M. Albrecht, *J. Am. Chem. Soc.* **2013**, *135*, 13193-13203; b) F. Lazreg, D. B. Cordes, A. M. Z. Slawin and C. S. J. Cazin, *Organometallics* **2015**, *34*, 419-425.

[25] a) I. J. B. Lin and C. S. Vasam, *Comments Inorg. Chem.* **2004**, *25*, 75-129; b) C. E. Strasser, E. Stander-Grobler, O. Schuster, S. Cronje and H. G. Raubenheimer, *Eur. J. Inorg. Chem.* **2009**, 1905-1912.

Chapter 4

A Corannulene-Bridged Bis-N-Heterocyclic Carbene: Synthesis, Coordination and Supramolecular Properties

4.1 Introduction

During the last few years, a great effort has been devoted to the preparation of di- and tris-N-heterocyclic carbene ligands connected by polyaromatic linkers, because they were thought to be beneficial for the development of improved materials with applications in homogeneous catalysts and materials chemistry.[1] In this context, our group actively contributed to the field by developing a series of rigid di- and tris-N-heterocyclic carbene ligands (Chart 4.1).[2]
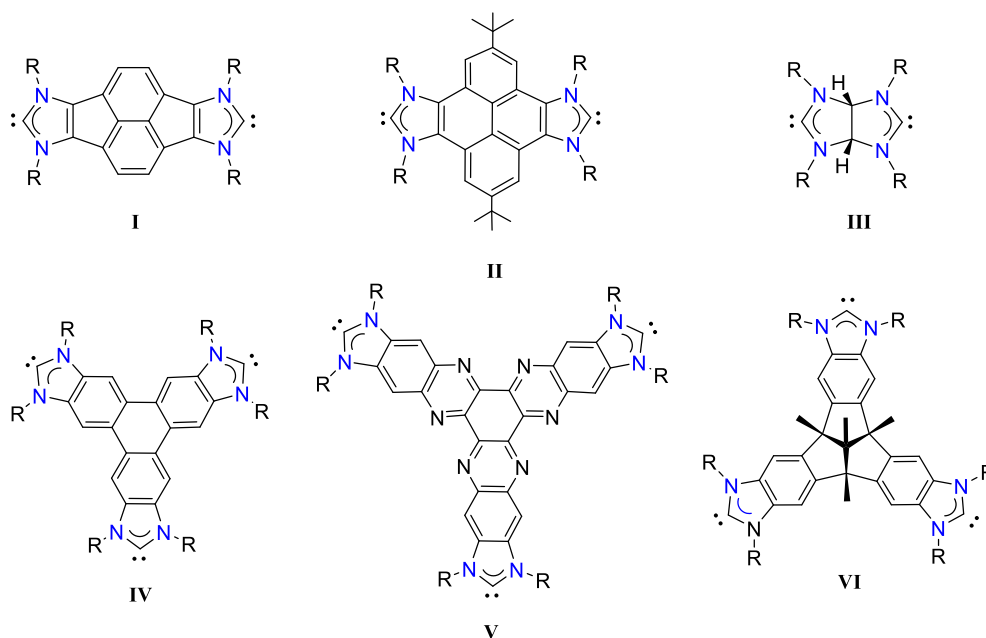
Chart 4.1. Examples of di- (**I**, **II**, **III**) and tris-N-heterocyclic (**IV**, **V**, **VI**) carbene ligands

In a continuation of this research, we turned our attention to corannulene as an alternative to the known planar polyaromatic linkers used in the design of previous rigid bis-NHC ligands. Corannulene is a bowl-shaped polyaromatic hydrocarbon with unique electronic and topologic features.[3] We thought that a corannulene derivative bearing bis-NHC moieties in its periphery could be applied not only in catalysis but also in supramolecular binding studies with fullerenes.
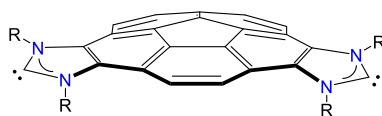
Chart 4.2. Corannulene-based NHC ligand

Shape complementary is probably the most important factor to consider in the design of supramolecular-based receptors. Since the discovery of fullerenes, the interaction of their curved conjugated surfaces with properly assembled polyaromatic systems has been an area of intense research.[4] The main target of this research is to find effective receptors that provide selective association of specific fullerenes to facilitate their separation from complex mixtures.[5] Bowl-shaped polyaromatic hydrocarbons, such as corannulene, which can now be prepared on the kg scale,[6] have demonstrated to be among the best candidates to build fullerene receptors, due to the complementarity of their concave and convex surfaces.[3c] However, although it has been computationally demonstrated that the complexation of corannulene to C_{60} should be energetically favorable in the gas phase,[7] and it has also been detected in the solid state,[8] no evidence of significant binding affinity of the two has been reported in solution. Some sophisticated receptors combining several tethered corannulene subunits, so-called 'buckycatchers', showed affinity for the formation of host-guest complexes with fullerenes in solution (some representative examples are **VII-IX**, shown in Chart 4.3).[9]
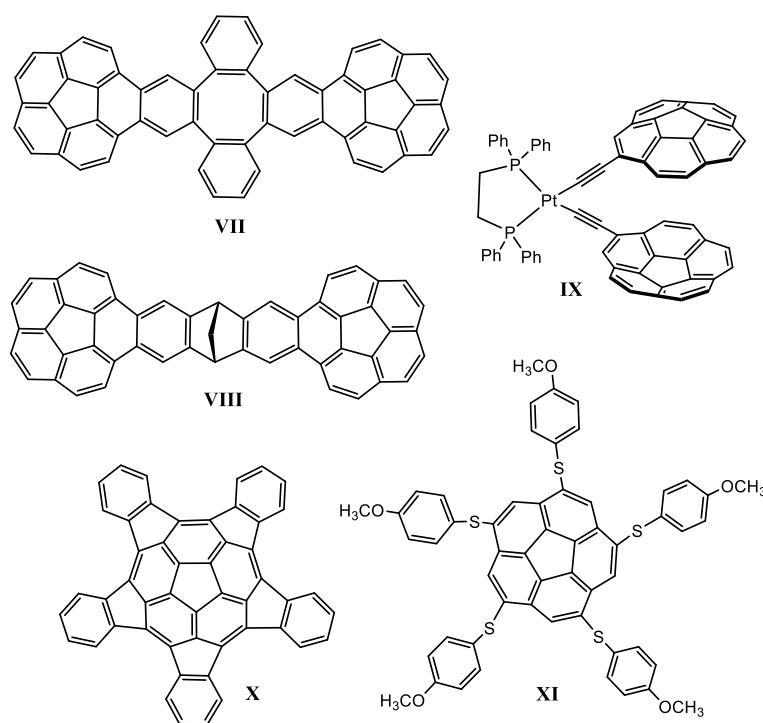
Chart 4.3. Examples of compounds based on the corannulene core

On the other hand, pentaindenocorannulene (**X**) displays a cap curvature similar to corannulene, but the presence of the five benzofingers creates a larger surface area and also a larger bowl depth.[7d, 10] In this context, a recent study described the formation of assemblies of pentaindenocorannulene with C_{60} in solution and in the solid state,[11] thus evidencing that this extended form of corannulene is a better receptor for recognizing fullerenes. Similarly, corannulene derivatives with geodesic electron-rich arms (**XI**) were found to form 1:1 complexes with C_{60} in toluene solution, with association constants ranging from 200 to 400 M^{-1}.[12] This finding was interpreted as a consequence of the enhanced attractive noncovalent interaction between the electronically complementary surfaces of the functionalized corannulene and C_{60}, due to the introduction of the electronrich arms.

This Chapter describes the synthesis of a set of corannulene-adorned bis-imidazolium salts, along with their coordination to $Rh^{(I)}$ and $Au^{(I)}$. The Chapter will also include molecular recognition studies focused on the interaction between a bowl-shaped gold complex and C_{60}-fullerene, by means of *host-guest* supramolecular techniques based on ^1H NMR spectroscopy, fluorescence spectroscopy, calorimetric studies and computational calculations.

The work described in this Chapter is the result of the collaboration with three different research groups. The starting material (1,2,5,6-tetrabromocorannulene), was provided by the group of Prof. Jay S. Siegel (Tianjin University, China). The group of Prof. Pau Ballester (Institut Català d'Investigació Química-ICIQ, Tarragona) performed the ITC (Isothermal Titration Calorimetry) measurements and provided guidance in the interpretation of the results derived from the supramolecular studies. Finally, Prof. Dmitri Gusev (Wilfrid Laurier University, Canada) carried out the computational studies, and provided key data for the interpretation of the results.

4.2 Results and discussion

4.2.1 Synthesis and characterization of corannulene-linked bis-imidazolium salts

The synthetic procedures employed for the preparation of the two bis-imidazolium salts with a corannulene linker are depicted in Scheme 4.1. First, tetrabromocorannulene **E**[6] is tetra-aminated with *tert*-butylamine *via* a palladium-catalyzed Buchwald-Hartwig amination[2f, 13] [the palladium catalyst is generated *in situ* from the reaction between

Pd(OAc)$_2$ and IPr·HCl (1,3-bis(2,6-diisopropylphenyl)imidazolium chloride) in the presence of NaO*t*Bu]. The reaction generates the tetraamino-corannulene **F** in almost quantitative yield (97%). The bis-annulation of **F** in neat tri-*n*-butyl orthoformate in the presence of ammonium hexafluorophosphate generates the bis-imidazolium salts **[H$_2$G^{tBu}](PF$_6$)$_2$** or **[H$_2$G^{nBu}](PF$_6$)$_2$**, depending on the reaction conditions used. The bis-azolium salt **[H$_2$G^{tBu}](PF$_6$)$_2$** (bearing *tert*-butyl N-substituents) was obtained when the reaction was carried out at room temperature during several days. In contrast, when the reaction mixture was heated at 150 ºC overnight, the bis-azolium salt **[H$_2$G^{nBu}](PF$_6$)$_2$** (with *n*-butyl wingtips) was the major product obtained. The replacement of the *tert*-butyl group by the *n*-butyl in the cyclization of *tert*-butyl substituted bis-ammino compounds using tri-*n*-butyl orthoformate, was previously observed for the preparation of several bis-azolium salts in our group,[2d, f] and it was justified as being a consequence of the steric constraints imposed during the rehybridation of the nitrogen atoms from *sp*^{3} to *sp*^{2}.
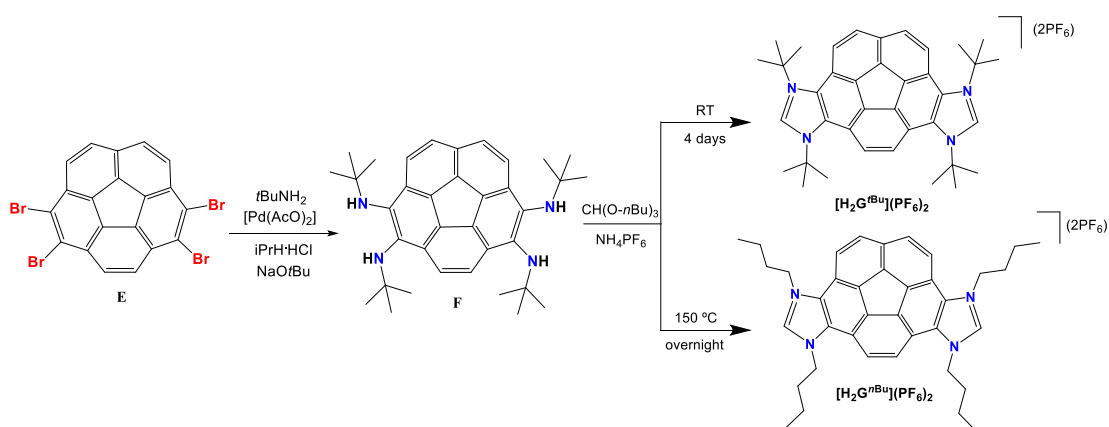
Scheme 4.1. Synthetic routes to bis-imidazolium salts **[H$_2$G^{nBu}](PF$_6$)$_2$**) and (**[H$_2$G^{tBu}](PF$_6$)$_2$**

Compounds **F**, **[H$_2$G^{nBu}](PF$_6$)$_2$** and **[H$_2$G^{tBu}](PF$_6$)$_2$** were characterized by means of NMR spectroscopy, Mass Spectrometry and Elemental Analysis. A common feature of their NMR spectra is that they are consistent with their predicted *Cs*-symmetry. As an illustrative example, the ^{1}H NMR spectrum of **[H$_2$G^{tBu}](PF$_6$)$_2$** is described below. All details regarding the synthesis and spectroscopic features of compounds **F**, **[H$_2$G^{nBu}](PF$_6$)$_2$** can be found in the Experimental Section (Chapter 5).

^{1}H NMR spectrum of [H$_2$G^{tBu}](PF$_6$)$_2$

Figure 4.1 shows the ^{1}H NMR spectrum of **[H$_2$G^{tBu}](PF$_6$)$_2$**. The singlet due to the acidic protons of the NC*H*N fragments (**e**) is displayed at 9.55 ppm. The signals assigned to the protons of the corannulene core (**a**, **b** and **c**) are displayed at 9.13(s), 8.90(d) and 8.54(d) ppm, respectively. Finally, the signal due to the protons of the *tert*-butyl groups appears at 2.32 ppm (**d**).
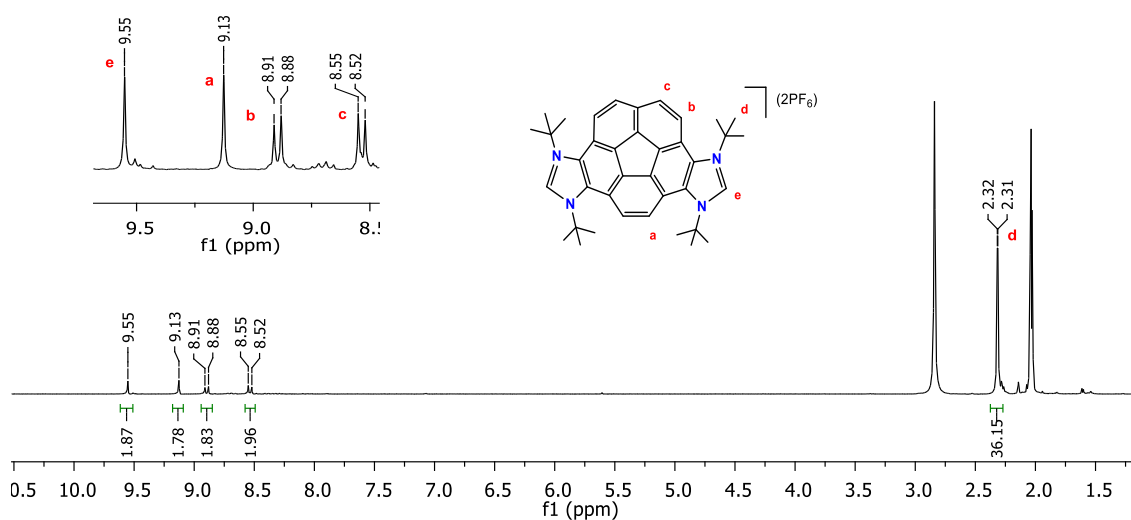
Figure 4.1. ^{1}H NMR spectrum of **[H$_2$G^{tBu}](PF$_6$)$_2$** in (CD$_3$)$_2$CO

Molecular structure of [H$_2$G^{tBu}](PF$_6$)$_2$

The molecular structure of **[H$_2$G^{tBu}](PF$_6$)$_2$** was unequivocally confirmed by single crystal X-ray diffraction (Figure 4.2). The structure reveals the presence of the two imidazolium rings bridged by the corannulene linker.
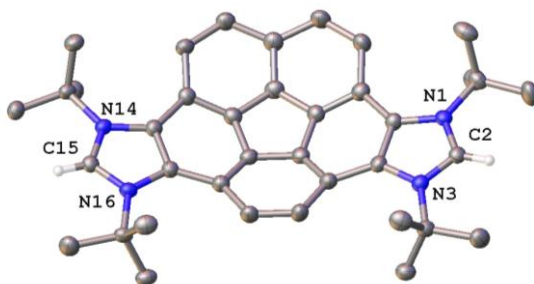
Figure 4.2. Molecular structure of **[H$_2$G^{tBu}](PF$_6$)$_2$**. Hydrogen atoms (except those hydrogen atoms bond to C2 and C15)and conterions have been omitted for clarity. Ellipsoids at 50 % of probability

The bowl-shape conformation of the corannulene unit induces a dihedral angle between the planes of the two azoles of 169.4º (Figure 4.3), thus making the two imidazolium fragments no co-planar.
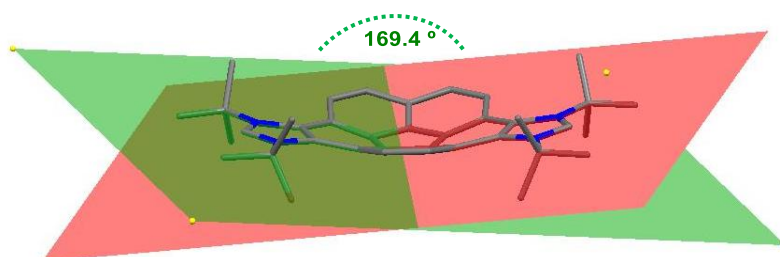
Figure 4.3. Dihedral angle between the planes of the two azoles of **[H₂Gᵗᴮᵘ](PF₆)₂**

The *tert*-butyl substituents of the nitrogen atoms adopt the less hindered conformation by pointing one of the methyl groups toward the coordination plane of a potential metal fragment, assuming that a N-heterocyclic carbene complex could eventually be formed. Based on the X-ray structure of **[H₂Gᵗᴮᵘ](PF₆)₂**, the potential metal-to-metal distance for a putative dimetallic complex bound to this di-NHC precursor would approximately be of 11.9 Å.

The steric hindrance of the potential bis-NHC ligand generated from the deprotonation of **[H₂Gᵗᴮᵘ](PF₆)₂**, was estimated by calculating the percent of buried volume (% V_{Bur}). The % V_{Bur} is defined as the percentage of the total volume of a sphere centred in the metal, which is occupied by the reference ligand.[14] This parameter, first introduced by Nolan and Cavallo, and now is commonly employed for measuring the steric bulk of NHC ligands.[15] Based on the molecular structure of **[H₂Gᵗᴮᵘ](PF₆)₂**, the percent of steric bulk assigned to the putative di-NHC ligand was calculated by using the Samb*V*ca free software developed by Cavallo and co-workers[16] resulting on a 45.1% (assuming a M-C distance of 2Å).[16]

Maximum steric constrain
%V = 45.1

%V = 36.1
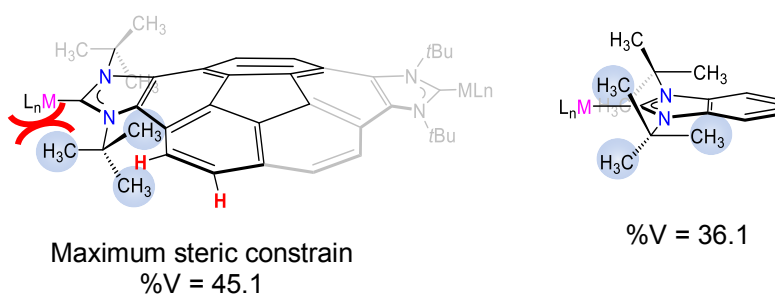
Scheme 4.2. Schematic representation of buried volumes (% V_{Bur})

This value is significantly larger than the steric bulk exhibited by other related *t*Bu-substituted NHC ligands (see Scheme 4.2).[14, 17] The larger steric bulk observed for our corannulene-based bis-NHC[2d] may be explained by the spatial orientation exhibited by the *t*Bu-wingtips, where one of methyl groups is enforced towards the coordination sphere of a putative metal, therefore affording a higher steric hindrance than other benzimidazolylidene ligands in which the orientation of the *t*Bu groups may allow a less hindered situation.

4.2.2 Isolation of a corannulene-based bis-NHCs

The availability of free and stable carbenes (persistent carbenes) can give access to the preparation of metal complexes which cannot be prepared otherwise.[18] In addition, stable carbenes and related metal-free species can activate small molecules and stabilize highly reactive intermediates.[19] Traditionally, carbenes were considered as curiosities and were only studied indirectly, e.g. by trapping reactions. This situation has changed dramatically with the emergence of persistent carbenes. Although they are very reactive molecules (i.e. they can dimerize) many of them can be isolated as pure substances,[20] specially if bulky substituents are incorporated avoiding potential dimerization reactions.

Deprotonation of the bis-imidazolium salt **[H₂G$^{t\textbf{Bu}}$](PF₆)₂** was carried out in C_6D_6 using sodium bis(trimethylsilyl)amide (NaHMDS, 1M in THF) and a catalytic amount of NaO^{t}Bu, as shown in Scheme 4.2. The resulting free bis-NHC, **G$^{t\textbf{Bu}}$**, which is stable in C_6D_6 solution for several days, was characterized by NMR spectroscopy.
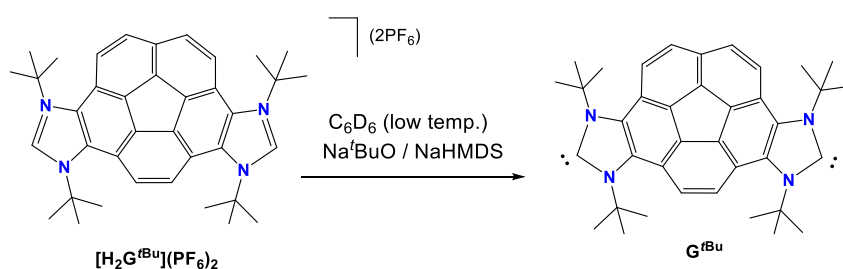
Scheme 4.3. Isolation of bis-N-heterocyclic carbene ligand **G$^{t\textbf{Bu}}$**

The $^{13}C\{^1H\}$ NMR spectrum of **G$^{t\textbf{Bu}}$** displayed the diagnostic signal of the carbene carbon at 219.89 ppm, in the same region as shown by other previously published

benzimidazole-based carbenes.[2e, 13b, 21] All other details regarding the $^{13}C\{^{1}H\}$ NMR spectrum may be found in the Experimental Section (Chapter 5). The ^{1}H NMR spectrum of G^{tBu} is described below.

^{1}H NMR spectrum of G^{tBu}

Figure 4.4 shows the ^{1}H NMR spectrum of an *in situ* prepared solution of G^{tBu} in C_6D_6. The absence of the acidic signal of the NC*H*N groups of the salt precursor is an indication of the deprotonation of $[H_2G^{tBu}](PF_6)_2$. The signals corresponding to the protons of corannulene core (**a**, **b** and **c**) are displayed at 8.55, 8.48 and 7.86 ppm, respectively. In addition, the signal due to the protons of the *tert*-butyl groups appears at 2.09 ppm (**d**).
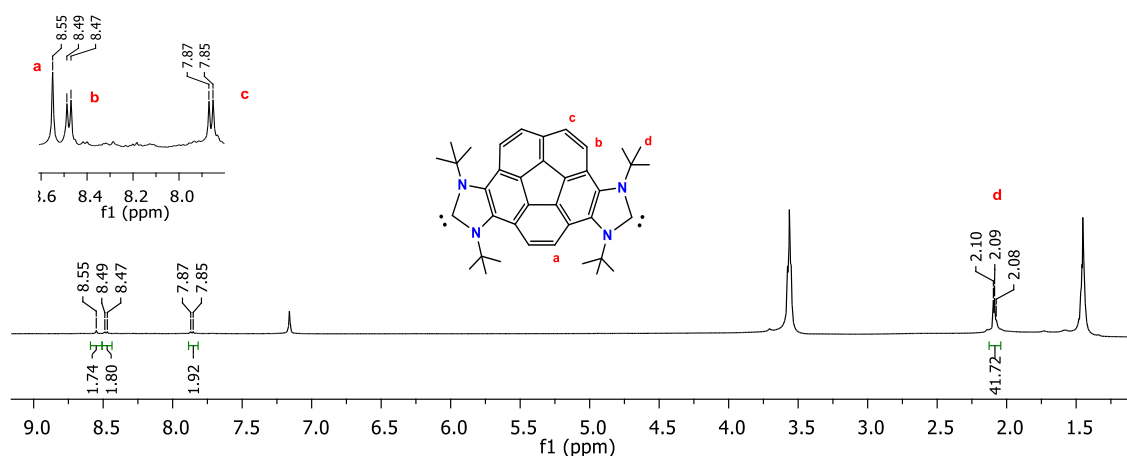
Figure 4.4. ^{1}H NMR spectrum of G^{tBu} in C_6D_6

4.2.3. Coordination of corannulene-based bis-NHCs

The coordination abilities of the bis-NHC ligands resulting from the deprotonation of the bis-azoliums $[H_2G^{nBu}](PF_6)_2$ and $[H_2G^{tBu}](PF_6)_2$ (Chart 4.4) were probed by using $[RhCl(COD)]_2$ and $[AuCl(SMe_2)]$ as metal sources. In the following sections, the preparation and characterization of the complexes $1G^{nBu}$, $2G^{nBu}$ and $3G^{tBu}$ will be described.
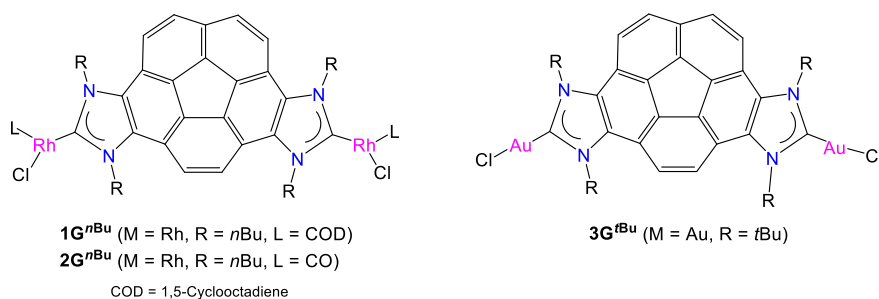
Chart 4.4. Bimetallic complexes $1G^{nBu}$, $2G^{nBu}$ and $3G^{tBu}$

4.2.3.1 Synthesis and characterization of rhodium complexes

The corannulene-based bis-NHC rhodium complexes $1G^{nBu}$ and $2G^{nBu}$ were obtained following the synthetic route depicted in Scheme 4.4. The reaction between $[H_2G^{nBu}](PF_6)_2$ and $[RhCl(COD)]_2$ in refluxing acetone in the presence of K_2CO_3, allowed the preparation the di-rhodium complex $1G^{nBu}$ in 30 % of yield (Scheme 4.4). The related tetra-carbonylated complex $2G^{nBu}$, was obtained by bubbling CO through a dichloromethane solution of $1G^{nBu}$ at 0 ºC.
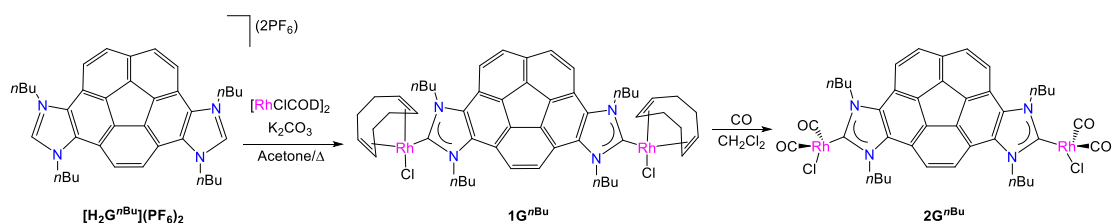
Scheme 4.4. Synthesis of complexes $1G^{nBu}$ and $2G^{nBu}$

Both complexes were characterized by NMR spectroscopy, Mass Spectrometry and Elemental Analysis. The ^1H and $^{13}C\{^1H\}$ NMR spectra are consistent with their predicted two-fold symmetries. Single resonances due to the metallated carbene carbons are found in the $^{13}C\{^1H\}$ NMR spectra, showing the characteristic $^1J_{Rh-C}$ couplings ($1G^{nBu}$: 190.5 ppm, $^1J_{Rh-C} = 52$ Hz; $2G^{nBu}$: 185.14 ppm, $^1J_{Rh-C} = 54$ Hz).

As an illustrative example, the ^1H and $^{13}C\{^1H\}$ NMR spectra of $1G^{nBu}$ are described below. All details regarding the characterization of $2G^{nBu}$ can be found in the Experimental Section (Chapter 5).

^1H NMR spectrum of $1G^{nBu}$

Figure 4.5 shows the ^1H NMR spectrum of $1G^{nBu}$. The absence of the signal due to the protons of the NC*H*N groups, and the appearance of the signals corresponding to the COD ligand are indicative of the coordination of the bis-NHC ligand G^{nBu} to the Rh$^{(I)}$

fragment. The signals assigned to the protons of the corannulene core (**a**, **b** and **c**) are displayed at 8.17, 8.05 and 8.02 ppm, respectively. The signals due to the protons of the *n*-butyl groups appear at 5.21, 2.05, 1.83 and 1.24 ppm (**d**, **e**, **f** and **g**, respectively). The rest of the signals corresponding to the protons of the COD ligands are shown on the spectrum.
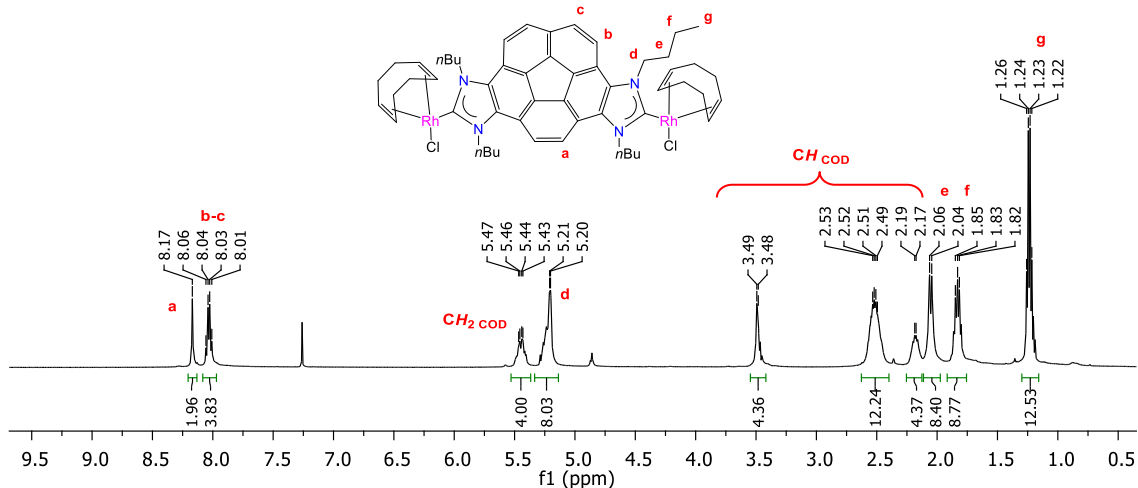
Figure 4.5. ^{1}H NMR spectrum of **1G^{nBu}** in CDCl$_3$

^{13}C{^{1}H} NMR spectrum of **1G^{nBu}**

Figure 4.6 shows the ^{13}C{^{1}H} NMR spectrum of **1G^{nBu}**. The most characteristic signal is the doublet attributed to the metallated carbene-carbon (**1**) at 190.5 ppm ($^1J_{\text{Rh-C}}$ = 52 Hz). The signals assigned to the corannulene core are shown between 133.5-117.9 ppm. The signals due to the carbons of the *n*-butyl groups appear between 33.4 and 14.3 ppm. The rest of the signals corresponding to the COD carbons are conveniently displayed on the spectrum.
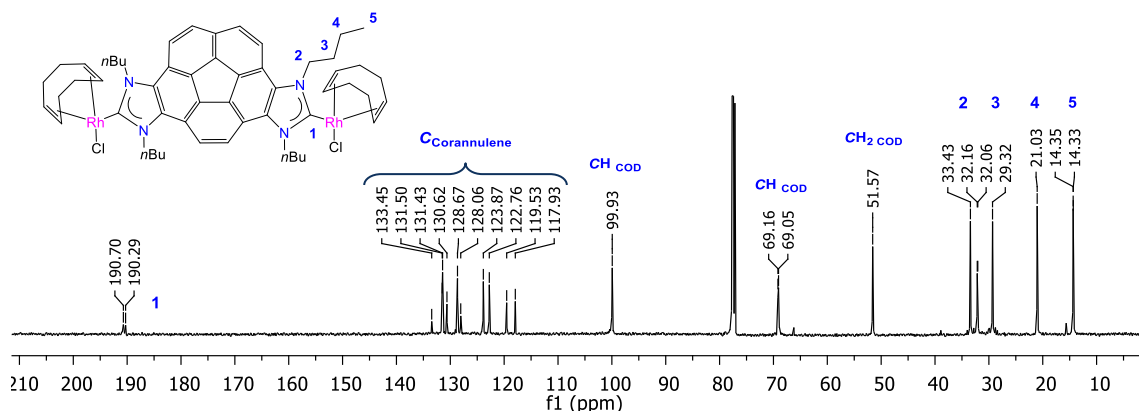
Figure 4.6. ^{13}C{^{1}H} NMR spectrum of **1G^{nBu}** in CDCl$_3$

4.2.3.2 Synthesis and characterization of a gold complex

The corannulene-based bis-NHC $\mathbf{G}^{tBu}$ ligand presents a very large steric bulk around the carbene carbon, due to the spatial orientation of the *tert*-butyl wingtips, where two methyl groups are enforced towards the coordination sphere of the metal (Chart 4.3). We envisaged that the coordination of this ligand should only be possible if a linear metal complex was obtained. For this reason, we decided to try the coordination of this bis-NHC ligand to $Au^{(I)}$-Cl.

The reaction of $[\mathbf{H_2G}^{tBu}](\mathbf{PF_6})_2$ with $[AuCl(SMe_2)]$ in THF, in the presence of KHMDS, afforded the bis-NHC complex ($\mathbf{3G}^{tBu}$) in moderate yield (40 %) (Scheme 4.5). The gold complex $\mathbf{3G}^{tBu}$ was characterized by NMR spectroscopy, Mass Spectrometry and Elemental Analysis. The mass spectrum (ESI-TOF-MS) of the complex revealed two main peaks at *m/z* ratios of 787.3 and 1041.3, which were assigned to $[M-AuCl+H]^+$ and $[M+Na]^+$, respectively. The $^{13}C\{^1H\}$ NMR spectrum of complex $\mathbf{3G}^{tBu}$ displayed a signal at 178.72 ppm, assigned to the resonance of the carbene carbon.

The ^1H NMR spectrum of $\mathbf{3G}^{tBu}$ is described below. All other details regarding the full characterization of $\mathbf{3G}^{tBu}$ may be found in the Experimental Section (Chapter 5).
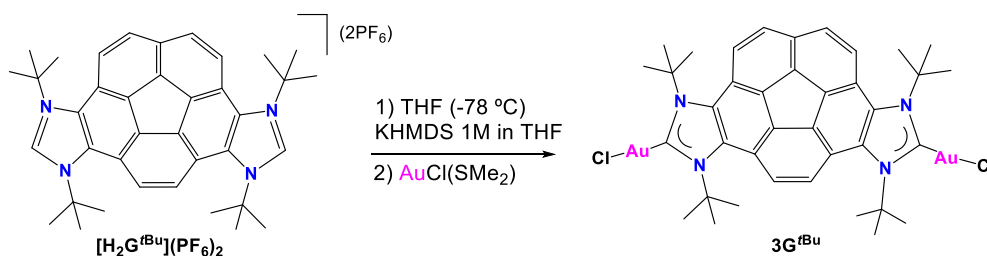
Scheme 4.5. Synthesis of complex $\mathbf{3G}^{tBu}$

^1H NMR spectrum of $\mathbf{3G}^{tBu}$

Figure 4.7 shows the ^1H NMR spectrum of $\mathbf{3G}^{tBu}$. The absence of the signal due to the protons of the NC*H*N groups is the first indication that the coordination of the bis-NHC ligand $\mathbf{G}^{tBu}$ to the $Au^{(I)}$ fragment has taken place. The signals assigned to the protons of the corannulene core (**a**,**b** and **c**) are displayed at 8.39-8.34 and 7.97 ppm. The signals due to the protons of the four *tert*-butyl groups appear at 2.37 ppm (**d**)
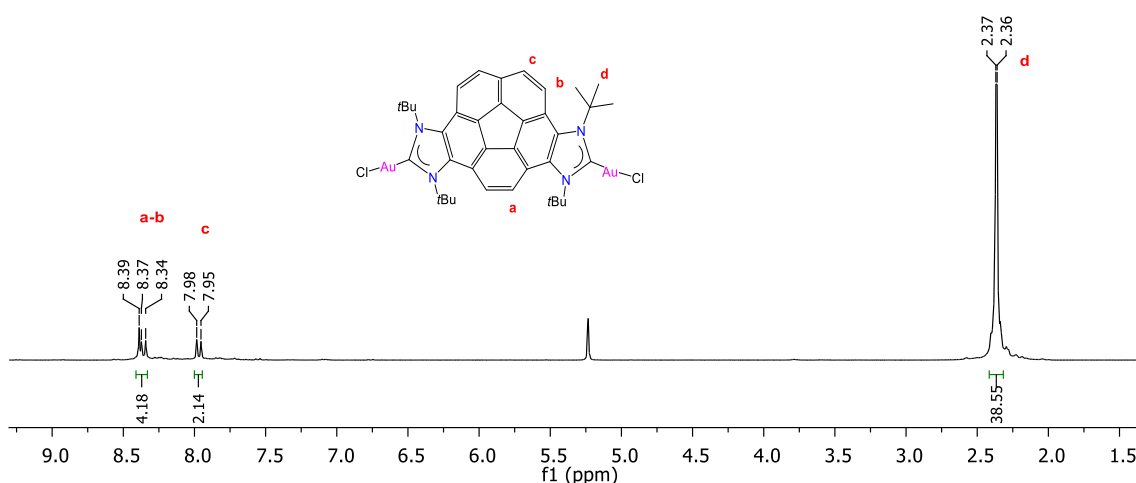
Figure 4.7. ^{1}H NMR spectrum of **3G^{tBu}** in CD$_2$Cl$_2$

4.2.4. Electronic properties of the corannulene-based bis-NHC ligand

The electron-donating strength of the ligand **G^{nBu}** in complexes **1G^{nBu}** and **2G^{nBu}**, was experimentally evaluated by means of Cyclic Voltammetry (CV) and Infrared spectroscopy (IR).

Electronic studies

The cyclic voltammetry diagram of the bis-Rh$^{(I)}$ complex **1G^{nBu}** is shown in Figure 4.8, along with the relevant section of the Differential Pulse Voltammetry (DPV) plot. The complex showed an irreversible redox event at E$_{oxid}$ = 1.07 V, which is attribuited to the Rh$^{(I)}$/Rh$^{(II)}$ couple.
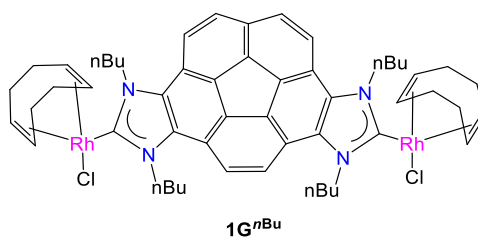
Chart 4.5. Bimetallic rhodium derivative

The analysis of the DPV generated for **1G^{nBu}**, indicates that there is only one rhodium-centered redox event taking place, thus indicating that the bi-metallic complex **1G^{nBu}** contains two essentially decoupled rhodium fragments.
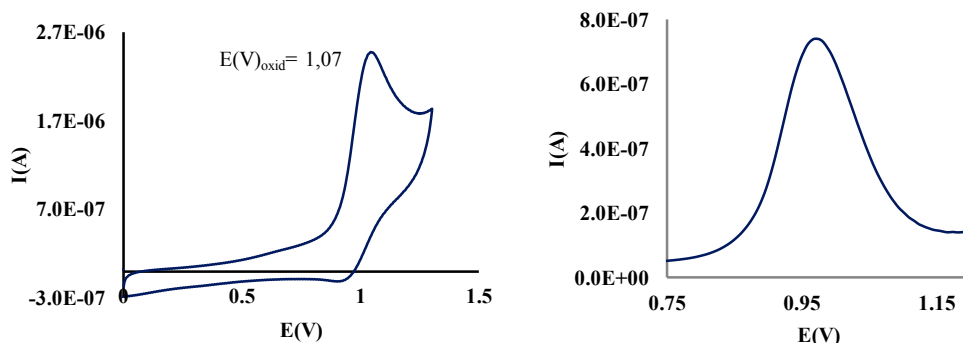
Figure 4.8. CV plot (left) and relevant DPV section (right) of complex **1G$^{n\text{Bu}}$** (1mM in dry CH_2Cl_2 with 0.1M [NBu$_4$][PF$_6$] as the supporting electrolyte, 50 mVs^{-1} scan rate, Fc$^+$/Fc used as internal standard with E$_{1/2}$ (Fc/Fc$^+$) = 0.44 V *vs.* SCE).
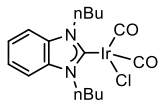
IR studies and Tolman Electronic Paramenter (TEP)

The electron-donating strength of our bis-NHC ligand can also be determined by studying the IR spectrum of the rhodium tetracarbonyl complex **2G$^{n\text{Bu}}$**.

The IR spectrum of **2G$^{n\text{Bu}}$** was carried out in CH_2Cl_2 solution, and showed two CO stretching bands at 2083 and 2003 cm^{-1}. The average value of the two stretching frequencies ($\nu_{av}(CO)$) is 2043.0 cm^{-1}, from which a TEP value of 2055.0 cm^{-1} can be derived by employing the well-known correlations.[17, 22]

In addition, the DFT calculated TEP[23] value for **G$^{n\text{Bu}}$** (determined by Prof. Dmitri Gusev, from the Wilfrid Laurier University) is 2054 cm^{-1}, thus differing only in one TEP unit from the experimental one.

Table 4.1. Carbonyl stretching frequencies and TEP (cm^{-1})

Complex	$\nu(CO)_{av}$ (cm^{-1})	TEP (calculated)	TEP (from DFT)
2G$^{n\text{Bu}}$	2043.0	2055.0	2054.0
	2026.8	2052.7[24]	-

Scheme 4.6 displays the calculated TEP values of a series of NHCs bearing *n*Bu N-substituents. From the data shown, it can be observed that there is a large difference between the TEP value of the imidazolylidene (I^{n}Bu) and the rest of the NHC ligands bearing aromatic rings at the backbone, all showing lower electron-donating character. The difference in the electron-donating character of all three arene-decorated NHCs is

very similar, with a maximum difference of 0.7 cm^{-1} between the TEP values shown for the benzoimidazolylidene and our corannulene-bis-NHC.
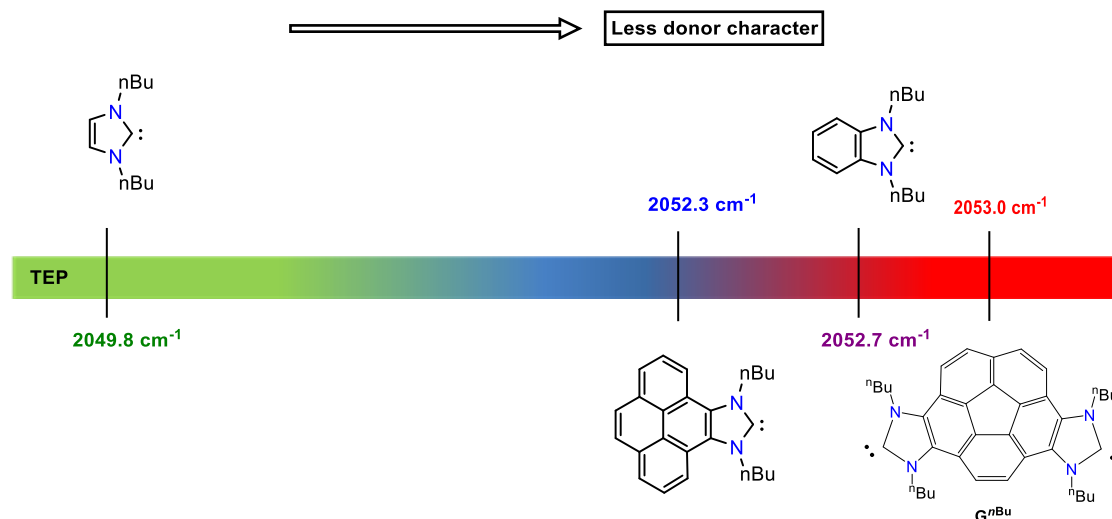
Scheme 4.6. Variation of the TEP (cm^{-1}) values of some NHC ligands

4.2.5. Catalytic studies of the corannulene-bis-NHC di-Au$^{(I)}$ complexes

As previously stated in the introduction, our research group has been recently working on the design and development of poly-N-heterocyclic carbene ligands linked by polycyclic aromatic hydrocarbons.[25] The ultimate goal was the preparation of homogeneous metal-based catalysts with enhanced properties.[2] In particular, the use of polymetallic metal complexes based on a polyaromatic core allowed the supramolecular interaction of the ligand with the substrates, enhancing their catalytic performance, exhibiting better activity than their related monometallic counterpart lacking this polycyclic aromatic core. Among them, two trimetallic gold complexes featuring electron deficient polyaromatic ligands resulted in very efficient catalysts towards the hydroamination of alkynes.[2d, 26] It is worth mentioning that the catalytic activity of gold catalysts has often been related to the ability of the gold center to behave as an electrophile. For this reason and given the low electron-donating character of the corannulene based bis-NHC ligand in **G^{nBu}**, we chose **3G^{tBu}** to evaluate its catalytic activity against two different catalytic transformations: the hydroamination of alkynes and the cyclization reaction of 2,5-dimethylfuran with alkynes because we thought that this complex should yield good catalytic efficiencies.

Unfortunately, as will be described in the following section, the catalytic performance of **3G^{tBu}** towards both catalytic processes resulted in low activities.

94

Hydroamination of alkynes

The catalytic activity of the bis-NHC-gold complex **3G^{tBu}** was tested towards the hydroamination of phenylacetylene using three different anilines (aniline, 2,4,6-trimethylaniline and 2,6-diisopropylaniline) following the methodology reported in the literature.[2b, d, 27]

Table 4.2 summarizes the catalytic results. The reactions were carried out at 90 °C in acetonitrile, in the presence of AgBF$_4$ and using a catalyst loading of 0.5 mol % during 6 hours.

Table 4.2. Hydroamination of Phenylacetylene with arylamines
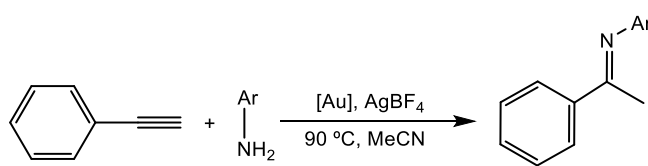
Entry	Ar	Conv. (%)^b
1		9
2		20
3		19

^{a} Reaction conditions: 0.5 mmol of phenylacetylene, 0.55 mmol of aryl amine, 0.5 mol % of the catalyst, 1 mol % of AgBF$_4$, 1 mL of dry CH$_3$CN at 90 °C, 6 h. ^{b}Conversions determined by gas chromatography (GC), using anisole as internal standard

Cyclization of 2,5-dimethylfuran with terminal alkynes

In view of the poor catalytic performances observed in the hydroamination of alkynes, we decided to test a different catalytic reaction. In this case, we betted on the synthesis of phenols obtained by cyclization reaction of 2,5-dimethylfuran with alkynes.[28] The reactions were carried out following a method previously described, where 2,5-dimethylfuran is reacted at room temperature with the alkyne in dichloromethane, using

1.5 mol % of catalyst and 1.5 mol % of NaBArF (tetrakis[3,5bis(trifluoromethyl)-phenyl]borate]) during 24 hours.

Table 4.3. Intermolecular gold(I)-catalyzed cyclization of 2,5-dimethylfuran with terminal alkynes
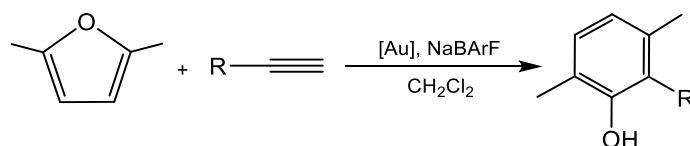
Entry	Alkyne	Temperature	Yield (%)[b]
1	phenylacetylene	R.T	17
2	phenylacetylene	40 °C	29
3	1-octyne	40 °C	-
4	3-ethynyltoluene	40 °C	14

[a]Conditions: 2 mmol of 2,5-dimethylfuran, 1 mmol of alkyne, 1.5 mol % of the catalyst, 1.5 mol % of NaBArF, dry CH_2Cl_2, 24 h. [b]Yields of the isolated products

The low performance of complex **3G**^{tBu} observed in both catalytic transformations was rather disappointing, and we ascribed to be likely due to catalyst decomposition during the reaction course. As a result of the poor catalytic activity shown by the di-gold complex, we considered the possibility of exploiting the size and shape of **3G**^{tBu}, as molecular receptor for fullerene recognition.

4.2.6. Corannulene-bis-NHC di-Au$^{(I)}$ complex and recognition of C$_{60}$

As mentioned in the introduction, bowl-shaped polyaromatic hydrocarbons, such as corannulene, are among the best binding motifs for the preparation of effective fullerene receptors.[29] This is mainly due to the complementarity shape that exists between the shallow concave cavity of the corannulene and the convex surfaces of fullerenes.[3c] For this reason, and inspired by the existing literature, we decided to study the interaction of the bowl-shaped gold complex **3G**^{tBu} with fullerene. Our studies were carried out by using different titration techniques, such as ^{1}H NMR spectroscopy, fluorescence spectroscopy and calorimetric studies, and were also supported by DFT calculations.

We decided to use the di-gold complex $3G^{tBu}$ for this study because we thought that the linear coordination of the metal fragment on the bis-NHC ligand should enhance the shape complementarity between the corannulene-based compound and fullerene, since the linear AuCl branches should probably behave as an extension of the receptor, increasing the contact surface with fullerenes. The corannulene rhodium complexes described in this chapter should show lower binding affinities due to the steric bulk provided by the more sterically crowded metal fragment.

Host-guest studies by ^{1}H NMR titrations

We first studied the affinity of $3G^{tBu}$ (host) *versus* two different shaped polyaromatic guests, *fullerene* (C_{60}) and *coronene* (Chart 4.6). With these two model substrates we aimed to illustrate the importance of shape complementarity on the binding affinities of our corannulene-based host compound.
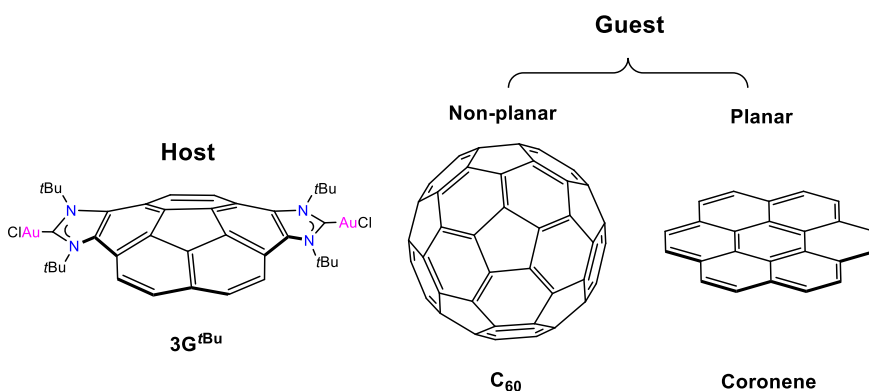
Chart 4.6. Host ($3G^{tBu}$) vs. Guest (C_{60} and Coronene)

Toluene-d_8 was chosen as solvent for all titrations due to the optimal solubility observed for all reagents. In addition, the ^{1}H NMR spectrum of $3G^{tBu}$ in toluene-d_8 solution showed sharp and well-defined signals in the aromatic region. The H_a proton resonates as a singlet at 8.07 ppm, while the signals due to the protons H_b and H_c appear as two separated doublets at 8.08 and 7.56 ppm, respectively (see Figure 4.9).
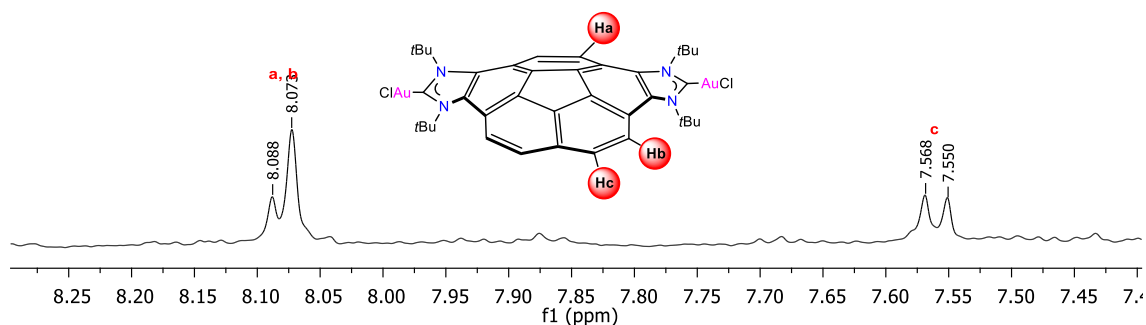
Figure 4.9. Representative region of the ^{1}H NMR spectrum of **3G^{tBu}** in toluene-d_8

The titrations were performed at constant concentrations of host (1.55 mM). In order to do this, two solutions were prepared: a host solution (1.55 mM) and a titrating solution that contained guest (2 mM) and host (1.55 mM). Unfortunately, we could not use higher concentrations of fullerene due to its low solubility in toluene. In a typical experiment, aliquots of titrant solution (guest + host) were gradually added into a NMR tube containing the titrand (host) solution.
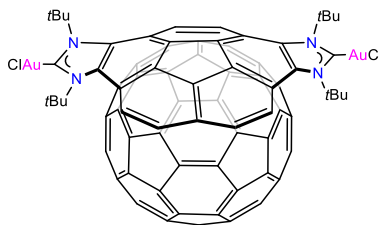
Chart 4.7. π-π Donor-acceptor interactions between **3G^{tBu}** and C$_{60}$

We observed that the incremental addition of C$_{60}$ (guest) to the solution of **3G^{tBu}** (host) induced a downfield shift of the corannulene proton signals in **3G^{tBu}**, as can be observed from the series of spectra shown in Figure 4.11. The addition of 0.5 equivalents of C$_{60}$ produced a downfield shift of 0.4 ppm for the signal assigned to H$_a$. The signals due to H$_b$ and H$_c$ also experienced downfield shifts although to a lesser extent. The chemical shift changes experienced by the proton resonances of the corannulene unit in **3G^{tBu}** are indicative of a binding process with C$_{60}$ that showed fast kinetics on the NMR timescale. We assumed that the bimetallic complex **3G^{tBu}** interacts with C$_{60}$ through π-π donor-acceptor interactions.

Figure 4.10 shows the binding isotherm resulting from the representation of the chemical shift changes experienced by the signal of the H$_a$ proton in **3G^{tBu}** during the

titration with C_{60}. Assuming the formation of a 1:1 binding complex, the nonlinear regression gave a good fit, and returned a binding constant of $K_{11} = 2750 \pm 300$ M^{-1} for the formation of a potential $C_{60}@\mathbf{3G}^{t\mathbf{Bu}}$ complex.
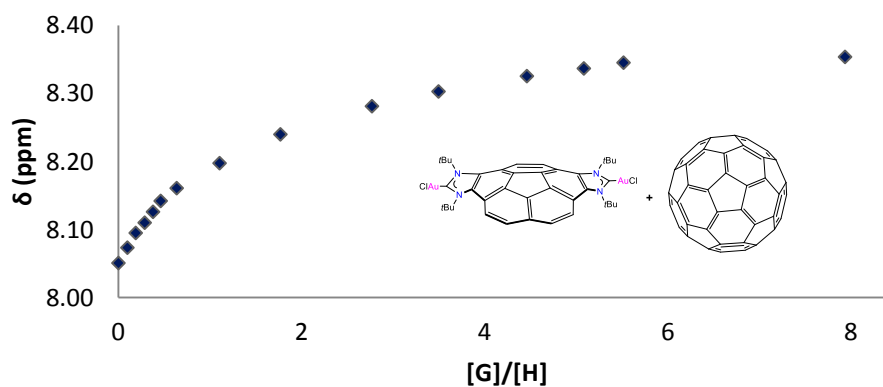
Figure 4.10. ^{1}H NMR chemical shifts δ(ppm) plotted against [G]/ [H].
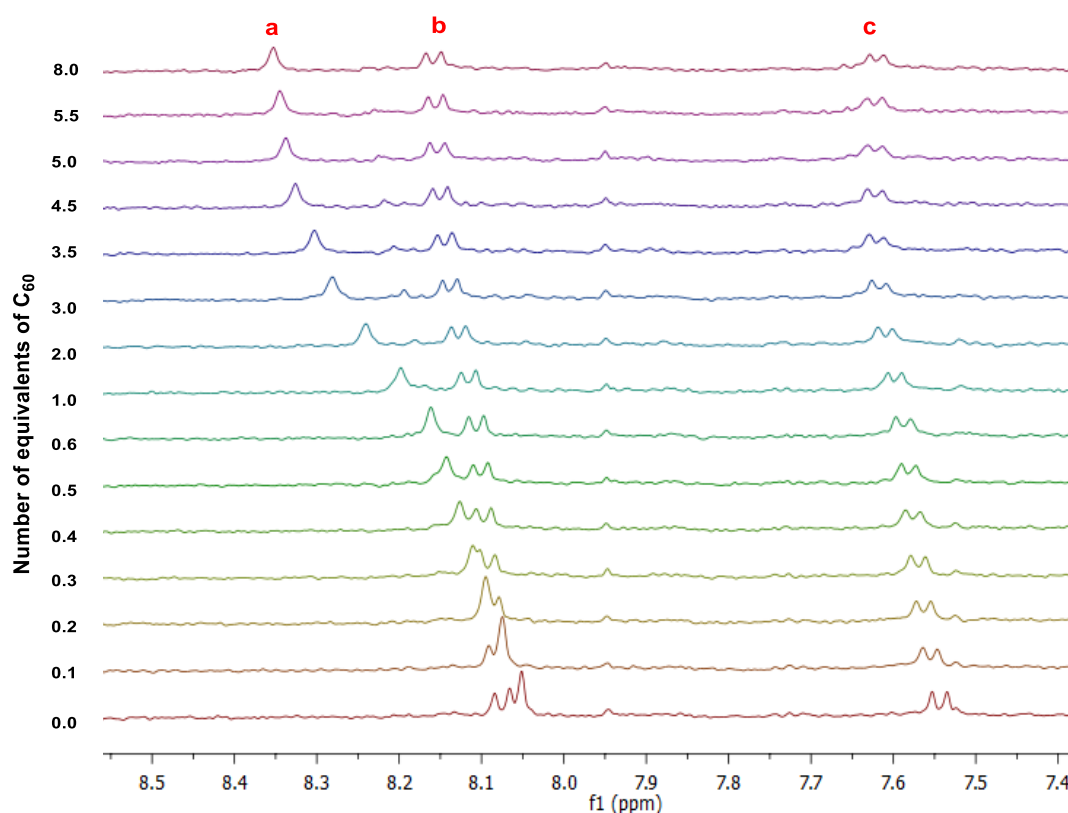
Figure 4.11. Selected regions of the ^{1}H NMR (500 MHz, toluene-d_8, 298 K) spectra acquired during the titration of $\mathbf{3G}^{t\mathbf{Bu}}$ with incremental amounts of C_{60}. The concentration of $\mathbf{3G}^{t\mathbf{Bu}}$ was maintained constant (1.55 mM) throughout the titration

The experimental data obtained in the NMR titration data with C_{60} also displayed good fits for 1:2 or 1:3 binding models. The analysis was performed by considering that the

binding constants for the single binding steps leading to $C_{60}@(3G^{tBu})_2$ and $C_{60}@(3G^{tBu})_3$ were identical and independent, and returned a value that was coincident for the formation of 1:1 complex $K_a(C_{60}@3G^{tBu})$ = 2750 M^{-1}. Unfortunately, the monotonic shift experienced by the analyzed proton signal of corannulene derivative $3G^{tBu}$ upon binding C_{60} did not allow us to establish an irrefutable binding model based on the fit of the NMR titration data.

Taking all this together, the results indicate that a) corannulene $3G^{tBu}$ interacts with C_{60} in solution at millimolar concentration, b) the chemical exchange between free and complexed $3G^{tBu}$ is fast on the NMR timescale; c) the binding constant for the interaction of $3G^{tBu}$ with C_{60} is on the order of 10^3 M^{-1}, and d) most likely, complexes of larger stoichiometry than the simple 1:1 $C_{60}@3G^{tBu}$ are formed in the investigated range of millimolar concentrations.

We were also interested in studying if $3G^{tBu}$ could also be used as a receptor of planar polyaromatic hydrocarbons (*PAHs*). As a model guest, we used coronene for our studies.
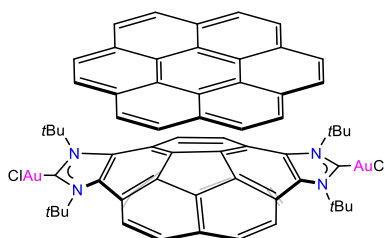
Chart 4.8. π-π donor-acceptor interactions between $3G^{tBu}$ and coronene

The addition of incremental amounts of coronene to a millimolar solution of host $3G^{tBu}$ in toluene-d_8 produced changes in the chemical shift of all the siganals of aromatic protons of the host. The signals of H_b and H_c experienced a downfield shift whereas the signal of H_a moved upfield.
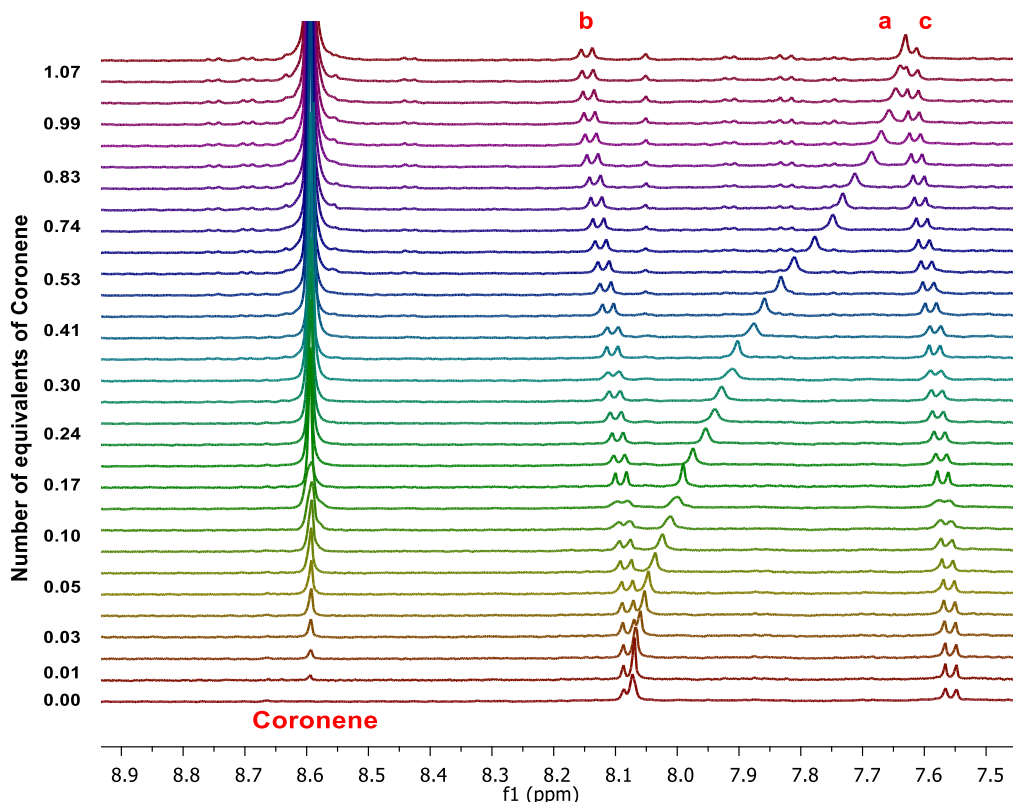
Figure 4.12. Selected regions of the ^{1}H NMR (500 MHz, toluene-d_8, 298 K) spectra acquired during the titration of **3G^{tBu}** with incremental amounts of coronene. The concentration of **3G^{tBu}** was maintained constant throughout the titration

The NMR titration data for the H_a signal were mathematically analyzed using a 1:1 binding model. The fit was good and returned an association constant value for the formation of a coronene@**3G^{tBu}** complex of K_{11}= 239 $\pm$ 25 M^{-1}. This constant is significantly lower than that found for the binding with fullerene, pressumably as a consequence of the much lower shape complementarity. However, this result illustrates how the concave surface of corannulene can be adapted to the recognition of large planar polycyclic aromatic hydrocarbons.

Host-guest studies by fluorescence spectroscopy

In order to provide a further insight into the binding affinity of **3G^{tBu}** and C$_{60}$ in toluene, we carried out UV-Vis and fluorescence titrations. In these experiments, the host solution was transferred into an UV-cell and aliquots of the solution of host+guest were added, in the same way as in the NMR experiments. These spectrocopic techniques allow the use of lower concentrations than those required for ^{1}H NMR titrations. We carried out the fluorescence spectroscopy experiments with concentrations of 1.55x10^{-5}

M and 1.55×10^{-4} M for **3G^{tBu}** and C$_{60}$, respectively. By working at such low concentrations of **3G^{tBu}**, we expected to disfavour the formation of the aggregates of higher stoichiometry, *e.g.* 1:2 and 1:3 complexes, and therefore, to gain more information about the formation of the 1:1 inclusion complex. Unfortunately, the UV-Vis spectroscopic titration with C$_{60}$ did not show any noticeable change in the absorption spectrum of **3G^{tBu}**. Conversely, the emission of **3G^{tBu}** changed significantly in the presence of increasing amounts of C$_{60}$. Figure 4.13 shows the changes observed in the emission spectra of **3G^{tBu}** (1.55×10^{-5} M) in toluene solution upon incremental addition of C$_{60}$. The titration showed two phases. In the initial phase, the incremental addition of C$_{60}$ provoked an increase in the intensity of the emission band of **3G^{tBu}** centered at 528 nm. However, when the ratio of [C$_{60}$]/[**3G^{tBu}**] > 0.4 the intensity of the emission band started to decrease. We inteprete this observation as a consequence of an absorption increase at the excitation wavelenght produced by the addition of C$_{60}$ (inner filter effect). Consequently, the obtained emision titration data are not suitable for the mathematical analysis using theoretical binding models, but they clearly indicate that the interaction of **3G^{tBu}** with C$_{60}$ occurs even at micromolar concentration.
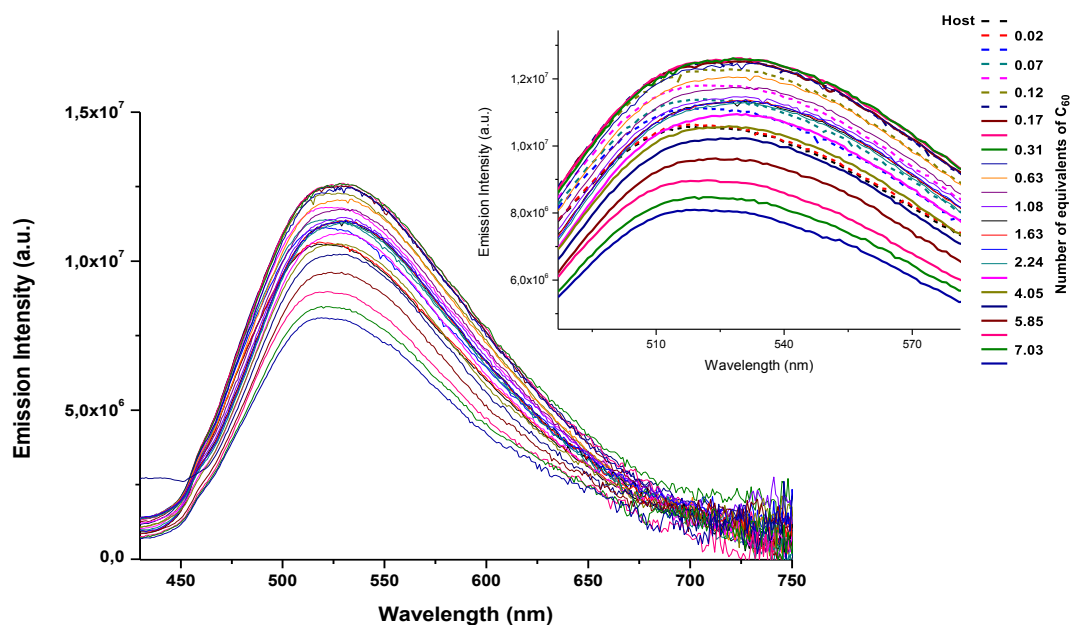
Figure 4.13. Fluorescence spectra during the titration of **3G^{tBu}** (1.55×10^{-5} M) with C$_{60}$ (1.55×10^{-4}M) in toluene at 298 K ($\lambda_{ex} = 403$ nm).
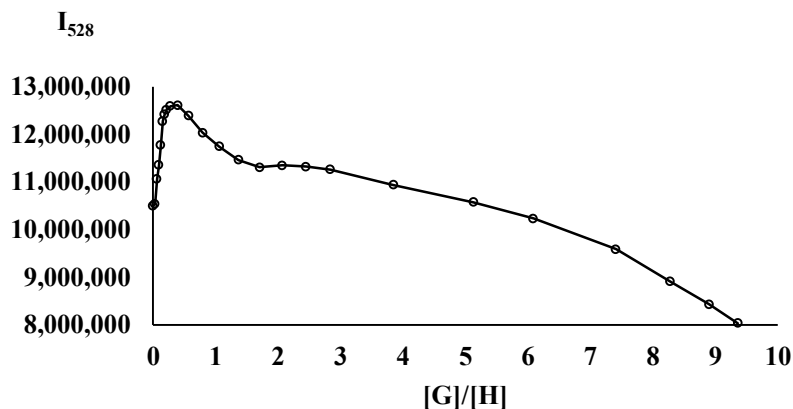
Figure 4.14. Plot of the data values from the titration study of $3G^{tBu}$ with C_{60}. I_{528} *vs.* equivalents of [G]/[H]

Isothermal Titration Calorimetry (ITC)

We then considered that Isothermal Titration Calorimetry (ITC) experiments should help us to obtain additional information on the interaction of complex $3G^{tBu}$ with C_{60}. ITC is a thermodynamic technique that directly measures the heat released or absorbed upon sequential and incremental addition of a solution of one compound to another in the same solvent (toluene). The work was done in collaboration with the group of Prof. Pau Ballester (ICIQ of Tarragona, Spain). Due to solubility problems, the titrant ($3G^{tBu}$ + C_{60}) and titrand ($3G^{tBu}$) concentrations used in the ITC experiment were suboptimal considering a tentative binding affinity for the $C_{60}@3G^{tBu}$ 1:1 complex in the order of 10^3 M^{-1}, as determined by ^1H NMR titrations (*vide supra*). The ITC experiments were performed by incremental addition of a toluene solution of C_{60} (3.8 mM) to a toluene solution of $3G^{tBu}$ (0.6 mM) located in the cell. The addition of C_{60} to the solution of $3G^{tBu}$ produced the observation of significant evolved heat in the initial injections, indicating an exothermic process. The experimentally obtained binding isotherm was fitted using the "one set of sites" theoretical binding model implemented in the Microcal software. We obtained the best fit for a model that considers the formation of a 1:3 inclusion complex of the type $C_{60}@(3G^{tBu})_3$ (Figure 4.15).
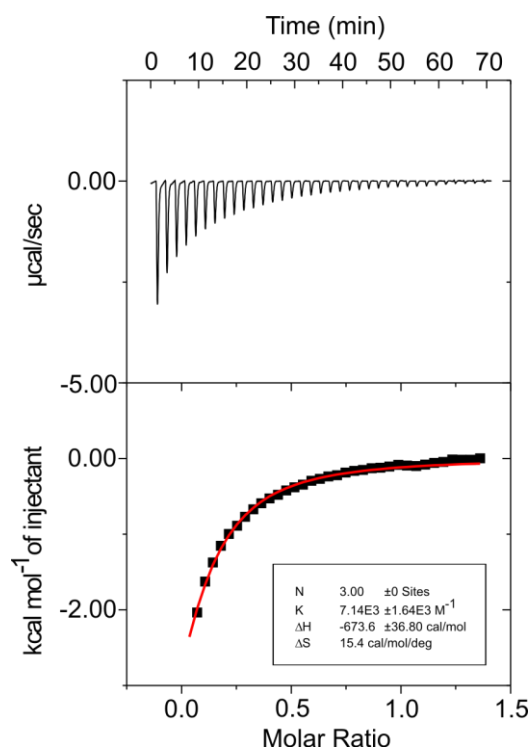
Figure 4.15. ITC experiment of **3G^{tBu}** (0.6 mM) with C$_{60}$ (3.8 mM) in toluene performed at 298 K. Heat *vs*. time plot for the titration of guest C$_{60}$ into host **3G^{tBu}** (top). "One set of sites" binding isotherm (red line) fit to the experimental data assuming that the complex of higher stoichiometry formed by the two binding partners is C$_{60}$@(**3G^{tBu}**)$_3$ (bottom). This binding model assumes that all binding sites are almost identical. The thermodynamic constants returned in the fitting procedure are shown in the panel inset.

This finding suggested that C$_{60}$ interacted with **3G^{tBu}**, in the range of studied concentration, forming complexes of 1:1, 2:1 and 3:1 stoichiometry, a result which is in agreement with the ^{1}H NMR titration experiments. The fit of the experimental data to the theoretical model also allowed the determination of an average value for the binding constant of C$_{60}$ with **3G^{tBu}** and the average enthalpy of binding (ΔH) for this process. The free energy (ΔG) and the entropy (ΔS) terms were derived from the thermodynamic constants measured experimentally. The average stability constant found was 7.1 ± 0.7 x 10^3 M^{-1}, for each individual step leading to C$_{60}$@(**3G^{tBu}**)$_3$. This value is in agreement with the one obtained using ^{1}H NMR spectroscopy. The average enthalpy per step and per mol of **3G^{tBu}** in the formation of the C$_{60}$@(**3G^{tBu}**)$_3$ complex was determined as -0.67 ± 0.07 kcal mol^{-1}. An important point is that the entropic term, TΔS, was found to be 4.6 ± 0.5 kcal mol^{-1}, therefore contributes significantly to the free binding energy that was calculated to be -5.3 ± 0.5 kcal mol^{-1}. These results indicate that the binding of C$_{60}$ with **3G^{tBu}** in toluene solution is enthalpically and entropically favored, although

entropy is the dominant parameter. This result is in clear contradiction with the previous assumptions that the association of single-based corannulene receptors with corannulene should be entropically disfavored,[29] but are in the line of recent findings regarding the positive entropies found when receptors containg more than one corannulene unit are used.[9a] Our interpretation of this result is that solvent effects are playing an important role in the process, and for this reason solvation/desolvation processes of the binding process shoud be also take into account.

DFT calculations

In order to gain more insight on the behaviour of our complex in the presence of C_{60}, DFT calculations were performed to determine the structures and binding energies of **3G^{tBu}** with C_{60}. These studies were carried out by Prof. Dmitri Gusev (Wilfrid Laurier University, Canada).

The principal objective of the study was to establish any trends upon the formation of $C_{60}@($**3G^{tBu}**$)_n$ with n=1–3. Along with **3G^{tBu}**, we calculated a smaller version of this complex possessing all N-CH$_3$ groups **3G^{Me}** (Figure 4.16). For the comparison of the energy minimized structures of these complexes, it could be observed that the *bulkier* complex **3G^{tBu}** presents a deeper cavity compared to **3G^{Me}**. Therefore, the former was assumed to have the most favourable shape for the association with a fullerene.
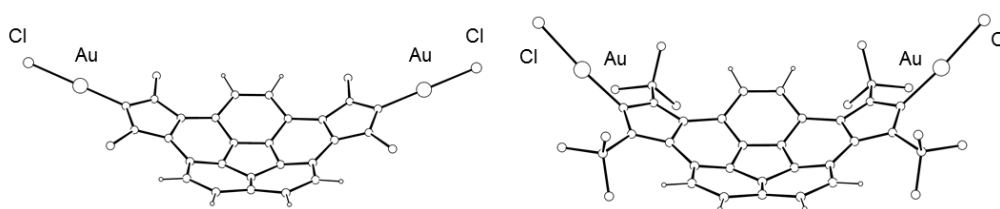
Figure 4.16. Schematic representation of **3G^{Me}** (left) and **3G^{tBu}** (right)

The computational calculations allowed us to conclude that the formation of the aggregate $C_{60}@$**3G^{tBu}** is more favourable than $C_{60}@$**3G^{Me}** (see Tables 5.7 and 5.8 in Experimetal Section), a fact that can be related to the more extended and deeper cavity of **3G^{tBu}** *vs.* **3G^{Me}**. This is translated into a better shape–size complementarity of **3G^{tBu}** and C_{60} and thus the stronger dispersion attractive forces in $C_{60}@$**3G^{tBu}**.

C$_{60}$@(**3G^{Me}**) C$_{60}$@(**3G^{Me}**)$_2$ C$_{60}$@(**3G^{Me}**)$_3$
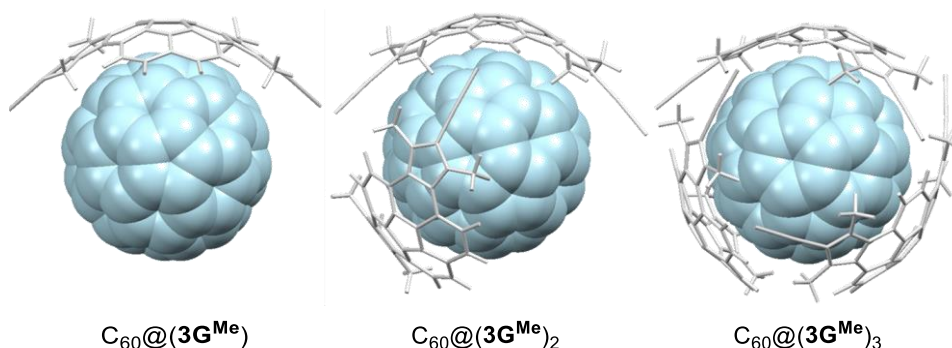
Figure 4.17. Optimized geometries of C$_{60}$@(**3G^{Me}**)$_n$ (n =1–3)

Unfortunately, the calculations were too costly to allow the optimization of the structure of the aggregate C$_{60}$@(**3G^{tBu}**)$_3$, so for the determination of the relative energies associated to the formation of aggregates with different stoichiometries (1:1, 1:2 and 1:3), complex **3G^{Me}** was used as model. Interestingly, the optimized structure of C$_{60}$@(**3G^{Me}**)$_3$ (Figure 4.17, right) has five of the six chlorides engaged in close Cl···H contacts, thus adding further stabilization to the complex with three bis-carbenes forming an interlocked molecular "puzzle" templated on C$_{60}$.

The free energy of formation of C$_{60}$@(**3G^{Me}**)$_3$ is −8.2 kcal/mol. As mentioned above, C$_{60}$@(**3G^{tBu}**)$_3$ could not be calculated, however, its free formation energy can be estimated by applying the energy difference between C$_{60}$@(**3G^{Me}**)$_3$ and C$_{60}$@(**3G^{Me}**)$_2$ (ΔG = −1.7 kcal/mol) toward the energy of formation of C$_{60}$@(**3G^{tBu}**)$_2$ (ΔG = −7.2 kcal/mol). This gives the estimated $\Delta G \leq$ −8.9 kcal/mol for C$_{60}$@(**3G^{tBu}**)$_3$, suggesting somewhat tighter bonding in the product *vs*. ITC experiment. The entropy change upon the formation of C$_{60}$@(**3G^{tBu}**)$_3$ should be $\Delta S \leq$ 17 cal·K^{-1}·mol^{-1}, which in full agreement with the ITC experiment.

4.3 Conclusions

In this Chapter we described the synthesis and characterization of two bis-imidazolium salt precursors based on a corannulene core.

The deprotonation of one of the corannulene-based bis-azolium salt featuring bulkier substituents allowed the preparation and characterization by NMR of the free corannulene based bis-imidazolylidene carbene ligand, which is stable in solution for a few days.

A series of dimetallic rhodium and gold complexes featuring corannulene-based bis-

NHC ligands were prepared and fully characterized by standard spectroscopic techniques.

In particular, the tetracarbonyl Rh$^{(I)}$ complex was used to determine the corannulene-based bis-carbene ligand electron-donating character by means of IR spectroscopy and electrochemical measurements. As a result, it was found that the corannulene-based bis-NHC ligand is slightly less donating that its benzoimidazolylidene counterpart.

In addition, di-gold$^{(I)}$ complex was found to be a good receptor for the recognition of fullerene C_{60} and coronene. In the case of C_{60}, host:guest stoichiometry of 3:1 and a high association constants were evidenced by the combination of NMR and ITC titrations. The formation of 3:1 complexes between the di-gold$^{(I)}$ complex and C_{60} which is favoured by the presence of the two linearly-opposed NHC-Au-Cl fragments, was confirmed by DFT calculations. In contrast, in the case of coronene, a moderate binding affinity and a host:guest stoichiometry of 1:1, were observed.

4.4 References

[1]   a) E. Peris, *Chem. Commun.* **2016**, *52*, 5777-5787; b) A. J. Boydston, K. A. Williams and C. W. Bielawski, *J. Am. Chem. Soc.* **2005**, *127*, 12496-12497.

[2]   a) A. Prades, E. Peris and M. Alcarazo, *Organometallics* **2012**, *31*, 4623-4626; b) S. Ibanez-Maella, M. Poyatos and E. Peris, *Chem. Commun.* **2017**; c) A. Prades, M. Poyatos, J. A. Mata and E. Peris, *Angew. Chem. Int. Ed.* **2011**, *50*, 7666-7669; d) S. Gonell, M. Poyatos and E. Peris, *Angew. Chem. Int. Ed.* **2013**, *52*, 7009-7013; e) C. Segarra, J. Linke, E. Mas-Marza, D. Kuck and E. Peris, *Chem. Commun.* **2013**, *49*, 10572-10574; f) S. Gonell, M. Poyatos and E. Peris, *Chem. Eur. J.* **2014**, *20*, 9716-9724; g) G. Guisado-Barrios, J. Hiller and E. Peris, *Chem. Eur. J.* **2013**, *19*, 10405-10411.

[3]   a) T. A. Jin, J. Zhao, N. Asao and Y. Yamamoto, *Chem. Eur. J.* **2014**, *20*, 3554-3576; b) X. Q. Hou, Y. T. Sun, L. Liu, S. T. Wang, R. L. Geng and X. F. Shao, *Chin. Chem. Lett.* **2016**, *27*, 1166-1174; c) X. Li, F. Kang and M. Inagaki, *Small* **2016**, *12*, 3206-3223.

[4]   F. Diederich and M. Gomez-Lopez, *Chem. Soc. Rev.* **1999**, *28*, 263-277.

[5]   a) D. Canevet, M. Gallego, H. Isla, A. de Juan, E. M. Perez and N. Martin, *J. Am. Chem. Soc.* **2011**, *133*, 3184-3190; b) Y. Shoji, K. Tashiro and T. Aida, *J. Am. Chem. Soc.* **2010**, *132*, 5928-5929; c) E. Huerta, G. A. Metselaar, A. Fragoso, E. Santos, C. Bo and J. de Mendoza, *Angew. Chem. Int. Ed.* **2007**, *46*, 202-205; d) E. Huerta, E. Cequier and J. de Mendoza, *Chem. Commun.* **2007**, 5016-5018.

[6]   A. M. Butterfield, B. Gilomen and J. S. Siegel, *Org. Process Res. Dev.* **2012**, *16*, 664-676.

[7]   a) T. Janowski, P. Pulay, A. A. S. Karunarathna, A. Sygula and S. Saebo, *Chem. Phys. Lett.* **2011**, *512*, 155-160; b) P. A. Denis, *Chem. Phys. Lett.* **2011**, *516*, 82-87; c) Y. Zhao and D. G. Truhlar, *Phys. Chem. Chem. Phys.* **2008**, *10*, 2813-2818; d) E. A. Jackson, B. D. Steinberg, M. Bancu, A. Wakamiya and L. T. Scott, *J. Am. Chem. Soc.* **2007**, *129*, 484-485.

[8]   L. N. Dawe, T. A. AlHujran, H. A. Tran, J. I. Mercer, E. A. Jackson, L. T. Scotc and P. E. Georghiou, *Chem. Commun.* **2012**, *48*, 5563-5565.

[9]   a) V. H. Le, M. Yanney, M. McGuire, A. Sygula and E. A. Lewis, *J. Phys. Chem. B* **2014**, *118*, 11956-11964; b) C. Muck-Lichtenfeld, S. Grimme, L. Kobryn and A. Sygula, *Phys. Chem. Chem. Phys.* **2010**, *12*, 7091-7097; c) A. Sygula, F. R.

Fronczek, R. Sygula, P. W. Rabideau and M. M. Olmstead, *J. Am. Chem. Soc.* **2007**, *129*, 3842-3843; d) C. M. Alvarez, L. A. Garcia-Escudero, R. Garcia-Rodriguez, J. M. Martin-Alvarez, D. Miguel and V. M. Rayon, *Dalton Trans.* **2014**, *43*, 15693-15696; e) M. Yanney, F. R. Fronczek and A. Sygula, *Angew. Chem. Int. Ed.* **2015**, *54*, 11153-11156; f) M. Yanney and A. Sygula, *Tetrahedron Lett.* **2013**, *54*, 2604-2607; g) A. Sygula, M. Yanney, W. P. Henry, F. R. Fronczek, A. V. Zabula and M. A. Petrukhina, *Cryst. Growth Des.* **2014**, *14*, 2633-2639.

[10] a) A. S. Filatov, L. T. Scott and M. A. Petrukhina, *Cryst. Growth Des.* **2010**, *10*, 4607-4621; b) B. D. Steinberg, E. A. Jackson, A. S. Filatov, A. Wakamiya, M. A. Petrukhina and L. T. Scott, *J. Am. Chem. Soc.* **2009**, *131*, 10537-10545.

[11] S. Lampart, L. M. Roch, A. K. Dutta, Y. Wang, R. Warshamanage, A. D. Finke, A. Linden, K. K. Baldridge and J. S. Siegel, *Angew. Chem. Int. Ed.* **2016**, *55*, 14648-14652.

[12] S. Mizyed, P. E. Georghiou, M. Bancu, B. Cuadra, A. K. Rai, P. C. Cheng and L. T. Scott, *J. Am. Chem. Soc.* **2001**, *123*, 12770-12774.

[13] a) K. A. Williams and C. W. Bielawski, *Chem. Commun.* **2010**, *46*, 5166-5168; b) Y.-T. Wang, M.-T. Chang, G.-H. Lee, S.-M. Peng and C.-W. Chiu, *Chem. Commun.* **2013**, *49*, 7258-7260.

[14] H. Clavier and S. P. Nolan, *Chem. Commun.* **2010**, *46*, 841-861.

[15] A. C. Hillier, W. J. Sommer, B. S. Yong, J. L. Petersen, L. Cavallo and S. P. Nolan, *Organometallics* **2003**, *22*, 4322-4326.

[16] A. Poater, B. Cosenza, A. Correa, S. Giudice, F. Ragone, V. Scarano and L. Cavallo, *Eur. J. Inorg. Chem.* **2009**, 1759-1766.

[17] R. A. Kelly, III, H. Clavier, S. Giudice, N. M. Scott, E. D. Stevens, J. Bordner, I. Samardjiev, C. D. Hoff, L. Cavallo and S. P. Nolan, *Organometallics* **2008**, *27*, 202-210.

[18] J. Bouffard, B. K. Keitz, R. Tonner, G. Guisado-Barrios, G. Frenking, R. H. Grubbs and G. Bertrand, *Organometallics* **2011**, *30*, 2617-2627.

[19] a) D. Bourissou, O. Guerret, F. P. Gabbai and G. Bertrand, *Chem. Rev.* **2000**, *100*, 39-91; b) M. Soleilhavoup and G. Bertrand, *Acc. Chem. Res.* **2015**, *48*, 256-266.

[20] a) A. J. Arduengo, R. L. Harlow and M. Kline, *J. Am. Chem. Soc.* **1991**, *113*, 361-363; b) E. Aldeco-Perez, A. J. Rosenthal, B. Donnadieu, P. Parameswaran, G. Frenking and G. Bertrand, *Science* **2009**, *326*, 556-559; c) G. Guisado-Barrios, J.

Bouffard, B. Donnadieu and G. Bertrand, *Angew. Chem. Int. Ed.* **2010**, *49*, 4759-4762; d) G. Guisado-Barrios, J. Bouffard, B. Donnadieu and G. Bertrand, *Organometallics* **2011**, *30*, 6017-6021.

[21] a) F. E. Hahn, L. Wittenbecher, D. Le Van and R. Fröhlich, *Angew. Chem. Int. Ed.* **2000**, *39*, 541-544; b) D. M. Khramov, A. J. Boydston and C. W. Bielawski, *Angew. Chem. Int. Ed.* **2006**, *45*, 6186-6189; c) J. A. V. Er, A. G. Tennyson, J. W. Kamplain, V. M. Lynch and C. W. Bielawski, *Eur. J. Inorg. Chem.* **2009**, 1729-1738; d) K. A. Williams and C. W. Bielawski, *Chem. Commun.* **2010**, *46*, 5166-5168; e) F. E. Hahn, L. Wittenbecher, R. Boese and D. Blaser, *Chem. Eur. J.* **1999**, *5*, 1931-1935.

[22] a) A. R. Chianese, X. W. Li, M. C. Janzen, J. W. Faller and R. H. Crabtree, *Organometallics* **2003**, *22*, 1663-1667; b) D. J. Nelson and S. P. Nolan, *Chem. Soc. Rev.* **2013**, *42*, 6723-6753.

[23] A. G. Tennyson, D. M. Khramov, C. D. Varnado, P. T. Creswell, J. W. Kamplain, V. M. Lynch and C. W. Bielawski, *Organometallics* **2009**, *28*, 5142-5147.

[24] a) H. Valdes, M. Poyatos and E. Peris, *Inorg. Chem.* **2015**, *54*, 3654-3659; b) H. Valdes, M. Poyatos and E. Peris, *Organometallics* **2014**, *33*, 394-401.

[25] L. T. Scott, *Chem. Soc. Rev.* **2015**, *44*, 6464-6471.

[26] S. Ibanez, M. Poyatos, L. N. Dawe, D. Gusev and E. Peris, *Organometallics* **2016**, *35*, 2747-2758.

[27] a) M. J. Pouy, S. A. Delp, J. Uddin, V. M. Ramdeen, N. A. Cochrane, G. C. Fortman, T. B. Gunnoe, T. R. Cundari, M. Sabat and W. H. Myers, *Acs Catalysis* **2012**, *2*, 2182-2193; b) M. Katari, M. N. Rao, G. Rajaraman and P. Ghosh, *Inorg. Chem.* **2012**, *51*, 5593-5604; c) L. Canovese, F. Visentin, C. Levi and C. Santo, *Inorg. Chim. Acta* **2012**, *391*, 141-149; d) E. Alvarado, A. C. Badaj, T. G. Larocque and G. G. Lavoie, *Chem. Eur. J.* **2012**, *18*, 12112-12121; e) S. Gaillard, J. Bosson, R. S. Ramon, P. Nun, A. M. Z. Slawin and S. P. Nolan, *Chem. Eur. J.* **2010**, *16*, 13729-13740.

[28] a) A. S. K. Hashmi, M. C. Blanco, E. Kurpejovic, W. Frey and J. W. Bats, *Adv. Synth. Catal.* **2006**, *348*, 709-713; b) N. Huguet, D. Leboeuf and A. M. Echavarren, *Chem. Eur. J.* **2013**, *19*, 6581-6585.

[29] A. Sygula, *Synlett* **2016**, *27*, 2070-2080.

Chapter 5

Experimental Section

5.1 Analytical techniques

Nuclear Magnetic Resonance (NMR)

^1H, $^{13}C\{^1H\}$ NMR spectra were recorded on the following spectrometers at 298 K:

- Varian Innova 300 MHz (^1H 300 MHz, ^{13}C 75 MHz)
- Varian Innova 400 MHz (^1H 400 MHz, ^{13}C 100 MHz)
- Varian Innova 500 MHz (^1H 500 MHz, ^{13}C 125 MHz)
- Bruker Avance 200 MHz (^1H 200 MHz, ^{13}C 50 MHz)
- Bruker Avance 300 MHz (^1H 300 MHz, ^{13}C 75 MHz)
- Bruker Avance 400 MHz (^1H 400 MHz, ^{13}C 100 MHz)

Chemical shifts are given in ppm (δ), referred to the residual peak of the deuterated solvent ($CDCl_3$, CD_2Cl_2, CD_3CN, CD_3OD, $(CD_3)_2CO$, toluene-d_8 and DMSO-d_6) and reported downfield of $SiMe_4$.

Electrospray Mass Spectra (ESI-MS) and High Resolution Mass Spectroscopy (HR-MS)

Electrospray Mass Spectra (ESI-MS) were recorded on a Micromass Quatro LC instrument; CH_3OH or CH_3CN were used as mobile phase and nitrogen was employed as drying and nebulizing gas. High Resolution Mass Spectra (HR-MS) were recorded on a QTOF I (quadrupole-hexapole-TOF) mass spectrometer with an orthogonal Z-spray-electrospray interface (Micromass, Manchester, UK). The drying gas as well as nebulizing gas was nitrogen at a flow of 400 L/h and 80 L/h respectively. The temperature of the source block was set to 120 ºC and the desolvation temperature to 150 ºC. A capillary voltage of 3.5 kV was used in the positive scan mode and the cone voltage was set to 30V.

Elemental Analysis (EA)

Elemental analyses were carried out on a EuroEA3000 Eurovector Analyzer.

Gas Chromatography: GC and GC/MS

GC analyses were obtained on a Shimadzu GC-2010 apparatus equipped with a FID and a Technokroma (TRB-5MS, 30 m x 0.25 mm x 0.25 μm) column was used.

Infrared Spectroscopy (IR)

Infrared spectra (FT-IR) were performed on a JASCO FT/IR-6200 spectrometer with a spectral window of 4000-500 cm^{-1}. The samples were prepared as KBr disks and in CH_2Cl_2 solution.

UV/Vis Spectroscopy

UV/Vis absorption spectra were recorded on a Varian Cary 300 BIO spectrophotometer using CH_3CN or toluene under ambient conditions. Extinction coefficients (ε) were determined from Beer's law measurements.

Fluorescence Spectroscopy

Emission spectra were recorded in a modular Horiba FluoroLog®-3 spectrofluorometer employing degassed CH_3CN or toluene. Quantum yields were determined relative to quinine bisulphate in degassed 1N sulfuric acid solution as standard (ϕ_f) with excitation at 290 nm.

Electrochemical Measurements

Electrochemical studies were carried out by using an Autolab Potentiostat, Model PGSTAT101 using a three-electrode cell. The cell was equipped with platinum working and counter electrodes, as well as a silver wire reference electrode. In all experiments, $[NBu_4][PF_6]$ (0.1 M in dry CH_2Cl_2) was used as the supporting electrolyte with analyte concentration of approximately 1 mM. Measurements were performed between 50 and 150 mVs^{-1} scan rates. All redox potentials were referenced to the Fc^+/Fc couple as internal standard with $E_{1/2}(Fc/Fc^+)$ vs. SCE = +0.44 V.

X-Ray Diffraction

Diffraction data were collected on a Agilent SuperNova diffractometer equipped with an Altas CCD detector using Cu Kα radiation (λ = 1.54184 Å). Single crystal was mounted on a MicroMount polymer tip (MiteGen) in a random orientation. The structures were solved by direct methods in SHELXS-97[1] and refined by the full-matrix method based on F^2 with the program SHELXL-97 using the OLEX software package.[1-2] Key details of the crystals and structures refinement data are summarized in the following tables. Table 5.10-14**.** Further crystallographic data may be found in the corresponding CIF file which was deposited at the Cambridge Crystallographic Data Centre CCDC, Cambridge, UK.

ITC

Isothermal titration calorimetry (ITC) experiments were carried out by using Microcal ITC Data Analysis Module.

5.2 Synthesis and characterization

All manipulations were carried out by using standard Schlenk techniques under nitrogen atmosphere unless otherwise stated. Anhydrous solvents were dried using a solvent purification system (SPS M BRAUN) or purchased from Aldrich and degassed prior to use by purging with dry nitrogen and kept over molecular sieves. All other reagents were used as received from commercial suppliers (1,3,5-tris(4-bromophenyl)benzene, 1,3-bis(2,6-diisopropylphenyl)imidazolium chloride (IPr.HCl), 1-phenylimidazole, coronene, fullerene (C_{60}), NiCp$_2$, Ag$_2$O, CuI and [RhCl(COD)]$_2$. 1,3,5-tris(4-ethynylphenyl)benzene,[3] 1,3-dimesityltriazine,[4] [IrCl(COD)]$_2$[5] and [AuCl(SMe$_2$)][6] was obtained as described in the literature. 1,2,5,6-tetrabromocorannulene has been provided by Jay S. Siegel research group.[7]

5.2.1 Synthesis and characterization of azolium and triazolium salts: Chapter 2 and 3

Synthesis of A
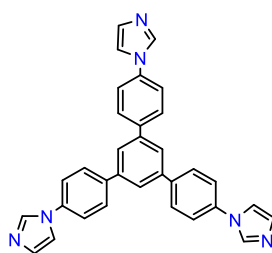
A round bottomed flask was loaded with 1,3,5-tris(4-bromophenylbenzene) (1 g, 1.84 mmol), K$_2$CO$_3$ (1.25 g, 9.05 mmol), imidazole (0.75 g, 11.02 mmol) and CuSO$_4$ (5 mg, 0.03 mmol). DMSO (5 mL) was added and the reaction mixture was heated to 185 ºC for 2 days. Then the solvent was removed by distillation. The crude mixture was redissolved in methylene chloride and washed with water. The resulting organic solution was dried with MgSO$_4$, and the solvent was removed under vacuum to yield a yellow solid, 0.60 g (65 %). ^{1}H NMR (300 MHz, CDCl$_3$): δ (ppm) 7.94 (s, 3H, NC*H*N), 7.82 (m, 9H, C*H*$_{Imid}$, C*H*$_{Ar}$), 7.55 (d, *J* = 6.6 Hz, 6H, C*H*$_{Ar}$), 7.36 (s, 3H, C*H*$_{Ar}$), 7.26 (s, 3H, C*H*$_{Imid}$). ^{13}C{^{1}H} NMR (75 MHz, CDCl$_3$): δ (ppm) 141.6 (*C*$_{Ar}$), 140.1 (*C*$_{Ar}$), 137.1 (*C*$_{Ar}$), 135.7 (*C*$_{Imid}$), 130.8 (*C*$_{Imid}$), 128.9 (*C*$_{Ar}$), 125.4 (*C*$_{Imid}$), 122.0 (*C*$_{Ar}$), 118.3 (*C*$_{Ar}$). Electrospray MS (20 V, *m/z*): 253.3 [M+2H]$^{2+}$. Elemental analysis calcd (%) for C$_{33}$H$_{24}$N$_6$·2H$_2$O: C, 73.3; H, 5.2; N,

15.5; found C 73.3; H 3.9; N 15.4. Melting point: 148 ºC. Decomposition temperature: 243 ºC.

Synthesis of [H₃B^{Et}](BF₄)₃
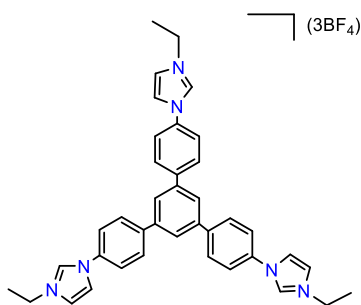
Triethyloxonium tetrafluoroborate (0.844 g, 4.44 mmol) was added to a Schlenk tube containing a solution of 1,3,5-tris(4-imidazolylphenylbenzene) (**A**) (0.5 g, 0.99 mmol) in dry methylene chloride (30 mL). Instantaneously, a white precipitate crashed out. The solid was filtered, washed with hexane and MeOH to yield 0.462 g of a white powder (55 %). ^{1}H NMR (300 MHz, DMSO-d_6): δ (ppm) 9.86 (s, 3H, NC*H*N), 8.41 (d, J = 8.4 Hz, 3H, C*H*$_{Ar}$), 8.29-8.15 (m, 9H, C*H*$_{Imid}$, C*H*$_{Ar}$), 8.10 (d, J = 8.1 Hz, 3H, C*H*$_{Imid}$), 7.96 (d, J = 8.4 Hz, 6H, C*H*$_{Ar}$), 4.33 (q, J = 7.3 Hz, 6H, C*H*$_2$), 1.55 (t, J = 7.3 Hz, 9H, C*H*$_3$). ^{13}C{^{1}H} NMR (75 MHz, DMSO-d_6): δ (ppm) 140.9 (C_{Ar}), 140.2 (C_{Ar}), 135.1 (NCHN), 134.4 (C_{Ar}), 129.0 (C_{Ar}), 125.4 (C_{Ar}), 123.0 (C_{Imid}), 122.2 (C_{Ar}), 121.1 (C_{Imid}), 44.8 (CH_2), 14.8 (CH_3). Electrospray MS (20 V, m/z): 196.9 [M]$^{3+}$, 339.3 [M+BF₄]$^{2+}$. Elemental analysis calcd (%) for C₃₉H₃₉N₆B₃F₁₂·2H₂O: C, 52.7; H, 4.9; N, 9.5; found C, 52.8; H, 5.1; N, 9.5. Decomposition temperature: 174 ºC

Synthesis of [H₃B^{Et}](Br)₃
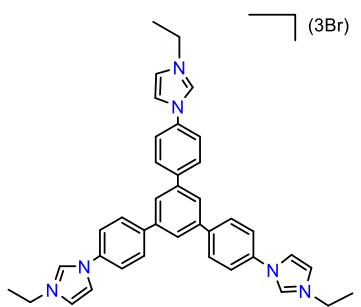
A sample of compound **A** (0.316 g, 0.63 mmol) and ethyl bromide (0.409 g, 3.76 mmol) were dissolved in DMF (10 mL) and the solution was heated to 100 °C for 48 h. A white solid precipitated over this period. After cooling of the reaction mixture to ambient temperature, the white precipitate was filtered off, washed with diethyl ether and dried *in vacuo* to give the salt **[H₃B^{Et}](Br)₃**. Yield: 0.344 g (66%). ^{1}H NMR (400 MHz, DMSO-d_6): δ (ppm) 10.05 (s, 3H, NC*H*N), 8.46 (s, 3H, C*H*$_{Imid}$), 8.29 (d, J = 8.7 Hz, 6H, C*H*$_{Ar}$), 8.17 (s, 3H, C*H*$_{Ar}$), 8.14 (s, 3H, C*H*$_{Imid}$), 8.00 (d, J = 8.7 Hz, 6H, C*H*$_{Ar}$), 4.35 (q, J = 7.3 Hz, 6H, C*H*$_2$), 1.55 (t, J = 7.3 Hz, 9H, C*H*$_3$). ^{13}C{^{1}H} NMR (100 MHz, DMSO-d_6): δ (ppm) 140.7 (C_{Ar}), 140.1 (C_{Ar}), 135.1 (NCHN), 134.3 (C_{Ar}), 128.9 (C_{Ar}), 125.3 (C_{Ar}), 123.0 (C_{Imid}), 122.1 (C_{Ar}), 121.0 (C_{Imid}), 44.8 (CH_2), 14.8 (CH_3). HR-MS (m/z): 197.1073 [M]$^{3+}$. Elemental analysis calcd (%) for C₃₉H₃₉N₆Br₃·H₂O: C, 55.1; H, 4.9; N, 9.9; found C, 55.1; H, 5.3; N, 9.9.

Synthesis of [H₃Bᴱᵗ](PF₆)₃
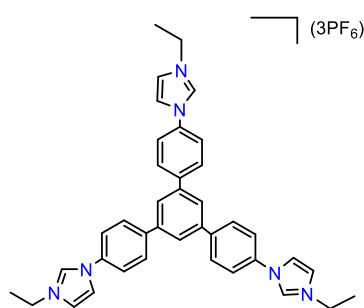
A methanolic solution of NH_4PF_6 (0.270 g, 1.66 mmol in 5 mL of MeOH) was added to a methanolic solution of **[H₃Bᴱᵗ](Br)₃** (0.344 g, 0.41 mmol in 10 mL of MeOH). The hexafluorophosphate salt **[H₃Bᴱᵗ](PF₆)₃** precipitated as white solid. The solid was collected by filtration, washed with cold methanol and diethyl ether and dried *in vacuo*. Yield: 0.334 g (79%). ¹H NMR (400 MHz, DMSO-d_6): δ (ppm) 9.88 (s, 3H, NCHN), 8.42 (s, 3H, CH_{Imid}), 8.29 (d, J = 8.6 Hz, 6H, CH_{Ar}), 8.18 (s, 3H, CH_{Ar}), 8.10 (s, 3H, CH_{Imid}), 7.96 (d, J = 8.6 Hz, 6H, CH_{Ar}), 4.33 (q, J = 7.3 Hz, 6H, CH_2), 1.56 (t, J = 7.3 Hz, 9H, CH_3). ¹³C{¹H} NMR (100 MHz, DMSO-d_6): δ (ppm) 140.8 (C_{Ar}), 140.1 (C_{Ar}), 135.1 (NCHN), 134.4 (C_{Ar}), 128.9 (C_{Ar}), 125.3 (C_{Ar}), 123.0 (C_{Imid}), 122.1 (C_{Ar}), 121.0 (C_{Imid}), 44.8 (CH_2), 14.7 (CH_3). HR-MS (*m/z*): 197.1073 $[M]^{3+}$.

Synthesis of [H₃Bᴹᵉ](CF₃SO₃)₃
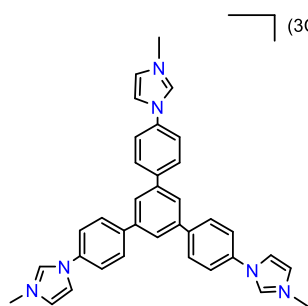
Methyl trifluoromethanesulfonate (143 μL 1.31 mmol) was added to a Schlenk containing a solution of 1,3,5-tris(4-imidazolylphenylbenzene) (**A**) (0.2 g, 0.40 mmol) in 1,2-dichloroethane (10 mL). The solution was heated at 100ºC overnight. An oily precipitate was obtained after evaporating the solvent. MeOH was added to dissolve the oily crude, and the addition of hexane yielded a light brown solid, 0.264 g (72 %). ¹H NMR (300 MHz, CD₃OD): δ (ppm) 9.52 (s, 3H, NCHN), 8.12-8.05 (m, 12H, CH_{Imid}, CH_{Ar}), 7.88-7.81 (m, 9H, CH_{Imid}, CH_{Ar}), 4.08 (s, 9H, CH_3). ¹³C{¹H} NMR (75 MHz, CD₃CN): δ (ppm) 142.8 (C_{Ar}), 141.6 (C_{Ar}), 136.3 (NCHN), 135.4 (C_{Ar}), 130.1 (C_{Ar}), 126.8 (C_{Ar}), 125.3 (C_{Imid}), 123.6 (C_{Ar}), 122.4 (C_{Imid}), 37.2 (CH_3). Electrospray MS (20 V, *m/z*): 183.2 $[M]^{3+}$. Elemental analysis calcd (%) for $C_{39}H_{33}N_6 S_3O_9F_9 \cdot H_2O$: C, 46.2; H, 3.5; N, 8.3; found C, 46.2; H, 4.5; N, 7.9. Decomposition temperature: 184 ºC.

117
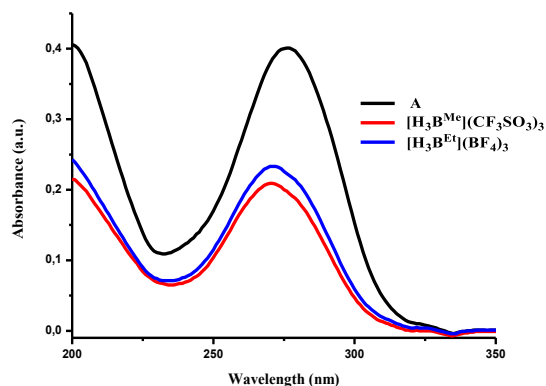
Figure 5.1. UV spectra of compounds **A**, **[H₃B^{Me}](CF₃SO₃)₃** and **[H₃B^{Et}](BF₄)₃** recorded in MeCN
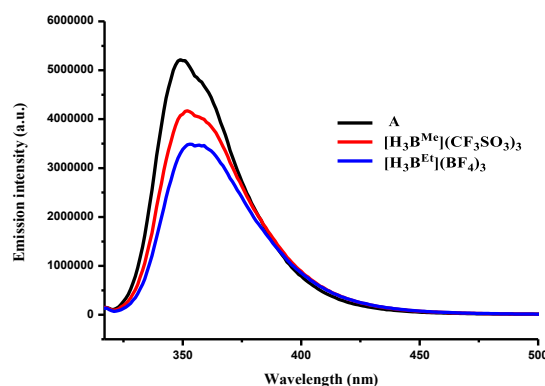
Figure 5.2. Emission spectra of compounds **A**, **[H₃B^{Me}](CF₃SO₃)₃** and **[H₃B^{Et}](BF₄)₃** at 290 nm in MeCN

Synthesis of [H₃C^{Mes}](PF₆)₃
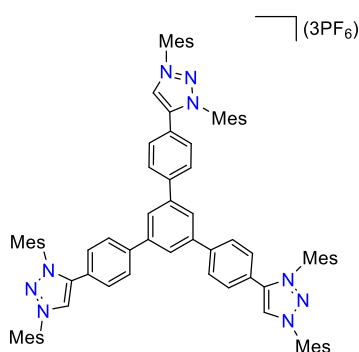
In a Schlenk tube, a mixture of wrapped with aluminum foil containing 1,3,5-tris-(4-ethynylphenyl)benzene (270 mg, 0.71 mmol), 1,3-dimesityltriazene (1.50 g, 4.10 mmol) and KPF₆ (990 mg, 5.38 mmol) in CH₂Cl₂ was cooled down to -78 °C and stirred during 30 min. Then ^{t}BuOCl (486 mg, 0.53 mmol) was added dropwise over the period of one hour at -78 °C and the reaction mixture was stirred at -78 °C during 6 hours. The reaction was allowed to slowly warm up and stirred at room temperature overnight. The resulting solution was filtrated, and the filtrate was evaporated. The resulting white solid was washed with diethyl ether and MeOH (yield: 1.1 g. 93%). ^{1}H NMR (300 MHz, CDCl₃): δ (ppm) 9.08 (s, 3H, NC*H*N), 7.77 (m, 9H, C*H*_Ar), 7.60 (m, 6H, C*H*_Ar), 7.14 (d, 12H, *J* = 6 Hz C*H*_Ar), 2.43 (bs, 18H,

118

CH_3), 2.22 (bs, 18H, CH_3), 2.06 (bs, 18H, CH_3). $^{13}C\{^1H\}$ NMR (75 MHz, CDCl$_3$): δ (ppm) 144.7 (C_{Ar}), 144.0 (C_{Ar}), 143.9 (C_{Ar}), 143.1 (C_{Ar}), 140.7 (C_{Ar}), 134.4 (C_{Ar}), 134.1 (C_{Ar}), 131.3 (NCHN), 130.8 (C_{Ar}), 130.2 (C_{Ar}), 128.7 (C_{Ar}), 126.0 (C_{Ar}), 120.7 (C_{Ar}), 21.5 (CH_3), 21.4 (CH_3), 17.5 (CH_3), 17.3 (CH_3). Electrospray MS (20 V, *m/z*): 406.6 $[M]^{3+}$, 682.5 $[MPF_6]^{2+}$. Elemental analysis calcd (%) for $C_{84}H_{84}N_9P_3F_{18}.3CH_2Cl_2$: C, 54.7; H, 4.7; N, 6.6; found C, 54.3; H, 5.0; N, 7.2.

Synthesis of [HD^{Et}](BF$_4$)
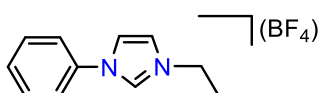
Triethyloxonium tetrafluoroborate was added (0.450 g, 2.37 mmol) to a Schlenk tube containing a solution of 1-phenylimidazole (200 μL, 1.60 mmol) in dry methylene chloride (10 mL) at room temperature. After 30 minutes, the solvent was removed affording an oil that was broken by hexane addition to yield 0.332 g of a white powder (81 %). ^1H NMR (300 MHz, CD$_3$CN): δ (ppm) 8.95 (s, 1H, NCHN), 7.78 (t, J = 1.8 Hz, 1H, CH_{Imid}), 7.69 – 7.56 (m, 6H, CH_{Imid}, CH_{Ar}), 4.31 (q, J = 7.3 Hz, 2H, CH_2), 1.55 (t, J = 7.3 Hz, 3H, CH_3). $^{13}C\{^1H\}$ NMR (75 MHz, CD$_3$CN): δ (ppm) 135.8 (C_{Ar}), 135.3 (C_{Ar}), 131.2 (C_{Ar}), 131.1 (C_{Ar}), 123.8 (NCHN), 123.3 (C_{Imid}), 122.6 (C_{Imid}), 46.3 (CH_2), 15.2 (CH_3). Electrospray MS (20 V, *m/z*): 173.0 $[M]^+$. Elemental analysis calcd (%) for $C_{11}H_{13}N_2BF_4$: C, 50.8; H, 5.0; N, 10.8; found C, 50.0; H, 4.7; N, 10.6.

5.2.2 Synthesis and characterization of azolium salts: Chapter 4

Synthesis of F
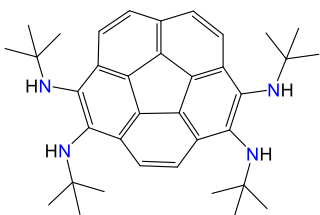
To a flame dried Schlenk (A) containing a suspension of 1,2,5,6-tetrabromocorannulene (300 mg, 0.53 mmol) in dry toluene (20 mL) was added NaO^{t}Bu (2 M in THF, 1.27 mL, 2.54 mmol). In parallel, to a flame dried Schlenk (B), containing a suspension of [Pd(OAc)$_2$] (8.36 mg, 0.037 mmol), IPr.HCl (31.75 mg, 0.074 mmol) in dry toluene (5 mL) was added NaO^{t}Bu (2 M in THF, 57 μL, 0.11 mmol). Both Schlenk tubes were stirred for 15 min at room temperature. Then, the solution from Schlenk (B) was transferred to Schlenk (A) *via* oven-dried cannula. Finally, *tert*-butyl amine (280 μL, 2.6 mmol) was added and the resulting mixture was refluxed overnight. The reaction mixture was allowed to cool down to room temperature and filtered over Celite. The solvent was evaporated under reduced pressure, yielding the desired product as an orange solid. Yield: 275 mg (97 %).

119

^{1}H NMR (500 MHz, CDCl$_3$): δ (ppm) 7.84 (d, *J* = 8.8 Hz, 2H, C*H*$_{Ar}$), 7.82 (s, 2H, C*H*$_{Ar}$), 7.63 (d, *J* = 8.8 Hz, 2H, C*H*$_{Ar}$), 4.51 (s, 2H, N*H*), 4.22 (s, 2H, N*H*), 1.31 (m, 36H, C(C*H*)$_3$). ^{13}C{^{1}H} NMR (100.8 MHz, CDCl$_3$): δ (ppm) 137.4 (*C*$_{Ar}$), 135.6 (*C*$_{Ar}$), 132.0 (*C*$_{Ar}$), 132.0 (*C*$_{Ar}$), 131.9 (*C*$_{Ar}$), 131.2 (*C*$_{Ar}$), 129.7 (*C*$_{Ar}$), 126.1 (*C*$_{Ar}$), 125.9 (*C*$_{Ar}$), 125.5 (*C*$_{Ar}$), 125.4 (*C*$_{Ar}$), 55.3 (N*C*(CH$_3$)$_3$), 55.3 (N*C*(CH$_3$)$_3$), 31.4 (NC(*C*H$_3$)$_3$), 31.4 (NC(*C*H$_3$)$_3$). HR-MS (*m/z*): 535.37 [M+H]$^+$. Elemental analysis calcd (%) for C$_{36}$H$_{46}$N$_4$.C$_7$H$_8$: C, 82.4; H, 8.7; N, 8.9; found C, 82.7; H, 8.5; N, 8.8.

Synthesis of [H$_2$G^{nBu}](PF$_6$)$_2$
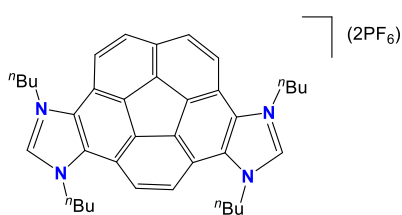
A Schlenk tube containing a mixture of compound **F** (150 mg, 0.28 mmol), 4 mL of tributyl orthoformate and NH$_4$PF$_6$ (150 mg, 0.92 mmol) was heated at 150 ºC for 12h. A sticky precipitate crashed out from an orange solution. The solution was discarded and the precipitate was dissolved in copious amount of methanol. The solution was filtrated and removed under vacuum obtained a pale orange solid. Yield: 168 mg (71 %). The solid was purified by liquid-liquid extraction in H$_2$O/CH$_2$Cl$_2$, then the aqueous phase was removed in vacuum obtained a yellow solid. ^{1}H NMR (300 MHz, CD$_3$OD): δ (ppm) 9.86 (s, 2H, NC*H*N), 8.50 (bs, 2H, C*H*$_{Ar}$), 8.33 (d, *J* = 8.8 Hz, 2H, C*H*$_{Ar}$), 8.22 (d, *J* = 8.7 Hz, 2H, C*H*$_{Ar}$), 5.04 (m, 8H, NC*H*$_2$CH$_2$CH$_2$CH$_3$), 2.31 (m, 8H, NCH$_2$C*H*$_2$CH$_2$CH$_3$), 1.75-1.62 (m, 8H, NCH$_2$CH$_2$C*H*$_2$CH$_3$), 1.16 (m, 12H, NCH$_2$CH$_2$CH$_2$C*H*$_3$). ^{13}C{^{1}H} NMR (75.6 MHz, CD$_3$OD): δ (ppm) 140.7 (N*C*HN), 133.6 (*C*$_{Ar}$), 132.1 (*C*$_{Ar}$), 130.5 (*C*$_{Ar}$), 130.2 (*C*$_{Ar}$), 129.9 (*C*$_{Ar}$), 129.3 (*C*$_{Ar}$), 125.4 (*C*$_{Ar}$), 123.8 (*C*$_{Ar}$), 119.4 (*C*$_{Ar}$), 118.9 (*C*$_{Ar}$), 50.8 (N*C*H$_2$CH$_2$CH$_2$CH$_3$), 31.7 (NCH$_2$*C*H$_2$CH$_2$CH$_3$), 20.3 (NCH$_2$CH$_2$*C*H$_2$CH$_3$), 13.9 (NCH$_2$CH$_2$CH$_2$*C*H$_3$). HR-MS (*m/z*): 278.2 [M]$^{2+}$ Elemental analysis calcd (%) for C$_{38}$H$_{44}$N$_4$(PF$_6$): C, 53.9; H, 5.2; N, 6.6; found C, 53.2; H, 5.6; N, 6.3.

Synthesis of [H$_2$G^{tBu}](PF$_6$)$_2$
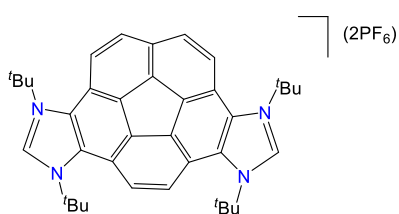
A Schlenk tube containing a mixture of compound **F** (150 mg, 0.28 mmol), 4 mL of tributyl orthoformate and NH$_4$PF$_6$ (150 mg, 0.92 mmol) was stirred at room temperature for 4 days. After this period of time a precipitate crashed out from an orange solution. Acetone was added over the suspension and filtered over Celite. The solvent was removed under vacuum to yield an orange solid, which was washed with diethyl ether.

The residue was dissolved in a copious amount of CH_2Cl_2 filtered over Celite and the solution was dried under vacuum. The final product was obtained as a yellow solid. Yield: 158 mg (67 %). ^{1}H NMR (300 MHz, $(CD_3)_2CO$): δ (ppm) 9.55 (s, 2H, NC*H*N), 9.13 (s, 2H, C*H*$_{Ar}$), 8.89 (d, $J = 9$ Hz, 2H, C*H*$_{Ar}$), 8.54 (d, $J = 9$ Hz, 2H, C*H*$_{Ar}$), 2.32 (m, 36H, NC(C*H*$_3$)). ^{13}C{^{1}H} NMR (100.8 MHz, $(CD_3)_2CO$): δ (ppm) 137.8 (N*C*HN), 134.1 (C_{Ar}), 132.4 (C_{Ar}), 132.3 (C_{Ar}), 131.6 (C_{Ar}), 130.5 (C_{Ar}), 129.8 (C_{Ar}), 129.1 (C_{Ar}), 120.2 (C_{Ar}), 119.2 (C_{Ar}), 64.1 (N*C*(CH$_3$)$_3$), 64.0 (N*C*(CH$_3$)$_3$), 27.7 (NC(*C*H$_3$)$_3$). HR-MS (*m/z*): 278.2 $[M]^{2+}$ Elemental analysis calcd (%) for $C_{38}H_{44}N_4(PF_6)$: C, 53.9; H, 5.2; N, 6.6; found C, 53.2; H, 5.6; N, 6.3.

Synthesis of G*^{tBu}*
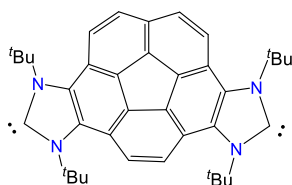
Under inert atmosphere, a NMR tube with a Teflon-lined cap was charged with **[H₂G*^{tBu}*](PF₆)₂** (16 mg, 0.018 mmol), NaO*^{t}*Bu (1.8 mg, 0.018 mmol) and dried C_6D_6 (0.6 mL). To this suspension, NaHMDS (1 M in THF, 49 µL, 0.049 mmol) was added and the reaction mixture was stirred at room temperature for 2 h. ^{1}H NMR (500 MHz, C_6D_6): δ (ppm) 8.55 (s, 2H, C*H*$_{Ar}$), 8.48 (d, $J = 10.0$ Hz, 2H, C*H*$_{Ar}$), 7.86 (d, $J = 10.0$ Hz, 2H, C*H*$_{Ar}$), 2.09 (m, 36H, NC(C*H*$_3$)$_3$ ^{13}C{^{1}H} NMR (126 MHz, C_6D_6): δ (ppm) 219.9 ($C_{Carbene}$), 132.4 (C_{Ar}), 131.1 (C_{Ar}), 130.0 (C_{Ar}), 128.0 (C_{Ar}), 127.9 (C_{Ar}), 126.3 (C_{Ar}), 120.3 (C_{Ar}), 118.0 (C_{Ar}), 58.0 (N*C*(CH$_3$)$_3$), 31.3-31.2 (NC(*C*H$_3$)$_3$).

5.2.3 Synthesis and characterization of metal complexes: Chapter 2

Synthesis of 1B^{Me}
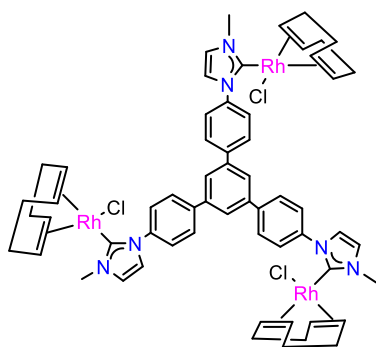
To a Schlenk containing a solution of **[H₃B^{Me}](CF₃SO₃)₃** (0.100 g, 0.10 mmol) and [RhCl(COD)]₂ (0.074 g, 0.15 mmol) in THF (15 mL) at -78 ºC, was added dropwise a solution of KHMDS (0.5 M in toluene, 662 µL, 0.33 mmol). The mixture was stirred overnight to room temperature. After removal of the volatiles, the crude solid was dissolved in CH_2Cl_2 and purified by column chromatography using silica gel. An orange product was obtained (72 mg). Yield: 56 %. ^{1}H NMR (300 MHz, CDCl₃): δ (ppm) 8.38 (d, $J = 8.5$ Hz, 6H, C*H*$_{Ar}$), 7.93 (m, 9H, C*H*$_{Imid}$, C*H*$_{Ar}$), 7.25 (s, 3H, C*H*$_{Ar}$), 7.02 (d, $J = 2.0$ Hz, 3H, C*H*$_{Imid}$), 5.06 (m, 3H, C*H*$_{COD}$), 4.24 (s, 9H, C*H*$_3$), 3.29 (br s, 3H, C*H*$_{COD}$), 2.64 (br s, 3H,

CH_{COD}), 2.36-2.17 (m, 12H, CH_{2COD}), 1.61 (m, 12H, CH_{2COD}). $^{13}C\{^{1}H\}$ NMR (75 MHz, CDCl$_3$): δ (ppm) 183.8 (d, J = 51.2 Hz, Rh-$C_{carbene}$), 141.9 (C_{Ar}), 140.4 (C_{Ar}), 140.0 (C_{Ar}), 127.8 (C_{Ar}), 125.4 (C_{Ar}), 125.3 (C_{Ar}), 123.0 (C_{Imid}), 121.2 (C_{Imid}), 98.3 (C_{COD}), 68.7 (C_{COD}), 68.5 (C_{COD}), 68.3 (C_{COD}), 68.1 (C_{COD}), 54.0 (CH_3), 38.6 (C_{COD}), 32.1 (C_{COD}), 31.0 (C_{COD}), 29.4 (C_{COD}), 28.7 (C_{COD}). Electrospray MS (20 V, *m/z*): 627.7 [M-2Cl+MeCN]$^{2+}$.

Synthesis of 2B^{Et}
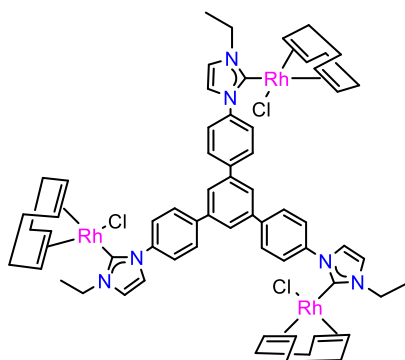
To a Schlenk containing a solution of **[H$_3$B^{Et}](BF$_4$)$_3$** (0.100 g, 0.12 mmol) and [RhCl(COD)]$_2$ (0.087 g, 0.18 mmol) in THF (15 mL) at -78 ºC, a solution of KHMDS (0.5M in toluene, 774 µL, 0.39 mmol) was added dropwise. The mixture was stirred overnight to room temperature. After removal of the volatiles, the crude solid was dissolved in methylene chloride and purified by column chromatography using silica gel. Using mixtures of CH$_2$Cl$_2$/acetone, an orange product (87 mg) was obtained. Yield: 56 %. ^{1}H NMR (300 MHz, CDCl$_3$): δ (ppm) 8.39 (d, J = 8.4 Hz, 6H, CH_{Ar}), 7.96 (m, 9H, CH_{Imid}, CH_{Ar}), 7.30 (s, 3H, CH_{Ar}), 7.06 (d, J = 2.0 Hz, 3H, CH_{Imid}), 5.14 (m, 3H, CH_{COD}), 4.98 (m, 3H, CH_{COD}), 4.78 (m, 6H, CH_2), 3.28 (br s, 3H, CH_{COD}), 2.67 (br s, 3H, CH_{COD}), 2.36 (m, 12H, CH_{2COD}), 2.17 (m, 12H, CH_{2COD}), 1.86 (m, 9H, CH_3). $^{13}C\{^{1}H\}$ NMR (75 MHz, CDCl$_3$): δ (ppm) δ 182.9 (d, J = 51.3 Hz, Rh-$C_{carbene}$), 141.9 (C_{Ar}), 140.32 (C_{Ar}), 140.2 (C_{Ar}), 127.7 (C_{Ar}), 125.4 (C_{Ar}), 125.3 (C_{Ar}), 121.6 (C_{Imid}), 120.6 (C_{Imid}), 97.9 (C_{COD}), 68.9 (C_{COD}), 68.8 (C_{COD}), 68.5 (C_{COD}), 68.3 (C_{COD}), 46.6 (CH_2), 33.5 (C_{COD}), 32.0 (C_{COD}), 29.8 (C_{COD}), 29.2 (C_{COD}), 28.6 (C_{COD}), 16.2 (CH_3). Electrospray MS (20 V, *m/z*): 648.8 [M-2Cl+MeCN]$^{2+}$. Elemental analysis calcd (%) for C$_{63}$H$_{72}$N$_6$Rh$_3$Cl$_3\cdot$2H$_2$O$\cdot$CH$_2$Cl$_2$: C, 53.0; H, 5.4; N, 5.8; found C, 53.0; H, 6.0; N, 5.6.

Synthesis of 3B^{Et}
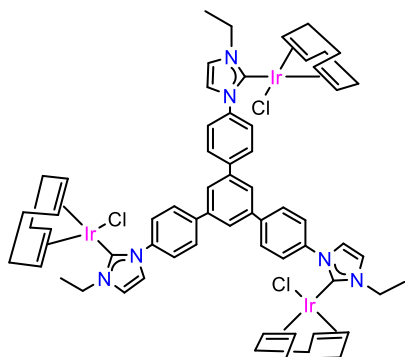
A solution of KHMDS (0,5M in toluene, 774 μL, 0.39 mmol) was added dropwise to a Schlenk tube containing a solution of **[H$_3$B^{Et}](BF$_4$)$_3$** (0.10 g, 0.12 mmol) and [IrCl(COD)]$_2$ (0.12 g, 0.18 mmol) in THF (15 mL) at -78 ºC. The mixture was stirred overnight at room temperature. After removal of the volatiles, the crude mixture was dissolved in CH$_2$Cl$_2$ and purified by column chromatography using silica gel (CH$_2$Cl$_2$/acetone), to yield 79 mg of an orange product. Yield: 42 %. ^{1}H NMR (300 MHz, CDCl$_3$): δ (ppm) 8.20 (d, J = 8.4 Hz, 6H, CH_{Ar}), 7.92-7.83 (m, 9H, CH_{Imid}, CH_{Ar}), 7.23 (d, J = 1.9 Hz, 3H, CH_{Ar}), 7.06 (d, J = 2.0 Hz, 3H, CH_{Imid}), 4.72-4.51 (m, 12H, C$H_{COD}$, C$H_2$), 2.89 (m, 3H, C$H_{COD}$), 2.34-2.14 (m, 12H, C$H_{2COD}$), 1.91-1.84 (m, 3H, C$H_{COD}$), 1.61-1.47 (m, 21H, C$H_{2COD}$, C$H_3$). ^{13}C{^{1}H} NMR (75 MHz, CDCl$_3$): δ (ppm) δ 180.3 (Ir-$C_{carbene}$), 142.0 (C_{Ar}), 140.3 (C_{Ar}), 140.0 (C_{Ar}), 127.6 (C_{Ar}), 125.8 (C_{Ar}), 125.4 (C_{Ar}), 121.4 (C_{Imid}), 120.4 (C_{Imid}), 84.3 (C_{COD}), 83.8 (C_{COD}), 68.6 (C_{COD}), 52.3 (C_{COD}), 52.2 (C_{COD}), 46.4 ($C H_2$), 34.1 (C_{COD}), 32.8 (C_{COD}), 29.8 (C_{COD}), 29.6 (C_{COD}), 29.5 (C_{COD}), 28.0 (C_{COD}), 16.1 ($C H_3$). Electrospray MS (20 V, m/z): 783.2 [M-2Cl+MeCN]$^{2+}$. Elemental analysis calcd (%) for C$_{63}$H$_{72}$N$_6$Ir$_3$Cl$_3$·2H$_2$O·2CH$_2$Cl$_2$: C, 43.3; H, 4.5; N, 4.7; found C, 43.0; H, 3.3; N, 4.5.

Synthesis of 4B^{Et}
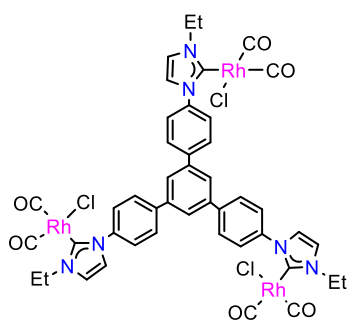
CO gas was bubbled through a solution of **1B^{Me}** in dichloromethane (10 mL) at 0 ºC for 30 min. The solution was concentrated by evaporation of the solvent under reduced pressure. Addition of hexanes allowed the precipitation of **4B^{Et}** as a yellow solid (59 mg). Yield: 90 %. ^{1}H NMR (300 MHz, CDCl$_3$): δ (ppm) 7.92-7.87 (m, 15H, CH_{Ar}), 7.36 (br s, 3H, CH_{Imid}), 7.20 (br s, 3H, CH_{Imid}), 4.98 (br s, 6H, CH_2), 1.61 (s, 9H, CH_3). ^{13}C{^{1}H} NMR (75 MHz, CDCl$_3$): δ (ppm) 185.6 (d, J = 54.3 Hz, Rh-$C_{carbene}$), 182.2 (d, J = 74.7 Hz, Rh-CO), 173.9 (d, J = 43.6 Hz, Rh-CO), 141.1 (C_{Ar}), 141.0 (C_{Ar}), 139.2 (C_{Ar}), 128.0 (C_{Ar}), 125.8 (C_{Ar}), 125.4 (C_{Ar}), 122.7 (C_{Imid}), 121.6 (C_{Imid}), 46.8 ($C H_2$), 16.0 ($C H_3$). Electrospray MS (20 V, m/z): 1188.8 [M-CO-Cl+2MeCN]$^+$, 1106.8 [M-CO-Cl]$^+$. Elemental analysis calcd (%) for

$C_{45}H_{36}N_6Rh_3Cl_3O_6 \cdot 2H_2O$: C, 44.8; H, 3.3; N, 6.8; found C, 44.4; H, 3.8; N, 6.8; IR (cm^{-1}): 2072, 1991; TEP: 2045.
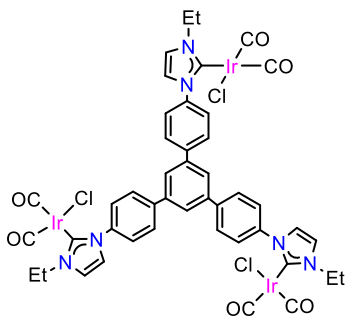
Synthesis of 5B^{Et}

CO was bubbled through a solution of **3B^{Et}** in dichloromethane (10 mL) at 0 ºC for 30 min. The solution was concentrated by evaporation of the solvent under reduced pressure. A yellow precipitate was obtained after addition of hexanes to the residue (78 mg). Yield: 87 %. ^{1}H NMR (300 MHz, CDCl$_3$): δ (ppm) 7.90 (br s, 3H, CH_{Ar}), 7.84 (br s, 12H, CH_{Ar}), 7.32 (br s, 3H, CH_{Imid}), 7.21 (br s, 3H, CH_{Imid}), 4.52 (br s, 6H, CH_2), 1.59 (s, 9H, CH_3). ^{13}C{^{1}H} NMR (75 MHz, CDCl$_3$): δ (ppm) 181.1 (Ir-$C_{carbene}$), 173.3 (Ir-CO), 167.8 (Ir-CO), 141.4 (C_{Ar}), 141.3 (C_{Ar}), 139.1 (C_{Ar}), 128.1 (C_{Ar}), 126.7 (C_{Ar}), 125.7 (C_{Ar}), 122.8 (C_{Imid}), 121.4 (C_{Imid}), 46.9 (CH$_2$), 16.0 (CH$_3$). Electrospray MS (20 V, *m/z*): 1506.9 [M-3Cl-3CO+6MeCN]$^+$. IR (cm^{-1}): 2061, 1975; TEP: 2045 cm^{-1}.

Synthesis of 1D^{Et}
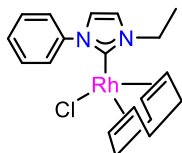
To a Schlenk tube containing a solution of **[HD^{Et}](BF$_4$)** (0.100 g, 0.38 mmol) and [RhCl(COD)]$_2$ (0.095 g, 0.19 mmol) in THF (15 mL) at -78 ºC, a solution of KHMDS was added dropwise (0.5M in toluene, 845 µL, 0.42 mmol). The mixture was stirred overnight at room temperature. After removal of the volatiles, the crude solid was dissolved in methylene chloride and purified by column chromatography using the mixture of (CH$_2$Cl$_2$/acetone) to yield 0.142 g of a yellow solid. Yield: 89 %. ^{1}H NMR (300 MHz, CDCl$_3$): δ (ppm) 8.18-8.15 (m, 2H, CH_{Ar}), 7.56-7.44 (m, 3H, CH_{Ar}), 7.14 (d, *J* = 1.9 Hz, 1H, CH_{Imid}), 7.01 (d, *J* = 1.9 Hz, 1H, CH_{Imid}), 5.08 (m, 1H, CH_{COD}), 4.93 (m, 1H, CH_{COD}), 4.82-4.67 (m, 2H, CH_2), 3.21 (m, 1H, CH_{COD}), 2.54 (m, 1H, CH_{COD}), 1.81-1.77 (m, 4H, CH_{COD}), 1.62-1.57 (m, 3H, CH_3). ^{13}C{^{1}H} NMR (75 MHz, CDCl$_3$): δ (ppm) 182.6 (d, *J* = 51.2 Hz, Rh-$C_{carbene}$), 140.4 (C_{Ar}), 128.8 (C_{Ar}), 127.8 (C_{Ar}), 124.7 (C_{Ar}), 121.4 (C_{Imid}), 120.3 (C_{Imid}), 97.7 (C_{COD}), 97.6 (C_{COD}), 97.5 (C_{COD}), 97.4 (C_{COD}), 68.6 (C_{COD}), 68.1 (C_{COD}), 46.3 (CH$_2$), 33.4 (C_{COD}), 31.7 (C_{COD}), 28.9 (C_{COD}), 28.4 (C_{COD}), 16.0 (CH$_3$). Electrospray MS (20 V, *m/z*): 383.2 [M-Cl], 424.2 [M-Cl+MeCN]$^+$. Elemental analysis calcd (%) for $C_{19}H_{24}N_2RhCl$: C, 54.5; H, 5.8; N, 6.7; found C, 53.3; H, 6.7; N, 6.9.

Figure 5.3. CV plot of complexes **2B**[Et] and **1D**[Et] (1mM in dry CH$_2$Cl$_2$ with 0.1M [NBu$_4$][PF$_6$] as the supporting electrolyte, 50 mVs^{-1} scan rate, Fc$^+$/Fc used as internal standard with E$_{1/2}$ (Fc/Fc$^+$) = 0.44 V vs. SCE).

Figure 5.4. DPV section of complexes **2B**[Et] and **1D**[Et] (1mM in dry CH$_2$Cl$_2$ with 0.1M [NBu$_4$][PF$_6$] as the supporting electrolyte, 50 mVs^{-1} scan rate, Fc$^+$/Fc used as internal standard with E$_{1/2}$ (Fc/Fc$^+$) = 0.44 V vs. SCE).

Synthesis of 2D[Et]
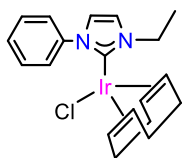
To a Schlenk containing a solution of **[HD**[Et]**](BF$_4$)** (0.100 g, 0.38 mmol) and [IrCl(COD)]$_2$ (129 mg, 0.18 mmol) in THF (15 mL) at -78 ºC, a (0.5M in toluene solution) of KHMDS (980 μL, 0.49 mmol) was added dropwise. The mixture was stirred overnight at room temperature. After removal of the volatiles, the crude was dissolved in methylene chloride and purified by column chromatography using silica gel (CH$_2$Cl$_2$/acetone), to yield 0.130 g of a yellow solid. Yield: 60 %. ^{1}H NMR (300 MHz, CDCl$_3$): δ (ppm) 8.01-7.98 (m, 2H, C*H*$_{Ar}$), 7.49-7.41 (m, 3H, C*H*$_{Ar}$), 7.14 (d, *J* = 1.9 Hz, 1H, C*H*$_{Imid}$), 7.01 (d, *J* = 1.9 Hz, 1H, C*H*$_{Imid}$), 4.71-4.46 (m, 4H, C*H*$_{2COD}$, C*H*$_2$), 2.84 (m, 1H, C*H*$_{COD}$), 2.25-2.11 (m, 4H, C*H*$_{2COD}$), 1.95-1.83 (m, 1H, C*H*$_{COD}$) , 1.58-1.49 (m, 6H, C*H*$_{2COD}$, C*H*$_3$), 1.39-1.20 (m, 1H, C*H*$_{2COD}$). ^{13}C{^{1}H} NMR (75 MHz, CDCl$_3$): δ (ppm)

180.1 (Ir-$C_{carbene}$), 140.3 (C_{Ar}), 128.7 (C_{Ar}), 127.8 (C_{Ar}), 125.3 (C_{Ar}), 121.4 (C_{Imid}), 120.2 (C_{Imid}), 84.0 (C_{COD}), 83.4 (C_{COD}), 52.1 (C_{COD}), 52.0 (C_{COD}), 46.2 (CH_2), 34.1 (C_{COD}), 32.6 (C_{COD}), 29.5 (C_{COD}), 29.4 (C_{COD}), 16.2 (CH_3). Electrospray MS (20 V, *m/z*): 514.1 [M-Cl+MeCN]$^+$. Elemental analysis calcd (%) for $C_{19}H_{24}N_2IrCl.1/2(C_6H_{14}).H_2O$: C, 46.4; H, 5.8; N, 4.9; found C, 46.1; H, 6.5; N, 5.5.
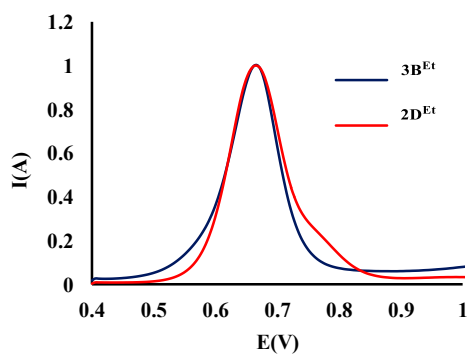
Figure 5.5. DPV section of complexes **3B**^{Et} and **2D**^{Et} (1mM in dry CH_2Cl_2 with 0.1M [NBu$_4$][PF$_6$] as the supporting electrolyte, 50 mVs^{-1} scan rate, Fc$^+$/Fc used as internal standard with $E_{1/2}$ (Fc/Fc$^+$) = 0.44 V vs. SCE).
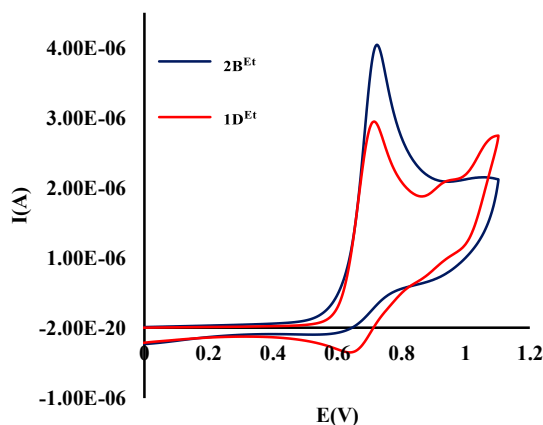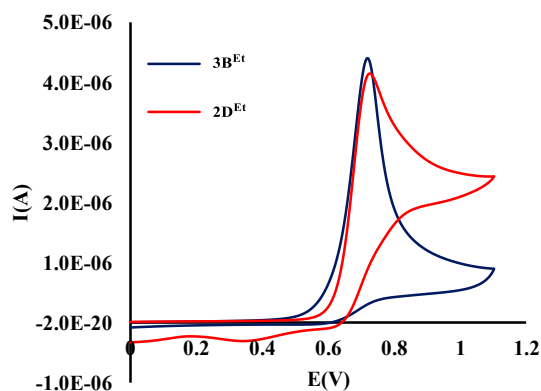

Figure 5.6. CV plot of complexes **3B**^{Et} and **2D**^{Et} (1mM in dry CH_2Cl_2 with 0.1M [NBu$_4$][PF$_6$] as the supporting electrolyte, 50 mVs^{-1} scan rate, Fc$^+$/Fc used as internal standard with $E_{1/2}$ (Fc/Fc$^+$) = 0.44 V vs. SCE).
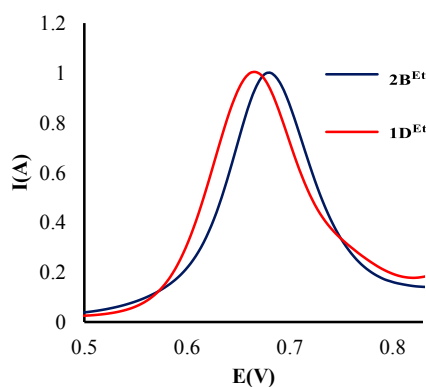
Synthesis of 1C^{Mes}
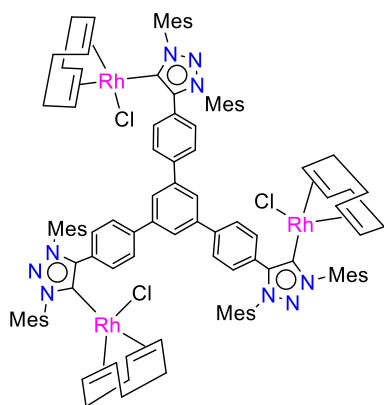
To a Schlenk containing a solution of tris-triazolium salt **[H₃C^{Mes}](PF₆)₃** (0.05 g, 0.03 mmol) and [RhCl(COD)]₂ (0.031 g, 0.06 mmol) in THF (15 mL) at -78 ºC, was added dropwise a solution of KHMDS (0.5 M in toluene, 400 µL, 0.20 mmol). The mixture was allowed to warm up to room temperature and stirred overnight. After removal of the volatiles, the crude solid was dissolved in CH_2Cl_2 and purified by column chromatography using silica gel and a DCM/Acetone mixture, to yield 55 mg of an orange solid. Yield: 84 %. ^{1}H NMR (300 MHz, CDCl₃): δ (ppm) 8.32 (d, *J* = 7.9 Hz, 6H, C*H*₍Ar₎), 7.84 (s, 3H, C*H*₍Ar₎), 7.72 (d, *J* = 8.6 Hz, 6H, C*H*₍Ar₎), 7.14-7.02 (m, 12H, C*H*₍Ar₎), 4.82 (m, 6H, C*H*₍COD₎), 3.27 (m, 6H, C*H*₍COD₎), 3.39 (m, 36H, C*H*₃), 2.11-1.98 (m, 42H, C*H*₃, C*H*₍COD₎). ^{13}C{^{1}H} NMR (75 MHz, CDCl₃): δ (ppm) 173.4 (d, *J* = 41.5 Hz, Rh-*C*₍carbene₎), 145.8 (*C*₍Ar₎), 141.6 (*C*₍Ar₎), 141.2 (*C*₍Ar₎), 140.0 (*C*₍Ar₎), 136.7 (*C*₍Ar₎), 135.0 (*C*₍Ar₎), 134.1 (*C*₍Ar₎), 133.9 (*C*₍Ar₎), 132.3 (*C*₍Ar₎), 129.9 (*C*₍Ar₎), 128.3 (*C*₍Ar₎), 127.9 (*C*₍Ar₎), 126.9 (*C*₍Ar₎), 125.3 (*C*₍Ar₎), 95.9 (), 95.4 (*C*₍COD₎), 69.3 (*C*₍COD₎), 67.1 (*C*₍COD₎), 33.7 (*C*₍COD₎), 32.0 (*C*₍COD₎), 29.4 (*C*₍COD₎), 28.5 (*C*₍COD₎), 21.4 (*C*H₃), 19.6 (*C*H₃), 17.9 (*C*H₃), 17.7 (*C*H₃). HR-MS (*m/z*): 616.6 [M]$^{3+}$, 942.3 [M-Cl]$^{2+}$.

Synthesis of 2C^{Mes}
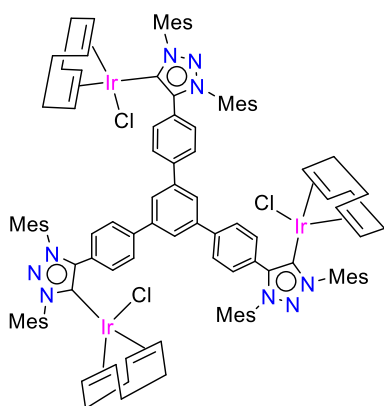
A Schlenk was charged with tris-triazolium salt **[H₃C^{Mes}](PF₆)₃** (0.05 g, 0.03 mmol), [IrCl(COD)]₂ (0.043 g, 0.06 mmol) and K₂CO₃ (0.54 g, 0.39 mmol). The resulting mixture was suspended in acetone (10 mL) and stirred for 1 day at 60 ºC. After this period of time the solid was filtered and washed several times with acetone. The crude mixture was dissolved in CH_2Cl_2 and purified by filtration through a pad of celite. The resulting solution was concentrated to dryness obtained 40 mg of a yellow solid. Yield: 60 %. ^{1}H NMR (300 MHz, CDCl₃): δ (ppm) 8.05 (d, *J* = 7.4 Hz, 6H, C*H*₍Ar₎), 7.78 (s, 3H, C*H*₍Ar₎), 7.63 (d, *J* = 7.8 Hz, 6H, C*H*₍Ar₎), 7.08-7.00 (m, 12H, C*H*₍Ar₎), 4.40 (m, 6H, C*H*₍COD₎), 2.94 (m, 6H, C*H*₍COD₎), 2.57-2.27 (m, 36H, C*H*₃), 2.04 (m, 42H, C*H*₃, C*H*₍COD₎). ^{13}C{^{1}H} NMR (75 MHz, CDCl₃): δ (ppm) 172.1 (Ir-*C*₍carbene₎), 146.3 (*C*₍Ar₎),

141.6 (C_{Ar}), 141.3 (C_{Ar}), 141.2 (C_{Ar}), 140.0 (C_{Ar}), 136.5 (C_{Ar}), 135.1 (C_{Ar}), 134.2 (C_{Ar}), 134.0 (C_{Ar}), 132.3 (C_{Ar}), 130.1 (C_{Ar}), 130.0(C_{Ar}), 129.7 (C_{Ar}), 128.3 (C_{Ar}), 127.5 (C_{Ar}), 126.7 (C_{Ar}), 125.3 (C_{Ar}), 81.8 (C_{COD}), 81.1 (C_{COD}), 52.8 (C_{COD}), 50.7 (C_{COD}), 34.2 (C_{COD}), 32.9 (C_{COD}), 30.1 (C_{COD}), 29.8 (C_{COD}), 29.1 (C_{COD}), 21.4 (CH_3), 19.6 (CH_3), 18.1 (CH_3), 17.7 (CH_3). HR-MS (*m/z*): 1075.6 [M-Cl]$^{2+}$.
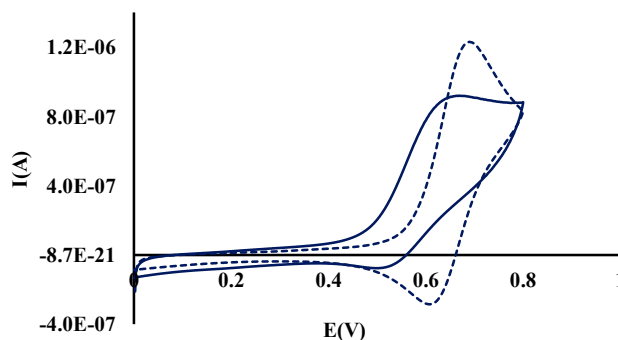
Figure 5.7. CV plots of complexes **1C^{Mes}** (continuous line), and **2C^{Mes}** (discontinuous line). Experiments carried out using 1mM solutions of the complexes in dry CH_2Cl_2 with 0.1M [NBu$_4$][PF$_6$] as the supporting electrolyte, 100 mVs^{-1} scan rate, Fc$^+$/Fc used as internal standard with $E_{1/2}$ (Fc/Fc$^+$) = 0.44 V vs. SCE.

Synthesis of 3C^{Mes}
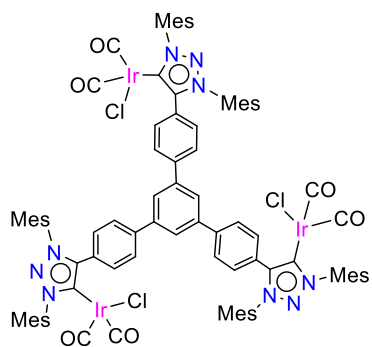
To a solution of **2C^{Mes}** (0.050 g, 0.02 mmol) in dichloromethane (10 mL) in round a bottomed flask, CO gas was bubble through at 0 ºC for 30 min. The solution was concentrated under reduced pressure. Addition of hexanes allows to precipitate a yellow solid 0.043 g. Yield: 93 %. ^{1}H NMR (300 MHz, CDCl$_3$): δ (ppm) 7.80-7.60 (m, 15H, C*H*$_{Ar}$), 7.07-7.04 (m, 12H, C*H*$_{Ar}$), 2.41-2.06 (m, 56H, C*H*$_3$). ^{13}C{^{1}H} NMR (75 MHz, CDCl$_3$): δ (ppm) 181.0 (Ir-$C_{carbene}$), 168.7 (Ir-*C*O), 166.0 (Ir-*C*O), 148.6 (C_{Ar}), 141.8 (C_{Ar}), 141.2 (C_{Ar}), 140.7 (C_{Ar}), 135.8 (C_{Ar}), 134.5 (C_{Ar}), 131.4 (C_{Ar}), 130.3 (C_{Ar}), 129.8 (C_{Ar}), 129.3 (C_{Ar}), 127.0 (C_{Ar}), 125.8 (C_{Ar}), 125.4 (C_{Ar}), 21.3 (CH_3), 18.2 (CH_3), 17.5 (CH_3). HR-MS (*m/z*): 2073.5 [M-Cl+MeCN]$^+$, IR (cm^{-1}): 2057, 1972; TEP: 2042.

Synthesis of 4C^{Mes}
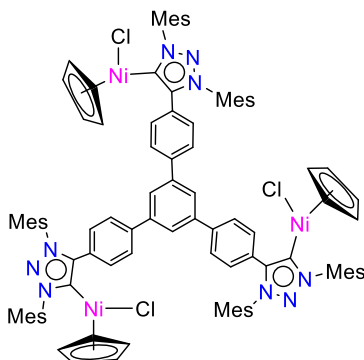
A Schlenk was charged with **[H₃C^{Mes}](PF₆)₃** (0.10 g, 0.06 mmol), NiCp₂ (0.46 g, 0.24 mmol) and NEt₄Cl (0.30 g, 0.18 mmol). The resulting mixture was suspended in 1,4-dioxane (8 mL) and stirred for 10 minutes at room temperature. Then, the reaction was heated to reflux overnight. The solution slowly turned from green to dark red. The crude mixture was cooled to RT and filtered through celite under nitrogen atmosphere. The solvent was removed under reduced pressure and the crude solid was washed with diethyl ether. The desired complex was purified by precipitation from a mixture of CH_2Cl_2/hexane to yield 40 mg of a red solid. Yield: 40 %. ^1H NMR (400 MHz, CDCl₃): δ (ppm) 8.44 (bs, 6H, CH_{Ar}), 7.92 (bs, 3H, CH_{Ar}), 7.81 (bs, 9H, CH_{Ar}), 7.18 (bs, 6H, CH_{Ar}), 7.04 (bs, 6H, CH_{Ar}), 4.79 (bs, 15H, CH_{Cp}), 2.36 (bs, 9H, CH_3), 2.23 (bs, 27H, CH_3), 1.99 (bs, 18H, CH_3). $^{13}C\{^1H\}$ NMR (100 MHz, CDCl₃): δ (ppm) 151.4 (Ni-$C_{carbene}$), 148.5 (C_{Ar}), 141.6 (C_{Ar}), 141.4 (C_{Ar}), 140.5 (C_{Ar}), 137.0 (C_{Ar}), 135.5 (C_{Ar}), 134.5 (C_{Ar}), 134.1 (C_{Ar}), 132.0 (C_{Ar}), 130.3 (C_{Ar}), 129.8 (C_{Ar}), 129.4 (C_{Ar}), 127.5 (C_{Ar}), 127.1 (C_{Ar}), 125.6 (C_{Ar}), 125.3 (C_{Ar}), 92.0 (CH_{Cp}), 21.4 (CH_3), 18.3 (CH_3), 17.7 (CH_3). HR-MS (*m/z*): 810.7 [M-2Cl]²⁺.
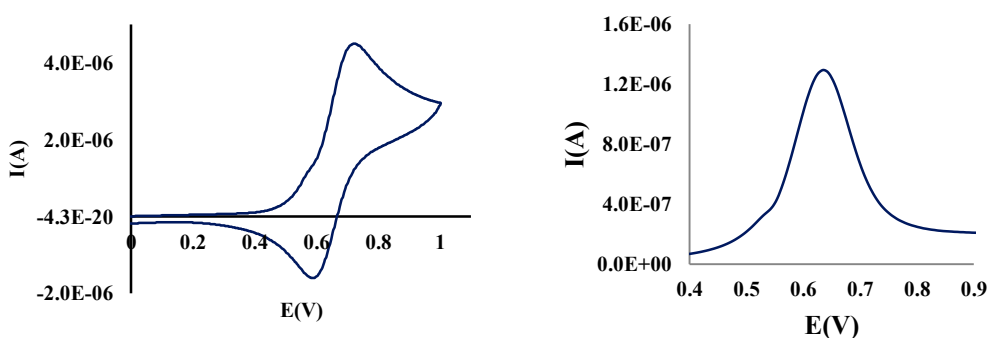
Figure 5.8. CV plot (left) and relevant DPV section (right) of complex **4C^{Mes}** (1mM in dry CH_2Cl_2 with 0.1M [NBu₄][PF₆] as the supporting electrolyte, 50 mVs⁻¹ scan rate, Fc⁺/Fc used as internal standard with $E_{1/2}$ (Fc/Fc⁺) = 0.44 V vs. SCE).

5.2.4 Synthesis and characterization of metal complexes: Chapter 3

Synthesis of 6B^{Et}
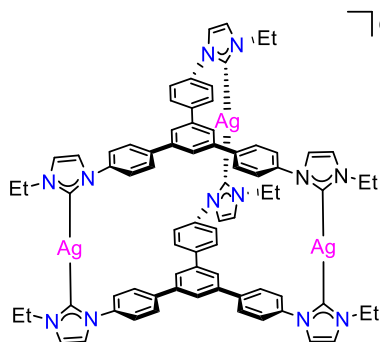
To a mixture of **[H$_3$B^{Et}](PF$_6$)$_3$** (0.080 g, 0.078 mmol) and Ag$_2$O (0.027 g, 0.117 mmol) was added acetonitrile (10 mL). The resulting suspension was heated to 60 °C for 48 h under exclusion of light. After cooling of the reaction mixture to ambient temperature, the obtained suspension was filtered through a pad of Celite to get a clear solution. The filtrate was concentrated to 3 mL and addition of 15 mL of diethyl ether resulted in the precipitation of a white solid. The precipitate was filtered off, washed with diethyl ether and dried *in vacuo*. Yield: 0.058 g (76%). ^{1}H NMR (400 MHz, DMSO-d_6): δ (ppm) 7.97 (s, 6H, C*H*$_{Imid}$), 7.87 (s, 6H, C*H*$_{Imid}$), 7.79 (s br, 24H, C*H*$_{Ar}$), 7.66 (s, 6H, C*H*$_{Ar}$), 4.43 (q, *J* = 7.3 Hz, 12H, C*H*$_2$), 1.60 (t, *J* = 7.3 Hz, 18H, C*H*$_3$). ^{13}C{^{1}H} NMR (100 MHz, DMSO-d_6): δ (ppm) δ 178.3 (Ag-$C_{carbene}$), 138.8 (C_{Ar}), 138.6 (C_{Ar}), 138.5 (C_{Ar}), 127.2 (C_{Ar}), 123.5 (C_{Ar}), 122.8 (C_{Ar}), 122.7 (C_{Imid}), 122.0 (C_{Imid}), 46.8 (*C*H$_2$), 16.9 (*C*H$_3$). HR-MS (*m/z*): 500.4 [M]$^{3+}$, 823.1 [MPF$_6$]$^{2+}$.

Synthesis of 7B^{Et}
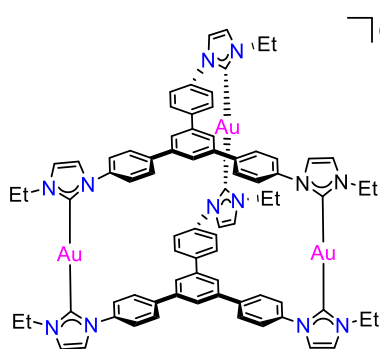
To a solution of **[H$_3$B^{Et}](PF$_6$)$_3$** (0.058 g, 0.030 mmol) in acetonitrile (5 mL) was added solid [AuCl(SMe$_2$)] (0.027 g, 0.092 mmol). Immediately after the addition a white solid started to precipitate. The reaction mixture was left stirring at ambient temperature for 16 h and was then slowly filtered through a pad of Celite until a clear filtrate was obtained. The filtrate was added slowly to diethyl ether (20 mL) to get a white solid which was collected by filtration, washed with diethyl ether and dried *in vacuo*. Yield: 0.046 g (70%). ^{1}H NMR (400 MHz, DMSO-d_6): δ (ppm) 7.96 (s, 6H, C*H*$_{Imid}$), 7.90 (s, 6H, C*H*$_{Imid}$), 7.84 (d, *J* = 8.3 Hz, 12H, C*H*$_{Ar}$), 7.77 (d, *J* = 8.3 Hz, 12H, C*H*$_{Ar}$), 7.71 (s, 6H, C*H*$_{Ar}$), 4.49 (q, *J* = 7.3 Hz, 12H, C*H*$_2$), 1.63 (t, *J* = 7.3 Hz, 18H, C*H*$_3$). ^{13}C{^{1}H} NMR (100 MHz, DMSO-d_6): δ (ppm) δ 180.6 (Au-$C_{carbene}$), 138.7 (C_{Ar}), 138.4 (C_{Ar}), 137.9 (C_{Ar}), 126.9 (C_{Ar}), 124.4 (C_{Ar}), 122.8 (C_{Imid}), 122.7 (C_{Imid}), 46.4 (*C*H$_2$), 16.7 (*C*H$_3$). HR-MS (*m/z*): 589.1 [M]$^{3+}$, 956.2 [MPF$_6$]$^{2+}$.

Synthesis of 8B^{Et}

$\rceil$ (3PF$_6$)
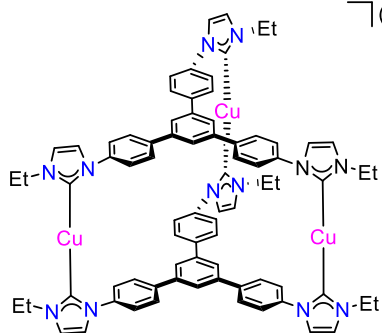
A sample of **[H₃B^{Et}](PF₆)₃** (0.058 g, 0.030 mmol) was dissolved in 10 mL of acetonitrile and to this solution was added solid CuI (0.018 g, 0.095 mmol). The reaction mixture was stirred for 16 h at ambient temperature. The resulting suspension was slowly filtered through a pad of Celite to get a clear solution. The filtrate was concentrated to 2 mL and addition of 10 mL diethyl ether resulted in the precipitation of a white solid. The white solid was filtered off, washed with diethyl ether and dried *in vacuo*. Yield: 0.034 g (63%). ¹H NMR (200 MHz, DMSO-*d₆*): δ (ppm) 7.98 (s, 6H, C*H*$_{Imid}$), 7.83 (s, 6H, C*H*$_{Imid}$), 7.78 (s, 24H, C*H*$_{Ar}$), 7.64 (s, 6H, C*H*$_{Ar}$), 4.45 (q, *J* = 7.2 Hz, 12H, C*H₂*), 1.61 (t, *J* = 7.2 Hz, 18H, C*H₃*). ¹³C{¹H} NMR (50 MHz, DMSO-*d₆*): δ (ppm) δ 174.3 (Cu-*C*$_{carbene}$), 137.9 (*C*$_{Ar}$), 137.3 (*C*$_{Ar}$), 126.1 (*C*$_{Ar}$), 126.1 (*C*$_{Ar}$), 122.3 (*C*$_{Ar}$), 121.9 (*C*$_{Ar}$), 121.5 (*C*$_{Imid}$), 120.6 (*C*$_{Imid}$), 45.9 (*C*H₂), 16.4 (*C*H₃). HR-MS (*m/z*): 455.8 [M]³⁺.

Synthesis of 5C^{Mes}

$\rceil$ (3PF$_6$)
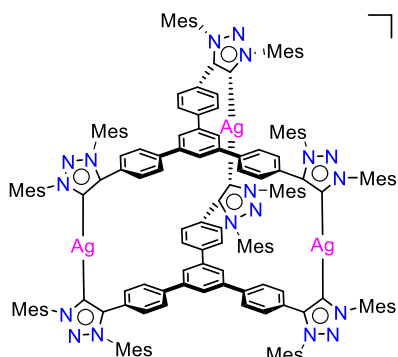
A mixture of **[H₃C^{Mes}](PF₆)₃** (100 mg, 0.085 mmol) and Ag₂O (30 mg, 0.13 mmol) in MeOH (7 mL) was heated at 60 °C overnight under exclusion of light. After cooling the reaction mixture to room temperature, the suspension was filtered through a pad of Celite, washed with CH₂Cl₂ to yield a clear solution, which was concentrated to dryness yielding a white solid. (yield: 114 mg. 42%). ¹H NMR (300 MHz, CD₂Cl₂): δ (ppm) 7.53-7.35 (m, 30H, C*H*$_{Ar}$), 7.06-7.00 (m, 24H, C*H*$_{Ar}$), 2.54 (bs, 18H, C*H₃*), 2.34 (bs, 18H, C*H₃*). ¹³C{¹H} NMR (75 MHz, CD₂Cl₂): δ (ppm) 169.7 (dd, *J* (C-Ag¹⁰⁷) = 165.0 Hz, *J* (C-Ag¹⁰⁹) = 190.5Hz, *C*$_{carbene}$), 150.3 (*C*$_{Ar}$), 150.1 (*C*$_{Ar}$), 142.6 (*C*$_{Ar}$), 141.2 (*C*$_{Ar}$), 141.0 (*C*$_{Ar}$), 139.8 (*C*$_{Ar}$), 136.2 (*C*$_{Ar}$), 134.3 (*C*$_{Ar}$), 131.8 (*C*$_{Ar}$), 130.4 (*C*$_{Ar}$), 129.8 (*C*$_{Ar}$), 129.3 (*C*$_{Ar}$), 127.1 (*C*$_{Ar}$), 123.9 (*C*$_{Ar}$), 21.8 (*C*H₃), 21.5 (*C*H₃), 17.9 (*C*H₃). Electrospray MS (20 V, *m/z*): 919.2 [M]³⁺, 1451.2 [M-Cl]²⁺. Elemental analysis calcd (%) for C₁₆₈H₁₆₂N₁₈Ag₃P₃F₁₈: C, 63.2; H, 5.1; N, 7.8 found C, 63.4; H, 5.3; N, 7.3.

Synthesis of 6C^{Mes}
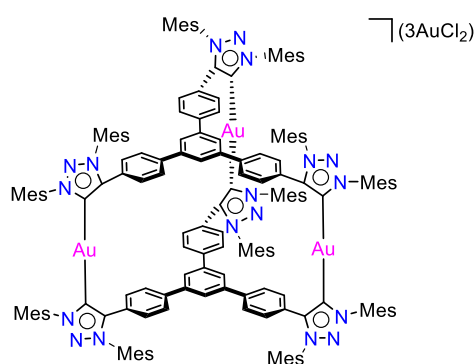
A solution of **5C^{Mes}** (55 mg, 0.017 mmol) and [AuCl(SMe$_2$)] (32 mg, 0.109 mmol) in acetonitrile (8 mL) was stirred at room temperature for 5 days. The resulting suspension was filtered through a pad of Celite, washed with CH$_2$Cl$_2$ to yield a clear solution, which was concentrated to dryness yielding a white solid. (yield: 38 mg. 58%). ^{1}H NMR (300 MHz, CD$_2$Cl$_2$): δ (ppm) 7.84 (s, 6H, C*H*$_{Ar}$), 7.77-7.69 (s, 24H, C*H*$_{Ar}$), 7.14-7.08 (m, 24H, C*H*$_{Ar}$), 2.43-2.39 (m, 36H, C*H*$_3$), 2.20 (s, 36H, C*H*$_3$), 2.05 (s, 36H, C*H*$_3$). ^{13}C{^{1}H} NMR (75 MHz, CD$_2$Cl$_2$): δ (ppm) 161.1 (dd, Au-$C_{carbene}$), 147.9 (C_{Ar}), 142.7 (C_{Ar}), 141.8 (C_{Ar}), 141.8 (C_{Ar}), 136.4 (C_{Ar}), 135.0 (C_{Ar}), 134.8 (C_{Ar}), 131.8 (C_{Ar}), 130.5 (C_{Ar}), 130.0 (C_{Ar}), 129.6 (C_{Ar}), 129.6 (C_{Ar}), 128.1 (C_{Ar}), 126.1 (C_{Ar}), 21.7 (C*H*$_3$), 21.6 (C*H*$_3$), 17.9 (C*H*$_3$). Electrospray MS (20 V, *m/z*): 1008.1 [M]$^{3+}$, 1645.6 [MAuCl$_2$]$^{2+}$. Elemental analysis calcd (%) for C$_{168}$H$_{162}$N$_{18}$Au$_3$(AuCl$_2$)$_3$: C, 52.7; H, 4.3; N, 6.6 found C, 53.5; H, 4.7; N, 6.2.

Synthesis of [1B^{Et}C^{Mes}](PF$_6$)$_3$
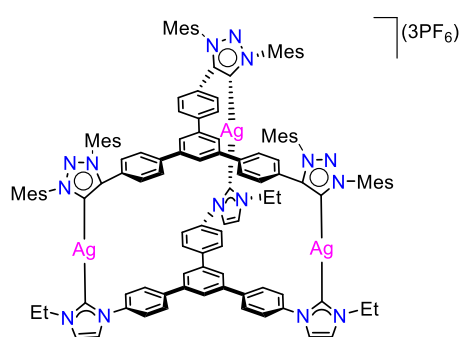
A mixture of **[H$_3$C^{Mes}](PF$_6$)$_3$** (60 mg, 0.04 mmol), **[H$_3$B^{Et}](PF$_6$)$_3$** (42 mg, 0.04 mmol) and Ag$_2$O (25 mg, 0.11 mmol) in MeOH (7 mL) was heated to 60 °C overnight under exclusion of light. The resultimg suspension was filtered through a pad of celite, and washed with CH$_2$Cl$_2$. Then the filtrate was concentrated to dryness, yielding a white solid (yield: 55 mg, 43%). ***Method i.*** A mixture of **5C^{Mes}** (20 mg, 0.006 mmol) and **6B^{Et}** (12 mg, 0.006 mmol) in MeOH (5 mL) was heated to 60 °C overnight under exclusion of light. The resulting suspension was filtered through a pad of Celite and washed with CH$_2$Cl$_2$. The filtrate was concentrated to dryness obtained a white solid (yield: 45%). ***Method ii.*** A mixture of **5C^{Mes}** (30 mg, 0.015 mmol) and **[H$_3$B^{Et}](PF$_6$)$_3$** (24 mg, 0.015 mmol) in MeOH (5 mL) was heated to 60 °C overnight under exclusion of light. The resulting suspension was filtered through a pad of celite and washed with CH$_2$Cl$_2$. The filtrate was concentrated to dryness obtained a white solid (yield: 55%). ***Method iii.*** A mixture of **[H$_3$C^{Mes}](PF$_6$)$_3$** (30 mg, 0.009 mmol) and **6B^{Et}** (10 mg, 0.009 mmol) in MeOH (5 mL) was heated to 60 °C overnight under exclusion of light. The resulting

suspension was filtered through a pad of celite and washed with CH_2Cl_2. The filtrate was concentrated to dryness obtained a white solid (yield: 45%). ^1H NMR (300 MHz, CD_2Cl_2): δ (ppm) 7.65-7.65 (m, 12H, CH_{Ar}), 7.55 (m, 6H, CH_{Ar}), 7.46 (m, 12H, CH_{Ar}), 7.20 (m, 12H, CH_{Ar}), 7.06 (m, 6H, CH_{Ar}), 3.72 (m, 6H, CH_2), 2.47 (s, 9H, CH_3), 2.34 (s, 9H, CH_3), 2.24 (s, 18H, CH_3), 2.05 (s, 9H, CH_3), 2.02 (s, 18H, CH_3). $^{13}C\{^1H\}$ NMR (75 MHz, CD_2Cl_2): δ (ppm) 180.9-178.1 (dd, J (C-Ag^{107}) = 179.6 Hz, J (C-Ag^{109}) = 179.4 Hz, $C_{carbene}$), 170.8-168.3 (dd, J (C-Ag^{107}) = 169.6 Hz, J (C-Ag^{109}) = 169.6 Hz, $C_{carbene}$), 150.2 (C_{Ar}), 150.0 (C_{Ar}), 142.5 (C_{Ar}), 141.9 (C_{Ar}), 141.6 (C_{Ar}), 141.0 (C_{Ar}), 140.6 (C_{Ar}), 139.8 (C_{Ar}), 137.3 (C_{Ar}), 134.9 (C_{Ar}), 134.7 (C_{Ar}), 131.5 (C_{Ar}), 130.3 (C_{Ar}), 129.8 (C_{Ar}), 129.0 (C_{Ar}), 128.7 (C_{Ar}), 127.7 (C_{Ar}), 126.5 (C_{Ar}), 124.7 (C_{Ar}), 122.6 (C_{Ar}), 122.6 (C_{Ar}), 122.0 (C_{Ar}), 46.6 (CH_2), 21.4 (CH_3), 21.3 (CH_3), 17.7 (CH_3), 17.6 (CH_3), 17.1 (CH_3). Electrospray MS (20 V, m/z): 709.5 [M]$^{3+}$, 1136.8 [MPF$_6$]$^{2+}$. Elemental analysis calcd (%) for $C_{123}H_{117}N_{15}Ag_3P_3F_{18}$: C, 57.6; H, 4.6; N, 8.2 found C, 57.0; H, 7.7; N, 7.5.

5.2.5 Synthesis and characterization of metal complexes: Chapter 4

Synthesis of 1G$^{n\text{Bu}}$
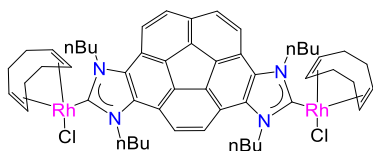
A Schlenk flask was loaded with **[H$_2$G$^{n\text{Bu}}$](PF$_6$)$_2$** (0.1 g, 0.12 mmol), [RhCl(COD)]$_2$ (0.58 g, 0.12 mmol) and K$_2$CO$_3$ (0.1 g, 0.34 mmol). The mixture was suspended in acetone (10 mL) and stirred for 12 h at 60 ºC. The resulting solid was filtered and washed several times with acetone. The crude mixture was dissolved in CH_2Cl_2 and purified by filtration through a pad of Celite. The resulting solution was concentrated to dryness obtained 28 mg of a yellow solid. Yield: 23 %. ^1H NMR (500 MHz, CDCl$_3$): δ (ppm) 8.17 (s, 2H, CH_{Ar}), 8.04 (m, 4H, CH_{Ar}), 5.46 (m, 4H, CH_{COD}), 5.24 (m, 8H, NCH_2CH$_2$CH$_2$CH$_3$), 3.49 (m, 4H, CH_{COD}), 2.52 (m, 12H, CH_{COD}), 2.18 (m, 4H, CH_{COD}), 2.05 (m, 8H, NCH$_2$CH_2CH$_2$CH$_3$), 1.83 (m, 8H, NCH$_2$CH$_2$CH_2CH$_3$), 1.24 (m, 12H, NCH$_2$CH$_2$CH$_2$CH_3). $^{13}C\{^1H\}$ NMR (126 MHz, CDCl$_3$): δ (ppm) 190.5 (d, J = 52 Hz, Rh-$C_{Carbene}$), 133.5 (C_{Ar}), 131.5 (C_{Ar}), 131.4 (C_{Ar}), 130.6 (C_{Ar}), 128.7 (C_{Ar}), 128.1 (C_{Ar}), 123.9 (C_{Ar}), 122.8 (C_{Ar}), 119.5 (C_{Ar}), 117.9 (C_{Ar}), 99.9 (C_{COD}), 69.1 (C_{COD}), 51.6 (NCH_2CH$_2$CH$_2$CH$_3$), 33.4 (NCH$_2$$CH_2CH_2CH_3$), 32.2 ($C_{COD}$), 32.1 ($C_{COD}$), 29.3 (NCH$_2$$CH_2CH_2CH_3$), 21.0 (NCH$_2CH_2$$CH_2CH_3$), 14.3 (NCH$_2CH_2CH_2$$CH_3$). HRMS ESI-TOF-MS (positive mode): 1011.3090 [M-Cl]$^+$
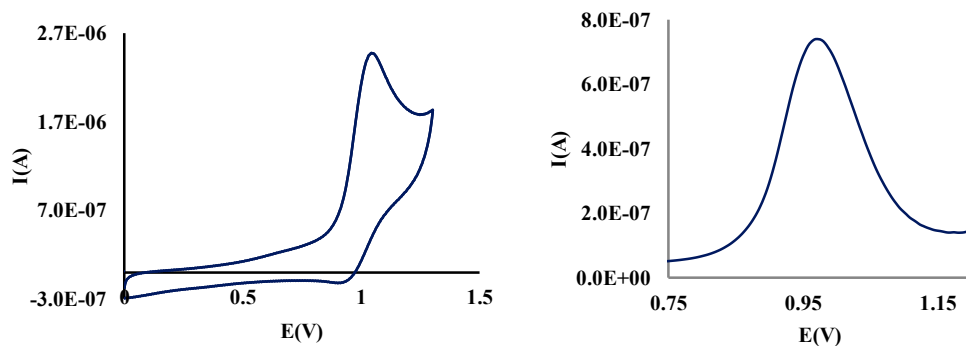
Figure 5.9. CV plot (left) and relevant DPV section (right) of complex **1G$^{n\text{Bu}}$** (1mM in dry CH$_2$Cl$_2$ with 0.1M [NBu$_4$][PF$_6$] as the supporting electrolyte, 50 mVs^{-1} scan rate, Fc$^+$/Fc used as internal standard with E$_{1/2}$ (Fc/Fc$^+$) = 0.44 V vs. SCE).

Synthesis of 2G$^{n\text{Bu}}$
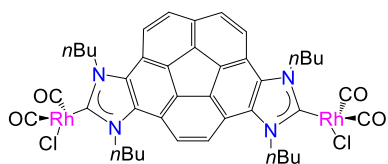
To a solution of **1G$^{n\text{Bu}}$** in dichloromethane (10 mL) in round a bottomed flask, CO gas was bubble through at 0 ºC for 2 h. The solution was concentrated under reduced pressure. Addition of hexanes allows to precipitate a yellow solid. Yield: 85 %. ^{1}H NMR (500 MHz, CDCl$_3$): δ (ppm) 8.25-8.02 (m, 6H, CH_{Ar}), 5.30-4.96 (m, 8H, NCH_2CH$_2$CH$_2$CH$_3$), 2.33-2.20 (m, 8H, NCH$_2$CH_2CH$_2$CH$_3$), 1.74 (m, 8H, NCH$_2$CH$_2$CH_2CH$_3$), 1.16 (m, 12H, NCH$_2$CH$_2$CH$_2$CH_3). ^{13}C{^{1}H} NMR (126 MHz, CDCl$_3$): δ (ppm) 185.6 (d, J = 54 Hz, Rh-C_{Carbene}), 182.6 (d, J = 74 Hz, Rh-C_{CO}), 180.2 (d, J = 78 Hz, Rh-C_{CO}), 131.0-117.0 (C_{Ar}), 51.4 (NCH$_2$CH$_2$CH$_2$CH$_3$), 31.6 (NCH$_2$$CH_2CH_2CH_3$), 29.6 (NCH$_2$$CH_2CH_2CH_3$), 27.9 (NCH$_2$$CH_2CH_2CH_3$), 20.2 (NCH$_2CH_2$$CH_2CH_3$), 13.9 (NCH$_2CH_2CH_2$$CH_3$); IR (cm^{-1}): 2083, 2003; TEP: 2055.

Synthesis of 3G$^{t\text{Bu}}$
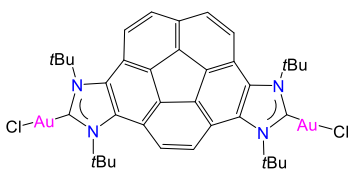
To a flame dried Schlenk containing a suspension of compound **[H$_2$G$^{t\text{Bu}}$](PF$_6$)$_2$** (50 mg, 0.06 mmol) in dry THF (8 mL) at -78 ºC, KHMDS (0.5 M in toluene, 260 μL, 0.130 mmol) was added dropwise. The mixture was stirred for 15 min at -78 ºC , then the resulting solution was transferred *via* oven-dried cannula to a second flame dried Schlenk containing a suspension of [Au(SMe$_2$)Cl] (35 mg, 0.12 mmol) in THF (5 mL) stirred at -78 ºC. The resulting solution was kept in the dark, allowed to warm up and stirred overnight. Then, the solvent was removed under vacuum. The crude mixture was dissolved in CH$_2$Cl$_2$ and stirred with activated charcoal for 30 min. The suspension was filtered through a pad of Celite. The resulting solution was concentrated and a mixture of diethyl ether/hexane was added to yield a white solid

precipitated. Yield: 37 mg (31 %). ^{1}H NMR (300 MHz, CD_2Cl_2): δ (ppm) 8.47 (s, 2H, CH_{Ar}), 8.44 (d, J = 9.0 Hz, 2H, CH_{Ar}), 8.05 (d, J = 9.0 Hz, 2H, CH_{Ar}), 2.43 (m, 36H, $NC(CH_3)_3$). ^{13}C{^{1}H} NMR (75 MHz, CD_2Cl_2): δ (ppm) 178.7 (Au-$C_{Carbene}$), 133.6 (C_{Ar}), 133.2 (C_{Ar}), 132.7 (C_{Ar}), 131.9 (C_{Ar}), 129.0 (C_{Ar}), 128.7 (C_{Ar}), 128.5 (C_{Ar}), 127.9 (C_{Ar}), 122.3 (C_{Ar}), 120.8 (C_{Ar}), 62.5 ($NC(CH_3)$), 62.3 ($NC(CH_3)$), 33.6 ($NC(CH_3)$). HRMS ESI-TOF-MS (positive mode): 787.3 $[M-AuCl+H]^+$; 1041.3 $[M+Na]^+$. Elemental analysis calcd (%) for $C_{38}H_{42}N_4Au_2Cl_2 \cdot 3CH_2Cl_2$: C, 38.6; H, 3.8; N, 4.4; found C, 38.6; H, 3.7; N, 4.9.

5.3 Catalytic experiments: Chapter 2 and 4

Addition of Aryl Boronic Acids to Acids to Cyclohex-2-enone

In a 50 mL high-pressure Schlenk tube, catalyst (0.2-0.02 mol %), 2-cyclohexen-1-one (0.5 mmol), arylboronic acid (0.6 mmol), KOH (0.09 mmol) and dry toluene (2 mL) were added. The mixture was stirred and heated at 100 ºC for 6h. The yields of the reaction were calculated by GC using anisole and 2,4,6-trimethylphenol as internal standard.

Hydroamination of Phenylacetylene with Aryl Amines

The Au[I] catalyst (0.5 mol % based on metal) and $AgBF_4$ (1 mol %, 0.01 mmol) were placed together in a thick-walled Schlenk tube fitted with a Teflon cap. The tube was then evacuated and filled with nitrogen three times. Afterward, 1 mL of CH_3CN was added, and the reaction mixture was stirred at room temperature for 5 min. After this time, the corresponding arylamine (0.55 mmol), phenylacetylene (0.5 mmol), and anisole as internal reference (0.5 mmol) were subsequently added. The resulting mixture was stirred at 90 °C for the appropriate time. The evolution of the reactions, yields, and conversions were determined by GC analysis. The products were identified by comparison to previously reported data.[8]

Cyclization of 2,5-Dimethylfuran with Different Terminal Alkynes

A solution of the alkyne (1 mmol), 2,5-dimethylfuran (2 mmol), the Au[I] catalyst (1.5 mol %), and NaBArF (2 mol %) in dry dichloromethane (2.5 mL) was stirred at room temperature or 40 ºC for 24 h. Then, a drop of trimethylamine was added, and the solvent was removed under vacuum. The crude was purified by flash column chromatography using different gradients of hexane, ethyl acetate, and dichloromethane

to obtain the desired products. The products were identified by comparison to previously reported data.[9]

5.4 DFT experiments: Chapter 3

All calculations were carried out in Gaussian 09[10] (revision D.01) using the M06L functional,[11] tight optimizations, and the ultrafine integration grid (a pruned (99,590) grid). The basis sets, listed by their corresponding Gaussian 09 keyword, included QZVP (with the QZVP ECP as implemented in Gaussian 09) for silver and TZVP[12] for all other atoms. The following density fitting basis sets were employed: QZVP (silver) and TZVPFit (all other atoms). The polarizable continuum model using the integral equation formalism (IEFPCM) was used for all calculations, with the radii and non-electrostatic terms of Truhlar and co-workers' SMD solvation model (scrf=smd).[13] The optimized geometries were verified to have no negative frequencies by frequency calculations, which also provided the enthalpies and free energies reported below. The energies were calculated at 298.15 K, under pressure (275 atm for benzene and 605 atm for methanol), following the approach of Martin and co-workers.[14]
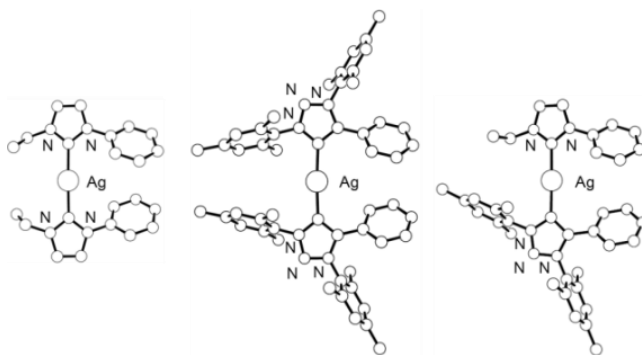
Figure 5.10. Calculated structures of $[Ag(NHC)_2]^+$, $[Ag(MIC)_2]^+$, and $[Ag(MIC)(NHC)]^+$ complexes (all hydrogen atoms are omitted for clarity)

Table 5.1. Calculated energies for the ground-state structures (Hartree)

Compound	Solvent	E	H	G
NHC (Carbene)	Methanol	-535.958446	-535.738644	-535.782130
MIC (Carbene)	Methanol	-1171.456758	-1170.962326	-1171.042564
$[Ag(NHC)]^+$	Methanol	-682.972172	-682.748679	-682.798568
$[Ag(MIC)]^+$	Methanol	-1318.473701	-1317.975867	-1318.062726
$[Ag(NHC)_2]^+$	Methanol	-1218.998969	-1218.553087	-1218.630025
$[Ag(NHC)_2]^+$	Benzene	-1218.985555	-1218.538735	-1218.616004
$[Ag(MIC)_2]^+$	Methanol	-2490.003772	-2489.009124	-2489.161157
$[Ag(MIC)_2]^+$	Benzene	-2489.997866	-2489.001076	-2489.149935
$[Ag(NHC)(MIC)]^+$	Methanol	-1854.501641	-1853.781108	-1853.895051
$[Ag(NHC)(MIC)]^+$	Benzene	-1854.493038	-1853.771150	-1853.885411

5.5 Titration experiments

Host-guest studies by ^1H NMR titrations with C_{60}

Stock solutions of **3G**^{tBu} and C_{60} were prepared in toluene-d_8: Solution A) 0.49 mM of **3G**^{tBu} and solution B) 2 mM of C_{60} and 0.49 mM of **3G**^{tBu}. Solution A was placed in a NMR tube and aliquots of solution B were added. The concentration of host **3G**^{tBu} was maintained constant throughout the titration. ^1H NMR spectra were directly recorded after each addition.

Figure 5.11. Selected region of the ^{1}H NMR (500 MHz, toluene-d_8, 298 K) spectra registered during the titration of **3G^{tBu}** with incremental amounts of C$_{60}$)

Table 5.2. Data values from the titration study of **3G^{tBu}** with C$_{60}$

[3G^{tBu}]	[C$_{60}$]	δ (ppm) for Ha	δ (ppm) for Hb	δ (ppm) for Hc	[3G^{tBu}]/[C$_{60}$]
0,49	0	8,051	8,083	7,552	0
0,49	0,05	8,074	8,090	7,564	0,10
0,49	0,10	8,095	8,095	7,571	0,19
0,49	0,14	8,110	8,101	7,578	0,29
0,49	0,19	8,126	8,106	7,585	0,38
0,49	0,23	8,142	8,110	7,590	0,47
0,49	0,31	8,161	8,116	7,597	0,64
0,49	0,54	8,198	8,124	7,606	1,11

0,49	0,87	8,240	8,136	7,618	1,77
0,49	1,36	8,281	8,147	7,626	2,77
0,49	1,71	8,303	8,153	7,630	3,49
0,49	2,19	8,326	8,159	7,630	4,46
0,49	2,49	8,337	8,163	7,630	5,08
0,49	2,71	8,345	8,165	7,630	5,51
0,49	3,89	8,354	8,167	7,627	7,92

Figure 5.12. ^{1}H NMR chemical shifts δ(ppm) plotted against [G]/ [H]
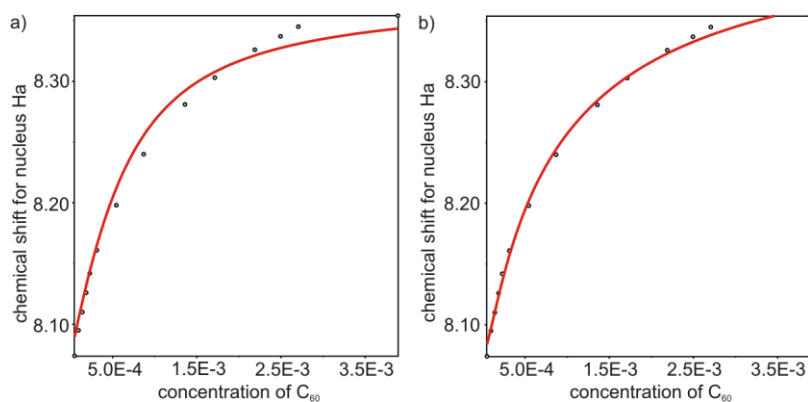
Figure 5.13. Non-linear least-squares fitting (red line) of the chemical shift changes of Ha during the titration of **3G^{tBu}** with C$_{60}$ to: a) 1:1 binding model, K$_a$ = 2750 ± 300 M^{-1} and b) 1:3 binding model assuming that the binding constants for the single binding steps leading to the C$_{60}$@(**3G^{tBu}**)$_2$ and C$_{60}$@(**3G^{tBu}**)$_3$ are identical and coincide with K$_a$ (C$_{60}$@**3G^{tBu}**) = 2750 ± 300 M^{-1}. HypNMR 2008 4.0.71
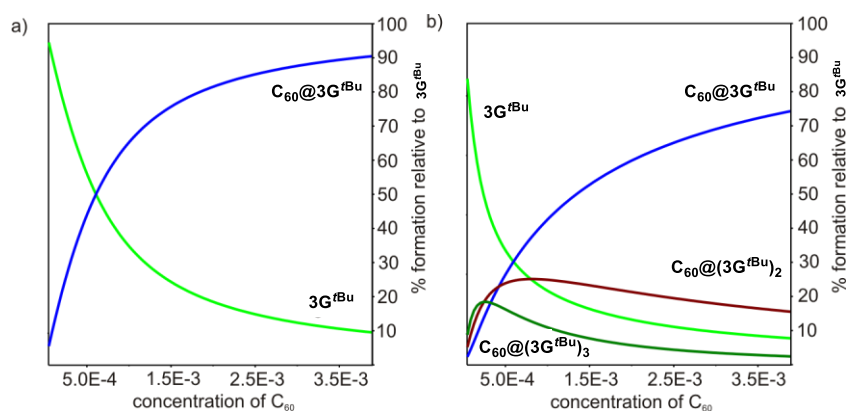
Figure 5.14. Speciation profiles for: a) 1:1 binding model, $K_a = 2750 \pm 300$ M^{-1} and b) 1:3 binding model assuming that the bindind constants for the single binding steps leading to the C$_{60}$@(**3G^{tBu}**)$_2$ and C$_{60}$@(**3G^{tBu}**)$_3$ are identical and coincide with K_a (C$_{60}$@**3G^{tBu}**) $= 2750 \pm 300$ M^{-1}. HypNMR 2008 4.0.71

Table 5.3. Calculated chemical shifts for the Ha protons in the C$_{60}$@(**3G^{tBu}**)$_n$ (n = 1; 2 and 3) complexes obtained in the non-linear least-squares fitting to a 1:1 and 1:3 binding models. HypNMR 2008 4.0.71

Binding model	δ (ppm) for Ha (n = 1)	δ (ppm) for Ha (n = 2)	δ (ppm) for Ha (n = 3)
1:1	8.37		
1:3	8.43	8.23	8.01

Host-guest studies by ^{1}H NMR titrations with Coronene

Stock solutions of **3G^{tBu}** and coronene were prepared in toluene-d_8. Solution A) 1.55 mM of **3G^{tBu}** and solution B) 2 mM of coronene and 1.55 mM of **3G^{tBu}**. Solution A was placed in a NMR tube and aliquots of solution B were added. The concentration of host **3G^{tBu}** was maintained constant throughout the titration. ^{1}H NMR spectra were directly recorded after each addition.
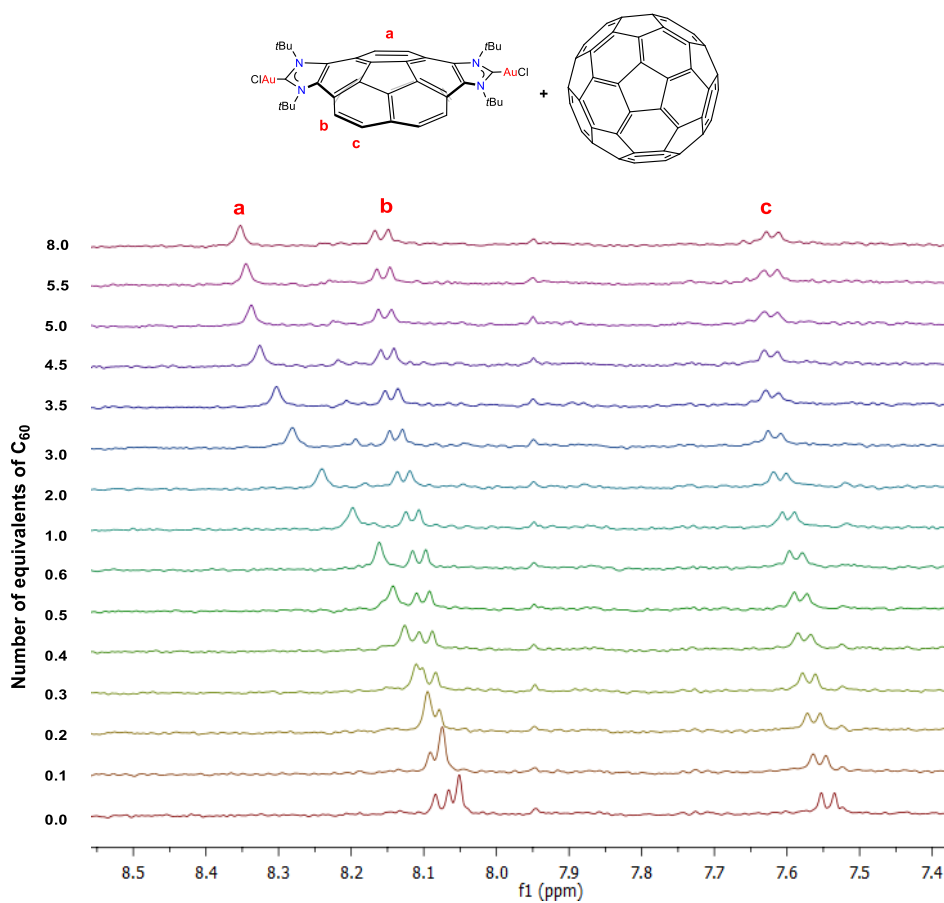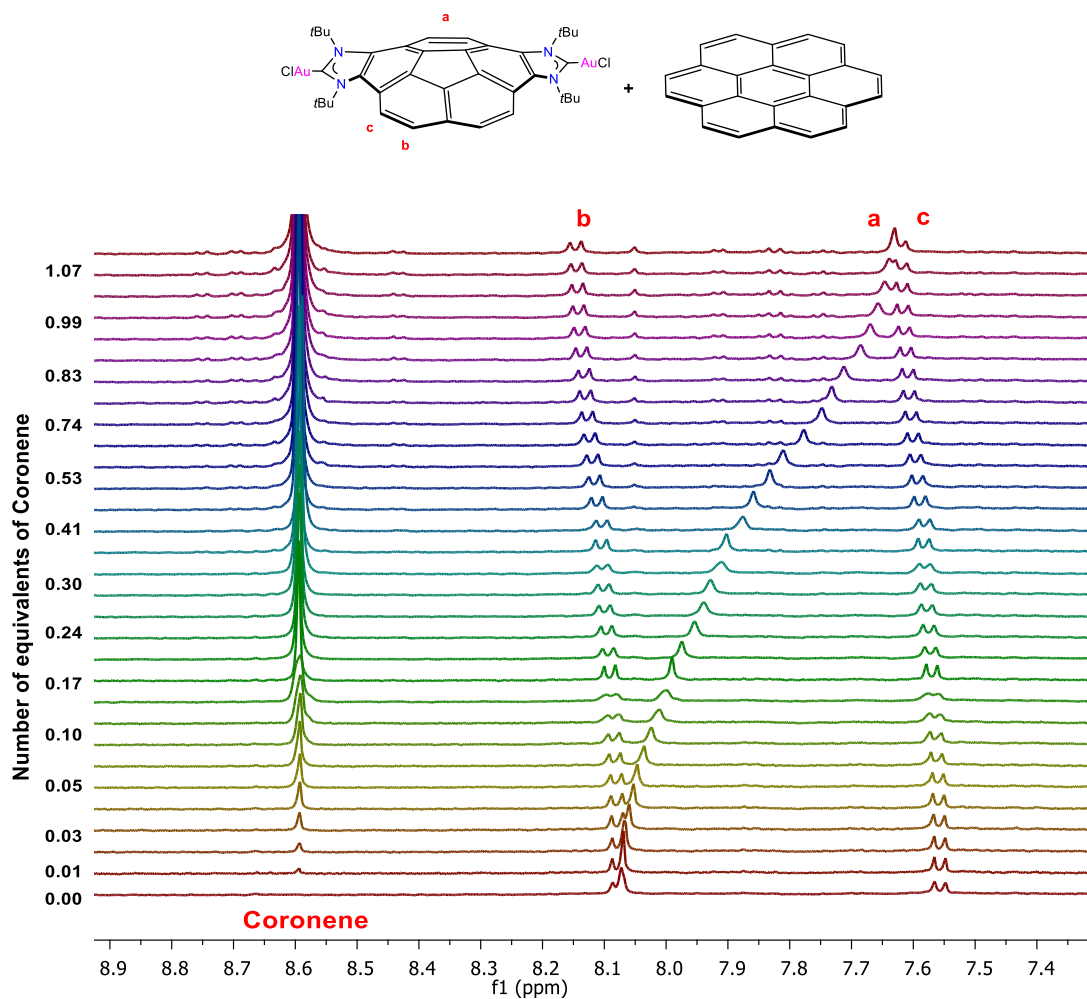
Figure 5.14. Selected region of the ^{1}H NMR (500 MHz, toluene-d_8, 298 K) spectra registered during the titration of **3G^{tBu}** with incremental amounts of coronene)

Table 5.4. Data values from the titration study of **3G^{tBu}** with Coronene

[3G^{tBu}]	[Coronene]	δ (ppm) for Ha	[3G^{tBu}]/[Coronene]
1,55	0	8,072	0
1,55	0,00995025	8,069	0,006437148
1,55	0,01980198	8,068	0,012810561
1,55	0,03921569	8,06	0,025369935
1,55	0,05825243	8,053	0,037685437
1,55	0,07692308	8,047	0,049764103
1,55	0,11320755	8,036	0,073237736

141

1,55	0,14814815	8,024	0,095841975
1,55	0,19004525	8,011	0,122946606
1,55	0,2300885	7,999	0,148851917
1,55	0,26839827	7,99	0,173635786
1,55	0,32285115	7,975	0,208863173
1,55	0,37398374	7,954	0,241942547
1,55	0,42209073	7,939	0,273064563
1,55	0,46743295	7,928	0,302397957
1,55	0,51024209	7,911	0,330092613
1,55	0,56373429	7,902	0,364698504
1,55	0,63713799	7,875	0,412185804
1,55	0,72408293	7,859	0,468433386
1,55	0,8183161	7,832	0,529395963
1,55	0,89958735	7,81	0,58197304
1,55	1,03264813	7,777	0,668054494
1,55	1,13700108	7,748	0,735563898
1,55	1,22103213	7,732	0,789926388
1,55	1,29015084	7,712	0,834641585
1,55	1,3971364	7,685	0,903854107
1,55	1,47609692	7,669	0,954936302
1,55	1,53676896	7,657	0,994187068
1,55	1,58484691	7,646	1,025290296
1,55	1,6238834	7,639	1,050544303
1,55	1,65620971	7,63	1,07145727

Host-guest studies by fluorescence spectroscopy

Stock solutions of $3G^{tBu}$ and C_{60} were prepared in toluene: Solution A) 0.02 mM of $3G^{tBu}$ and solution B) 0.2 mM of C_{60} and 0.02 mM of $3G^{tBu}$. Solution A was placed in a fluorescence cubette and aliquots of solution B were added. The fluorescence spectra (excitation wavelenght = 403 nm) of the titration of host $3G^{tBu}$ against C_{60} were directly recorded after each addition. The concentration of $3G^{tBu}$ was maintained constant throughout the titration.
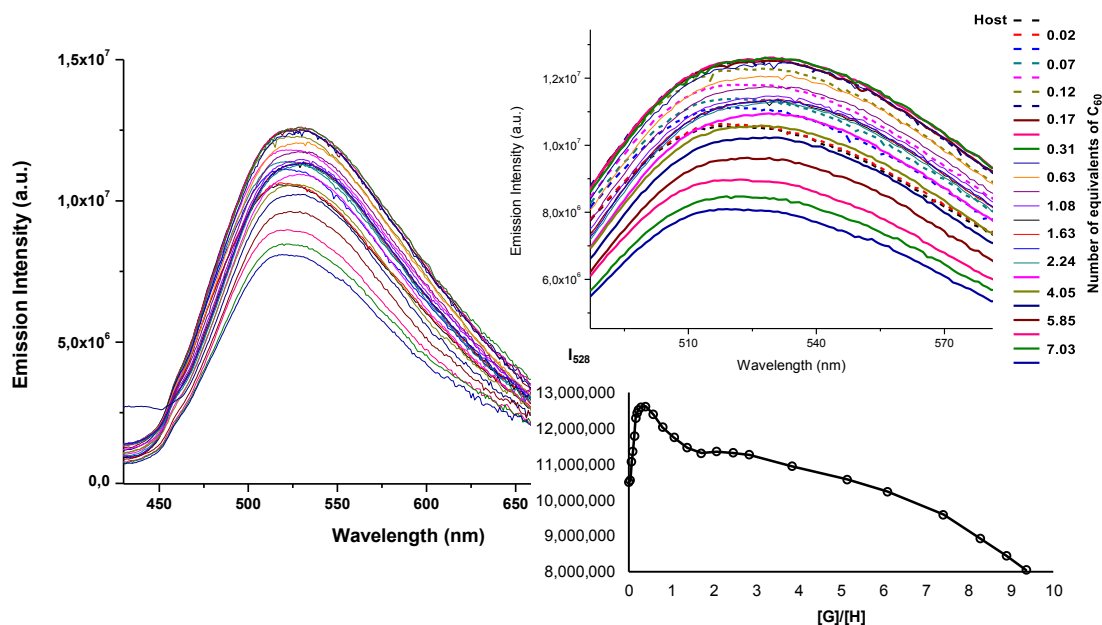
Figure 5.15. Fluorescence spectra registered during the titration of $3G^{tBu}$ with C_{60} in toluene at 298 K (excitation wavelenght = 403 nm) (Left) Emission intensity (528 nm) vs guest/host ratio plot (Bottom-Right)

Table 5.5. Data values from the titration study of $3G^{tBu}$ with C_{60}

[3G^{tBu}]	[C$_{60}$]	I(528 nm)	[3G^{tBu}]/[C$_{60}$]
1,55	0	1,05E+07	0
1,55	4,849E-07	1,05E+07	0,031283798
1,55	9,6739E-07	1,11E+07	0,062411955
1,55	1,4475E-06	1,14E+07	0,093385629
1,55	1,9252E-06	1,18E+07	0,124205969
1,55	2,4005E-06	1,23E+07	0,154874109

1,55	2,8736E-06	1,24E+07	0,185391175
1,55	3,3443E-06	1,25E+07	0,21575828
1,55	4,2787E-06	1,26E+07	0,276047007
1,55	6,1205E-06	1,26E+07	0,394872729
1,55	8,8173E-06	1,24E+07	0,568857409
1,55	1,2295E-05	1,20E+07	0,793231095
1,55	1,6463E-05	1,17E+07	1,062145781
1,55	2,122E-05	1,15E+07	1,369031939
1,55	2,6458E-05	1,13E+07	1,706960217
1,55	3,2069E-05	1,13E+07	2,068975838
1,55	3,795E-05	1,13E+07	2,448382049
1,55	4,4004E-05	1,13E+07	2,838959256
1,55	5,9648E-05	1,09E+07	3,848232422
1,55	7,9559E-05	1,06E+07	5,132807082
1,55	9,4344E-05	1,02E+07	6,086731893
1,55	0,00011484	9,59E+06	7,408752563
1,55	0,00012836	8,92E+06	8,281488384
1,55	0,00013796	8,44E+06	8,900706174
1,55	0,00014512	8,04E+06	9,362861747

Isothermal Titration Calorimetry (ITC)

Titration of host **3G$^{t\text{Bu}}$** with C$_{60}$ was carried out in toluene solution by the addition of small aliquots of C$_{60}$ (8 μL) of a solution of the guest (3.8 mM) into a solution of the host **3G$^{t\text{Bu}}$** (0.6 mM). The association constants and the thermodynamic parameters were obtained from the fit of the titration data to a 1:3 binding model (one set of sites) using the Microcal ITC Data Analysis Module indicating that the multitopic substrate

(C$_{60}$) was placed in the syringe. The reported data represent the averaged thermodynamic values for each site. The three sites are assumed to be non-cooperative.
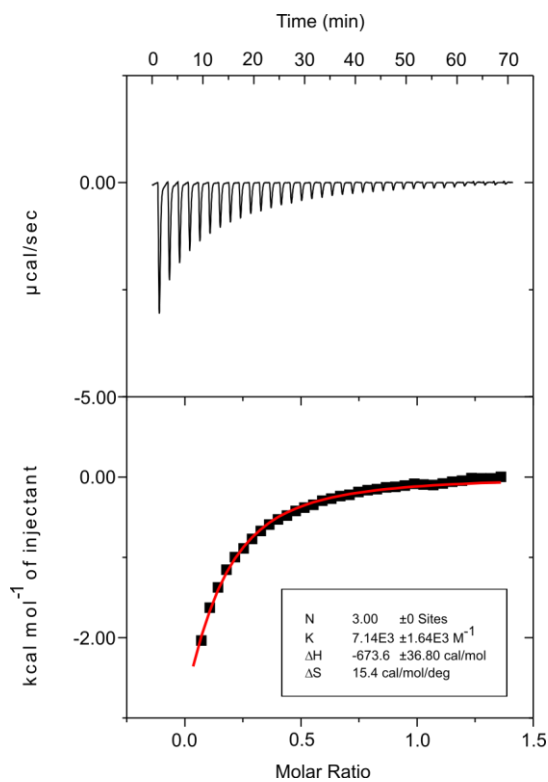
Figure 5.16. Heat vs time plot for the titration of guest C$_{60}$ into host **3G^{tBu}** (top). "One set of sites" binding isotherm (red line) fit to the experimental data assuming that the complex of higher stoichiometry formed by the two binding partners is C$_{60}$@(**3G^{tBu}**)$_3$ (bottom).The model assumes that all binding sites are almost identical.

Table 5.6 Thermodynamic parameters obtained from the ITC binding experiment (average data from two different experiments at 298 K). Errors (given as standard deviation) were determined from the experimental results

Complex	K$_a$ (M^{-1})	ΔH (kcal mol^{-1})	-TΔS (kcal mol^{-1})	ΔG (kcal mol^{-1})
C$_{60}$@(**3G^{tBu}**)$_3$	7.1 ± 0.3x10^3	-0.67 ± 0.07	-4.6 ± 0.5	-5.3 ± 0.5

DFT calculations

The calculations were carried out in Gaussian 09[10] (rev. D.01) using the M06-L,[11] B97D3,[15] B97D,[16] and ωB97X-D[17] functionals. In M06L-D3 calculations, the D3

145

version of Grimme's dispersion with the original D3 damping function[18] was added to M06-L with the "EmpiricalDispersion=GD3" keyword. The basis sets included def2-QZVP (with def2-ECP) for Au and def2-SVP for all other atoms together (when using the local finctionals) with the W06 density fitting basis set.[19] The polarizable continuum model (IEFPCM) was used in all calculations in toluene solvent, with the radii and non-electrostatic terms of Truhlar and co-workers' SMD solvation model (scrf=smd).[13] All geometry optimizations were accompanied by frequency calculations at 298.15 K, under pressure=230 atm, following the approach of Martin and co-workers.[14a] Ultimately, the calculated thermal corrections to enthalpy and Gibbs free energy were combined with the electronic energies from single-point calculations on the optimized geometries using the def2-QZVP basis set for all atoms.

Table 5.7 shows the enthalpies (kcal/mol) of toluene binding to $3G^{tBu}$ and $3G^{Me}$ in toluene at 298 K, per mole of toluene, calculated by different methods (M1-M5).

Table 5.7. Enthalpies of formation between di-gold complex and toluene

$3G^{tBu}$@toluene (kcal)		$3G^{tBu}$@toluene$_2$ (kcal)	
M1	-5.7	**M1**	-6.9
M2	-8.1	**M2**	-9.9
M3	-9.6	**M3**	-9.4
M4	-10.1	**M4**	-10.8
M5	-11.4	**M5**	-12.1

Table 5.8 shows the enthalpies (kcal/mol) and entropies (cal.K^{-1}.mol^{-1}) of formation in toluene at 298 K, per mole of $3G^{Me}$@toluene, calculated by different methods (M1-M4).

Table 5.8. Enthalpies and entropies of formation

Method	C_{60}@($3G^{Me}$)		C_{60}@($3G^{Me}$)$_2$		C_{60}@($3G^{Me}$)$_3$	
	ΔH	ΔS	ΔH	ΔS	ΔH	ΔS
M1	4.3	27	0.6	24	-2.6	19
M2	2.5	28	-2.1	21	-6.2	18
M3	2.2	18	-3.6	20	-7.7	18
M4	-0.2	21	-8.3	19	-12.8	16

Table 5.9 shows the enthalpies (kcal/mol) and entropies (cal.K^{-1}.mol^{-1}) of formation of C$_{60}$@$\mathbf{3G}^{t\mathbf{Bu}}$ and C$_{60}$@$(\mathbf{3G}^{t\mathbf{Bu}})_2$ in toluene at 298 K, per mol of $\mathbf{3G}^{t\mathbf{Bu}}$@toluene$_2$, calculated by different methods (M1-M4).

Table 5.9. Enthalpies and entropies of formation

Method	C$_{60}$@$(\mathbf{3G}^{t\mathbf{Bu}})$		C$_{60}$@$(\mathbf{3G}^{t\mathbf{Bu}})_2$	
	ΔH	ΔS	ΔH	ΔS
M1	3.8	19	-2.2	17
M2	1.1	16	6.4	17
M3	-1.2	21	-7.4	22
M4	-4.4	22	-11.8	19

5.6 X-Ray diffraction

Single crystal suitable for X-Ray Diffraction were mainly obtained by slow diffusion of hexane or Et$_2$O into a concentrated solution of the compound in different solvents or slow evaporation of a concentrated solution of the compound in the appropriated solvent. Diffraction data were collected on an Agilent SuperNova diffractometer equipped with an Atlas CCD detector. Single crystals were mounted on a MicroMount polymer tip (MiteGen) in a random orientation. Absortion corrections based on the multiscan method were applied.[20] The structures were solved by direct methods in SHELXS-97 and refined by the full-matrix method based on F^2 with the program SHELXL-97 using OLEX software package.[1-2]

Key details of the crystals and structures refinement data are summarized in the following tables.

Table 5.10 Structural parameters, register conditions and refinement of **[H₃B^Me](CF₃SO₃)₃**

	$[H_3B^{Me}](CF_3SO_3)_3$
Empirical formula	$C_{150}H_{132}F_{18}N_{24}O_{18}S_6$
Formula weight	515.52
Temperature/K	293(2)
Crystal system	Trigonal
Space group	R-3
a/Å	34.2772(14)
b/Å	34.2772(14)
c/Å	14.1208(6)
α/°	90
β/°	90
γ/°	120
Volume/Å³	14368.1(13)
Z	3
ρ_{calc} g/cm³	1.072
μ/mm⁻¹	1.294
F(000)	4806.0
Crystal size/mm³	0.18 × 0.13 × 0.11
2Θ range for data collection	6.932 to 121.99°
Index ranges	-38 ≤ h ≤ 34, -38 ≤ k ≤ 38, -14 ≤ l ≤ 15
Reflections collected	13623
Independent reflections	4812[R(int) = 0.0285]
Data/restraints/parameters	4812/0/331
Goodness-of-fit on F²	1.113
Final R indexes [I>=2σ (I)]	$R_1 = 0.0765$, $wR_2 = 0.02461$
Final R indexes [all data]	$R_1 = 0.0930$, $wR_2 = 0.2626$
Largest diff. peak/hole / e Å⁻³	0.23/-0.28

Table 5.11 Structural parameters, register conditions and refinement of **1D^{Et}**

	1D^{Et}
Empirical formula	$C_{24}HClN_7Rh$
Formula weight	418.77
Temperature/K	200(10)
Crystal system	Monoclinic
Space group	$P2_1/a$
a/Å	10.1941(3)
b/Å	17.6476(4)
c/Å	10.3104(3)
α/°	90
β/°	101.886(3)
γ/°	90
Volume/Å^3	1815.08(8)
Z	4
ρ_{calc} g/cm^3	1.45324
μ/mm^{-1}	1.089
F(000)	852.3
Crystal size/mm^3	$0.4043 \times 0.1787 \times 0.1169$
2Θ range for data collection	5.62 to 58.84°
Index ranges	$-13 \leq h \leq 13, -23 \leq k \leq 24, -13 \leq l \leq 14$
Reflections collected	39071
Independent reflections	4737[R(int) = 0.0605]
Data/restraints/parameters	4737/0/303
Goodness-of-fit on F^2	1.080
Final R indexes [I>=2σ (I)]	$R_1 = 0.0270$, $wR_2 = 0.0557$
Final R indexes [all data]	$R_1 = 0.0380$, $wR_2 = 0.0648$
Largest diff. peak/hole / e Å^{-3}	0.72/-0.63

Table 5.12 Structural parameters, register conditions and refinement of **[6B^{Et}](PF$_6$)$_3$**

	[6B^{Et}](PF$_6$)$_3$
Empirical formula	C$_{100}$H$_{125}$Au$_3$F$_{18}$N$_{13}$O$_5$P$_3$
Formula weight	2614.94
Temperature/K	153(2)
Crystal system	Monoclinic
Space group	P2$_1$/n
a/Å	20.4029(11)
b/Å	13.2486(8)
c/Å	33.8848(18)
α/°	90
β/°	93.936(3)
γ/°	90
Volume/Å^3	9137.8(9)
Z	4
ρ$_{calc}$ g/cm^3	1.901
μ/mm^{-1}	4.960
F(000)	5200.0
Crystal size/mm^3	0.23 × 0.07 × 0.03
2Θ range for data collection	2.26 to 62.1°
Index ranges	-29 ≤ h ≤ 29, -18 ≤ k ≤ 19, -48 ≤ l ≤ 48
Reflections collected	131138
Independent reflections	28577 [R(int) = 0.0841]
Data/restraints/parameters	28577/31/996
Goodness-of-fit on F^2	0.987
Final R indexes [I>=2σ (I)]	R$_1$ = 0.0585, wR$_2$ = 0.1473
Final R indexes [all data]	R$_1$ = 0.1105, wR$_2$ = 0.1632
Largest diff. peak/hole / e Å^{-3}	3.12/-2.46

Table 5.13 Structural parameters, register conditions and refinement of **[5C^{Mes}](PF$_6$)$_3$**

	[5C^{Mes}](PF$_6$)$_3$
Empirical formula	C$_{168}$H$_{162}$Ag$_3$F$_{18}$N$_{18}$P$_3$
Formula weight	3191.67
Temperature/K	150.00(14)
Crystal system	Trigonal
Space group	R-3
a/Å	35.4661(16)
b/Å	35.4661(16)
c/Å	26.1940(17)
α/°	90
β/°	90
γ/°	120
Volume/Å^3	28534(3)
Z	6
ρ$_{calc}$ g/cm^3	1.114
μ/mm^{-1}	3.228
F(000)	9864.0
Crystal size/mm^3	0.1117 × 0.1056 × 0.0466
2Θ range for data collection	6.672 to 129.874°
Index ranges	-36 ≤ h ≤ 36, -41 ≤ k ≤ 32, -29 ≤ l ≤ 30
Reflections collected	36807
Independent reflections	10546[R(int) = 0.1245]
Data/restraints/parameters	10546/238/652
Goodness-of-fit on F^2	1.054
Final R indexes [I>=2σ (I)]	R$_1$ = 0.0922, wR$_2$ = 0.2561
Final R indexes [all data]	R$_1$ = 0.1282, wR$_2$ = 0.2886
Largest diff. peak/hole / e Å^{-3}	1.35/-0.71

Table 5.14 Structural parameters, register conditions and refinement of **[H$_2$G^{tBu}](PF$_6$)$_2$**

	[H$_2$G^{tBu}](PF$_6$)$_2$
Empirical formula	C$_{40}$H$_{48}$Cl$_2$F$_{12}$N$_4$P$_2$
Formula weight	945.66
Temperature/K	293(2)
Crystal system	Monoclinic
Space group	P2$_1$/c
a/Å	8.36541(17)
b/Å	15.7033(3)
c/Å	32.4898(7)
α/°	90
β/°	90.02
γ/°	90
Volume/Å^3	4268.02(15)
Z	4
ρ_{calc} g/cm^3	1.472
μ/mm^{-1}	2.862
F(000)	1952.0
Crystal size/mm^3	0.15 × 0.14 × 0.13
2Θ range for data collection	7.83 to 146.44°
Index ranges	-6 ≤ h ≤ 10, -19 ≤ k ≤ 17, -39 ≤ l ≤ 39
Reflections collected	18156
Independent reflections	7693 [R(int) = 0.0365]
Data/restraints/parameters	7693/0/554
Goodness-of-fit on F^2	1.050
Final R indexes [I>=2σ (I)]	R$_1$ = 0.0499, wR$_2$ = 0.1357
Final R indexes [all data]	R$_1$ = 0.0570, wR$_2$ = 0.1436
Largest diff. peak/hole / e Å^{-3}	0.65/-0.51

5.7 References

[1]   O. V. Dolomanov, L. J. Bourhis, R. J. Gildea, J. A. K. Howard and H. Puschmann, *J. Appl. Crystallogr.* **2009**, *42*, 339-341.

[2]   G. M. Sheldrick, *Acta Crystallogr. Sect. A* **2008**, *64*, 112-122.

[3]   A. Nutton, P. M. Bailey and P. M. Maitlis, *Dalton Trans.* **1981**, 1997-2002.

[4]   J. Bouffard, B. K. Keitz, R. Tonner, G. Guisado-Barrios, G. Frenking, R. H. Grubbs and G. Bertrand, *Organometallics* **2011**, *30*, 2617-2627.

[5]   J. L. Herde, J. C. Lambert and C. V. Senoff, *Inorg. Synth.* **1974**, *14*, 18-20.

[6]   R. Uson, A. Laguna, M. Laguna, D. A. Briggs, H. H. Murray and J. P. Fackler, *Inorg. Synth.* **1989**, *26*, 85-91.

[7]   A. M. Butterfield, B. Gilomen and J. S. Siegel, *Org. Process Res. Dev.* **2012**, *16*, 664-676.

[8]   a) M. J. Pouy, S. A. Delp, J. Uddin, V. M. Ramdeen, N. A. Cochrane, G. C. Fortman, T. B. Gunnoe, T. R. Cundari, M. Sabat and W. H. Myers, *Acs Catalysis* **2012**, *2*, 2182-2193; b) S. Ibanez-Maella, M. Poyatos and E. Peris, *Chem. Commun.* **2017**; c) M. Katari, M. N. Rao, G. Rajaraman and P. Ghosh, *Inorg. Chem.* **2012**, *51*, 5593-5604; d) L. Canovese, F. Visentin, C. Levi and C. Santo, *Inorg. Chim. Acta* **2012**, *391*, 141-149; e) E. Alvarado, A. C. Badaj, T. G. Larocque and G. G. Lavoie, *Chem. Eur. J.* **2012**, *18*, 12112-12121; f) S. Gaillard, J. Bosson, R. S. Ramon, P. Nun, A. M. Z. Slawin and S. P. Nolan, *Chem. Eur. J.* **2010**, *16*, 13729-13740; g) S. Gonell, M. Poyatos and E. Peris, *Angew. Chem. Int. Ed.* **2013**, *52*, 7009-7013.

[9]   a) A. S. K. Hashmi, M. C. Blanco, E. Kurpejovic, W. Frey and J. W. Bats, *Adv. Synth. Catal.* **2006**, *348*, 709-713; b) N. Huguet, D. Leboeuf and A. M. Echavarren, *Chem. Eur. J.* **2013**, *19*, 6581-6585.

[10]   M. J. Frisch, G. W. Trucks, H. B. Schlegel, G. E. Scuseria, M. A. Robb, J. R. Cheeseman, G. Scalmani, V. Barone, B. Mennucci, G. A. Petersson, H. Nakatsuji, M. Caricato, X. Li, H. P. Hratchian, A. F. Izmaylov, J. Bloino, G. Zheng, J. L. Sonnenberg, M. Hada, M. Ehara, K. Toyota, R. Fukuda, J. Hasegawa, M. Ishida, T. Nakajima, Y. Honda, O. Kitao, H. Nakai, T. Vreven, J. A. Montgomery Jr., J. E. Peralta, F. Ogliaro, M. Bearpark, J. J. Heyd, E. Brothers, K. N. Kudin, V. N. Staroverov, R. Kobayashi, J. Normand, K. Raghavachari, A. Rendell, J. C. Burant, S. S. Iyengar, J. Tomasi, M. Cossi, N. Rega, J. M. Millam, M. Klene, J. E.

Knox, J. B. Cross, V. Bakken, C. Adamo, J. Jaramillo, R. Gomperts, R. E. Stratmann, O. Yazyev, A. J. Austin, R. Cammi, C. Pomelli, J. W. Ochterski, R. L. Martin, K. Morokuma, V. G. Zakrzewski, G. A. Voth, P. Salvador, J. J. Dannenberg, S. Dapprich, A. D. Daniels, Ö. Farkas, J. B. Foresman, J. V. Ortiz, J. Cioslowski and D. J. Fox, *Gaussian 09, Revision*, Gaussian, Inc., Wallinford, CT, **2009**, p.

[11] Y. Zhao and D. G. Truhlar, *J. Chem. Phys.* **2006**, *125*, 194101-194118.

[12] A. Schafer, C. Huber and R. Ahlrichs, *J. Chem. Phys.* **1994**, *100*, 5829-5835.

[13] A. V. Marenich, C. J. Cramer and D. G. Truhlar, *J. Phys. Chem. B* **2009**, *113*, 6378-6396.

[14] a) R. L. Martin, P. J. Hay and L. R. Pratt, *J. Phys. Chem. A* **1998**, *102*, 3565-3573; b) N. Sieffert and M. Buhl, *Inorg. Chem.* **2009**, *48*, 4622-4624.

[15] S. Grimme, S. Ehrlich and L. Goerigk, *J. Comput. Chem.* **2011**, *32*, 1456-1465.

[16] S. Grimme, *J. Comput. Chem.* **2006**, *27*, 1787-1799.

[17] J. D. Chai and M. Head-Gordon, *Phys. Chem. Chem. Phys.* **2008**, *10*, 6615-6620.

[18] S. Grimme, J. Antony, S. Ehrlich and H. Krieg, *J. Chem. Phys.* **2010**, *132*, 154104.

[19] a) F. Weigend and R. Ahlrichs, *Phys. Chem. Chem. Phys.* **2005**, *7*, 3297-3305; b) F. Weigend, *Phys. Chem. Chem. Phys.* **2006**, *8*, 1057-1065.

[20] R. C. Clark and J. S. Reid, *Acta Crystallogr. Sect. A* **1995**, *51*, 887-897.